

Fall 2016

LINEARLY EXTENDED PYRYLIUM SALTS (LEPS) AND LINEARLY EXTENDED THIOPYRYLIUM SALTS (LETS) AS ORGANIC SEMICONDUCTORS

Jianyu Zhao

University of New Hampshire, Durham

Follow this and additional works at: <https://scholars.unh.edu/dissertation>

Recommended Citation

Zhao, Jianyu, "LINEARLY EXTENDED PYRYLIUM SALTS (LEPS) AND LINEARLY EXTENDED THIOPYRYLIUM SALTS (LETS) AS ORGANIC SEMICONDUCTORS" (2016). *Doctoral Dissertations*. 1365.
<https://scholars.unh.edu/dissertation/1365>

This Dissertation is brought to you for free and open access by the Student Scholarship at University of New Hampshire Scholars' Repository. It has been accepted for inclusion in Doctoral Dissertations by an authorized administrator of University of New Hampshire Scholars' Repository. For more information, please contact nicole.hentz@unh.edu.

LINEARLY EXTENDED PYRYLIUM SALTS (LEPS) AND LINEARLY EXTENDED
THIOPYRYLIUM SALTS (LETS) AS ORGANIC SEMICONDUCTORS

By

Jianyu Zhao

B.S., Southwest University of China, 2008

M.S., Chinese Academy of Sciences, 2011

DISSERTATION

Submitted to the University of New Hampshire

in Partial Fulfillment of

the Requirements for the Degree of

Doctor of Philosophy

in

Chemistry

September, 2016

This dissertation has been examined and approved in partial fulfillment of the requirements for the degree of Doctor of Philosophy in Chemistry by:

Glen P. Miller, Dissertation Director
Professor of Chemistry and Materials Science

Erik Berda
Associate Professor of Chemistry and Materials Science

John Tsavalas
Associate Professor of Chemistry and Materials Science

Sterling A. Tomellini
Professor of Chemistry

Donald C. Sundberg
Professor of Materials Science

On June 2nd, 2016

Original approval signatures are on file with the University of New Hampshire Graduate School.

ACKNOWLEDGEMENT

My dissertation and the journey during my PhD study would not be completed without the help of numerous individuals. Here I would like to express my sincere gratitude to them.

First, I would like to express my deepest gratitude to my advisor Prof. Glen Miller. Without his consistent guidance and encouragement, numerous progresses in my research projects would be impossible. Without learning from Prof. Miller's in-depth knowledge, I would have not achieved the level of expertise in organic chemistry especially in the field of organic semiconductors. Without the freedom he allows in scientific research, I would have not formed the habit of independent thinking. Also, without his financial support, I would have not that sufficient time to focus on my research projects.

Also, I owe my sincere gratitude to the rest of my dissertation committee members for their guidance. I feel honored to have Prof. Erik Berda, Prof. John Tsavalas, Prof. Sterling Tomellini and Prof. Donald Sundberg in my dissertation committee. I appreciate your insightful comments and suggestions for my research project.

I would like to express my heartfelt thanks to Prof. Gonghu Li who kindly ran the ESR experiments for my samples. Also, I would like to express my sincere gratitude to professors who taught me in class, Prof. Arthur Greenberg in Advanced Organic Chemistry, Prof. Richard Johnson in Computational Chemistry, Prof. Charles Zercher in Organic Synthesis, Prof. Gary Weisman in NMR Spectroscopy, Prof. Matt Young in Spectroscopic Characterization of Organic Molecules and Prof. Roy Planalp in Advanced Inorganic Chemistry. Without your instructions, I would not build a solid background in Chemistry.

I would like to thank Jon Briggs for the help in crystal growing and single crystal X-ray analysis. I would also like to thank Dr. Chandrani Pramanik for the help in various experiments especially in cyclic voltammetry. I would also like to thank Dr. Weimin Lin for the practical suggestions in some experiments. I would also like to thank Dr. Jennifer Hodgson for the guidance in computational chemistry. Without the kind help from all of you, my research progress could not achieve this level.

I would like to thank Yi Xu, Hao Geng and Yushu Li for teaching me the practical experimental operations. I would like to thank Shunfu Hu for organic electronics device fabrication for my target materials. I am grateful for the friendship and the help of other current and previous group members Yanmei Rong, Xiaoyi Zhang, Lei Zhou, Claire Cho, Julia Chan, Jinyu Yang and Yadi Wang.

I would like to thank Dr. Pat Wilkinson for training me NMR operations and helping me all the time with the NMR problems. I would also like to thank John Wilderman's help in addressing the NMR instrumentation issues.

My thanks are continued to give office administrators Cindi Rowher and Peg Torch for their all-the-time kind help. Also, I would like to thank Bob Constantine for his enthusiastic assistance in reference searching.

Finally, I can never thank enough my parents for their consistent encouragement. The unconditional love and support from them provide me strong driving force to finish my PhD study. I owe all my achievements to them.

Thank you for reading my dissertation.

Table of Contents

ACKNOWLEDGEMENT.....	iii
LIST OF FIGURES.....	ix
LIST OF TABLES.....	xii
LIST OF SCHEMES.....	xiii
LIST OF NUMBERED STRUCTURES.....	xv
ABSTRACT.....	xxiv
CHAPTER 1.....	1
Introduction.....	1
1.1 Background.....	1
1.2 Organic semiconductor.....	2
1.2.1 General characteristics.....	2
1.2.2 Classification.....	3
1.2.2.1 Classification by molecular size.....	3
1.2.2.2 Classification by electronic behavior.....	5
1.3 Properties requirements for organic semiconductors.....	8
CHAPTER 2.....	10

Linearly extended pyrylium and thiopyrylium salts as organic semiconductors.....	10
2.1 Introduction.....	10
2.1.1 Pyrylium and thiopyrylium cations.....	10
2.1.2 Xanthylum and thioxanthylum cations.....	12
2.1.3 Linearly extended pyrylium salts (LEPS) and linearly extended thiopyrylium salts (LETS).....	14
2.2 Results and discussion.....	15
2.2.1 Computational study for LEPS and LETS compounds.....	15
2.2.1.1 Introduction.....	15
2.2.1.2 Computation for LEPS and LETS compounds.....	16
2.2.2 General synthetic routes design for LEPS and LETS compounds.....	17
2.2.3 Syntheses and study of dibenzoxanthenes and dibenzothioxanthenes.....	18
2.2.3.1 Synthesis of dibenzoxanthone 38	18
2.2.3.1.1 Synthesis of 38 through an LDA-mediated ring closure reaction.....	18
2.2.3.1.2 Synthesis of 38 through tandem intermolecular nucleophilic coupling involving a naphthalene intermediate.....	22
2.2.3.1.3 Attempted synthesis of 38 through Pd-catalyzed annulation.....	24
2.2.3.2 Synthesis of dibenzoxanthone 74 via an LDA-mediated ring closure	26

2.2.3.3 Synthesis of dibenzothioxanthone 80 via an LDA-mediated ring closure.....	27
2.2.3.4 Optical characteristics of dibenzoxanthenes and dibenzothioxanthenes.....	29
2.2.4 Syntheses of dibenzoxanthenols and dibenzothioxanthenols.....	32
2.2.4.1 Syntheses of aryl substituted dibenzoxanthenols and dibenzothioxanthenols.....	32
2.2.4.2 Syntheses of unsubstituted dibenzoxanthenol and dibenzothioxanthenol.....	35
2.2.5 Syntheses and study of LEPS and LETS compounds.....	36
2.2.5.1 Syntheses of LEPS and LETS compounds.....	36
2.2.5.2 Moisture resistance study of LEPS and LETS compounds.....	38
2.2.5.3 Solubilities of LEPS and LETS compounds.....	40
2.2.5.4 Charge delocalization of LEPS and LETS compounds.....	41
2.2.5.5 Optical properties of LEPS and LETS compounds.....	42
2.2.5.6 Single crystal X-ray diffraction study of LEPS and LETS compounds.....	46
2.2.5.7 Cyclic voltammetry of LEPS 99	49
2.2.5.8 Open-shell diradical character study.....	50
2.2.5.8.1 Introduction.....	50
2.2.5.8.2 Open-shell diradical character of LEPS and LETS compounds.....	56
Experimental.....	63

CHAPTER 3.....	90
Summary and conclusions.....	90
3.1 Summary.....	90
3.1.1 Summary of syntheses.....	90
3.1.2 Summary of properties.....	91
3.2 Conclusions and outlook.....	93
References.....	95
Appendix (NMR and Mass spectra).....	100

LIST OF FIGURES

Figure 1: Conjugated systems of organic semiconductors with overlapped p orbitals.

Figure 2: Chemical structures of common polymer organic semiconductors: **1** polypyrrole; **2** polyacetalene; **3** P3HT; **4** PPV.

Figure 3: Chemical structures of common small molecule organic semiconductors: **5** acenes; **6** oligothiophene; **7** porphyrins; **8** fullerenes; **9** perylene diimides.

Figure 4: Chemical structures of pentacene and its derivatives: **10** pentacene; **11** thiolated pentacene; **12** silylethynyl pentacene.

Figure 5: Proposed working process for organic photovoltaic devices involving (1) photoexcitation, (2) exciton dissociation and (3) charge separation and collection.

Figure 6: Chemical structures of p-type organic semiconductors: **10** pentacene; **13** tetracene; **14** thienoacene; **15** pyrene; **16** perylene.

Figure 7: Chemical structures of n-type organic semiconductors: **17** PCBM; **18** perfluoropentacene; **19** TCNQ; **20** NTCDI.

Figure 8: Structures of xanthylium cation **23**, thioxanthylium cation **24** and anthracene **25**.

Figure 9: Structures for linearly extended pyrylium salts (LEPS) **36** and linearly extended thiopyrylium salts (LETS) **37** with backbones and π -systems similar to those of pentacene **10**.

Figure 10: UV-Vis absorption spectra for dibenzoxanthenes **38**, **74** and dibenzothioxanthone **80**.

Figure 11: UV-Vis absorption spectra for dibenzoxanthenes **38** and **42** at 8.1×10^{-5} M in CHCl_3 .

Figure 12: Solubility order for LEPS compounds with different substituents.

Figure 13: ^1H NMR spectra in aromatic region for LEPS **99** and its precursor **83** both in CD_2Cl_2 .

Figure 14: UV-Vis-NIR absorption spectra of 3.4×10^{-5} M solutions of linear LEPS **99** and its phene-like isomer **100** in DCM.

Figure 15: UV-Vis-NIR absorption spectra of 3.4×10^{-5} M solutions of LEPS **99** and LETS **105** in DCM.

Figure 16: UV-Vis-NIR absorptions of 3.4×10^{-5} M solutions of LEPS and LETS compounds in DCM.

Figure 17: ORTEP diagrams (50% probability) of LEPS **99** and its packing structure.

Figure 18: ORTEP diagrams (50% probability) of LETS **105** and its packing structure.

Figure 19: Cyclic voltammogram of a 2×10^{-3} M solution of LEPS **99** in DCM with 0.1 M Bu_4NPF_6 as electrolyte, Ag/AgCl as reference electrode, Pt disk as working electrode and Pt wire as counter electrode. Scan rate is 100 mV/s.

Figure 20: Electronic configuration in NBMOs for singlet and triplet states.

Figure 21: Structures for bisanthene, teranthene and quarteranthene derivatives.

Figure 22: Temperature-related spin multiplicity switching of diradical with singlet ground state but accessible triplet excited state.

Figure 23: VT-NMR results for teranthene derivative **114** and quarteranthene derivative **115**.

Figure 24: ^1H NMR spectrum for dipyrilium salt **116**.

Figure 25: ^1H NMR and ^{13}C NMR for LETS **106** in CD_2Cl_2 at room temperature.

Figure 26: VT-NMR study for LETS **106** in CD_2Cl_2 .

Figure 27: Intramolecular electron transfer (IMET) process for LETS compounds.

Figure 28: Predicted LEPS and LETS structures with strong paramagnetic character.

LIST OF TABLES

Table 1: Energy calculations for LEPS-0, LETS-0 and pentacene with B3LYP/6-311+G**//B3LYP-6-31G*.

Table 2: Energy calculations for LEPS and LETS compounds with different substituents with B3LYP/6-311+G**//B3LYP-6-31G*.

Table 3: UV-Vis absorptions and emissions of dibenzoxanthenes and dibenzothioxanthenes in CHCl₃.

Table 4: Bond lengths (a-f) of the center ring and twist angle between the substituent and the backbone of LEPS and LETS compounds.

Table 5: ESR results for LEPS and LETS compounds and xanthylium derivatives.

LIST OF SCHEMES

Scheme 1: Pyrylium cation **21**.

Scheme 2: Thiopyrylium cation **22**.

Scheme 3: Syntheses of 9-arylxanthylium **28** and 9-arylthioxanthylium **31** tetrafluoroborates.

Scheme 4: Syntheses of xanthylium perchlorate **33** and thioxanthylium perchlorate **35**.

Scheme 5: Enhanced charge delocalization and stability for 9-phenyl xanthylium and thioxanthylium cations.

Scheme 6: General synthetic routes design for LEPS **36** and LETS **37**.

Scheme 7: Synthesis of dibenzoxanthone **38** via an LDA-mediated ring closure.

Scheme 8: Synthesis of 2-iodonaphthoic acid **43**.

Scheme 9: Formation of xanthone derivatives via Friedel-Crafts acylation/cyclization.

Scheme 10: Selective formation of linear xanthone derivatives via an LDA-mediated ring closure.

Scheme 11: Synthesis of dibenzoxanthone **38** via tandem intermolecular nucleophilic coupling.

Scheme 12: Formation of xanthonones **61** via tandem intermolecular nucleophilic coupling.

Scheme 13: Attempted synthesis of dibenzoxanthone **38** via a Pd-catalyzed annulation.

Scheme 14: Formation of xanthonones **61** via Pd-catalyzed annulation.

Scheme 15: Synthesis of dibenzoxanthone **74** via a selective LDA-mediated ring closure.

Scheme 16: Selective synthesis of dibenzothioxanthone **80** via an LDA-mediated ring closure.

Scheme 17: Syntheses of aryl substituted dibenzoxanthenols **82-87**.

Scheme 18: Syntheses of aryl substituted dibenzoxanthenols **88** and **89**.

Scheme 19: Syntheses of aryl substituted dibenzothioxanthenols **90-95**.

Scheme 20: Reduction of dibenzoxanthone **38** and its isomer **42** using hydride reagents.

Scheme 21: Reduction of dibenzothioxanthone **80** using sodium borohydride.

Scheme 22: Syntheses of LEPS **99** and its isomer **100**, LEPS **101**, LEPS **102**.

Scheme 23: Syntheses of LEPS **103** and LEPS **104**.

Scheme 24: Syntheses of LETS compounds (**105-110**).

Scheme 25: Nucleophilic attack of water on LEPS and LETS compounds.

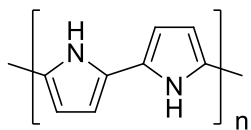
Scheme 26: *o*-Methyl groups on mesityl substituent shield the otherwise reactive C-13 of the LEPS and LETS backbones.

Scheme 27: Closed-shell and open shell resonance forms for quinoidal oligothiophenes.

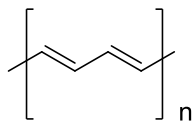
Scheme 28: Closed-shell and open shell resonance forms for anthene **112** with diradical character calculated at the CASSCF(2,2)/6-31G level.

Scheme 29: Intramolecular electron transfer (IMET) for dipyrilium salts **116**.

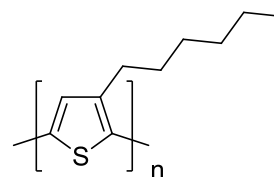
LIST OF NUMBERED STRUCTURES



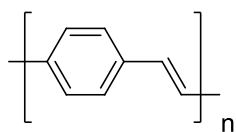
1



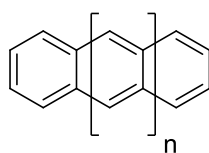
2



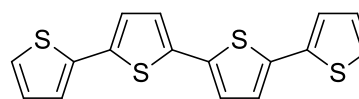
3



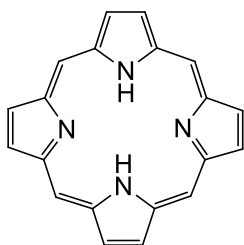
4



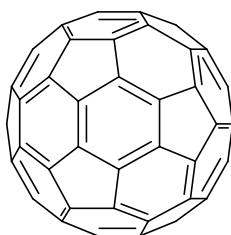
5



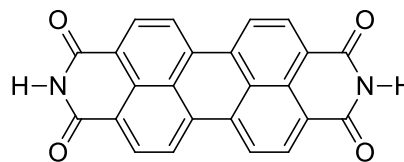
6



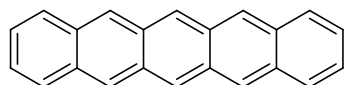
7



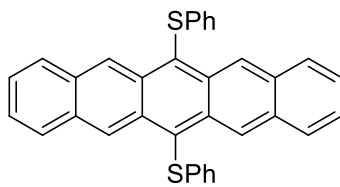
8



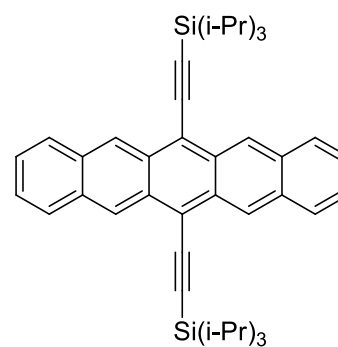
9



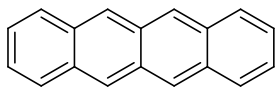
10



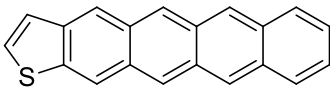
11



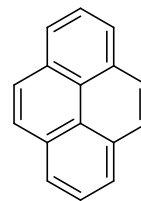
12



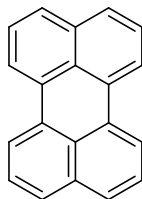
13



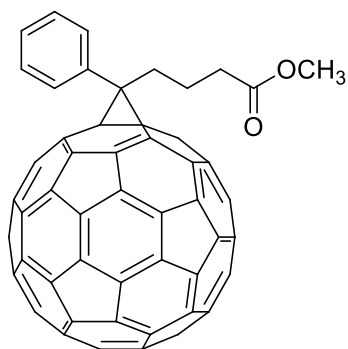
14



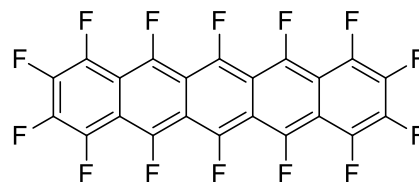
15



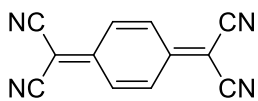
16



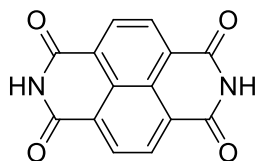
17



18



19



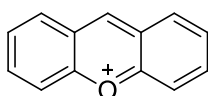
20



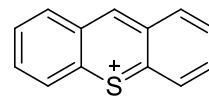
21



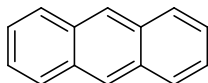
22



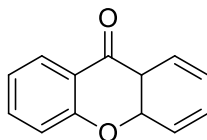
23



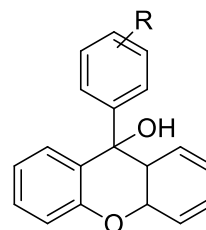
24



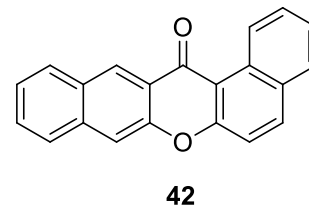
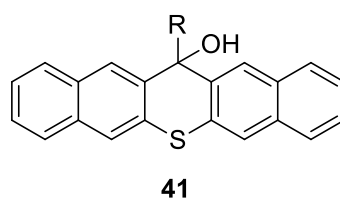
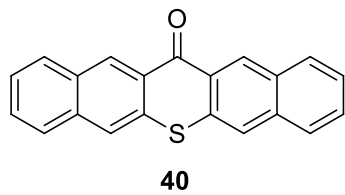
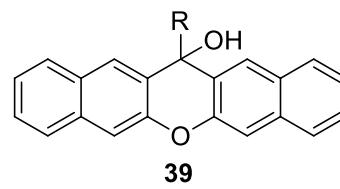
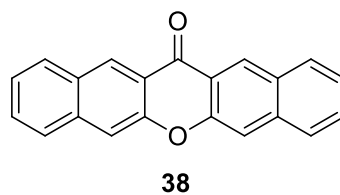
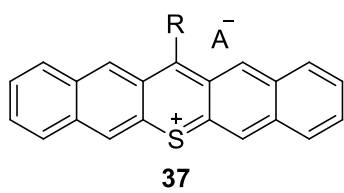
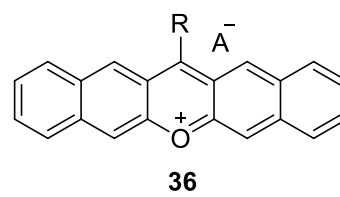
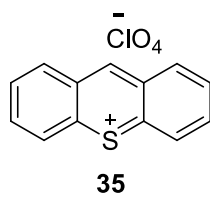
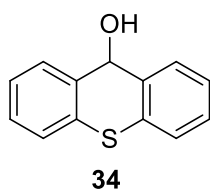
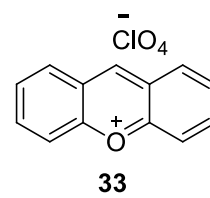
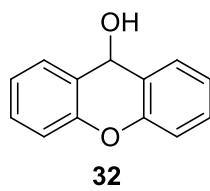
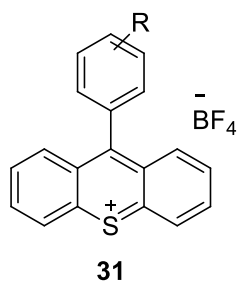
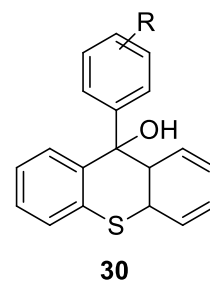
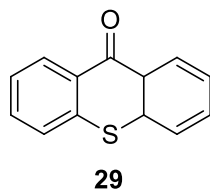
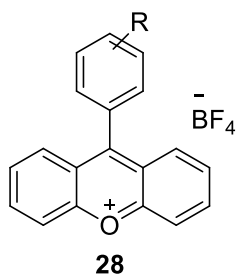
25

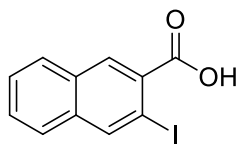


26

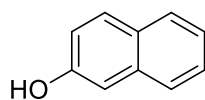


27

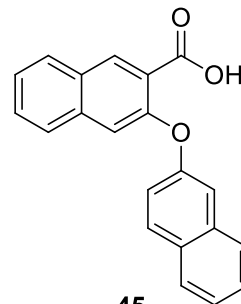




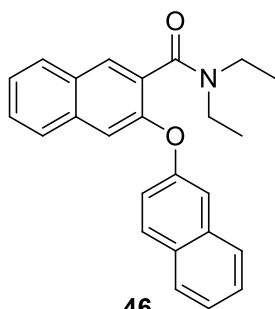
43



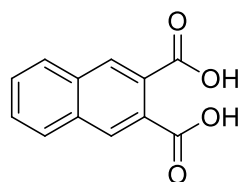
44



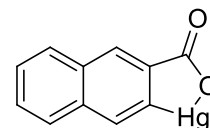
45



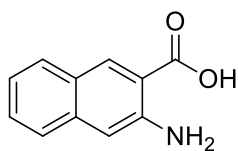
46



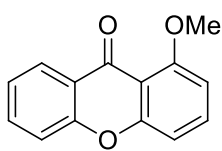
47



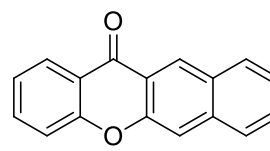
48



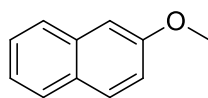
49



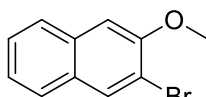
50



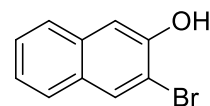
51



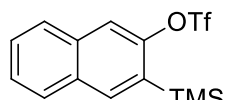
52



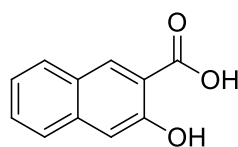
53



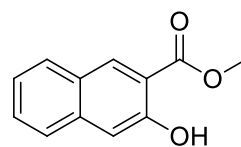
54



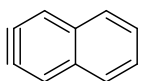
55



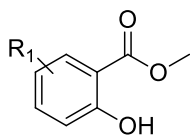
56



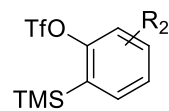
57



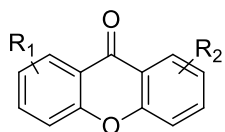
58



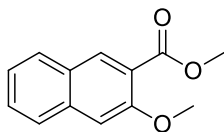
59



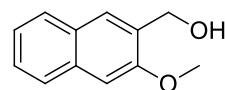
60



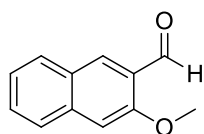
61



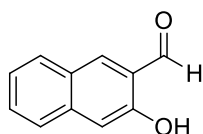
62



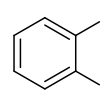
63



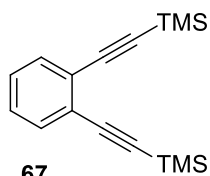
64



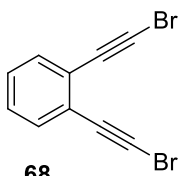
65



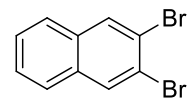
66



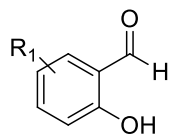
67



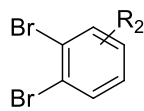
68



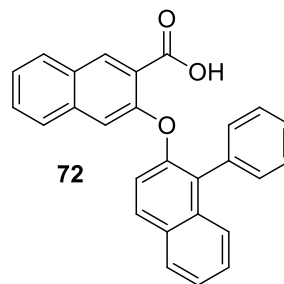
69



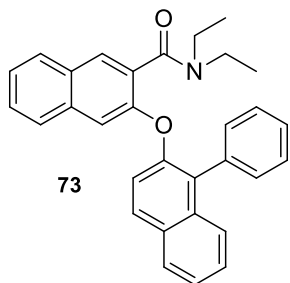
70



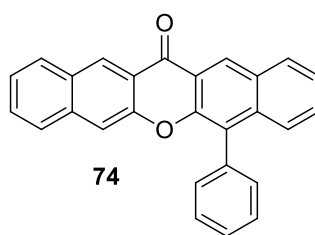
71



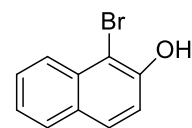
72



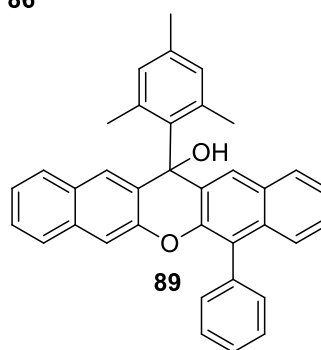
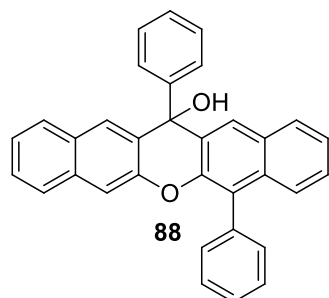
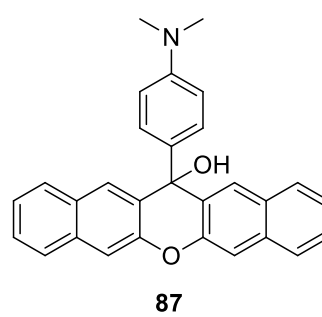
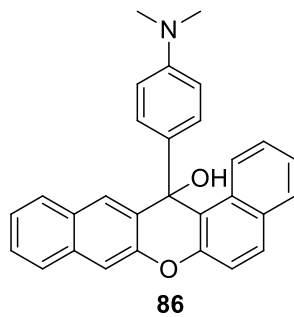
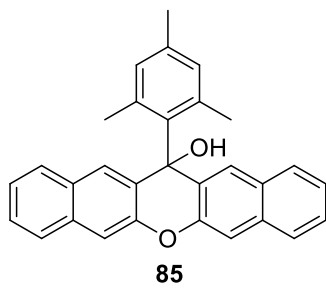
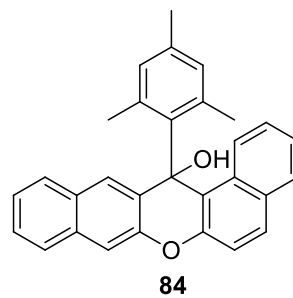
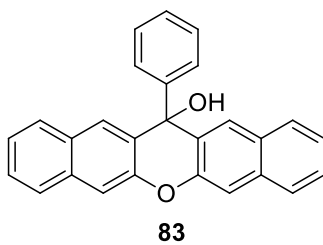
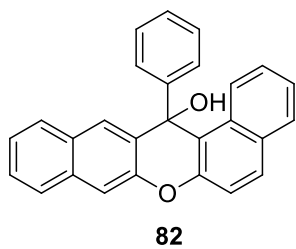
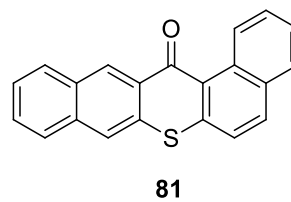
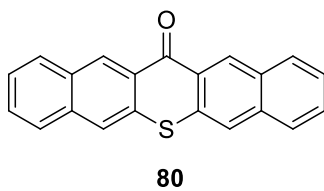
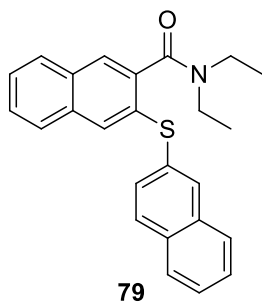
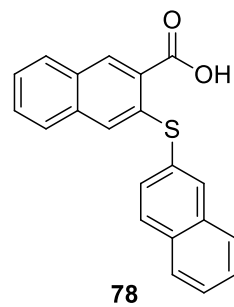
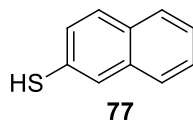
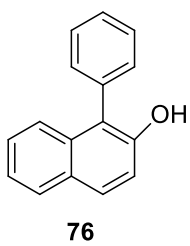
73

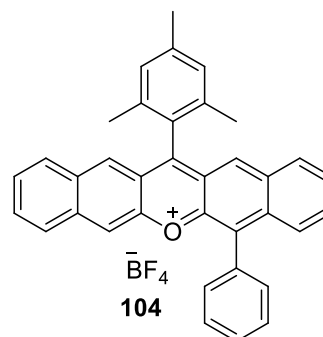
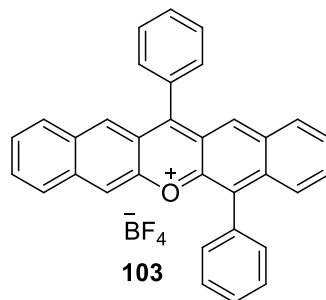
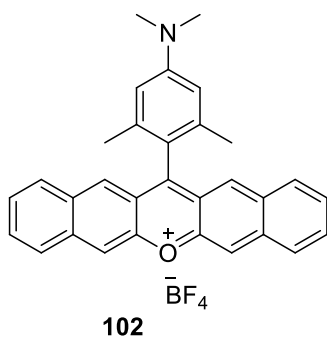
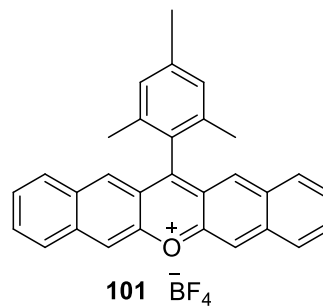
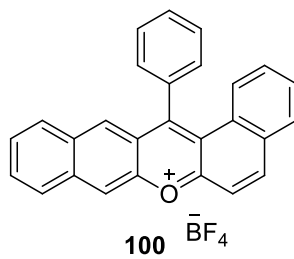
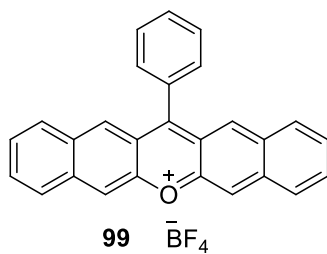
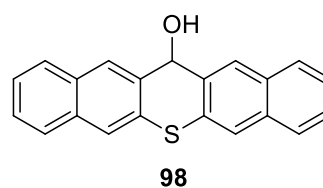
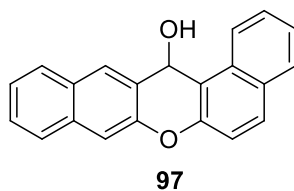
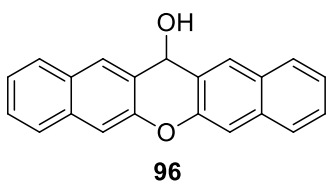
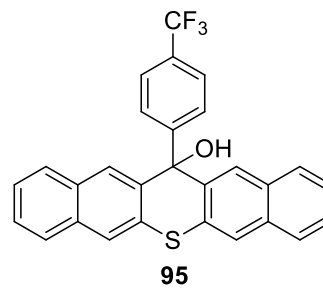
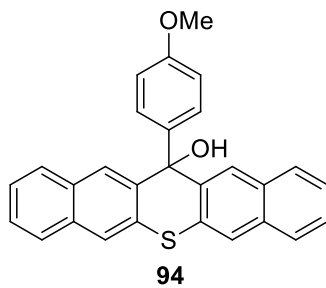
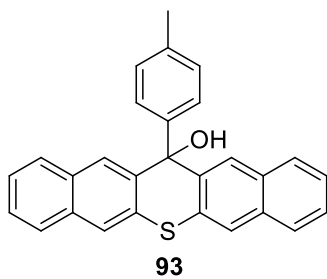
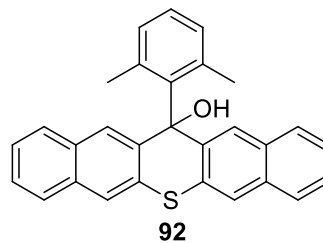
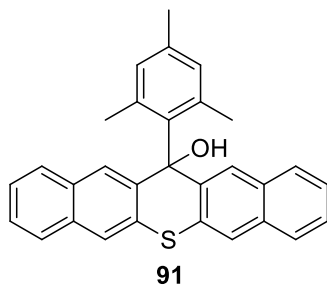
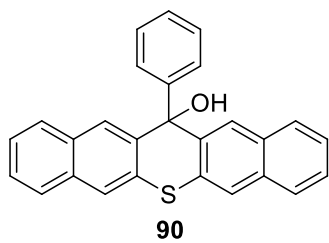


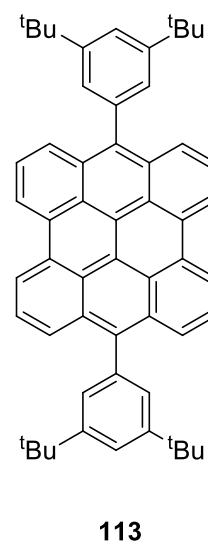
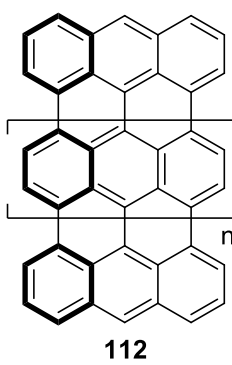
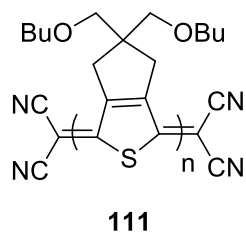
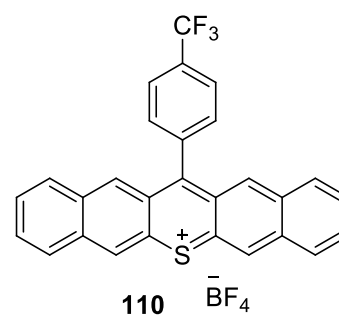
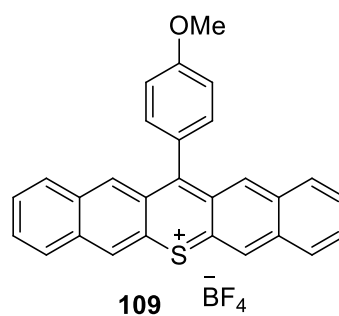
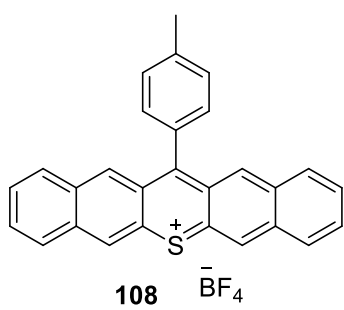
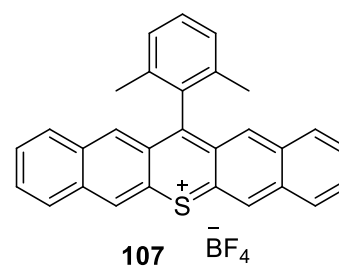
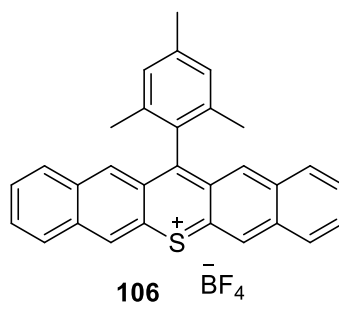
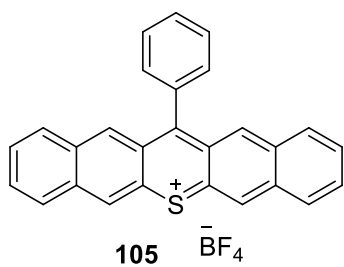
74

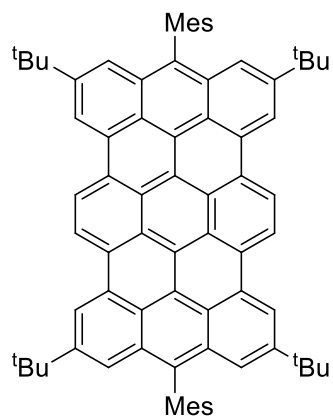


75



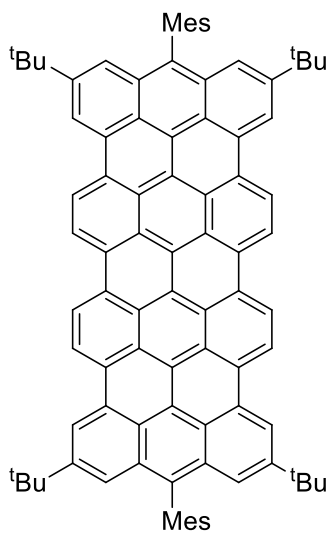




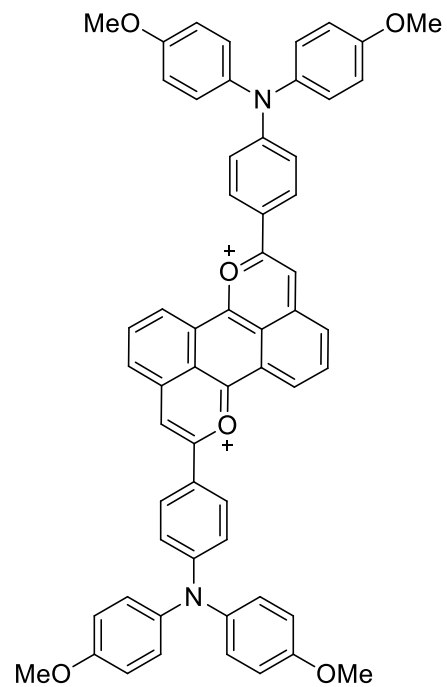


Mes=Mesityl

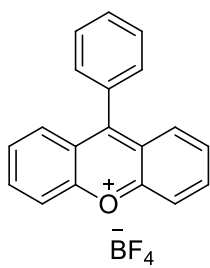
114



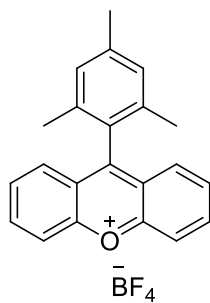
115



116



117



118

ABSTRACT

LINEARLY EXTENDED PYRYLIUM SALTS (LEPS) AND LINEARLY EXTENDED THIOPYRYLIUM SALTS (LETS) AS ORGANIC SEMICONDUCTORS

By

Jianyu Zhao

University of New Hampshire, September, 2016

Research focused on the development of a new class of n-type organic semiconductors called linearly extended pyrylium salts (LEPS) and linearly extended thiopyrylium salts (LETS). While a lot of progress has been made on p-type organic semiconductors over the last decade, less attention has been paid to n-type organic semiconductors. Pyrylium and thiopyrylium cations are aromatic structures akin to benzene but with one methine carbon (CH) replaced by either a positively charged oxygen or sulfur atom, respectively. This makes these aromatic π -systems very electron-deficient. With pentacene-like backbones, LEPS and LETS compounds combine linearly conjugated π -systems of acenes with the highly electron-deficient nature of pyrylium and thiopyrylium salts. The LEPS and LETS compounds described here were synthesized efficiently using new reactions. Their properties were calculated through high-level computation and studied experimentally by UV-Vis-NIR spectroscopy, cyclic voltammetry, single crystal X-ray diffraction, ESR and variable temperature NMR (VT-NMR) experiments.

The LEPS and LETS compounds described here show moderate to high solubilities in organic solvents like acetonitrile and dichloromethane. While they are resistant to oxidation due to their electron-deficient backbones, they are sensitive to nucleophiles like water. LEPS and LETS compounds with a mesityl or 2',6'-dimethylphenyl substituent have much higher resistance to moisture compared to other LEPS and LETS compounds due to shielding of the reactive site via the *o*-methyl groups of the phenyl substituents. LEPS and LETS compounds have broad absorptions in the UV-Vis-NIR region and possess small HOMO-LUMO gaps close to that of pentacene. They also exhibited reversible electrochemical behavior including remarkably easy reductions. Single crystal X-ray diffraction studies show that LEPS and LETS compounds form intermolecular face-to-face π - π stacking thin films. Broad and indiscernible NMR signals in the aromatic region and strong ESR signals were detected for LEPS and LETS compounds bearing a mesityl substituent. Weak to moderate ESR signals were also observed for most of other LEPS and LETS compounds. The broad aromatic NMR signals for LETS **106** bearing a mesityl substituent in CD₂Cl₂ sharpened upon gradually decreasing temperature in VT-NMR experiments. This indicates a switch from a paramagnetic triplet state to a diamagnetic singlet state. We propose that the LEPS and LETS compounds showing strong ESR signals and broadened NMR spectra have paramagnetic, triplet excited states that lie close in energy to their corresponding diamagnetic ground states. In these cases, populating the paramagnetic excited states via the thermal excitation is possible at or near room temperature.

CHAPTER 1

Introduction

1.1 Background

Semiconductors are materials that have conductivity between conductors like iron and insulators like glass. Semiconducting materials play important roles in the modern electronic industry. Elemental and compound materials are both important types of semiconductors.

Inorganic semiconductors are most commonly applied in industrial manufacturing. A variety of inorganic elements and compounds have semiconducting properties. Examples include the pure elements silicon and germanium, binary compounds gallium arsenide and silicon carbide, some oxides and alloys.¹

Organic semiconductors are organic molecules or polymers with π -conjugated aromatic backbones that are capable of transporting charge and interact effectively with light. These systems can function in similar ways as inorganic semiconductors in opto-electronic devices.² A lot of research has focused on organic semiconductors in recent decades. Although organic semiconductors exhibit comparable or lower electrical performance relative to inorganic semiconductors such as amorphous or crystalline silicon, they have other advantages. The structural versatility of organic semiconductors allows for property modification through synthetic tailoring. Also, they can be processed in either the vapor or solution phase during fabrication of the electronic devices. Moreover, they have good compatibility with different substrates including flexible substrates like plastics. Furthermore, because they can be solution-

processed, they can achieve high-rate manufacturing over large areas. Low cost and flexible next generation electronic devices with low power consumption, manufactured at high rates and over large areas, could all be realized using organic semiconductors.³

1.2 Organic Semiconductor

1.2.1 General characteristics

Holes and electrons in π -orbitals are the typical charge carriers in organic semiconductors. Charge transport typically depends on the ability of charge carriers to move from one molecule to another, which depends on the energy gap between highest occupied molecular orbital (HOMO) and lowest unoccupied molecular orbital (LUMO) levels. The smaller the HOMO-LUMO gap is, the easier the charge carriers can move. Increasing conjugation for molecules will decrease the HOMO-LUMO gap, so organic semiconductors typically have highly conjugated molecular backbones.⁴ Electrons and holes transport in the overlapped π -orbitals of the backbone. The backbone typically comprises alternating single and double bonds. The p orbitals of the sp^2 hybridized carbons in the backbone overlap with each other to form a planar conjugation system, which enables the charge carriers to transport inside and conduct the charges (**Figure 1**).⁵ For bulk materials in thin film applications, charge transport takes place in the overlapped π -orbitals of the neighboring organic semiconducting molecules when the crystalline film forms. Charge transport happens with thermally activated doping and tunneling between organic semiconducting molecules when the amorphous film forms.⁶

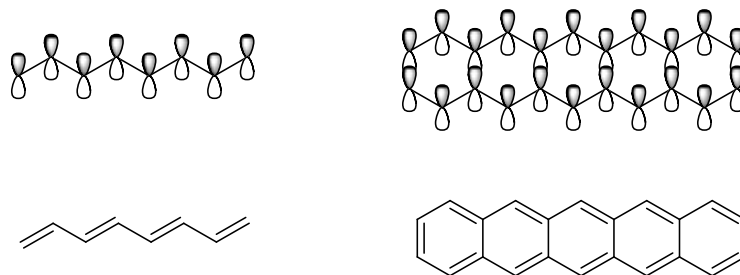


Figure 1: Conjugation systems of organic semiconductors with overlapped p orbitals.

1.2.2 Classification

1.2.2.1 Classification by molecular size

According to the molecular weight, the organic semiconductors can be classified as polymer organic semiconductors and small molecule organic semiconductors.

Polymer organic semiconductors typically comprise coupled aromatic monomer units, with extended π -conjugation along the polymer backbone. Aliphatic side chains can be attached to the backbone to increase the solubility.⁷ Polypyrrole **1**,⁸ polyacetalene **2**,⁹ poly(3-hexylthiophene) (P3HT) **3**,¹⁰ and poly(*p*-phenylene vinylene) (PPV) **4**¹¹ are well-known polymer organic semiconductors (**Figure 2**).

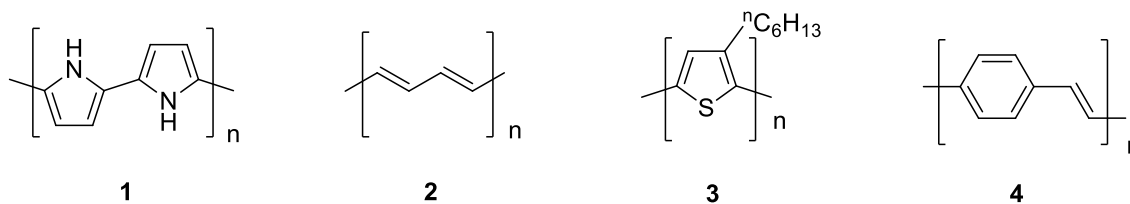


Figure 2: Chemical structures of common polymer organic semiconductors: **1** polypyrrole; **2** polyacetalene; **3** P3HT; **4** PPV.

Small molecule organic semiconductors generally have planar and highly conjugated backbones which are essential for lowering the HOMO-LUMO gap and promoting good

intermolecular π - π stacking for effective charge carrier transfer throughout the thin film of the material.¹² Acenes **5**,¹³ oligothiophenes **6**,¹⁴ porphyrins **7**,¹⁵ fullerenes **8**,¹⁶ and perylene diimides **9**¹⁷ are typical examples (**Figure 3**).

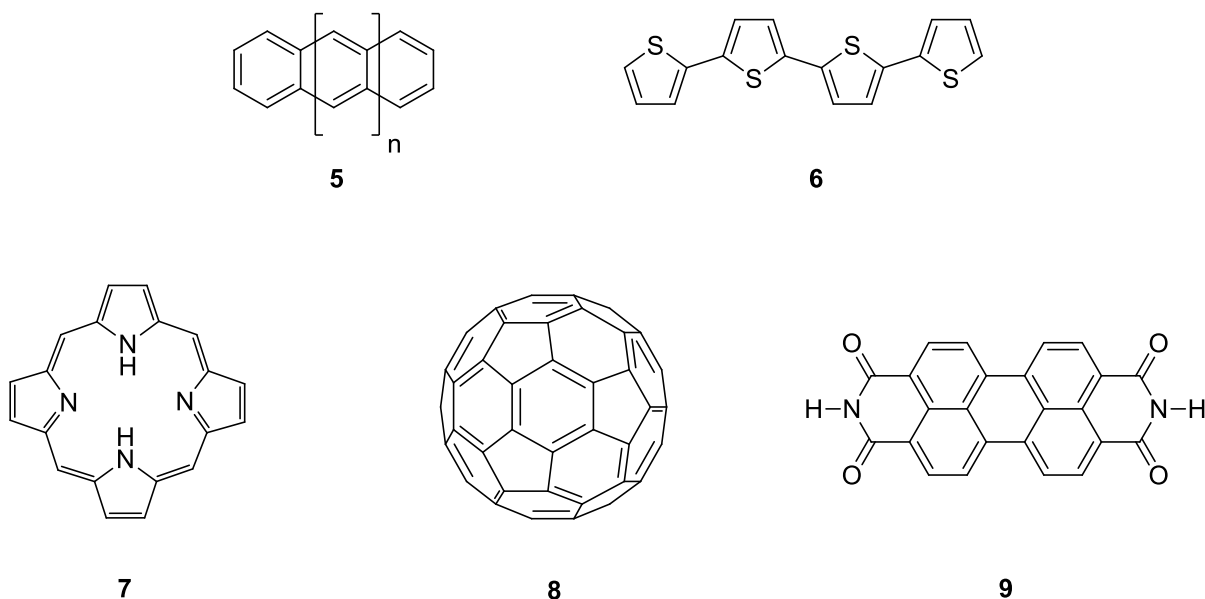


Figure 3: Chemical structures of common small molecule organic semiconductors: **5** acenes; **6** oligothiophene; **7** porphyrins; **8** fullerenes; **9** perylene diimides.

For the small molecule organic semiconductors, pentacene **10**¹⁸ is among the most widely explored molecules. Pentacene is a five ring acene possessing a linearly extended π -conjugated backbone. Thin films of pentacene possess relatively low band gaps (≤ 2 eV) and high charge carrier mobilities (up to ~ 3 cm²V⁻¹s⁻¹).⁴ Thin films prepared from other five-ring PAH (polycyclic aromatic hydrocarbon) molecules that lack the linear annelation of pentacene possess larger band gaps and smaller charge carrier mobilities, making them less interesting from an electronic applications perspective. Due to pentacene's poor solubility and facile photodegradation in the solution phase, pentacene derivatives bearing solubilizing and

stabilizing substituents, such as thiolated pentacenes **11**¹⁹ and silylethynyl pentacenes **12**¹³ were developed (**Figure 4**).

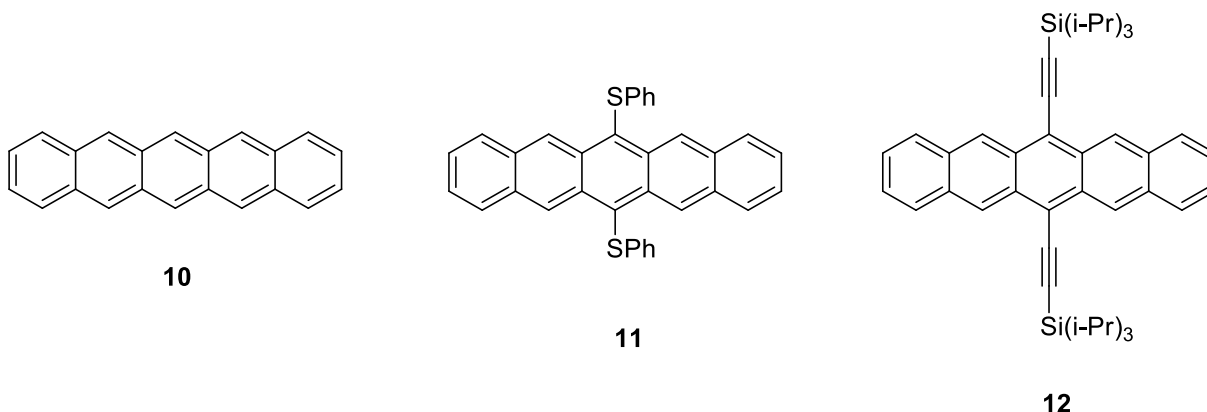


Figure 4: Chemical structures of pentacene and its derivatives: **10** pentacene; **11** thiolated pentacene; **12** silylethynyl pentacene.

1.2.2.2 Classification by electronic behavior

According to their electronic properties, organic semiconductors can be classified as p-type semiconductors which are electron-donors and n-type semiconductors which are electron-acceptors.

In an organic photovoltaic (OPV) device, the electrons in the HOMO of a p-type organic semiconductor are promoted to the LUMO upon excitation with light. Excitons, which are bound electron-hole pairs, are generated and move to the donor-acceptor interface, the region of the OPV material where p-type and n-type materials are contacting. Thus, the photoexcited p-type organic semiconductor can transfer an electron from its SOMO to the LUMO of an acceptor. The electron can then be transported through the conduction band of the acceptor thin film to an anode while the hole left can be transported through the donor thin film to the cathode, thus completing the electric circuit (**Figure 5**).⁴

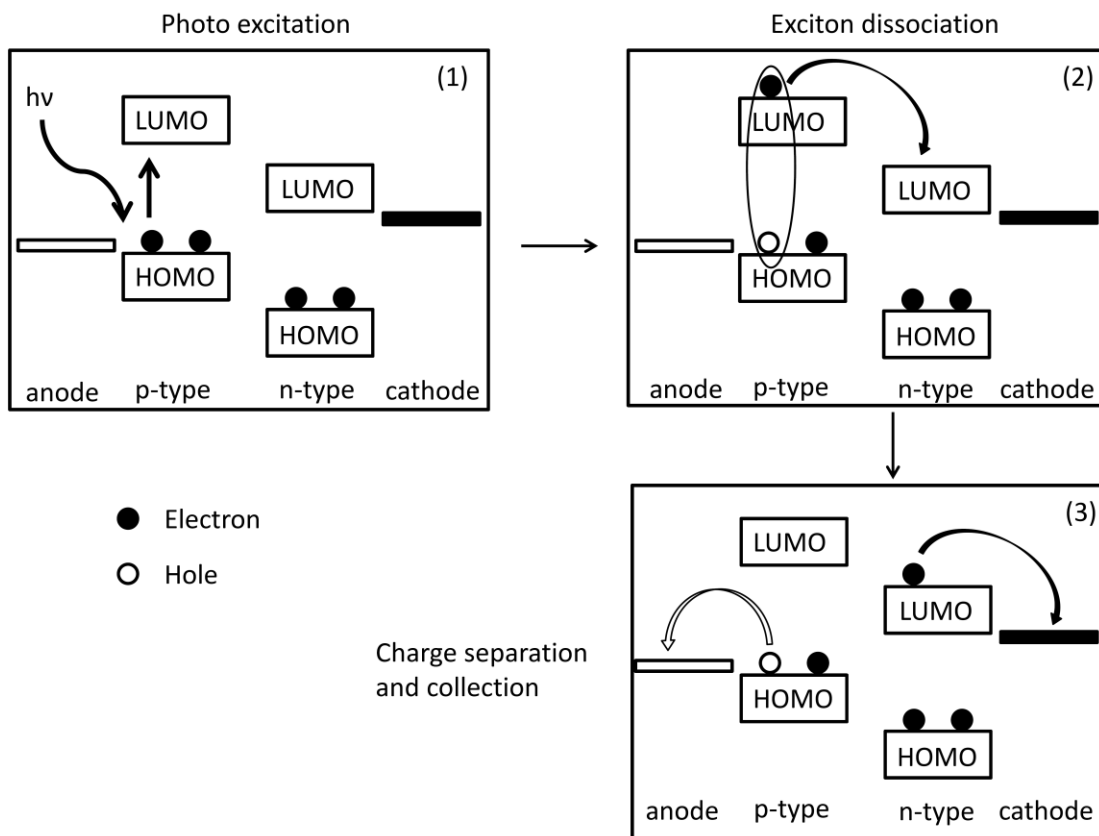


Figure 5: Proposed working process for organic photovoltaic devices involving (1) photoexcitation, (2) exciton dissociation and (3) charge separation and collection.

As electron-donors, p-type organic semiconductors usually contain electron-rich aromatic backbones.¹² Pentacene **10**,¹⁸ tetracene **13**,²⁰ thienoacene **14**,²¹ pyrene **15**,²² perylene **16**,²³ and their derivatives with electron-rich substituents are typical examples of p-type organic semiconductors (**Figure 6**).

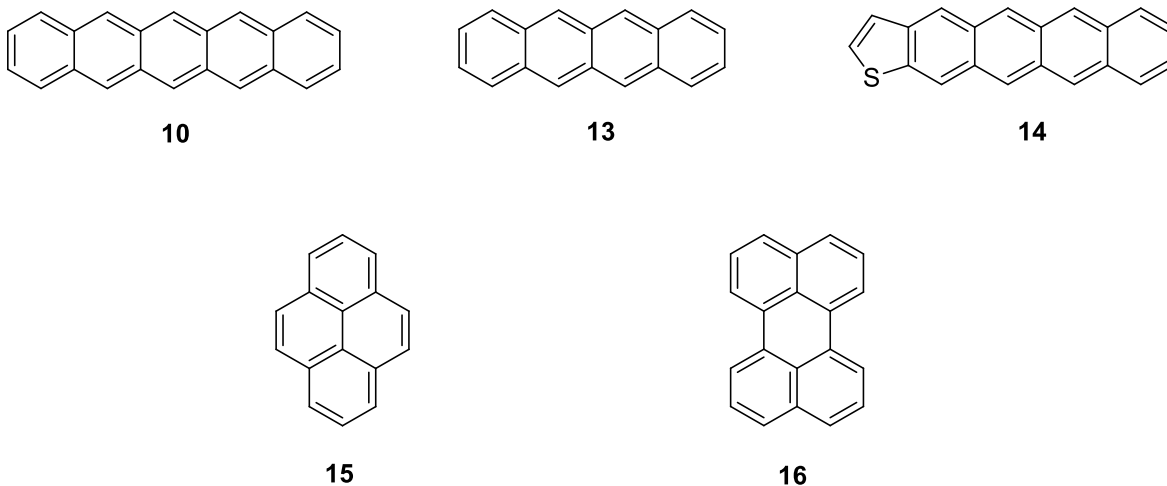


Figure 6: Chemical structures of p-type organic semiconductors: **10** pentacene; **13** tetracene; **14** thienoacene; **15** pyrene; **16** perylene.

As electron-acceptors, n-type organic semiconductors usually contain an electron-deficient aromatic backbone.¹² Fullerene **8** and its soluble derivative phenyl-C₆₁-butyric acid methyl ester (PCBM) **17**,²⁴ perfluoropentacene **18**,²⁵ tetracyanoquinodimethane (TCNQ) **19**,²⁶ naphthalene diimides (NTCDI) **20**²⁷ are examples of n-type organic semiconductors (**Figure 7**).

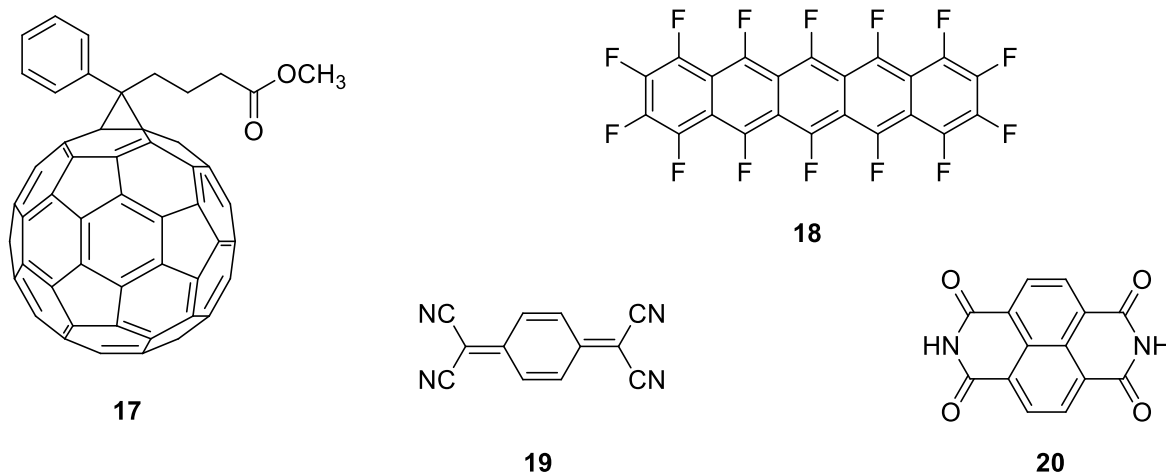


Figure 7: Chemical structures of n-type organic semiconductors: **17** PCBM; **18** perfluoropentacene; **19** TCNQ; **20** NTCDI.

1.3 Properties requirements for organic semiconductors

In order to achieve high-performance and long life-time organic electronic devices, the intrinsic properties of the organic semiconductors, the interaction between p-type and n-type organic semiconductors, device design and fabrication process are all important factors.

For the intrinsic properties of desirable organic semiconductors, there are several general requirements. First, they should have high stability under ambient condition and during device fabrication conditions. Because of the electron-rich conjugated backbone, many p-type organic semiconductors are readily subjected to photooxidation especially in the solution phase, which brings a problem for device fabrication. Second, they should have good solubility in an organic solvent, or in some cases, water. Vacuum deposition is commonly applied when the organic semiconductors have poor solubility. This device fabrication technique requires high temperatures, which is highly energy-consuming and harmful for the stability of the organic semiconductors. Also, a low HOMO-LUMO gap and suitable HOMO and LUMO energy levels are required to facilitate the charge carrier movement in p-type and n-type organic semiconductors. Moreover, for organic photovoltaic applications, they should have strong, broad absorption in the UV-Vis-NIR region to better utilize the solar energy spectrum. Furthermore, a strong intermolecular π - π stacking is preferred for efficient intermolecular charge transfer. Finally, a reversible electrochemical behavior is necessary for consistent functioning of the resulting device.

A lot of progress has been made on p-type organic semiconductors which are currently the leading class of organic semiconductors. However, high-performance n-type organic

semiconductors, which have the same significance in the development of organic electronic devices, are rare. The lack of availability of high performance n-type organic semiconductors provides an opportunity to explore and further develop this novel category.

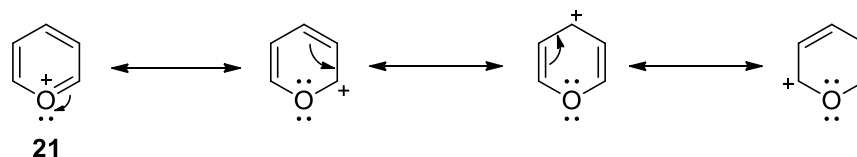
CHAPTER 2

Linearly extended pyrylium and thiopyrylium salts as organic semiconductors

2.1 Introduction

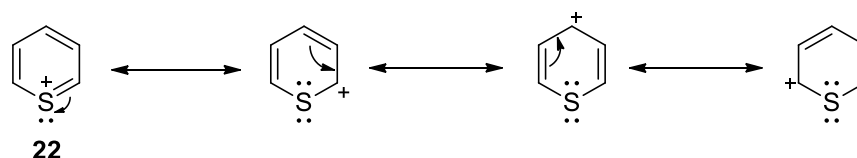
2.1.1 Pyrylium and thiopyrylium cations

Pyrylium cation **21** is an aromatic structure akin to benzene but with one methine carbon (CH) replaced by a positively charged oxygen atom (**Scheme 1**). The chemistry of pyrylium cation was introduced by Baeyer and Villiger in 1901.²⁸ Although the pyrylium ring is planar and has a full aromatic sextet of π -electrons, its chemical reactivity is quite different from that of benzene or even pyridine. The presence of O plus the formal positive charge perturbs the π -system profoundly, making the ring highly electron-deficient. Nucleophiles react readily with pyrylium cation and one-electron reductions take place readily to form radical species.²⁹ Pyrylium cations were recognized as exceptional examples of six π electron aromatic species, and a large number of stable derivatives have been prepared, most notably by Balaban.³⁰ In addition to being interesting species in their own right, pyrylium cations can function as intermediates in the syntheses of other interesting species including more stable pyridines, pyridinium cations, phosphabenzenes and thiopyrylium cations. Pyrylium cations can also be converted to 2-acylfurans, azulenes and indolizines.^{30b} Pyrylium cations also map directly onto a variety of materials with interesting applications such as natural pigments, food additives, photographic materials, photosensitizers, laser dyes, optical recording materials, fluorescent probes, anticorrosion agents and polymerization initiators.³¹



Scheme 1: Pyrylium cation **21**.

Thiopyrylium **22** (**Scheme 2**) is closely related to the corresponding oxygen-containing pyrylium **21**. Replacement of the oxygen heteroatom by the less electronegative sulfur produces a more stable species. Thiopyrylium cations were discovered nearly half a century after pyrylium cations and were first obtained upon reacting pyrylium salts with sodium sulfide.³² A comparison of their stability relative to those of pyrylium and seleno- and telluropyrylium cations shows the sulfur species to be more stable.^{30b} This is because sulfur has similar electronegativity as carbon, thereby increasing the aromaticity of the ring. Thiopyrylium salts show similar reactivity as their pyrylium counterparts.^{30b} They are utilized in photographic materials, in laser techniques, as infrared-absorbing dyes, and as electron-transfer photosensitizers or electrophotographic photoreceptors, as well as a photo-initiators for use in holographic recording.³²



Scheme 2: Thiopyrylium cation **22**.

2.1.2 Xanthylium and thioxanthylium cations

Xanthylium **23** and thioxanthylium **24** cations are linear dibenzo pyrylium or thiopyrylium cations, respectively, with backbones and π -systems similar to that of anthracene

25. (Figure 8)

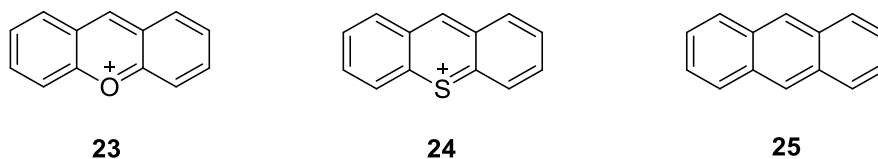
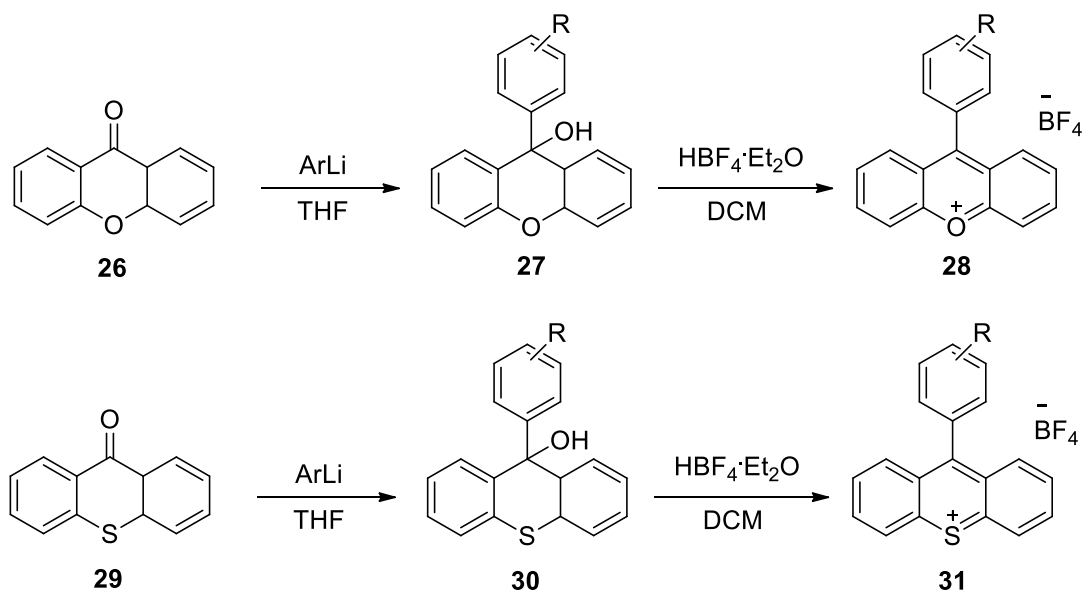


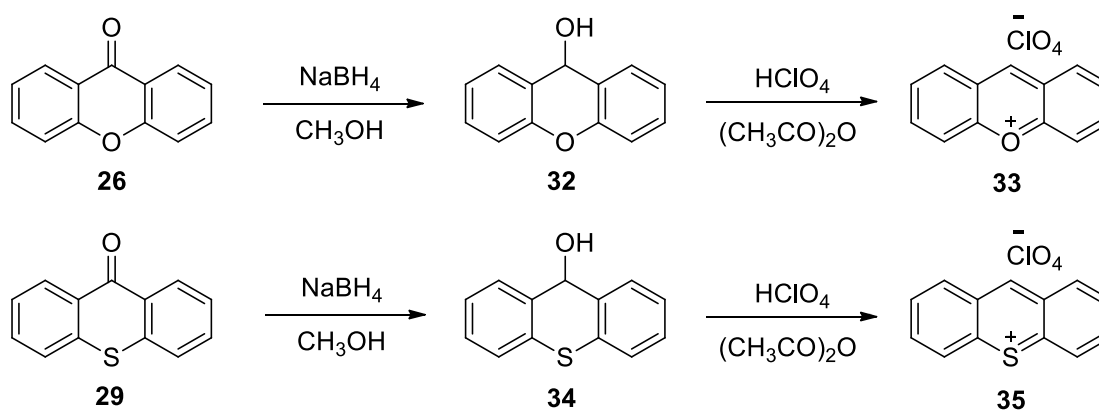
Figure 8: Structures of xanthylium cation **23**, thioxanthylium cation **24** and anthracene **25**.

A number of studies describing the syntheses and properties of xanthylium and thioxanthylium cations have been reported. In 1993, Valentino and co-workers reported the syntheses of several 9-arylxanthylium tetrafluoroborate salts **28** by treating 9-arylxanthen-9-ol **27** with propionic anhydride to create a reactive ester and fluoroboric acid to eliminate the ester.³³ The fluorescence quenching behaviors of these salts with water and alcohols were explored. These salts possess bright yellow or dark orange color and have strong absorptions in the UV-Vis region. Also, they have a broad unstructured and red-shifted fluorescence emissions band centered near 540 nm in acetonitrile solutions. In 2007, Hagel and co-workers reported syntheses of several 9-arylxanthylium **28** and 9-arylthioxanthylium **31** tetrafluoroborate salts by treating 9-arylxanthen-9-ol **27** or 9-arylthioxanthen-9-ol **30** with fluoroboric acid in ether (Scheme 3).³⁴ Compounds 9-arylxanthen-9-ol **27** and 9-arylthioxanthen 9-ol **30** were synthesized by treating xanthone **26** or thioxanthone **29** with aryllithium reagents. Reactivities of these xanthylium and thioxanthylium salts with sterically hindered bases were explored.



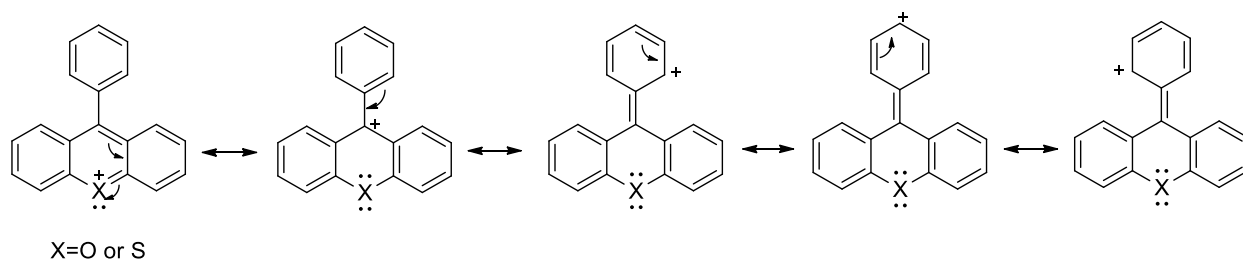
Scheme 3: Syntheses of 9-arylxanthylum **28** and 9-arylthioxanthylum **31** tetrafluoroborates.³⁴

In 2008, Zhu and coworkers reported the syntheses of xanthylum perchlorate **33** and thioxanthylum perchlorate **35** by treating 9-*H*-xanthanol **32** or 9-*H*-thioxanthanol **34** with acetic anhydride and perchloric acid (**Scheme 4**).³⁵ The two salts can be readily reduced with sodium borohydride to form xanthene and thioxanthene.



Scheme 4: Syntheses of xanthylum perchlorate **33** and thioxanthylum perchlorate **35**.³⁵

9-Arylxanthylum and 9-arylthioxanthylum cations are more stable than xanthylum and thioxanthylum cations because the former cations show greater delocalization of their charges and stronger steric shielding (**Scheme 5**).



Scheme 5: Enhanced charge delocalization and stability for 9-phenyl xanthylum and thioxanthylum cations.

2.1.3 Linearly extended pyrylium salts (LEPS) and linearly extended thiopyrylium salts (LETS)

Given that xanthylum and thioxanthylum salts have electron deficient and highly delocalized backbones, low HOMO-LUMO gaps, broad and strong absorptions and emissions in the UV-Vis region as well as good solubility and stability, we were keen to synthesize derivatives that could be utilized as n-type organic semiconductors which have been far less studied compared to p-type organic semiconductors. To the best of our knowledge, linearly extended five-ring pyrylium and thiopyrylium salts have never been prepared. Linearly extended polycyclic aromatic hydrocarbons like the 5-ring compound pentacene possess highly conjugated π -systems, low HOMO-LUMO gaps, and high charge carrier mobilities. We designed linearly extended pyrylium salts (LEPS) **36** and linearly extended thiopyrylium salts (LETS) **37** with the expectation that the pentacene-like backbone and π -system of these novel electron-deficient species would provide them interesting electronic properties (**Figure 9**). As with the xanthylum and thioxanthylum series, aryl substituted LEPS and LETS compounds were

expected to be more stable than unsubstituted LEPS and LETS compounds. Thus, appropriate substituted LEPS and LETS compounds were expected to possess small HOMO-LUMO gaps, broad and strong absorption and emission bands in the UV-Vis or even NIR regions, highly electron-deficient π -systems, good solubility and reasonable stability. If these expectations are met, then LEPS and LETS compounds will deserve careful consideration as n-type organic semiconductors.

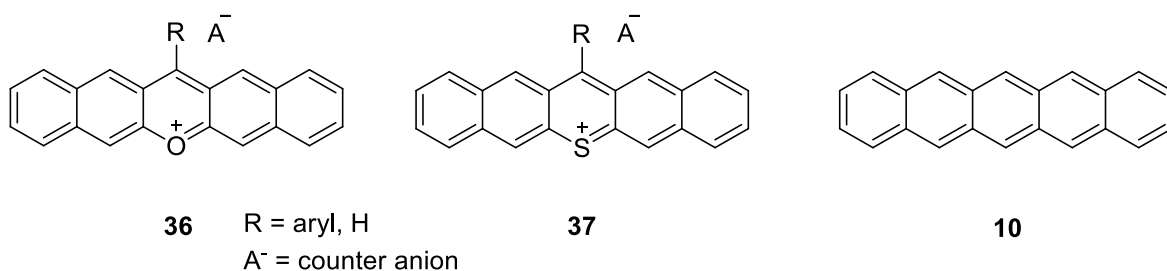


Figure 9: Structures for linearly extended pyrylium salts (LEPS) **36** and linearly extended thiopyrylium salts (LETS) **37** with backbones and π -systems similar to those of pentacene **10**.

2.2 Results and discussion

2.2.1 Computational study for LEPS and LETS compounds

2.2.1.1 Introduction

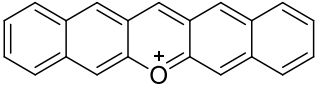
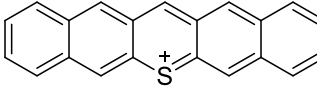
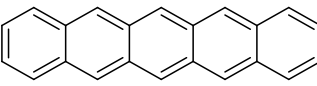
We have utilized density functional theory (DFT) to calculate the geometries and energies for pyrylium and thiopyrylium cations. B3LYP DFT calculations using a 6-31G* basis set have previously been utilized to calculate the geometry of pyrylium and thiopyrylium cations. For the energy calculations, B3LYP has been used with a variety of basis sets like 6-31G*,³⁶ 6-31G**,³⁷ 6-31+G*,³⁸ 6-31+G**.³⁹ For calculations of the energies of pentacene and its derivatives, B3LYP/6-311+G** with a larger basis set was utilized and the results fit well with

experiment.¹⁹ The triple- ζ quality AO basis sets enable more reliable energy calculations.⁴⁰ Since LEPS and LETS compounds are pyrylium and thiopyrylium salts with pentacene-like backbones and π -systems, we utilized B3LYP/6-31G* to calculate their geometries and B3LYP/6-311+G** to calculate their energies.

2.2.1.2 Computation for LEPS and LETS compounds

Computational results showed that unsubstituted LEPS cation (LEPS-0) and LETS cation (LETS-0) are both planar structures like pentacene. The HOMO-LUMO gaps for LEPS-0, LETS-0 and pentacene are similar, with LETS-0 possessing the smallest gap. The low-lying LUMOs for LEPS-0 and LETS-0 strongly suggest that these compounds will readily accept electrons, as required for an n-type organic semiconductor (**Table 1**).

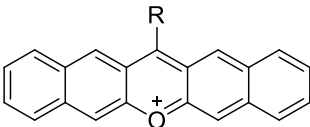
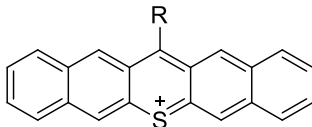
Table 1: Energy calculations for LEPS-0, LETS-0 and pentacene with B3LYP/6-311+G**//B3LYP/6-31G*.

Structure			
Name	LEPS-0	LETS-0	Pentacene
HOMO (eV)	-9.33	-9.12	-4.93
LUMO (eV)	-7.19	-7.10	-2.76
Gap (eV)	2.14	2.02	2.18

Geometry optimizations and energy calculations were also carried out for substituted LEPS and LETS compounds. The results show that the HOMO-LUMO gaps for different LEPS compounds are similar regardless of the substituent. This also applies to different LETS

compounds (**Table 2**). The geometries of the phenyl rings in the various phenyl, mesityl and 4'-dimethylaminophenyl derivatives are all nearly orthogonal as to the backbone, suggesting almost zero delocalization of π -electron density. The computational results are further corroborated by UV-Vis-NIR and X-ray single crystal structure studies which will be elaborated in later parts.

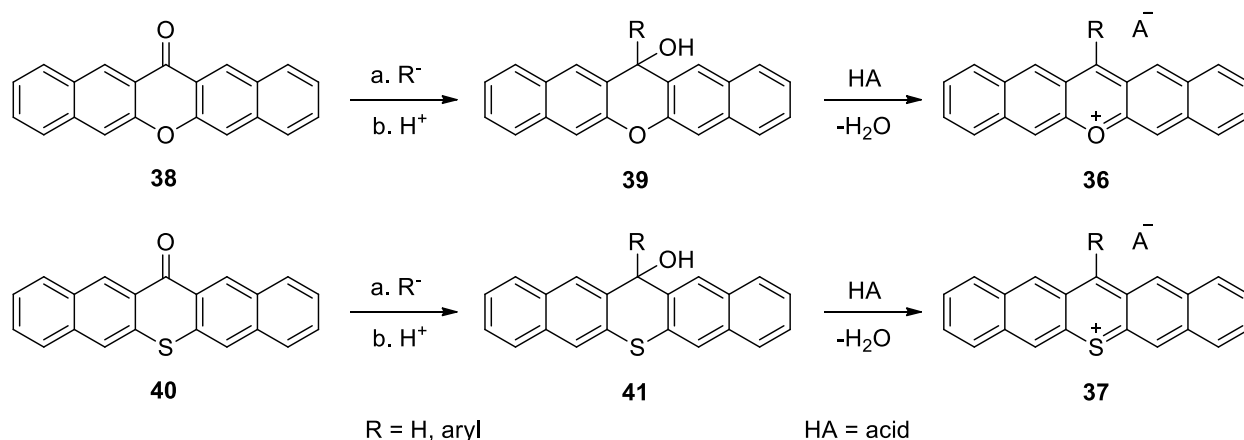
Table 2: Energy calculations for LEPS and LETS compounds with different substituents with B3LYP/6-311+G**//B3LYP-6-31G*.

	Gap (eV)		Gap (eV)
-H	2.14	-H	2.02
Phenyl	2.15	Phenyl	2.00
Mesityl	2.18	Mesityl	2.02
4'-Dimethylaminophenyl	2.20	4'-Dimethylaminophenyl	2.03

2.2.2 General synthetic routes design for LEPS and LETS compounds

In the synthesis of the xanthylium and thioxanthylium salts, commercially available xanthone and thioxanthone were typically utilized as starting materials. Then they were converted to alcohols by hydride reduction or nucleophilic addition at the carbonyl group. Finally, the alcohols were treated with acid to generate the corresponding xanthylium or thioxanthylium cations. For the syntheses of LEPS **36** and LETS **37**, the corresponding dibenzoxanthone **38** and dibenzothioxanthone **40** are important synthetic intermediates, surprisingly, they have never been synthesized before. These two intermediates can be

converted to the corresponding alcohols **39** and **41** using similar methods to those mentioned above for xanthone and thioxanthone. Treating the alcohols with acid could generate the corresponding desired LEPS and LETS compounds (**Scheme 6**).



Scheme 6: General synthetic routes design for LEPS **36** and LETS **37**.

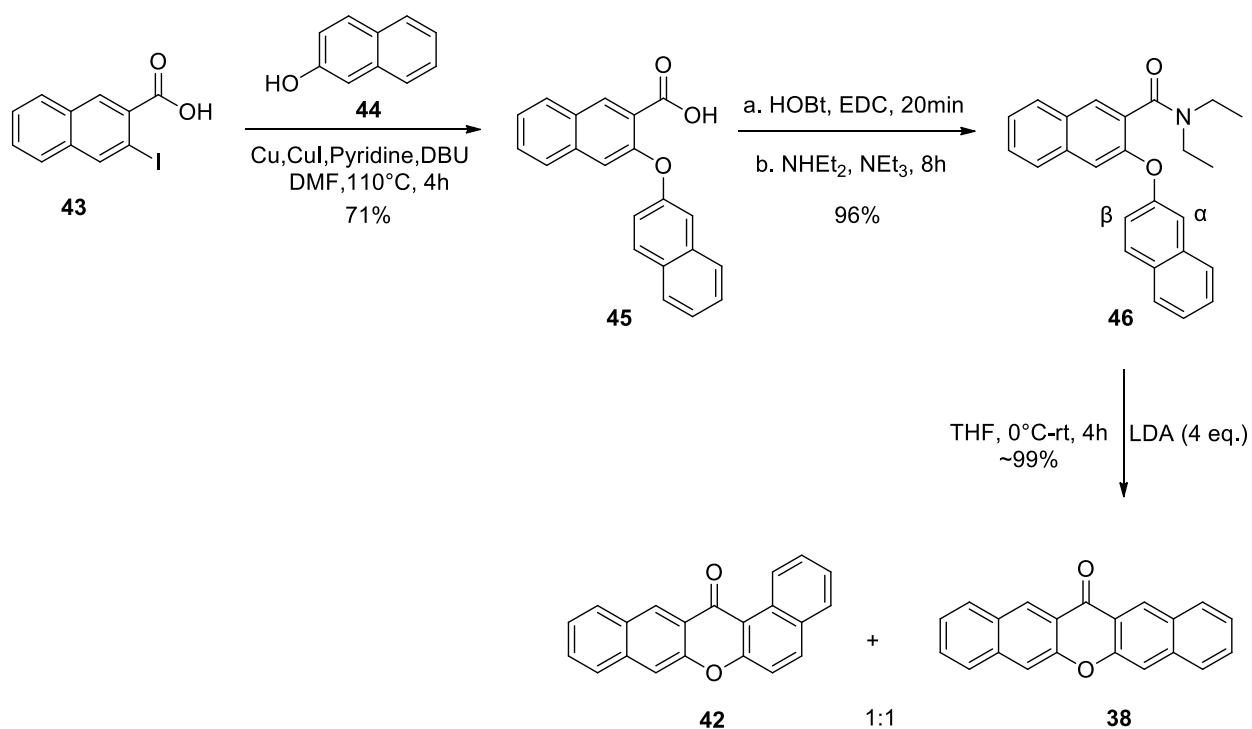
2.2.3 Syntheses and study of dibenzoxanthenes and dibenzothioxanthenes

2.2.3.1 Synthesis of dibenzoxanthone **38**

2.2.3.1.1 Synthesis of **38** through an LDA-mediated ring closure reaction

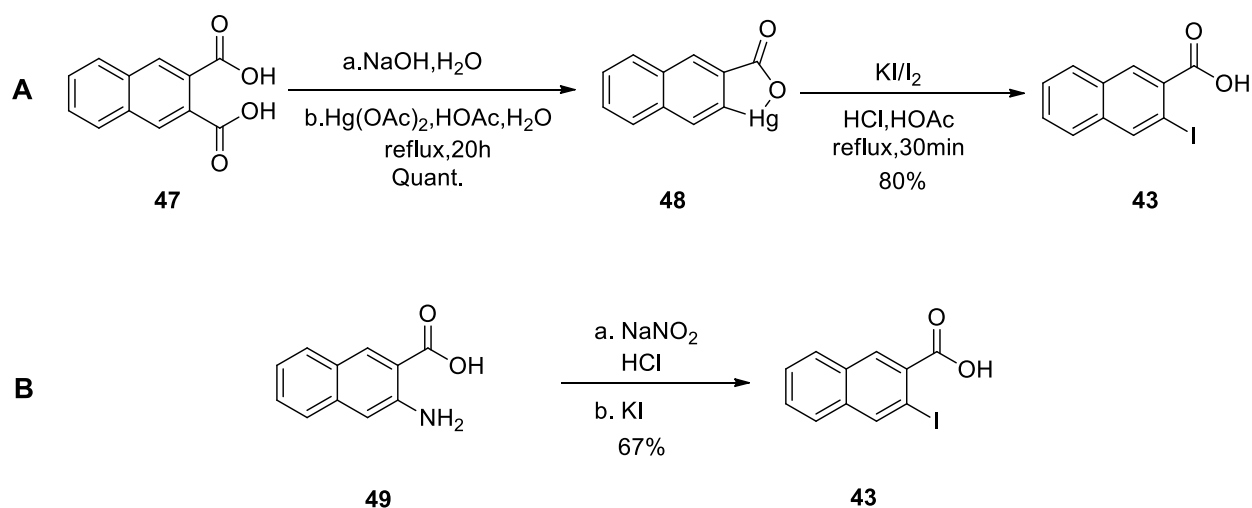
Using 3-iodo-2-naphthoic acid **43** and 2-naphthol **44** as starting materials, an Ullmann coupling reaction generated the corresponding acid intermediate **45** in good yield. This acid intermediate **45** was purified easily by base extraction followed by acidifying the basic solution. Then, the acid **45** was converted to the corresponding activated ester using HOBt. By treating the activated ester with diethylamine and triethylamine, the corresponding diethyl amide **46** was generated in high yield. The amide was subsequently treated with LDA to extract either an alpha or a beta aromatic proton, followed by nucleophilic attack at the carbonyl group to close

the ring. In this step, dibenzoxanthone **38** and its isomer **42** were formed in a 1:1 ratio according to the crude ^1H NMR spectra (**Scheme 7**). The ^1H NMR also showed there were few by-products formed. Due to the poor solubilities and similar polarities of the two ketones, their separation is difficult. Nonetheless, a small amount of mixture was separated using column chromatography with a large column and silica as stationary phase. In this way, pure **38** (35%) and **42** (27%) were isolated. The yield of separated products is low due largely to their poor solubilities in all mobile phase tested. For this reason, the availability of pure **38** was limited. Thus, the mixture of **38** and **42** was used as starting material for the next synthetic step. Subsequent products derived from **38** and **42** are much more soluble and possess more different polarities, enabling their separation. The choice of amide **46** as a precursor to **38** was based upon literature⁴¹ precedent in a similar but not identical reaction, as elaborated below.



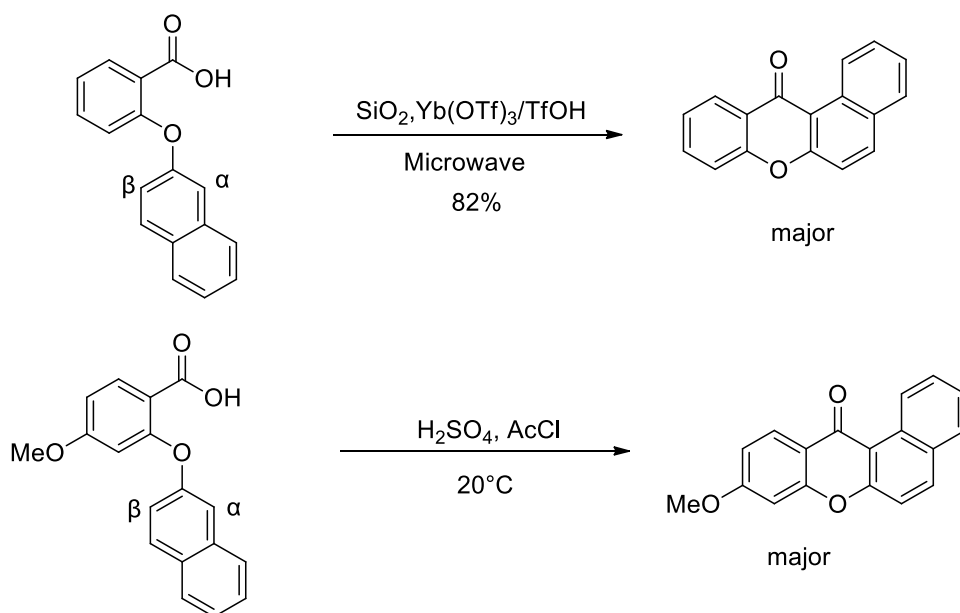
Scheme 7: Synthesis of dibenzoxanthone **38** via an LDA-mediated ring closure.

The synthesis of 3-iodo-2-naphthoic acid **43** can be achieved in two distinct manners. The first is Luis's method that includes the formation of a mercuric intermediate **48** which is itself derived from 2,3-naphthalene dicarboxylic acid **47** (**Scheme 8, Route A**).⁴² The second path to **43** involves a Sandmeyer reaction starting with 3-amino-2-naphthoic acid **49** (**Scheme 8, Route B**).⁴³ Although the first method has an overall higher yield, it is not environment friendly, requires a longer reaction time and more steps. The second method is preferred although the yield is a little bit lower.



Scheme 8: Synthesis of 2-iodonaphthoic acid **43**.

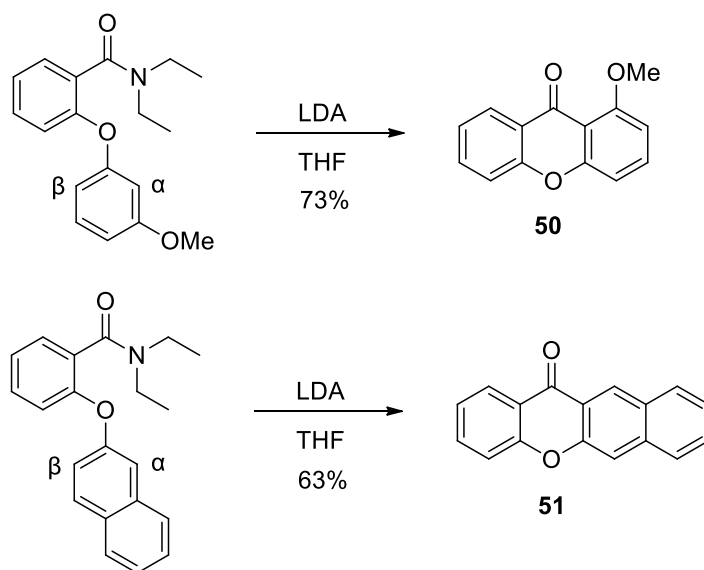
Prior to accomplishing the synthesis of **38** according to **scheme 7**, an alternative method involving Friedel-Crafts acylation/cyclization of **45** was considered. However, literature examples involving similar compounds (**Scheme 9**)⁴⁴ showed that acylation tends to occur more favorably at the undesired α -position of the naphthalene ring rather than the more highly desired β -position, leading to the formation of the major unwanted isomer.



Scheme 9: Formation of xanthone derivatives via Friedel-Crafts acylation/cyclization.⁴⁴

Due to the limitations of the Friedel-Crafts approach, an alternative method needed to be found. In 1997, Familoni and coworkers reported a general regioselective route to substituted and naturally occurring xanthenes (**Scheme 10**).⁴¹ This method utilized an LDA-mediated ring closure reaction that exploited Complex Induced Proximity Effects (CIPE)⁴⁵ and Directed Ortho Metalation (DOM).⁴⁶ During this reaction, LDA first forms a complex with the amide group. It then extracts a proton at the ortho position of the Directed Ortho Metalation Group (DOMG) to form an aromatic anion. DOMG's like $-\text{OR}$, $-\text{NR}_2$, $-\text{Cl}$ can stabilize this ortho aromatic anion. Attack of the anion on the carbonyl group closes the ring. In this way, xanthone **50** was obtained as the major product following α -ortho proton abstraction. Most important for our study, linear xanthone **51** involving β -ortho proton abstraction was selectively formed. A detailed reason for the regioselective cyclization leading to **51** was not provided.⁴¹ Nonetheless, the results were sufficiently compelling to lead us to attempt the synthesis of **38** according to

scheme 7. The lack of selectivity in the formation of **38** (**Scheme 7**) is contrary to expectations⁴¹ and disappointing. Nonetheless, this roadblock did not stall our progress towards LEPS and LETS compounds. We investigated other, potentially more selective routes to **38** (see below) while understanding that the synthesis detailed in **Scheme 7** was manageable.

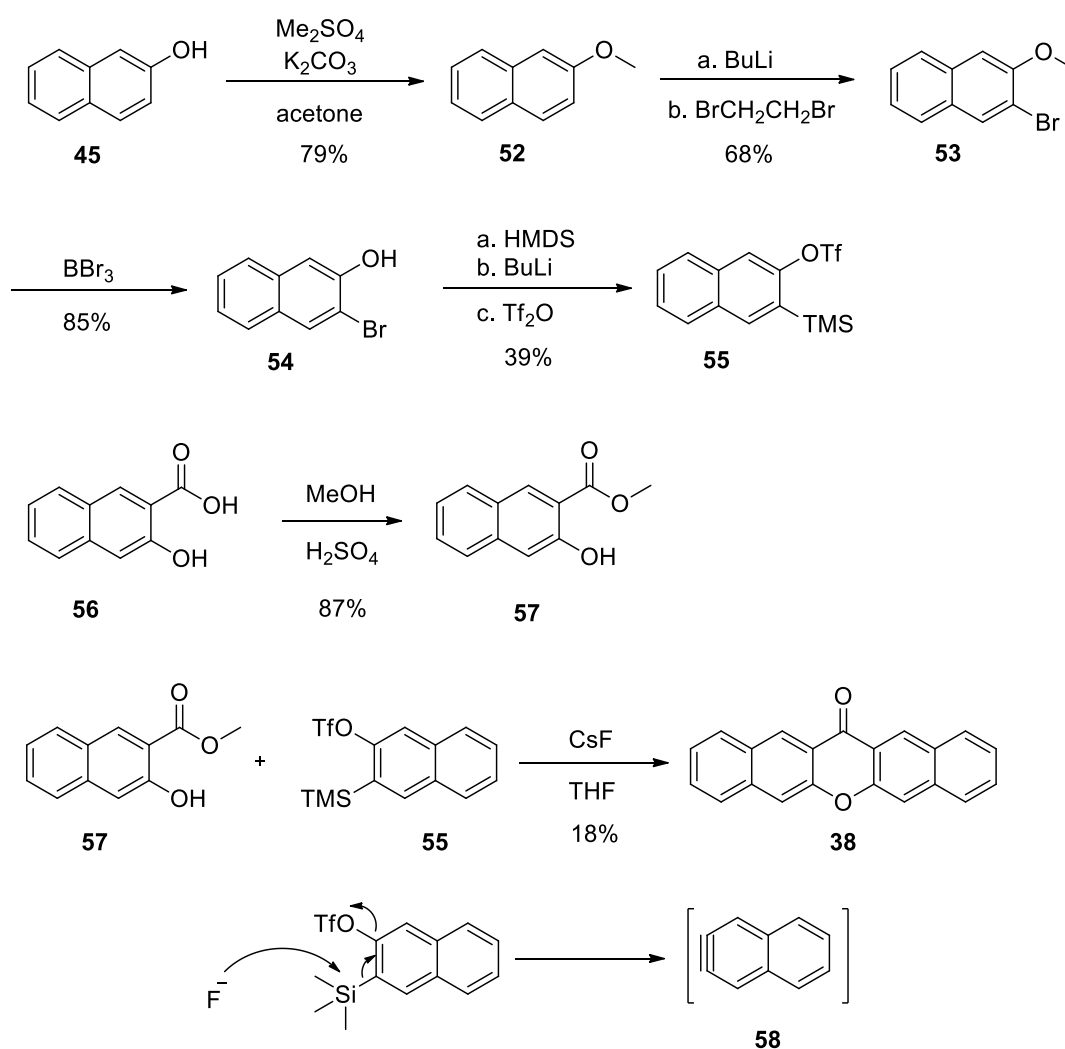


Scheme 10: Selective formation of linear xanthone derivatives via an LDA-mediated ring closure.⁴¹

2.2.3.1.2 Synthesis of **38** through tandem intermolecular nucleophilic coupling involving a naphthalene intermediate

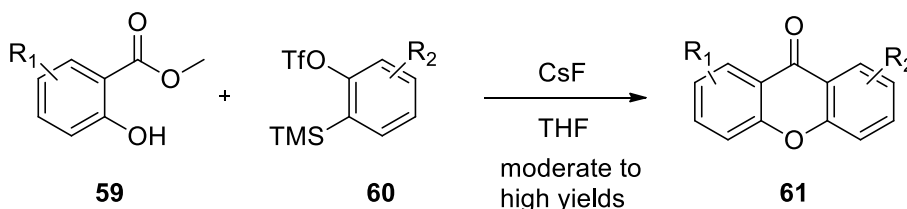
Commercially available 2-naphthol **44** was used as the starting material and converted to the methyl ether **52** to protect the hydroxyl group. Then **52** was treated with *n*-BuLi followed by 1,2-dibromoethane to generate the β -brominated naphthol methyl ether **53** which was easily separated from the α -brominated isomer through recrystallization. Then, **53** was treated with boron tribromide to deprotect the hydroxyl group. The resulting 3-bromo-2-naphthol **54** was converted to the naphthalene precursor **55** by treating with hexamethyldisilazane (HMDS)

followed by *n*-BuLi and then by triflic anhydride. Commercially available 3-hydroxyl-2-naphthoic acid **56** was also used as the starting material. It was converted to the corresponding methyl naphthoate **57** by reacting with methanol under the acidic conditions. In the final tandem intermolecular nucleophilic coupling reaction, cesium fluoride was added to convert the precursor **55** to naphthalene **58** which then coupled with **57** to generate dibenzoxanthone **38** in low yield (**Scheme 11**).



Scheme 11: Synthesis of dibenzoxanthone **38** via tandem intermolecular nucleophilic coupling.

The use of tandem intermolecular nucleophilic coupling to synthesize xanthenes **61** was reported by Zhao⁴⁷ and coworkers in 2007. The reaction of silylbenzyl triflates **60** which are precursors of benzyne, CsF, and 2-hydroxybenzoates **59** generated corresponding xanthenes **61** with moderate to high yields (**Scheme 12**).



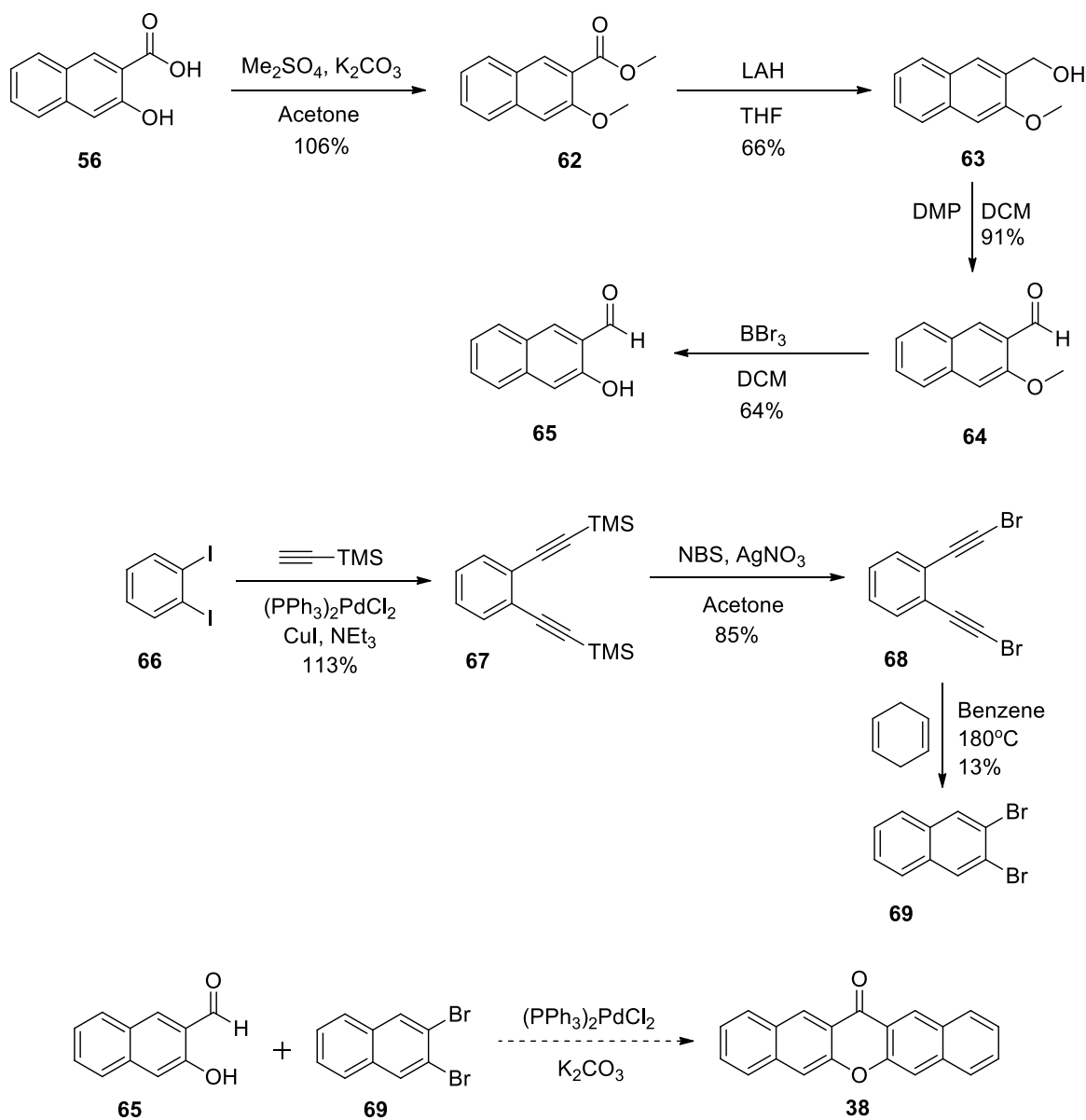
Scheme 12: Formation of xanthenes **61** via tandem intermolecular nucleophilic coupling.⁴⁷

During synthesis of dibenzoxanthone **38**, a naphthalene intermediate was generated instead of benzyne intermediate. The reaction was successful but occurred with a relatively low yield. Although no isomer **42** was generated in this reaction, a lot of byproducts were obtained. Also, there were small amounts of inseparable impurities mixing with dibenzoxanthone **38**.

2.2.3.1.3 Attempted synthesis of **38** through Pd-catalyzed annulation

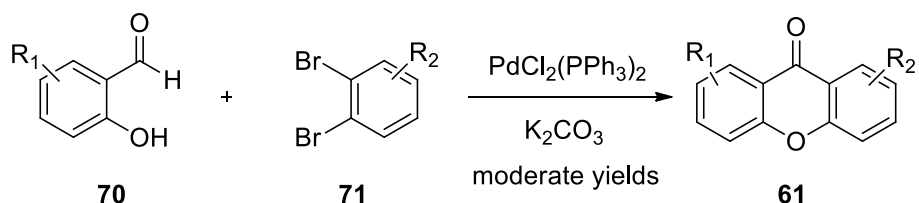
Using 3-Hydroxyl-2-naphthoic acid **56** as starting material, methyl 3-methoxy-2-naphthoate **62** was obtained via reaction with methyl sulfate. Then, the ester group in **62** was reduced by LAH to generate the benzyl alcohol derivative **63** which was oxidized with Dess–Martin periodinane (DMP) to produce benzaldehyde **64**. Compound **64** was deprotected with boron tribromide to yield 3-hydroxy-2-naphthaldehyde **65**. Commercially available 1,2-diodobenzene **66** was also used as starting material and converted to 1,2-bis((trimethylsilyl)ethynyl)benzene **67** after Sonogashira coupling. Terminal bromination of **67**

using NBS yielded 1,2-bis(bromoethynyl)benzene **68** which was converted to 2,3-dibromonaphthalene **69** in low yield via a Bergman cyclization (**Scheme 13**). In the syntheses of **62** and **67**, the greater than 100% yields were due to solvents or grease occluded in the oily products. The low yield of **69** was further complicated by inseparable impurities, hindering the next coupling reaction.



Scheme 13: Attempted synthesis of dibenzoxanthone **38** via a Pd-catalyzed annulation.

A Pd-catalyzed annulation to synthesize xanthenes **61** was reported by Wang⁴⁸ and coworkers in 2009. Dibromobenzenes **71** and salicylaldehydes **70** were coupled under the catalysis of a Pd complex to generate xanthenes **61** with moderate yields (**Scheme 14**).



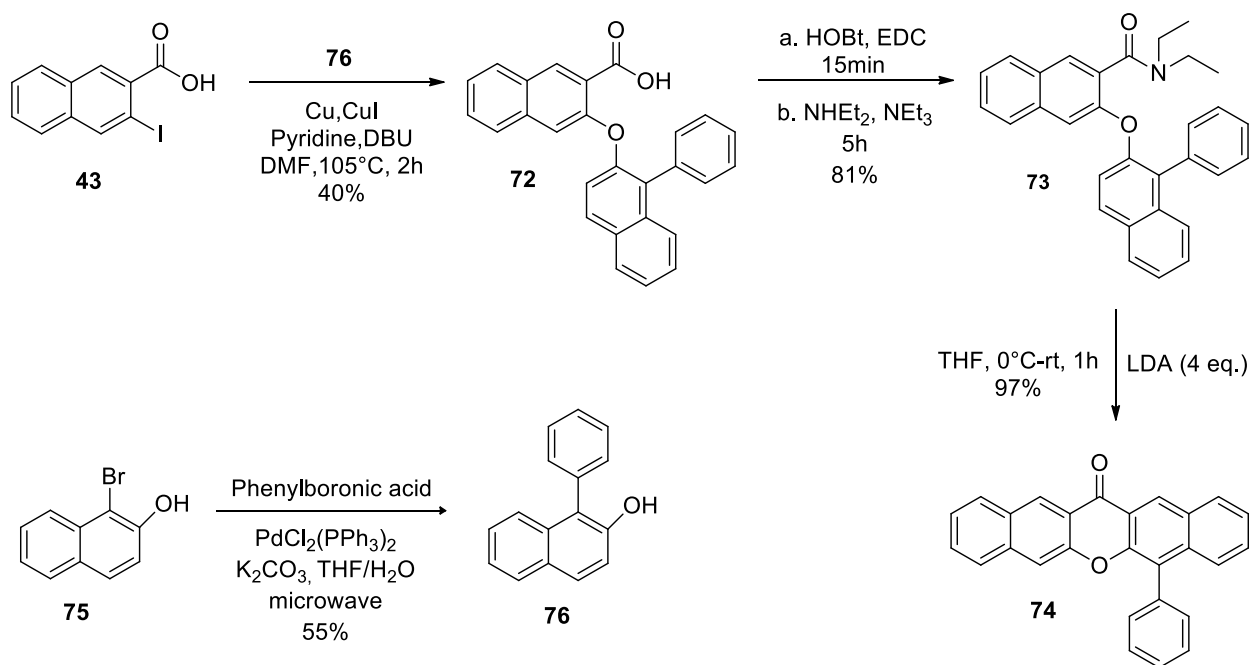
Scheme 14: Formation of xanthenes **61** via Pd-catalyzed annulation.⁴⁸

Compound 1,2-Dibromobenzene is commercially available; however, synthesis of 2,3-dibromonaphthalene **69** requires multiple steps. The Bergman cyclization in **Scheme 13** requires highly deoxygenated reaction conditions with high temperature and pressure.⁴⁹ The low yield of 2,3-dibromonaphthalene **69** and generation of inseparable byproducts may be due to the reaction conditions utilized which may not have complied very well with the required conditions. Meeting the required reaction conditions is necessary and new synthetic routes to **69** are under exploration.

2.2.3.2 Synthesis of dibenzoxanthone **74** via an LDA-mediated ring closure

Due to the issues of forming a hard-to-separate isomer and low yields in the synthesis of dibenzoxanthone **38** using an LDA-mediated ring closure reaction (section **2.2.3.1.1**), dibenzoxanthone **74** was designed and synthesized using an α -phenyl blocked amide intermediate **73**. Under Ullmann coupling reaction conditions, 3-iodo-2-naphthoic acid **43** reacted with 1-phenyl-2-naphthol **76** which was generated in a Suzuki reaction using 1-bromo-2-naphthol **75**. In this way, naphthoic acid intermediate **72** was prepared and converted to the

naphthamide intermediate **73**. Compound **73** was further converted to dibenzoxanthone **74** using an LDA-mediated ring closure reaction (**Scheme 15**). This last reaction occurred in high yield and without formation of additional isomers. The α -phenyl blocking group not only improves selectivity to linear **74** but also improves solubility compared to **38**.

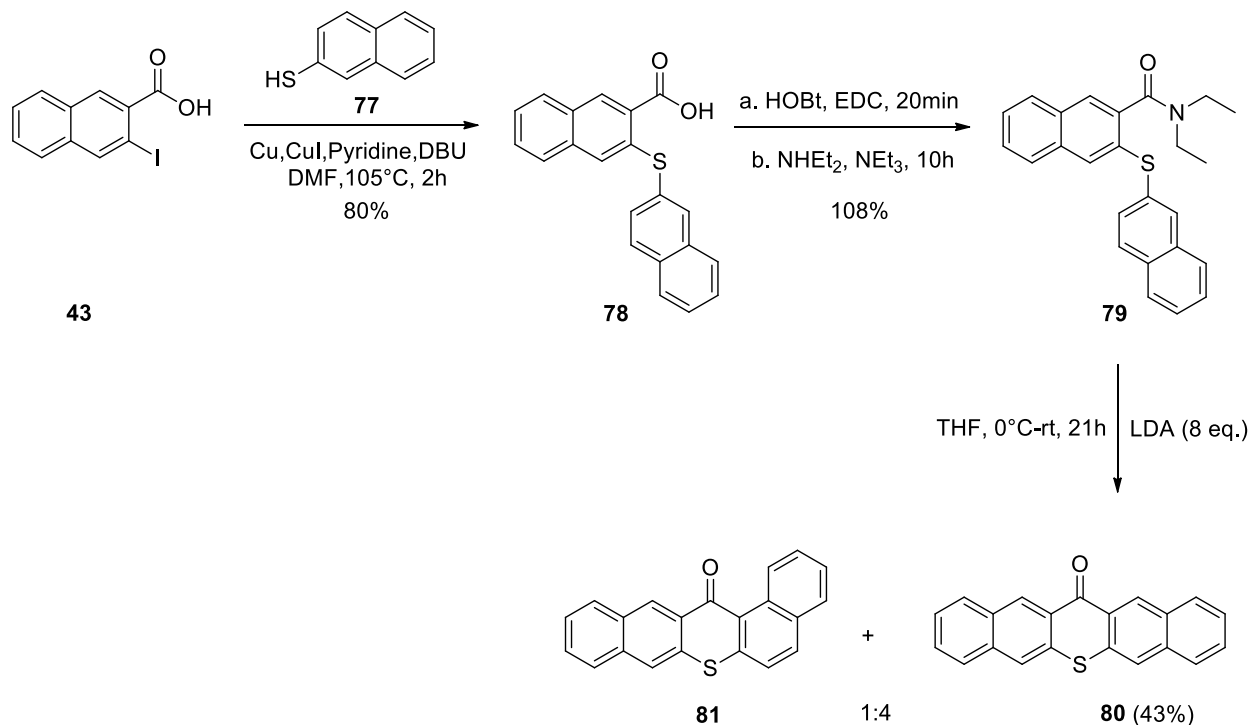


Scheme 15: Synthesis of dibenzoxanthone **74** via a selective LDA-mediated ring closure.

2.2.3.3 Synthesis of dibenzothioxanthone **80** via an LDA-mediated ring closure

The LDA-mediated ring closure to synthesize dibenzothioxanthone **80** is similar to that of dibenzoxanthone **38** which was previously discussed (section 2.2.3.1.1). The 2-Iodo-3-naphthoic acid **43** was used as starting material. Upon performing an Ullmann coupling reaction with 2-thionaphthol **77**, the corresponding acid intermediate **78** was obtained. Then **78** was converted to the corresponding diethyl amide intermediate **79** which was subsequently treated

with LDA to form dibenzothioxanthone **80** and its isomer **81** in a molar ratio of 4:1, respectively (Scheme 16).



Scheme 16: Selective synthesis of dibenzothioxanthone **80** via an LDA-mediated ring closure.

This ratio of **80** and its isomer **81** is quite different from the 1:1 ratio obtained for dibenzoxanthone **38** and its isomer **42**. The ring closing preference may indicate that $-SAr$ stabilizes the anion at the β -position more than the anion at the α -position. Unlike the synthesis of dibenzoxanthone **38** from amide **46** which occurred with little byproduct formation, the synthesis of dibenzothioxanthone **80** from amide **79** occurred with formation of a large amount of byproducts. Although **80** and its isomer **81** have similar polarities, their solubilities are quite different. Compound **80** shows very poor solubility in organic solvents like DCM while isomer **81** shows moderate to good solubility. With this difference, pure **80** was readily obtained by washing the crude reaction mixture with DCM.

2.2.3.4 Optical characteristics of dibenzoxanthenes and dibenzothioxanthenes

Dibenzoxanthone **38** and its isomer **42**, 5-phenyl dibenzoxanthone **74**, dibenzothioxanthone **80** and its isomer **81** are pale yellow to yellow solids. They show broad and strong UV-Vis absorptions due to their extended conjugation.

The UV-Vis absorptions for dibenzoxanthone **38** and 5-phenyl dibenzoxanthone **74** are quite similar with **74** only slightly red-shifted indicating that the extra phenyl substituent in **74** is not strongly conjugated to the dibenzoxanthone π -system. This means the phenyl substituent is far from co-planarity with the dibenzoxanthone backbone, which is due to the steric repulsion between the protons of the phenyl substituent and the backbone. The UV-Vis absorptions for dibenzothioxanthone **80**, on the other hand, are red-shifted compared to these of dibenzoxanthenes **38** and **74**, especially in the visible region (**Figure 10**). This implies more extensive conjugation and the increased significance of a pentacene-like resonance form for **80**. Similarly, thiopyrylium cation **22** shows greater aromaticity than pyrylium cation **21** as previously discussed.^{30b}

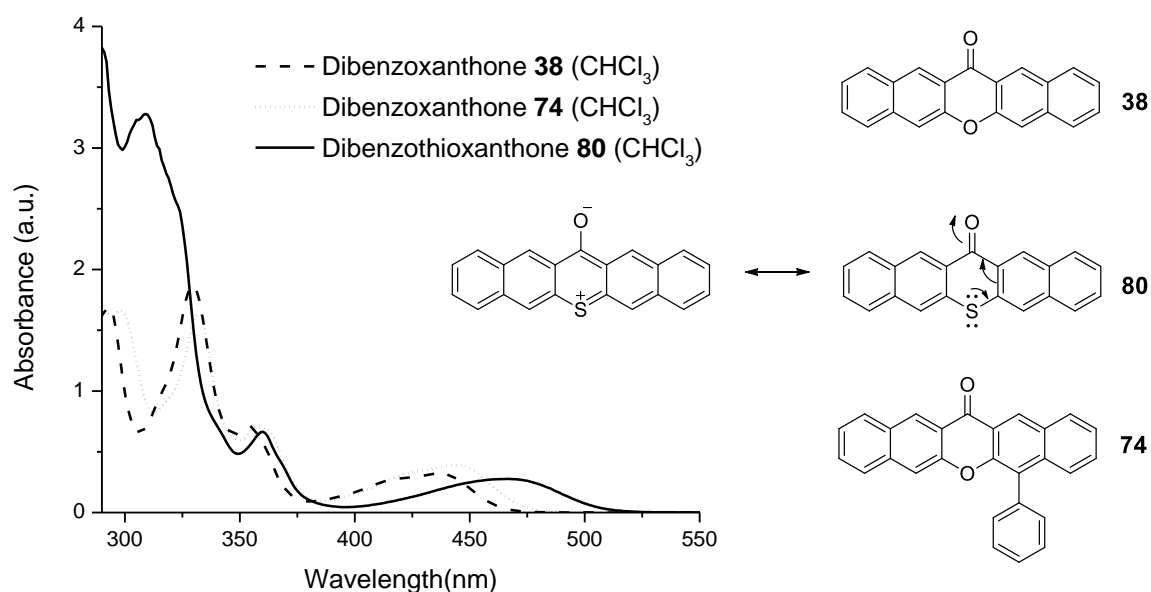


Figure 10: UV-Vis absorption spectra for dibenzoxanthones **38** and **74**, and dibenzothioxanthone **80**.

The UV-Vis absorption patterns for dibenzoxanthone **38** and its isomer **42** are quite different from one another, suggesting large difference in conjugation. Linear **38** has red-shifted absorptions compared to **42** (**Figure 11**), just as linear pentacene is red-shifted compared to any of its bent 5-ring isomers. The similar phenomenon was also observed between linear dibenzothioxanthone **80** and its bent isomer **81**.

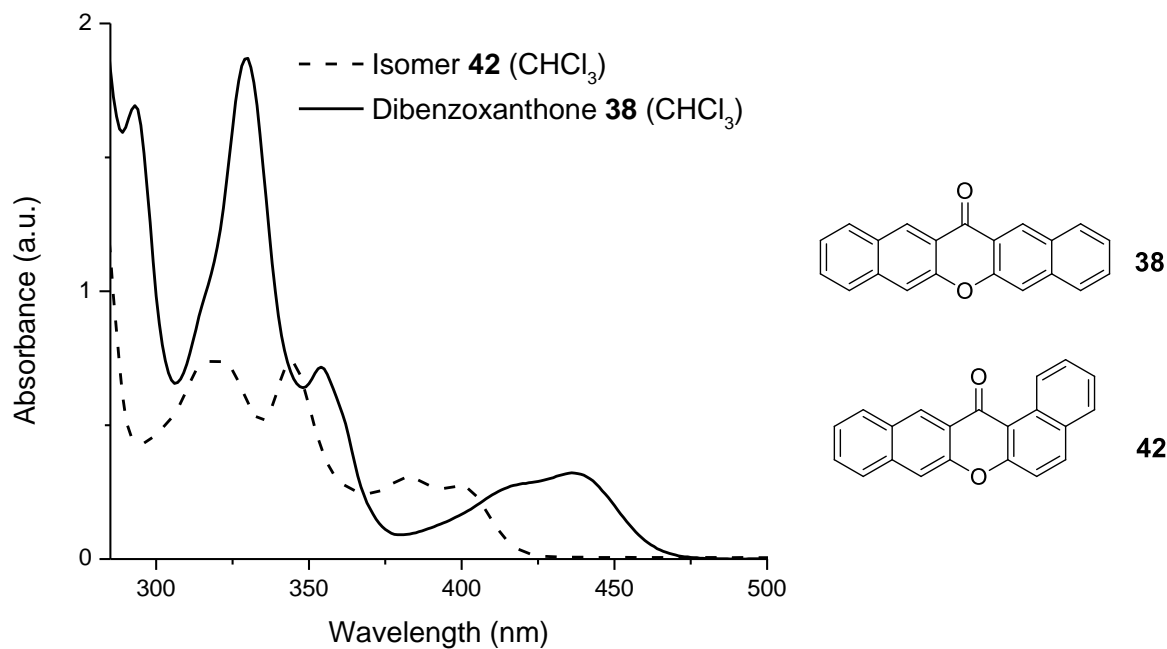
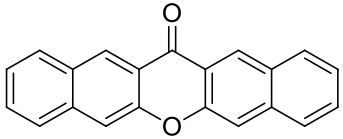
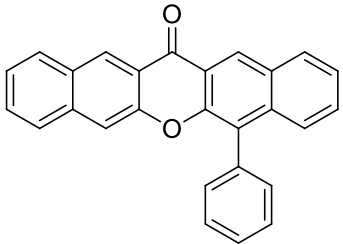
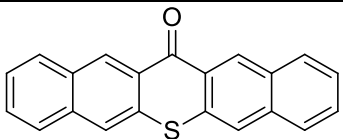
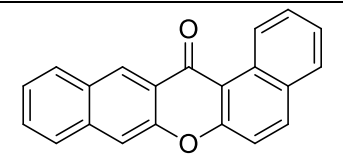
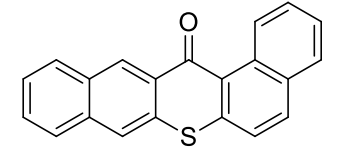


Figure 11: UV-Vis absorption spectra for dibenzoxanthenes **38** and **42** at 8.1×10^{-5} M in CHCl_3 .

Dibenzoanthrone and dibenzothioxanthone compounds all show broad and strong fluorescence emissions with Stokes shifts. Linear dibenzoxanthone **38** and **74** show longer wavelength emissions compared to the less conjugated **42**. Likewise, linear dibenzothioxanthone **80** shows a longer wavelength emission than that of bent isomer **81**. (Table 3).

Table 3: UV-Vis absorptions and emissions of dibenzoxanthenes and dibenzothioxanthenes in CHCl₃.

Structure	No.	Absorption (nm)	Emission (nm)	Fluorescence color
	38	330 354 436	476	Blue
	74	332 358 445	491	Greenish blue
	80	467 360	529	Green
	42	318 344 383 399	429	Purple
	81	334 350 432	466	Blue

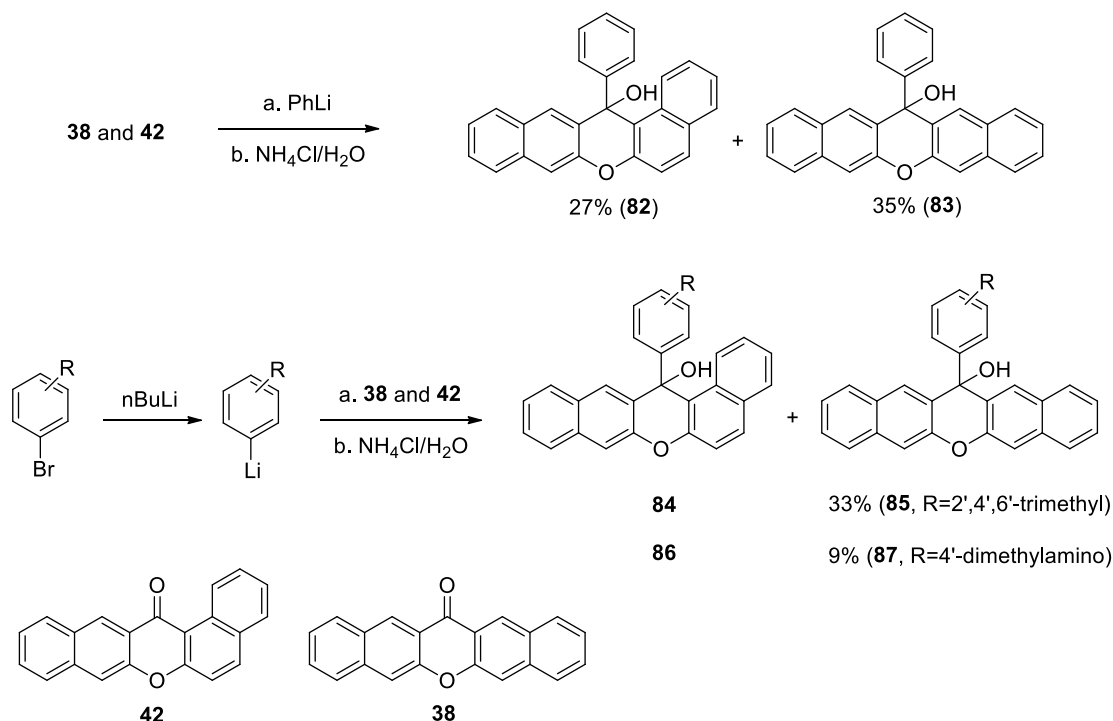
2.2.4 Syntheses of dibenzoxanthenols and dibenzothioxanthenols

2.2.4.1 Syntheses of aryl substituted dibenzoxanthenols and dibenzothioxanthenols

Aryl substituted dibenzoxanthenols and dibenzothioxanthenols are precursors for the corresponding LEPS and LETS compounds, respectively. In order to convert dibenzoxanthone and dibenzothioxanthone to these dibenzoxanthenols and dibenzothioxanthenols, respectively,

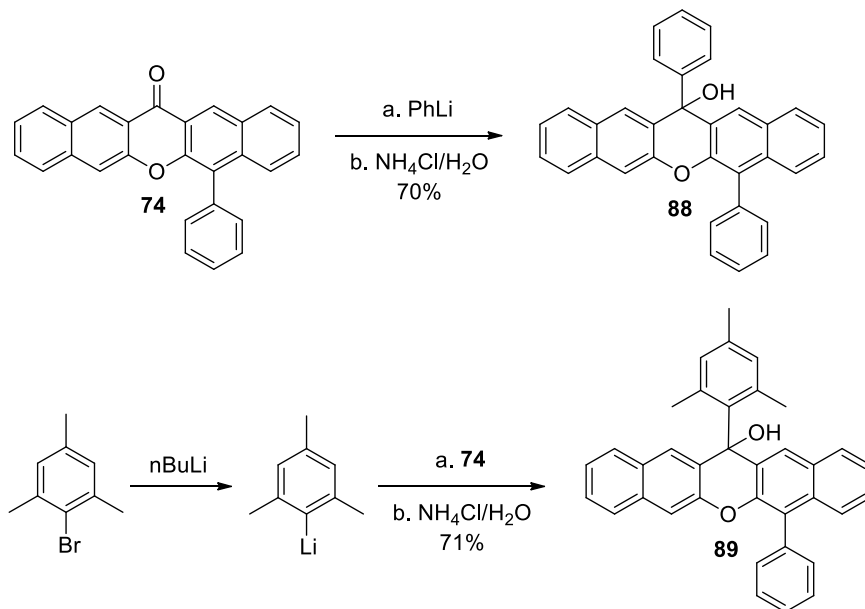
aryllithium reagents were used for nucleophilic attack at the carbonyl groups (**Scheme 17**). Except for the commercially available phenyllithium, other aryllithium reagents were prepared using halogen-lithium exchange reactions between *n*-butyllithium and the corresponding aryl bromide.

For the syntheses of aryl substituted dibenzoxanthenols, the mixture of dibenzoxanthone **38** and its isomer **42** were used as starting materials due to their difficult separation. The alcohol products show good solubility and are easily separable. The yields presented below were calculated based on the starting mixture (**Scheme 17**). The low yield for **87** is due to a low yielding halogen-lithium exchange reaction involving 4-dimethylamino phenyl bromide.



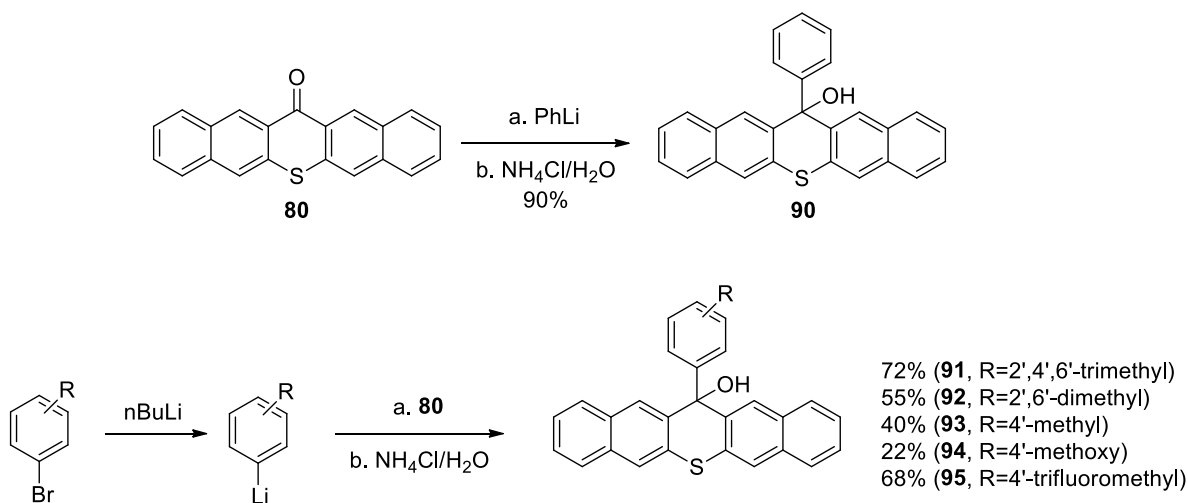
Scheme 17: Syntheses of aryl substituted dibenzoxanthenols **82-87**.

By treating dibenzoxanthone **74** with aryllithium reagents, the corresponding aryl substituted dibenzoxanthenol **88** and **89** were also obtained with high yields (**Scheme 18**).



Scheme 18: Syntheses of aryl substituted dibenzoxanthenols **88** and **89**.

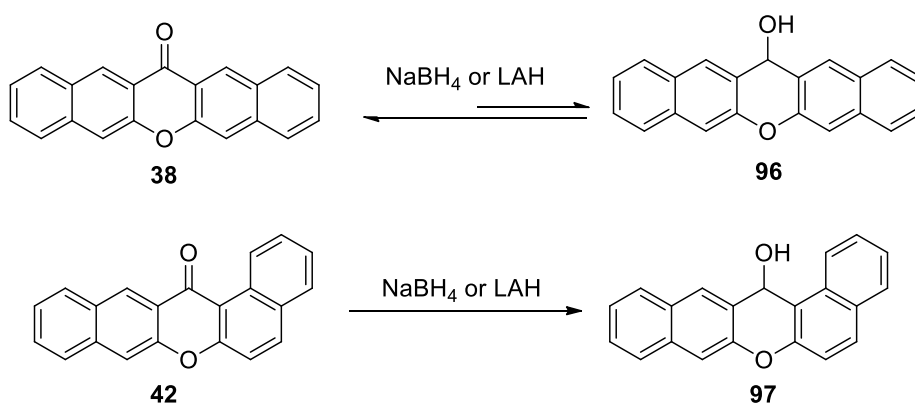
Also, reaction between dibenzothioxanthone **80** and aryllithium reagents generated aryl substituted dibenzothioxanthenols **90-95** in moderate to high yields (**Scheme 19**).



Scheme 19: Syntheses of aryl substituted dibenzothioxanthenols **90-95**.

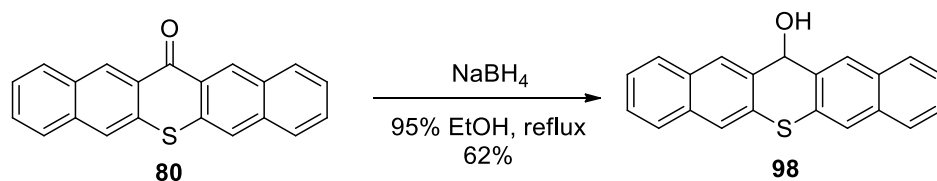
2.2.4.2 Syntheses of unsubstituted dibenzoxanthenol and dibenzothioxanthenol

Dibenzoxanthenol **96** is the precursor for an unsubstituted LEPS compound. By reducing dibenzoxanthone **38** with a hydride reagent like sodium borohydride or lithium aluminum hydride, dibenzoxanthenol **96** was generated. Unlike the relatively stable dibenzoxanthenol **97** derived from its isomer **42**, dibenzoxanthenol **96** was readily oxidized back to **38** and the two compounds exhibit similar solubility, making their separation difficult (**Scheme 20**).



Scheme 20: Reduction of dibenzoxanthone **38** and its isomer **42** using hydride reagents.

Unlike the reduction of **38**, reduction of dibenzothioxanthone **80** yielded stable dibenzothioxanthenol **98** in moderate yield (**Scheme 21**), a precursor to an unsubstituted LETS compound. Compound **98** is more soluble than **96** and does not easily reoxidize under ambient conditions. Pure **98** was obtained by precipitation upon adding water to the reaction mixture.



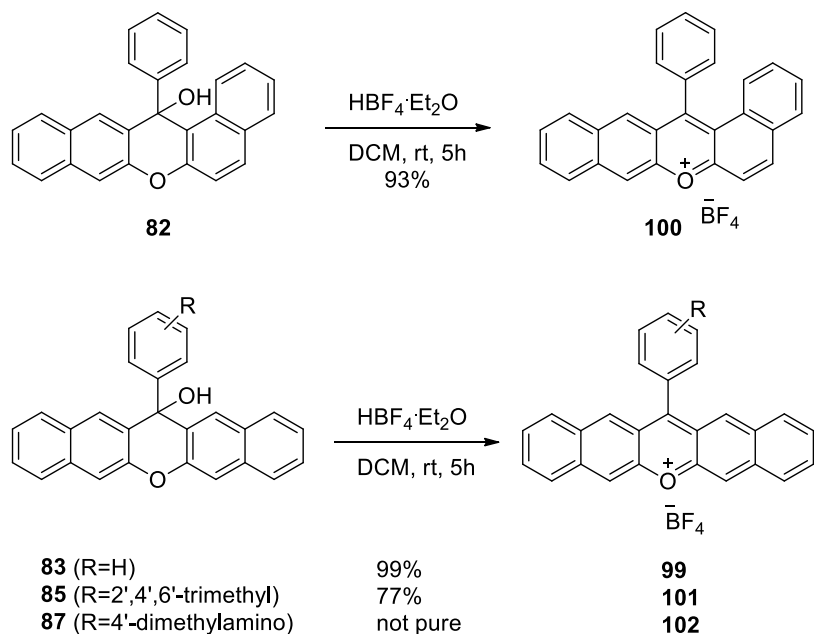
Scheme 21: Reduction of dibenzothioxanthone **80** using sodium borohydride.

2.2.5 Syntheses and study of LEPS and LETS compounds

2.2.5.1 Syntheses of LEPS and LETS compounds

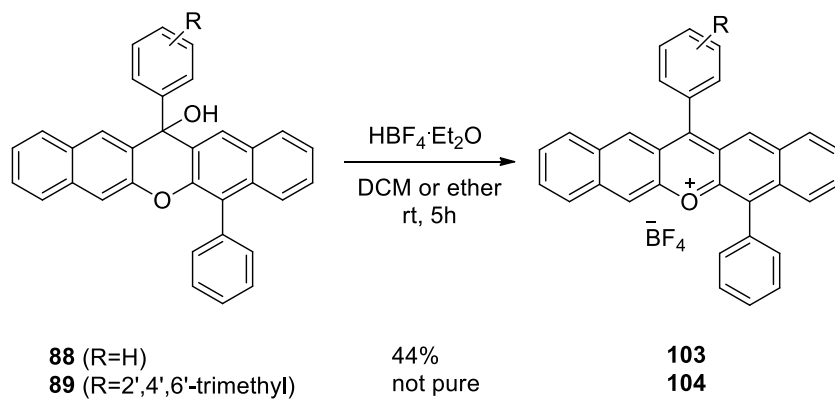
Using a similar method as that in the syntheses of xanthylum and thioxanthylum salts, dibenzoxanthenols and dibenzothioxanthenols were treated with acid to generate the corresponding LEPS and LETS compounds in good to excellent yields in all but one case. Non-oxidative fluoroboric acid⁵⁰ was used instead of the oxidizing perchloric acid.

The dibenzoxanthenols **82**, **83**, **85** and **87**, derived from dibenzoxanthone **38** and its isomer **42**, were successfully converted to the corresponding LEPS compounds **100**, **99**, **101**, and **102** respectively. LEPS **99** and its isomer **100** were both obtained in high yields. LEPS **99** was formed in the presence of only a little hydrolyzed impurity **83** while LEPS **100** showed even less (trace) **82**. LEPS **101** was also obtained in high yield with no detectable hydrolyzed impurity **85**. LEPS **102** is formed with a large percentage of hydrolyzed impurity **87** (**Scheme 22**). The facile hydrolysis of LEPS **102** bearing a 4'-dimethylamino substituent lends evidence that 13-phenyl substituents on LEPS and LETS compounds do not sit co-planar or even near co-planar with the acene-like backbone. If there was co-planarity or nearly co-planarity, then we would expect that the electron releasing resonance effect associated with amino substituents would stabilize LEPS **102** rendering it more difficult to hydrolyze than, for example, LEPS **99**. Since LEPS **102** is more easily hydrolyzed than LEPS **99**, it appears that an inductive effect may be destabilizing **102**.



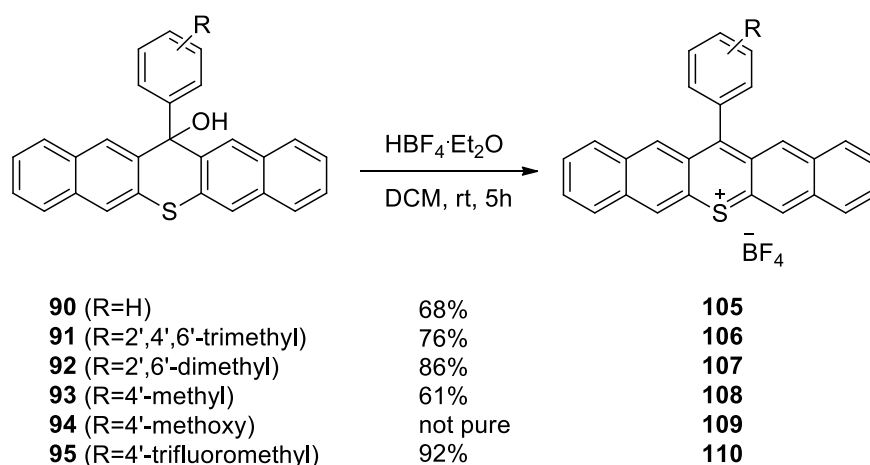
Scheme 22: Syntheses of LEPS **99** and its isomer **100**, LEPS **101**, LEPS **102**.

Also, dibenzoxanthenols **88** and **89** derived from 5-phenyl dibenzoxanthone **74** were successfully converted to the corresponding LEPS compounds. LEPS **103** was obtained in moderate yield in the presence of a little bit of hydrolyzed impurity **88**. LEPS **104** was formed in good yield but could not be purified using a precipitation method due to its excellent solubility (Scheme 23).



Scheme 23: Syntheses of LEPS **103** and LEPS **104**.

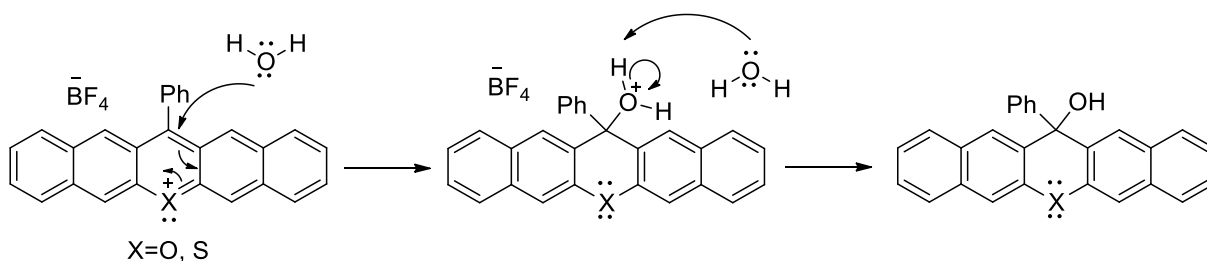
Dibenzothioxanthenols **90-95** derived from dibenzothioxanthone **80** were successfully converted to the corresponding LETS compounds in moderate to high yields. A small amount of hydrolyzed impurity was found in LETS **105**, LETS **108** and LETS **110** while a moderate amount of hydrolyzed impurity was found in LETS **109**. No hydrolyzed impurity was observed in LETS **106** and LETS **107** (**Scheme 24**). Dibenzothioxanthanol **98** was also converted to the corresponding unsubstituted LETS compound. However, it is highly unstable and easily decomposed under ambient condition.



Scheme 24: Syntheses of LETS compounds (**105-110**).

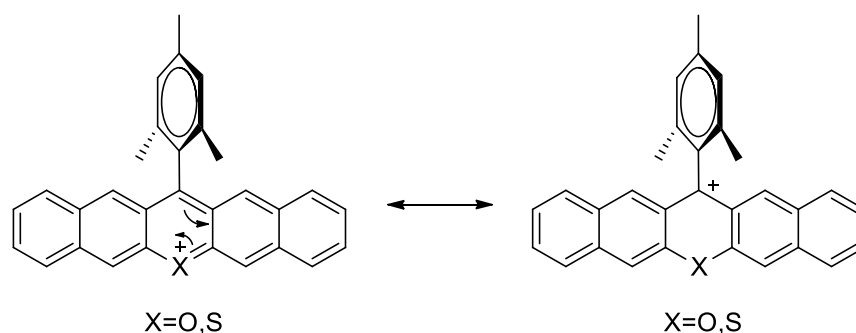
2.2.5.2 Moisture resistance study of LEPS and LETS compounds

As noted above, positively charged LEPS and LETS compounds are susceptible to nucleophilic attack by water. Upon reacting with water, LEPS and LETS compounds convert back to their starting alcohols (**Scheme 25**). The reaction is completely reversible with the position of the equilibrium depending upon the acidity and water content of the solvent. Thus, once formed, LEPS and LETS compounds should be kept dry.



Scheme 25: Nucleophilic attack of water on LEPS and LETS compounds.

Mesityl substituted LEPS **101**, LEPS **104**, LETS **106** and 2',6'-dimethylphenyl substituted LETS **107** show much greater moisture resistance compared to other LEPS and LETS compounds. No hydrolyzed impurity was observed by NMR for these compounds. Likewise, their colors persisted even in aqueous acetone while the color of other LEPS and LETS compounds disappeared quickly under similar conditions. Thus, the *o*-methyl groups on the phenyl substituent at C-13 effectively shield C-13, the otherwise most reactive carbon, from nucleophiles like water (**Scheme 26**). Clearly, the phenyl substituent at C-13 cannot lie planar to the LEPS and LETS backbones due to steric crowding of the methyl groups and aromatic hydrogens. Instead, a nearly orthogonal orientation is preferred. This explanation was further supported by high-level geometry calculations and single crystal structure studies.



Scheme 26: *o*-Methyl groups on mesityl substituent shield the otherwise reactive C-13 of the LEPS and LETS backbones.

2.2.5.3 Solubilities of LEPS and LETS compounds

All of the LEPS and LETS compounds synthesized above are soluble in organic solvents like acetonitrile and dichloromethane. Most are not soluble in ether and this was utilized for isolation. Thus, the slow diffusion of ether into reaction mixtures in DCM enabled precipitation of pure LEPS and LETS compounds. Structurally similar LEPS and LETS compounds possessing the same substituent show similar solubilities indicating that the choice of heteroatom (O vs. S) has little impact on the solubility. However, the number and types of substituents are key factors for solubility. Additional substituents seem to lead to better solubility. For example, LEPS **103** has better solubility than LEPS **99** while LEPS **104** has better solubility than LEPS **101**. Also, the presence of three additional aliphatic methyl groups renders the mesityl substituted LEPS and LETS compounds more soluble than simpler phenyl substituted structures. For example, LEPS **101** is more soluble than LEPS **99** while LEPS **104** is more soluble than LEPS **103** (**Figure 12**). Thus placement of a mesityl group at C-13 of LEPS and LETS compounds is beneficial in two distinct manners. The mesityl groups retard the addition of water (greater moisture resistance) while simultaneously improving solubility. The relatively low yield for LEPS **103** compared to LEPS **99** and LEPS **101** is due to its comparatively strong solubility in DCM. That is, ether diffusion into a solution of **103** in DCM does not effectively precipitate all of the **103**. The problem is even worse for LEPS **104** which shows the greatest solubility of all LEPS and LETS compounds. LEPS **104** is fully soluble in ether but insoluble in hexanes. A hexanes diffusion into a solution of **104** in ether leads to the complete precipitation of **104** but also a number of impurities. A method has yet to be developed to isolate highly soluble, relative stable LEPS **104**.

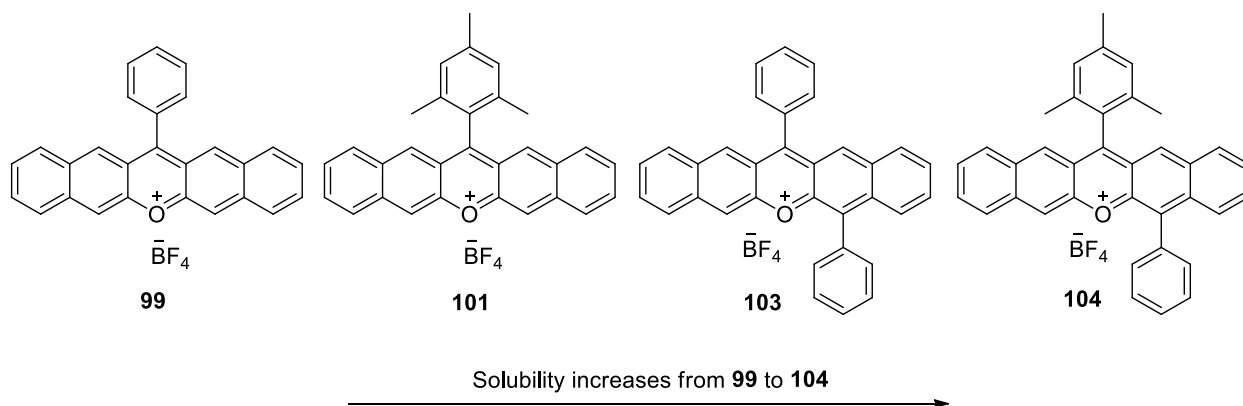


Figure 12: Solubility order for LEPS compounds with different substituents.

2.2.5.4 Charge delocalization of LEPS and LETS compounds

The positive charge in the π -system of LEPS and LETS compounds is delocalized and can be studied by examining the NMR chemical shifts. The chemical shifts of the aromatic protons are downfield compared to those in the starting alcohols. LEPS **99** has chemical shifts for aromatic protons between 7.7 and 9.0 ppm while its alcohol precursor **83** has the chemical shifts for aromatic protons between 7.1 and 8.2 ppm. For example, the chemical shifts for the two singlets of LEPS **99**, corresponding to the aromatic protons on the penultimate rings, shift about 1 ppm downfield compared to alcohol **83** (**Figure 13**). The delocalization of positive charge produces a highly electron-deficient π -system consistent with that desired for an n-type organic semiconductor.

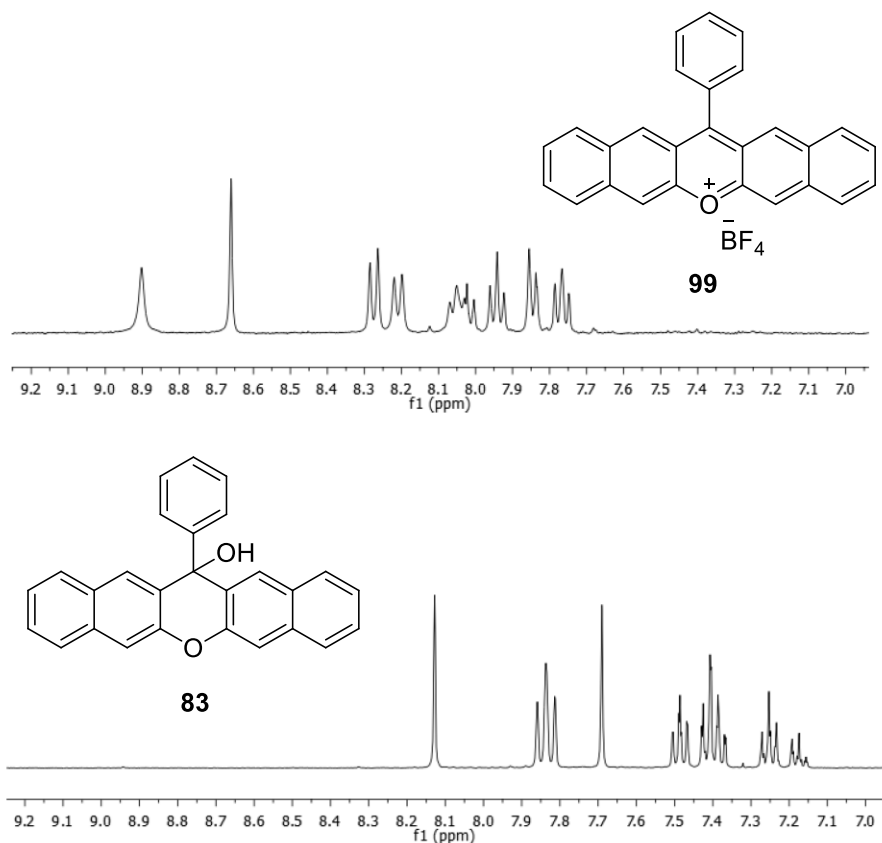


Figure 13: ^1H NMR spectra in aromatic region for LEPS **99** and its precursor **83** both in CD_2Cl_2 .

2.2.5.5 Optical properties of LEPS and LETS compounds

LEPS and LETS compounds have dark purple to black colors in the solid state and form dark red solutions upon addition of appropriate solvent. Due to the highly conjugated structures, they have a wide range of absorptions in the UV-Vis-NIR region. There are several strong absorption bands in the UV-Vis region as well as several broad and weak bands starting at about 600 nm and extending into the near-IR region. Linear LEPS **99** has red-shifted absorption bands compared to its isomer **100**, which is consistent with trends observed for linear acenes compared to their phene-like isomers (**Figure 14**). Based upon the absorption

bands at 555 and 500 nm, respectively, the optical HOMO-LUMO gap for LEPS **99** is approximately 2.1 eV while the same gap for phene-like isomer **100** is approximately 2.3 eV.

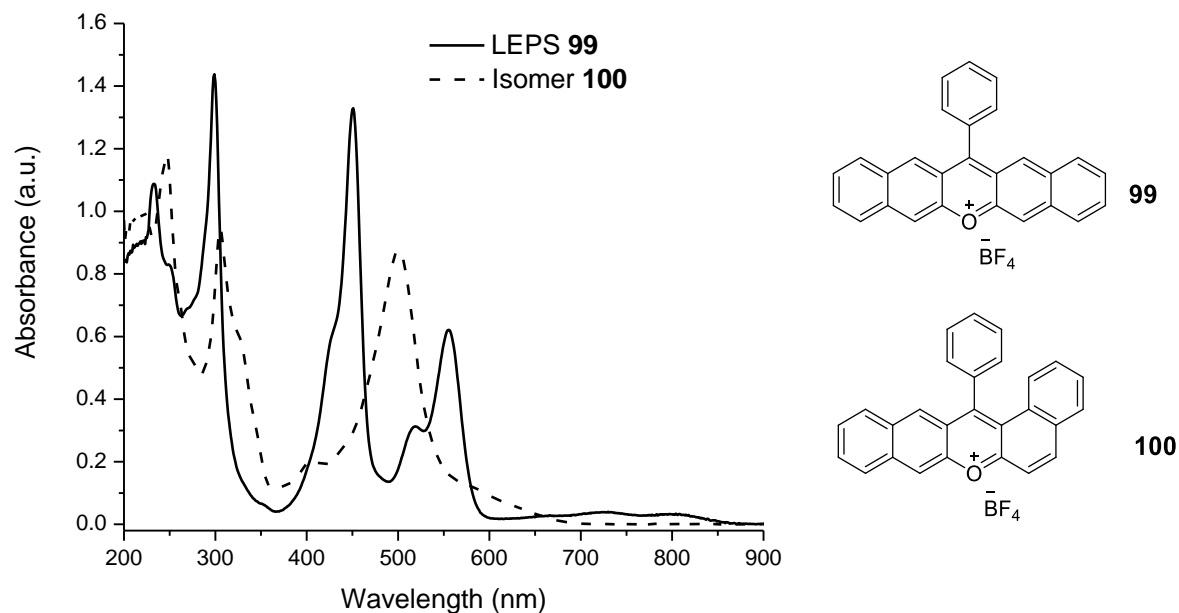


Figure 14: UV-Vis-NIR absorption spectra of 3.4×10^{-5} M solutions of linear LEPS **99** and its phene-like isomer **100** in DCM.

Although LEPS **99** and LETS **105** have different heteroatoms in their backbones, their absorption patterns are quite similar in the UV-Vis region with the band at approximately 300 nm red-shifted for LETS **105**. They both have broad and weak absorption bands that extend into the near-IR region. The longest wavelength band for LETS **105** centered at 916 nm is significantly red-shifted compared to the longest wavelength band for LEPS **99** centered at 804 nm (**Figure 15**). Based on the strong bands at approximately 550 nm, the optical HOMO-LUMO gaps for LETS **105** and LEPS **99** are approximately 2.1 eV, very close to the gap reported for pentacene, 2.08 eV¹⁹.

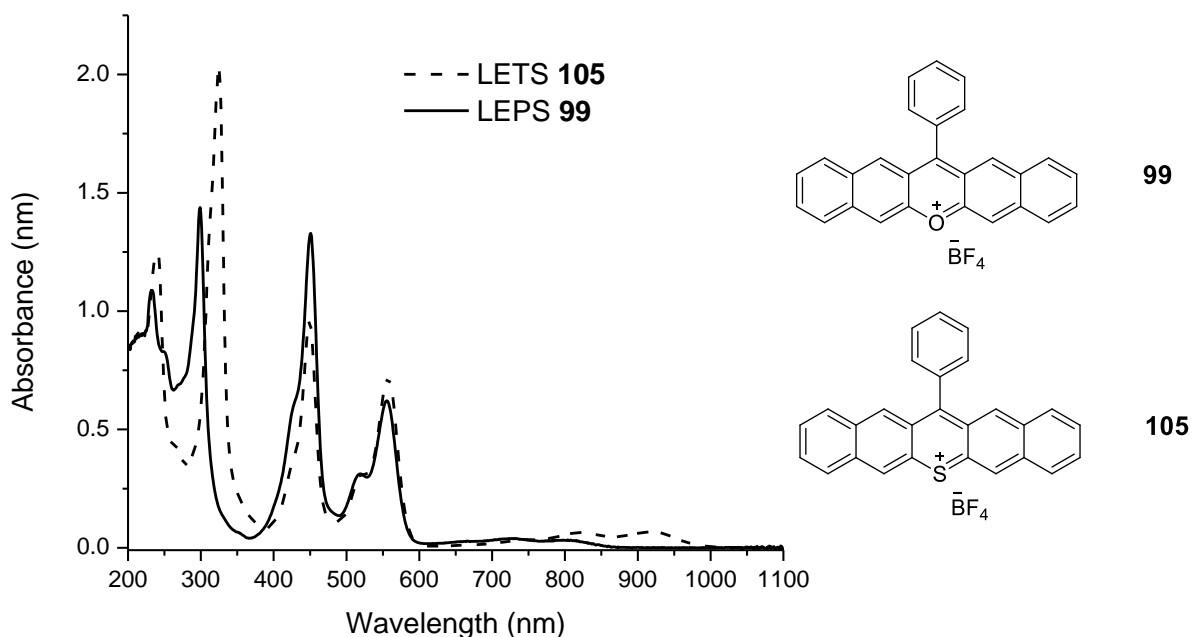


Figure 15: UV-Vis-NIR absorption spectra of 3.4×10^{-5} M solutions of LEPS **99** and LETS **105** in DCM.

Placement of phenyl substituents on either LEPS or LETS compounds has little effect on their UV-Vis-NIR absorptions. LEPS **99** with a phenyl substituent at C-13 and LEPS **101** with a mesityl substituent at C-13 have nearly the same UV-Vis-NIR absorption values. Compared to LEPS **99** with one phenyl substituent at C-13, LEPS **103** with two phenyl substituents at C-5 and C-13 has only a slightly red-shifted set of UV-Vis-NIR absorptions. Similarly, the UV-Vis absorption bands observed for LETS compounds were all but identical regardless of the substituents (**Figure 16**). Thus, we concluded that the phenyl substituents on LEPS and LETS compounds sit far from co-planar to the backbone such that they contribute little to the conjugation. These conclusions are consistent with those derived from the computational geometry optimizations for LEPS and LETS compounds.

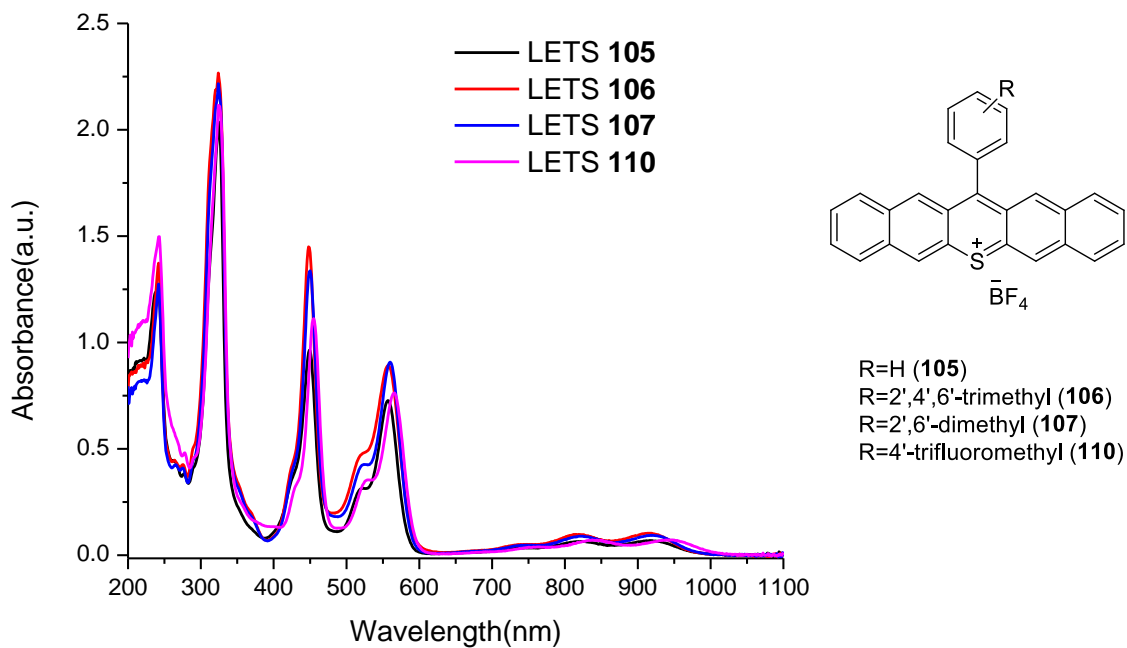
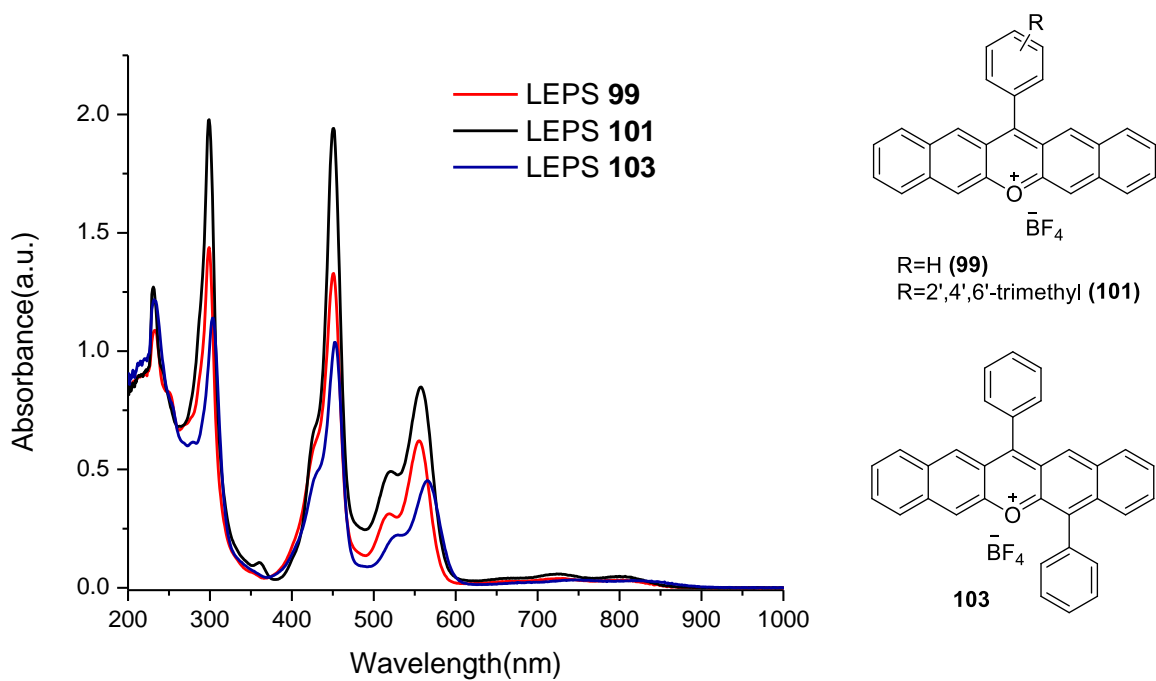


Figure 16: UV-Vis-NIR absorptions of 3.4×10^{-5} M solutions of LEPS and LETS compounds in DCM.

Unlike xanthylium and thioxanthylium compounds which have strong fluorescence, the fluorescence of LEPS and LETS compounds was not observed when exposed to UV light (254 nm, 302 nm, 365 nm) nor detected using a Cary 50 eclipse fluorometer with an effective detection range between 200 and 900 nm. Since LEPS and LETS compounds have absorptions that extended to the near-IR region, it is possible that they do fluoresce at longer wavelengths with significant Stokes shifts.

2.2.5.6 Single crystal X-ray diffraction study of LEPS and LETS compounds

Shiny, purple crystals of LEPS and LETS compounds were grown via the vapor diffusion method. Weak solvents, benzene or ether, were diffused into solutions containing the LEPS or LETS compound dissolved in a strong solvent, either acetonitrile or dichloromethane. The structures of LEPS **99** and its isomer **100**, LEPS **101**, LEPS **103**, LETS **105** and LETS **106** were all successfully characterized using single crystal X-ray diffraction. The backbone of bent LEPS isomer **100** is distorted from planarity due to the steric compression between the phenyl substituent and the benzo group of the backbone. Linear LEPS **99** and LETS **105** with one phenyl substituent each, have slightly more planar backbones compared to LEPS **101** and LETS **106** both of which include a mesityl substituent. This could be due to the steric repulsion between the backbone and the more bulky mesityl substituents. LEPS **99** and LETS **105** showed face to face intermolecular π - π stacking in their crystal structures. The phenyl substituent of LEPS **99** has a twist angle of 53° relative to the pentacene-like backbone. It shows a π - π stacking distance of 3.44 Å with the molecules orientated in a head-to-tail fashion such that steric compression between the 13-phenyl substituents is minimized (**Figure 17**). The phenyl substituent in LEPS

105 has a twist angle of 78° relative to its backbone. It stacks in a parallel displaced fashion with a π - π stacking distance of 3.40 \AA (**Figure 18**).

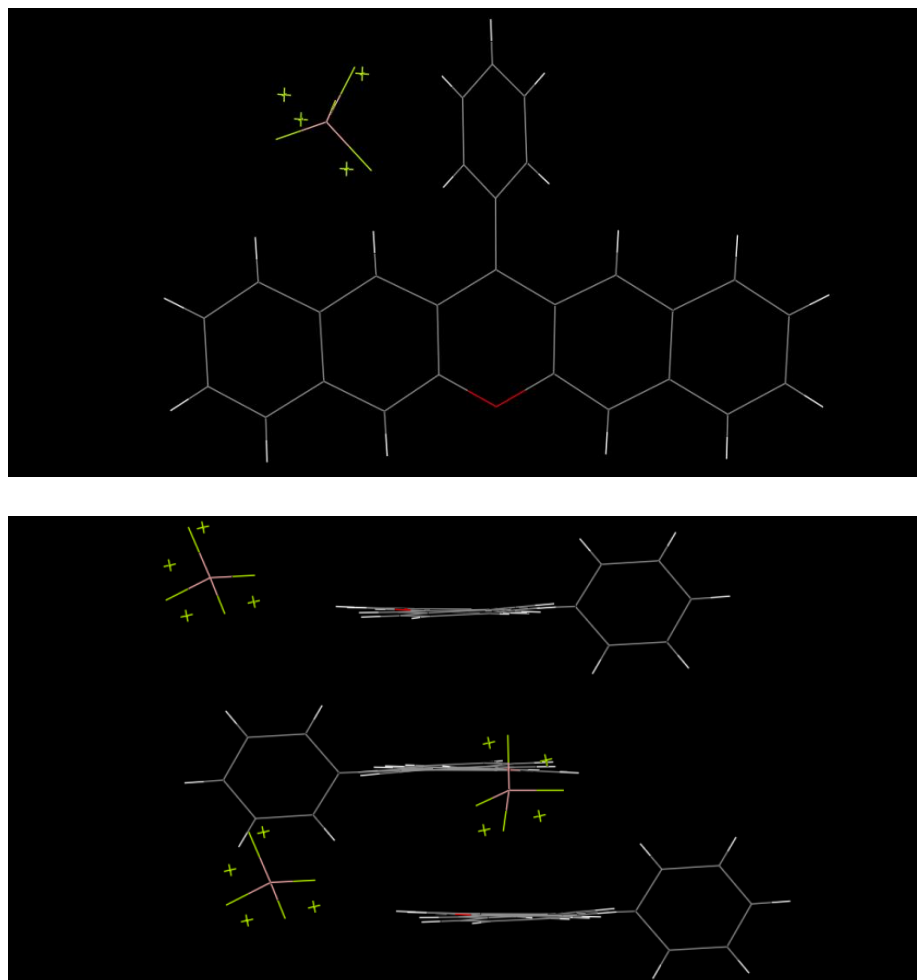


Figure 17: ORTEP diagrams (50% probability) of LEPS **99** and its packing structure.

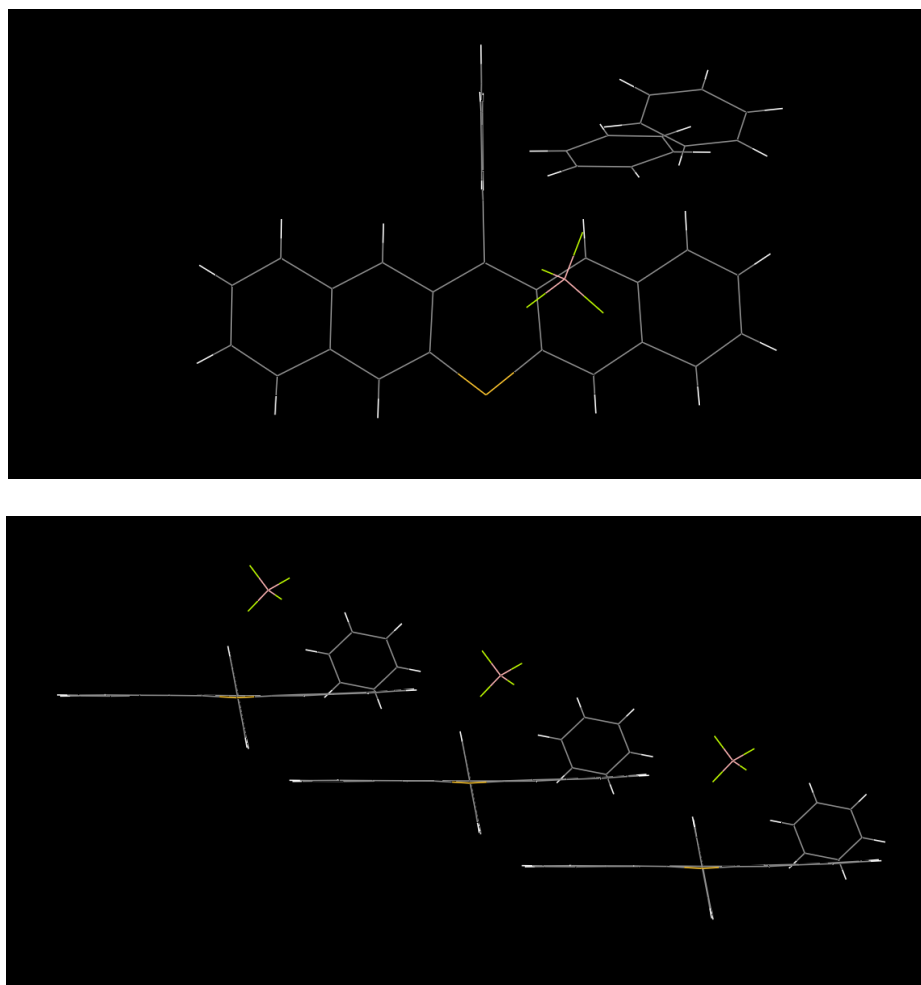
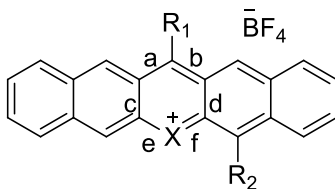


Figure 18: ORTEP diagrams (50% probability) of LETS **105** and its packing structure.

The C-O bond length in LEPS compounds is significantly shorter than the C-S bond length in LETS compounds ($\sim 1.37 \text{ \AA}$ vs. $\sim 1.71 \text{ \AA}$, **Table 4**). As the C-C bond lengths around the center rings of both LEPS and LETS compounds are approximately 1.42 \AA , there is little hexagonal distortion in the center rings of LEPS compounds, but significant hexagonal distortion in LETS compounds.

Table 4: Bond lengths (a-f) of the center ring and twist angle between the substituent and the backbone of LEPS and LETS compounds.



Compound	a (Å)	b (Å)	c (Å)	d (Å)	e (Å)	f (Å)	Twist angle (°)
LEPS 99 (X=O, R ₁ =Ph, R ₂ =H)	1.42	1.42	1.43	1.43	1.37	1.37	53
LEPS 101 (X=O, R ₁ =mesityl, R ₂ =H)	1.37	1.42	1.43	1.43	1.36	1.37	79
LEPS 103 (X=O, R ₁ =R ₂ =Ph)	1.41	1.44	1.44	1.44	1.37	1.37	57(R ₁), 56(R ₂)
LETS 105 (X=S, R ₁ =Ph, R ₂ =H)	1.42	1.42	1.44	1.44	1.71	1.71	78
LETS 106 (X=S, R ₁ =mesityl, R ₂ =H)	1.42	1.40	1.45	1.44	1.72	1.71	90

2.2.5.7 Cyclic voltammetry of LEPS 99

Cyclic voltammetry (CV) is a potentiodynamic electrochemical measurement. The oxidation and reduction waves for compounds can be observed using CV. Reversible electrochemical behavior was observed for LEPS **99**. A redox wave centered at approximately +270 mV (vs. Ag/AgCl) was observed, indicating the remarkable ease with which LEPS **99** is

reduced (**Figure 19**). The redox cycle is reversible, as required for organic semiconductors in solid-state device applications.

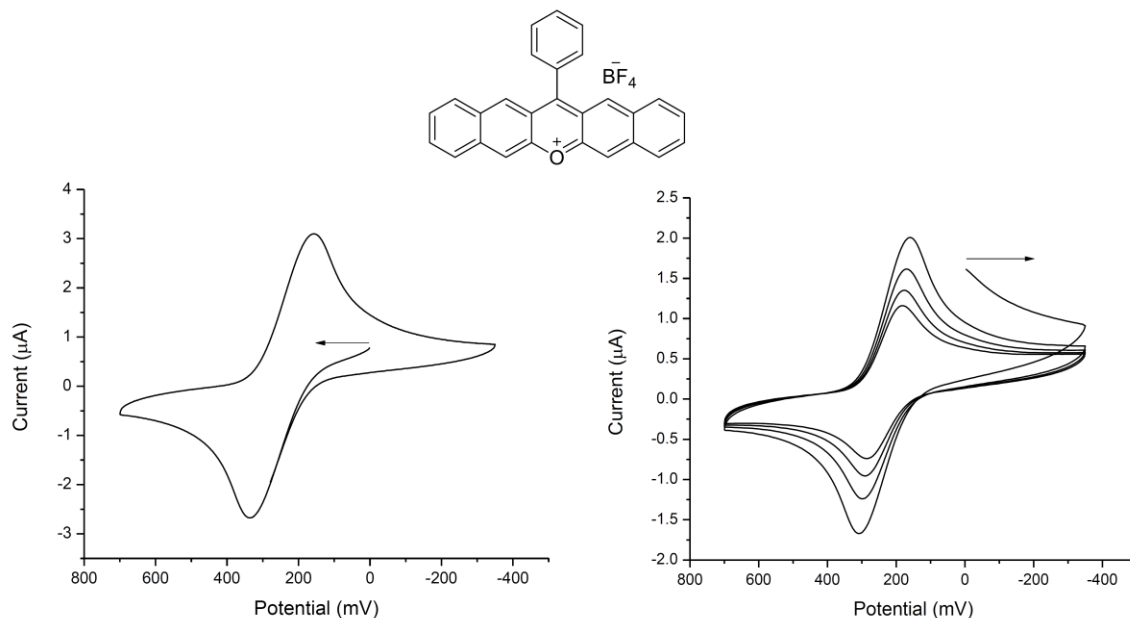


Figure 19: Cyclic voltammogram of a 2×10^{-3} M solution of LEPS **99** in DCM with 0.1 M Bu_4NPF_6 as the electrolyte, Ag/AgCl as the reference electrode, Pt disk as the working electrode and Pt wire as the counter electrode. Scan rate is 100 mV/s.

2.2.5.8 Open-shell diradical character study

2.2.5.8.1 Introduction

Open-shell molecules refer to molecules that have unpaired electrons. Free monoradicals are well known open-shell molecules that typically exist as reactive intermediates. Diradicals with two unpaired electrons represent another class of open-shell molecules.⁵¹ When two electrons are held in two distinct non-bonding molecular orbitals (NBMOs), there are six possible configurations for singlet and triplet states (**Figure 20**). Only the triplet states ($S=1$) are paramagnetic and can be detected by electron spin resonance (ESR). Singlet states ($S=0$), regardless of open-shell or closed-shell, are diamagnetic and cannot be detected by ESR.⁵²

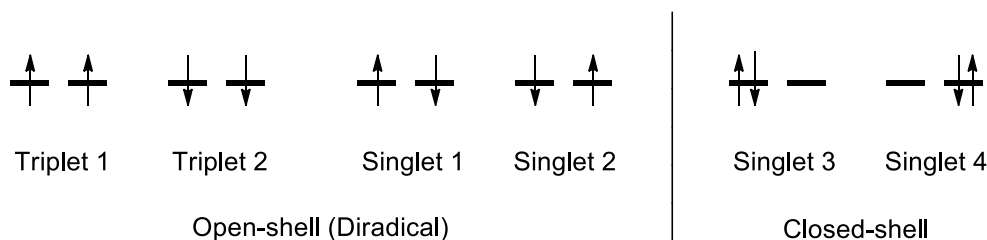
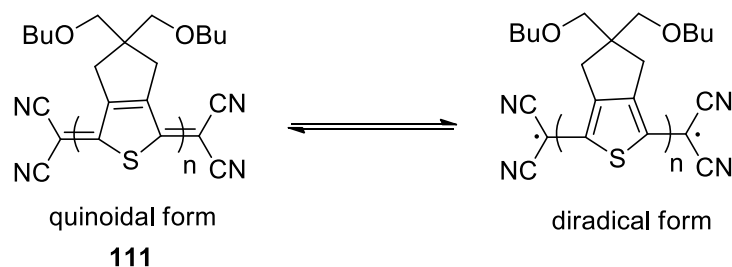


Figure 20: Electronic configuration in NBMOs for singlet and triplet states.

Diradicals species include dinitroxide,⁵³ benzyne,⁵⁴ carboryne,⁵⁵ disilaquinodimethane.⁵⁶ Diradicals were also reported in a series of highly conjugated organic molecules. When the HOMO-LUMO gap is low, it is relatively easy to promote one electron from HOMO to LUMO in order to form diradical species.⁵² In 2005, Takahashi and coworkers reported the syntheses of a series of stable extensive quinoidal oligothiophenes **111** that showed good solubilities and strong absorptions in the visible to near-infrared region (**Scheme 27**).⁵⁷ Higher homologues ($n > 4$, **Scheme 27**) started to show paramagnetic character which was indicated by broad ESR signals with a g value at about 2.0. Also, except for the signals assignable to the pendant butoxy carbons, no other signals corresponding to the backbone were observed in the ^{13}C NMR spectra. Diradicals were proposed as in **Scheme 27** where aromatic thiophenes and cyano substituents help to stabilize the diradical character. Like quinoidal oligothiophenes **111**, oligoporphyrins,⁵⁸ diphenoquinoid chromophores⁵⁹ and other dyes⁶⁰ with absorptions beyond 1000 nm normally show the open-shell character.

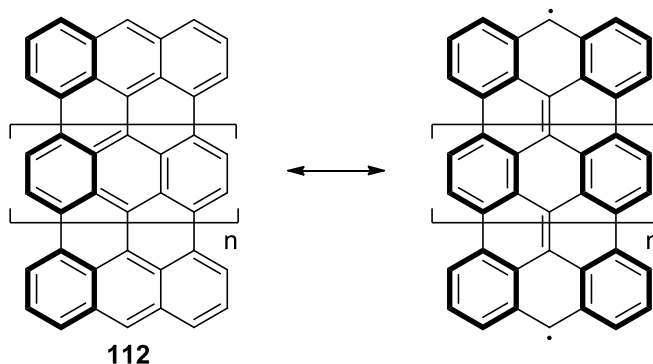


when $n=1-4$, "ESR-silent"

when $n>4$, "ESR-active"

Scheme 27: Closed-shell and open shell resonance forms for quinoidal oligothiophenes.⁵⁷

Anthenes **112** are *peri*-condensed anthracenes.⁶¹ According to calculations, the extent of the diradical character for anthenes increases with increasing anthracene units (**Scheme 28**).⁶² A simple way to understand this behavior is to consider that the formation of the aromatic sextets (depicted by bold lines) overwhelms the penalty of breaking one π -bond.



y = the extent of diradical character
 $n=0$, Bisanthene: $y=7\%$
 $n=1$, Teranthene: $y=54\%$
 $n=2$, Quarteranthene: $y=91\%$

Scheme 28: Closed-shell and open shell resonance forms for anthe **112** with diradical character calculated at the CASSCF(2,2)/6-31G level.⁶²

The computational results were corroborated by experimental data. At room temperature, the cores of the bisanthene derivatives⁶³ like **113**^{63c} showed sharp NMR signals

indicating little or no paramagnetic character. However, the cores of the teranthene derivative **114**⁶⁴ and the quarteranthene derivative **115**⁶² showed no NMR signals indicating significant paramagnetic character (**Figure 21**). Compound **115** also showed a broad ESR signal with g value at about 2.0 indicating obvious paramagnetic character.

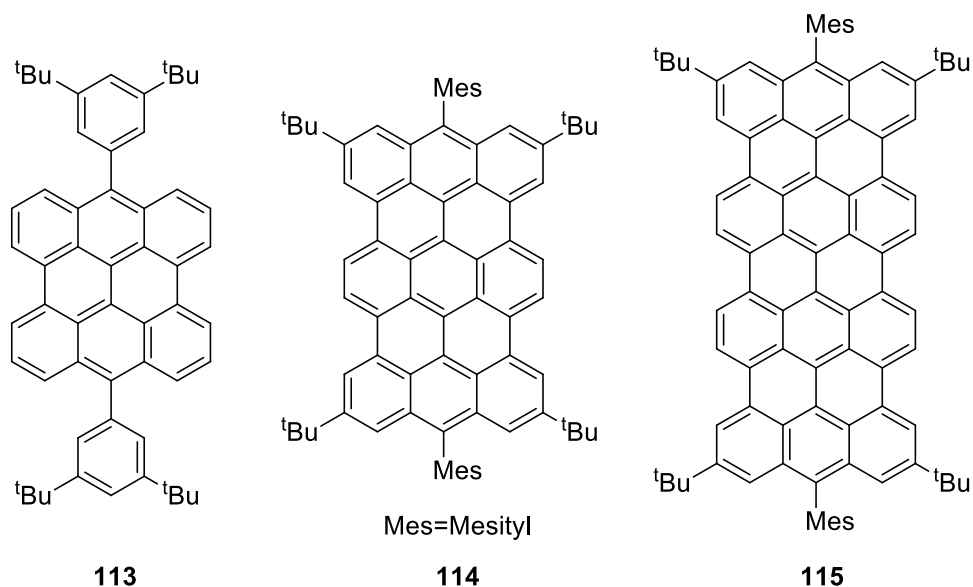


Figure 21: Structures for bisanthene, teranthene and quarteranthene derivatives.

Variable temperature NMR (VT-NMR) experiments can be applied when exploring organic diradicals with accessible singlet (diamagnetic) and triplet (paramagnetic) electronic states. Assuming that the singlet (diamagnetic) state is lower in energy, lowering the temperature will decrease the triplet character leading to a sharpening of the NMR signals (**Figure 22**).

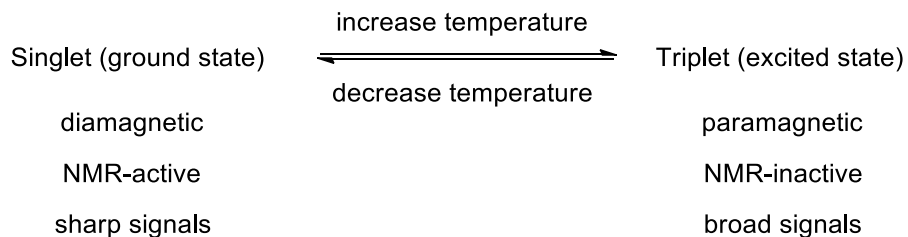


Figure 22: Temperature-related spin multiplicity switching of a diradical with singlet ground state but accessible triplet excited state.

VT-NMR studies were carried out for both the teranthene derivative **114**⁶⁴ and quarteranthene derivative **115**.⁶² The ¹H NMR signals for **114** began to sharpen with decreasing temperature from 30 °C down to -105 °C, indicating significant diradical character at room temperature with a singlet ground state. However, no significant sharpening of signals was observed for **115** even as the temperature was decreased from 20 °C to -90 °C, indicating that for this species, the triplet excited state lies closer in energy to the singlet ground state (**Figure 23**).

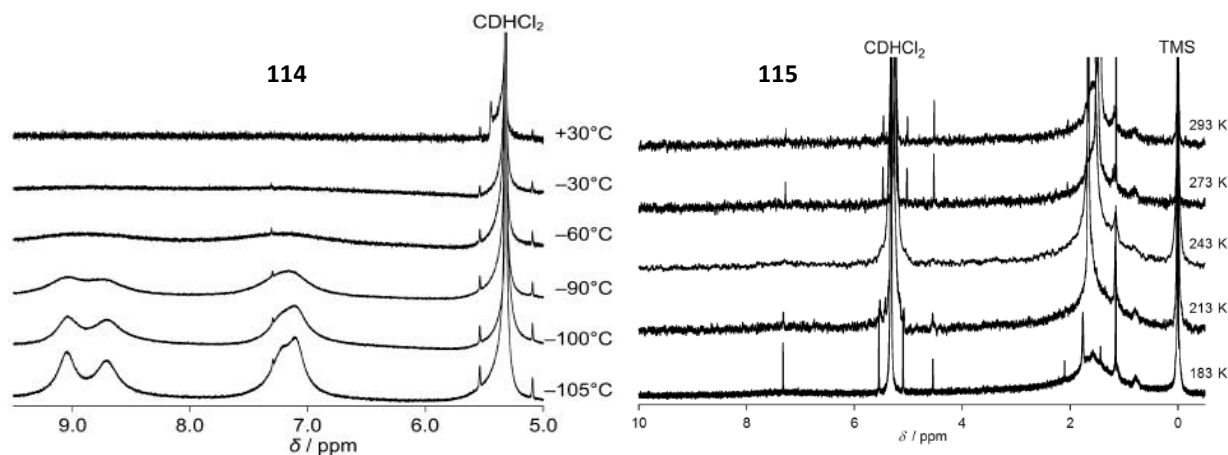
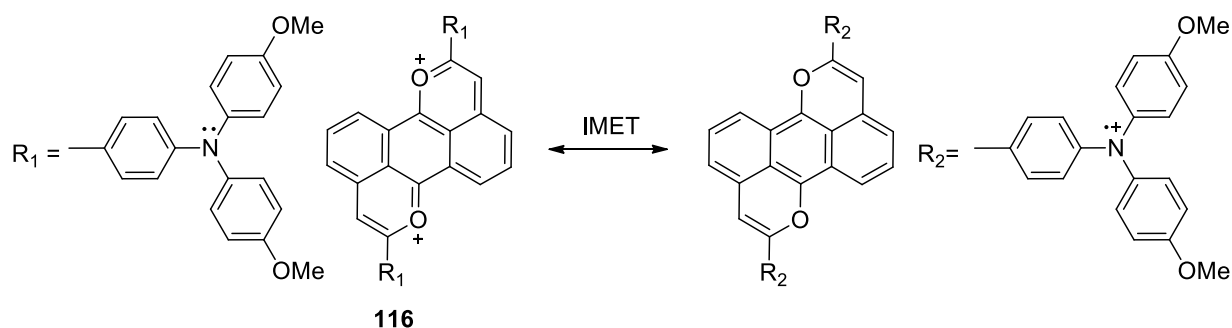


Figure 23: VT-NMR results for teranthene derivative **114**⁶⁴ and quarteranthene derivative **115**.⁶²

Certain pyrylium salts can also exist with paramagnetic character. Nishihara group reported a series of paramagnetic pyrylium salts in the past few years.⁶⁵ These pyrylium salts

have the highly electron-deficient pyrylium backbone connected to the electron-donating moiety. Diradical species can form after intramolecular electron transfer (IMET) from the donating moiety to the pyrylium backbone. For dipyrilium salt **116**,⁶⁵ⁱ one electron on each of the nitrogens of the triphenylamino groups is effectively transferred to the dipyrilium backbone, leaving the nitrogens as radical cations and the dipyrilium backbone as neutral (Scheme 29).



Scheme 29: Intramolecular electron transfer (IMET) for dipyrilium salts **116**.⁶⁵ⁱ

Dipyrilium salt **116** showed broad and indiscernible NMR signals which could not be integrated properly, suggesting paramagnetic character (**Figure 24**).⁶⁵ⁱ Also, it showed an ESR signal with a *g* value at about 2.0 which is a typical indication of π -radical formation.

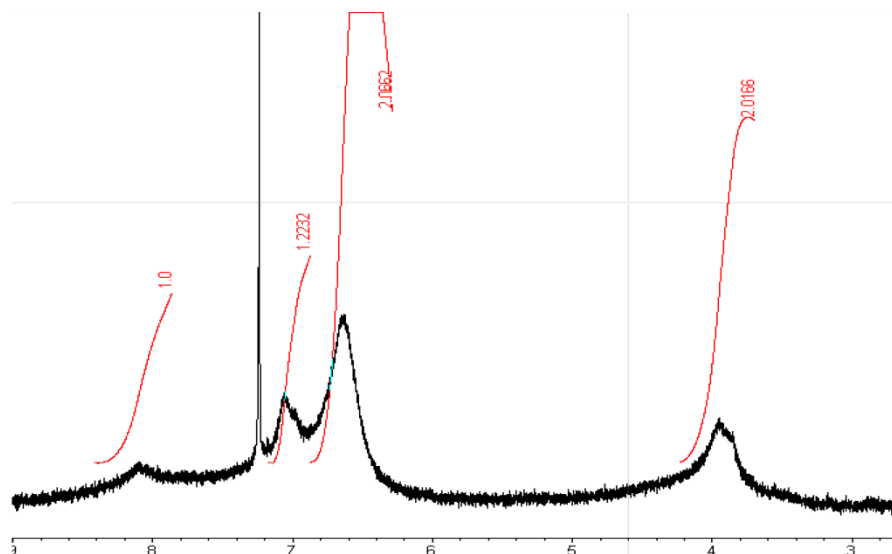


Figure 24 ^1H NMR spectrum for dipyrilium salt **116**.⁶⁵ⁱ

2.2.5.8.2 Open-shell diradical character of LEPS and LETS compounds

Among the synthesized LEPS and LETS compounds, LEPS **101**, LEPS **104** and LETS **106**, all with mesityl substituents, and LETS **107** with a 2',6'-dimethylphenyl substituent showed ^1H NMR spectra with broad and indiscernible signals indicating paramagnetic character. Previously, it was noted that the methyl groups at the 2,6-positions of the phenyl substituents effectively block attacking nucleophiles rendering the corresponding LEPS and LETS compounds moisture resistant. The same substituent at the C-13 position also appears to influence the paramagnetic character of the resulting LEPS or LETS compound. For example, the ^1H NMR spectrum for LETS **106** includes only two sharp signals corresponding to the methyl groups on the mesityl substituent (**Figure 25**). Several highly broadened aromatic signals were also observed between about 7 and 10 ppm. Likewise, the ^{13}C NMR spectrum for LETS **106** shows only four signals total including two methyl signals and two aromatic signals. All of this suggests that LETS **106** has a low lying triplet state that is partially accessed at room temperature. Conversely, the NMR

spectra for LEPS **99** and its isomer **100**, LEPS **103**, LETS **105** and xanthylium species **117** and **118** all show sharp ^1H NMR and ^{13}C NMR signals indicating little or no paramagnetic character.

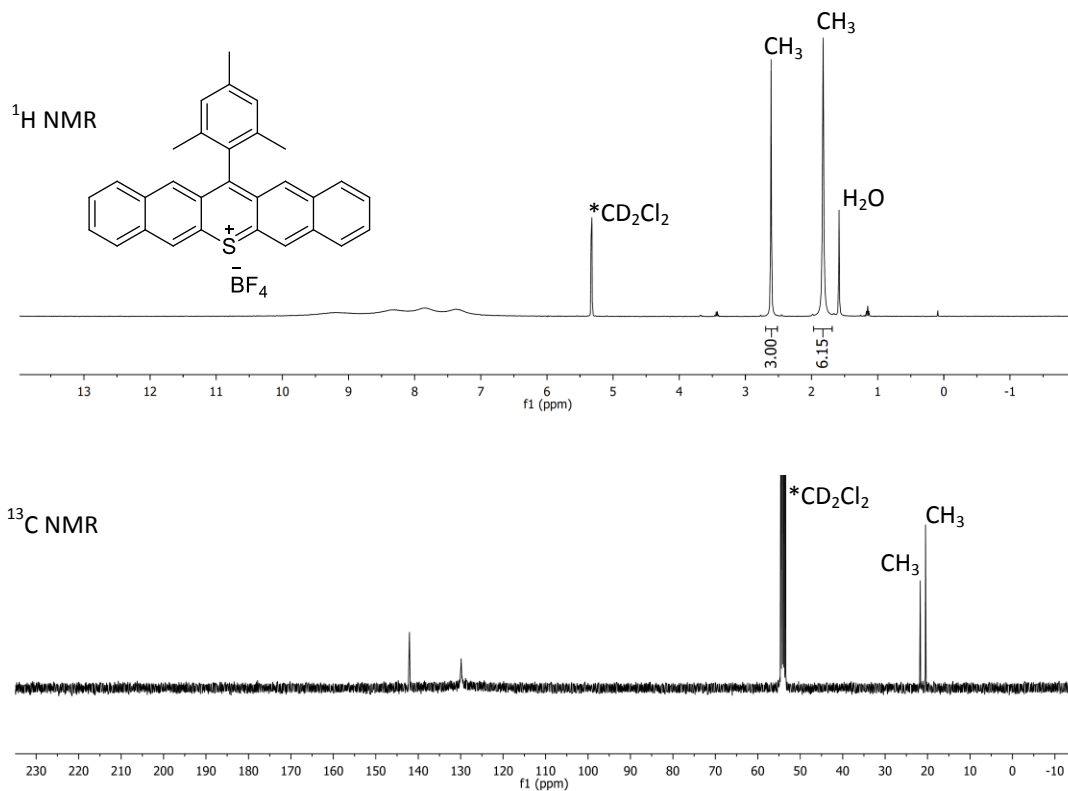


Figure 25: ^1H NMR and ^{13}C NMR spectra for LETS **106** in CD_2Cl_2 at room temperature.

ESR studies were carried out for the above mentioned mesityl substituted LEPS and LETS as well as others. The ESR results corroborate the NMR results well. Thus, those LEPS and LETS compounds with broad NMR signals all showed strong ESR signals with a g value at about 2.0 indicating π -radical formation. LETS **105** and LEPS **99** showed the ESR signal at about $g=2.0$ with moderate and weak intensities, respectively. No ESR signal could be detected for LEPS **103**, LEPS isomer **100**, xanthylium salts **117** and **118** (Table 5). The ESR and NMR results are clear. LEPS and LETS compounds with both five linearly fused rings and with a 2',6'-dimethylphenyl or a mesityl substituent at C-13 show strong paramagnetic behavior. For two species with

otherwise identical substituents, LETS compounds show greater paramagnetic character than LEPS compounds.

Table 5: ESR results for LEPS and LETS compounds and xanthylum derivatives.

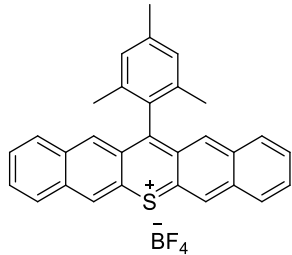
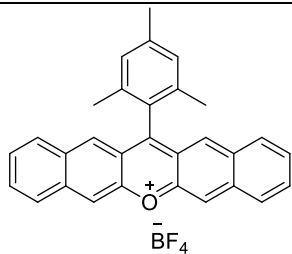
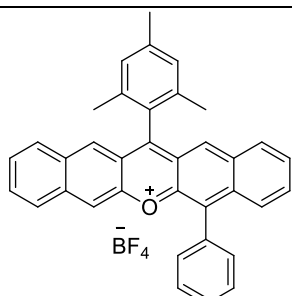
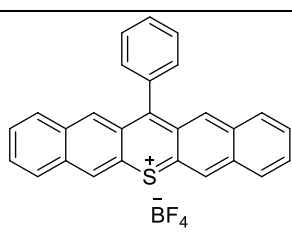
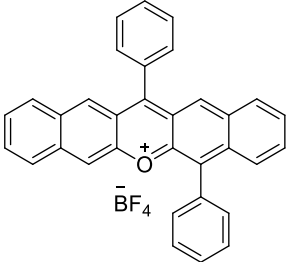
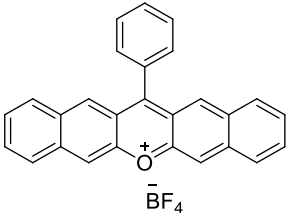
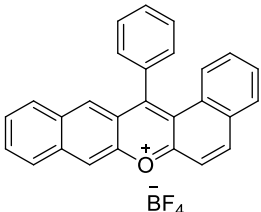
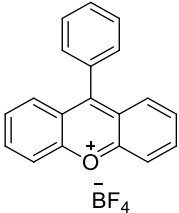
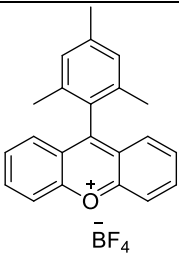
Compound	Structure	Signal intensity and shape	g value
LETS 106		strong and sharp	2.004
LEPS 101		strong and sharp	2.004
LEPS 104		strong and sharp	2.004
LETS 105		medium and sharp	2.004

Table is continued on the next page

LEPS 103		no signal	N/A
LEPS 99		weak and sharp	2.004
LEPS isomer 100		no signal	N/A
Xanthylium 117		no signal	N/A
Xanthylium 118		no signal	N/A

VT-NMR experiments with gradual temperature changes were carried out for select LEPS and LETS compounds that showed broadened NMR signals at room temperature. In these experiments, the temperature of the NMR probe was gradually lowered in an attempt to

increase the population of the singlet states relative to the triplet states, thus leading to a sharpening of NMR signals. Conversely, VT-NMR experiments in which the temperature of the NMR probe was gradually raised were carried out for LEPS and LETS compounds that showed sharp NMR signals at room temperature in an attempt to populate low-lying triplet excited states which will broaden the NMR signals. Only LETS **106** in CD_2Cl_2 showed obvious temperature-dependent change of the NMR signals. By decreasing the temperature from 22 °C to -27 °C, the peaks in the aromatic region of LETS **106** gradually sharpened (**Figure 26**). By raising the temperature to 22 °C again, the aromatic signals did not turn broad immediately. The reverse broadening process took roughly three weeks. In CD_3CN , LETS **106** did not show any change of its NMR spectrum upon lowering the temperature to -27 °C. Thus, solvent effects appear to play a large role.

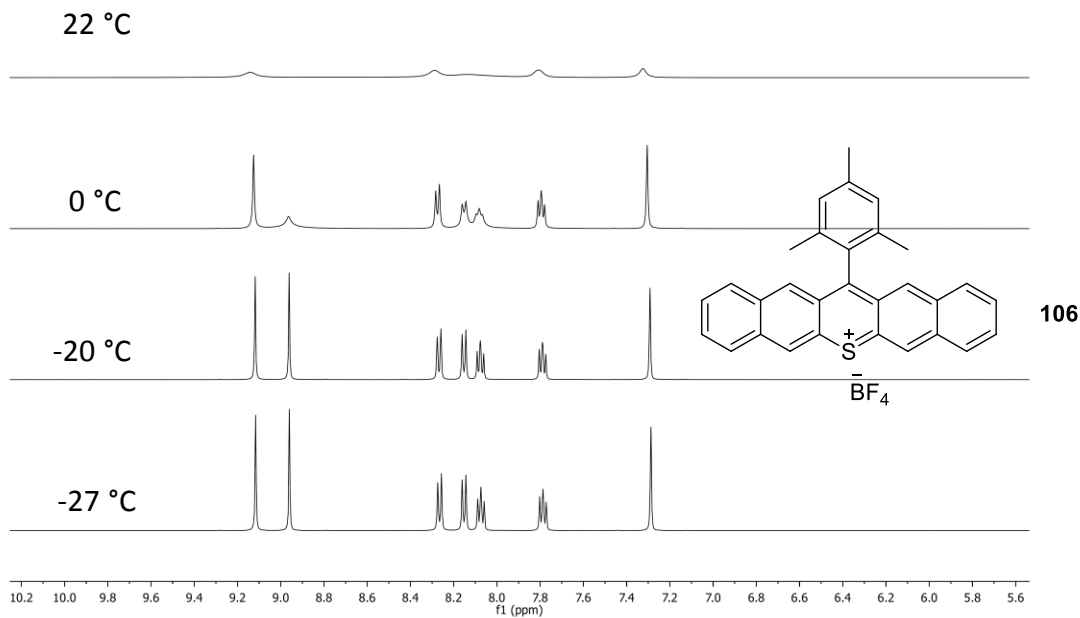


Figure 26: VT-NMR study for LETS **106** in CD_2Cl_2 .

Assuming that an IMET process (**Figure 27**) of dipyrilium salt **116**⁶⁵ⁱ is operating in LEPS and LETS compounds, we would expect one electron in an electron-rich mesityl ring to be transferred to the electron-deficient LEPS or LETS backbone, leading to the formation of a diradical species. In order to test this assumption, LETS **109** with an electron-rich 4-methoxyphenyl substituent and LETS **110** with an electron-deficient 4-trifluoromethylphenyl substituent were synthesized. A broadened NMR spectrum for **109** would indicate IMET from the electron-rich substituent to the electron-deficient LETS backbone. An NMR spectrum with sharp signals for **110** would indicate retarded IMET due to the electron-deficient substituent. However, the results showed that both **109** and **110** have sharp NMR signals suggesting that additional structural factors play an important role. Namely, neither **109** or **110** possessed 2',6'-dimethyl groups.

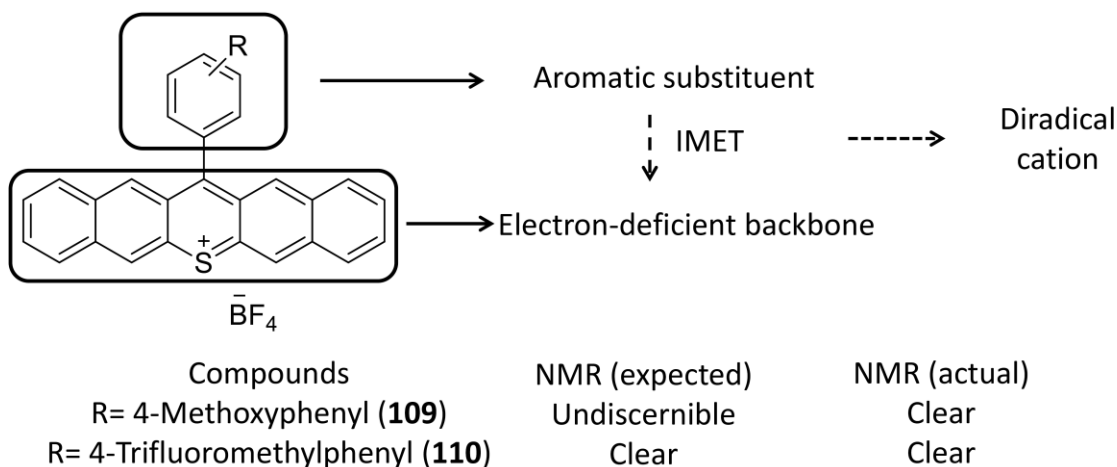


Figure 27: Intramolecular electron transfer (IMET) process for LETS compounds.

It is proposed that 2',6'-dimethyl groups are needed on the 13-phenyl substituent in order to prevent rapid reverse IMET processes from occurring. Thus, the 2',6'-dimethyl groups

ensure that the 13-phenyl substituent sits close to orthogonal to the pentacene-like π -system of the LEPS and LETS compounds. This essentially prevents the 2',6'-dimethylphenyl or mesityl substituents from experiencing π -conjugative effects with the LEPS and LETS π -systems. Based upon these findings, we predict that the following molecules (**Figure 28**) will show strong and lasting paramagnetic character.

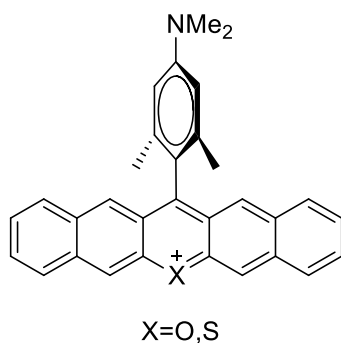


Figure 28: Predicted LEPS and LETS structures with strong paramagnetic character.

Experimental

Analytical Instrumentation

¹H NMR Spectra

¹H NMR spectra were obtained on a Varian Mercury Plus 400 FT-NMR operating at 399.768 MHz or a Varian INOVA 500 FT-NMR operating at 499.763 MHz. All chemical shift (δ_H) values are reported in parts per million (ppm) relative to (CH₃)₄Si (TMS) unless otherwise noted. All ¹H NMR experiments were carried out at room temperature unless otherwise noted.

¹³C NMR Spectra

¹³C NMR spectra were obtained on a Varian Mercury Plus 400 FT-NMR operating at 100.522 MHz or a Varian INOVA 500 FT-NMR operating at 125.666 MHz. All chemical shift (δ_C) values are reported in parts per million (ppm) relative to (CH₃)₄Si (TMS) unless otherwise noted. All ¹³C NMR experiments were carried out at room temperature unless otherwise noted.

Mass Spectroscopy

Matrix-assisted laser desorption ionization time-of-flight mass spectrometry (MALDI-TOF-MS) with sulfur as the matrix and Laser desorption ionization time-of-flight mass spectrometry (LDI-TOF-MS) were performed on a Shimadzu Kratos Axima-CFR running in reflectron mode. High-resolution mass spectra were recorded at the Notre Dame mass spectrometry facility.

UV-Vis-NIR Spectroscopy

UV-Vis-NIR spectra were obtained on a Thermo-Fisher Nicolet Evolution 300 spectrometer using 1 cm quartz cells. Solutions of dibenzoxanthone and dibenzothioxanthone were prepared using chloroform (ACS reagent grade). Solutions of LEPS and LETS compounds were prepared using dry dichloromethane from the dry-solvent delivery system.

Crystallographic Methods

Diffraction data for X-ray quality single crystals of the LEPS and LETS compounds were collected on a Bruker SMART X2S diffractometer using monochromated (doubly curved silicon crystal) Mo K α radiation (0.71073 Å).

Cyclic Voltammetry

Cyclic voltammetry (CV) studies of LEPS **99** were performed using a BAS-100B electrochemical analyzer in a three-electrode single-compartment cell with Pt disk as the working electrode, Ag/AgCl as the reference electrode, and Pt wire as the auxiliary electrode. Tetrabutylammonium hexafluorophosphate, TBAPF₆, was used as the supporting electrolyte (0.1 M), and dry dichloromethane from the solvent delivery system was used as the solvent. A scan rate of 100 mV/s was employed. The concentration of LEPS **99** was 2 mM.

Chromatography

Sand was obtained from Fisher Scientific Co.

Silica Gel (230-400 mesh) was obtained from Natland International Co.

Thin Layer Chromatography Plates (silica) were obtained from Fisher Scientific Co.

Solvents

Note: All solvents were used without further purification unless otherwise noted. Solvent drying was carried out for tetrahydrofuran, methylene chloride, diethyl ether and dimethyl formamide as needed by distillation from sodium (THF) or by passing through a silica column in a dry-solvent delivery system.

Acetic Acid ($\text{CH}_3\text{CO}_2\text{H}$) was obtained from VWR Chemical Co.

Acetone ($(\text{CH}_3)_2\text{CO}$) was obtained from Pharmco.

Acetonitrile (CH_3CN) was obtained from Fisher Scientific Co.

Chloroform (CHCl_3) was obtained from Fisher Scientific Co.

Deuterated NMR solvents were obtained from Cambridge Isotope Laboratories.

Dichloromethane (CH_2Cl_2) was obtained from Fisher Scientific Co.

Diethyl Ether ($(\text{CH}_3\text{CH}_2)_2\text{O}$) was obtained from Pharmco.

1,4-Dioxane ($(\text{CH}_2\text{CH}_2)_2\text{O}_2$) was obtained from Aldrich Chemical Co.

Ethanol ($\text{CH}_3\text{CH}_2\text{OH}$) was obtained from Pharmco.

Ethyl Acetate ($\text{CH}_3\text{CO}_2\text{CH}_2\text{CH}_3$) was obtained from Fisher Scientific Co.

Hexanes (C_6H_{14}) were obtained from Fisher Scientific Co.

Methanol (CH_3OH) was obtained from Pharmco.

Tetrahydrofuran (THF) ($(\text{CH}_2)_4\text{O}$) was obtained from Fisher Scientific Co.

Reagents

Aluminum foil (Al°) was obtained from Reynolds.

3-Amino-2-naphthoic acid ($\text{C}_{11}\text{H}_9\text{NO}_2$) was obtained from Chem-Impex International, Inc.

Ammonium chloride (NH_4Cl) was obtained from Fisher Scientific Co.

Bis(triphenylphosphine)palladium(II) dichloride ($\text{Pd}(\text{PPh}_3)_2\text{Cl}_2$) was obtained from Aldrich Chemical Co.

Boron tribromide (BBr_3) was obtained from Fluka Co.

4-Bromoanisole ($\text{C}_7\text{H}_7\text{BrO}$) was obtained from Aldrich Chemical Co.

4-Bromo-*N,N*-dimethylaniline ($\text{C}_8\text{H}_{10}\text{BrN}$) was obtained from Aldrich Chemical Co.

2-bromo-1,3-dimethylbenzene ($\text{C}_8\text{H}_9\text{Br}$) was obtained from Alfa Aesar Chemical Co.

2-Bromomesitylene ($\text{C}_9\text{H}_{11}\text{Br}$) was obtained from Aldrich Chemical Co.

1-Bromo-2-naphthol ($\text{C}_{10}\text{H}_7\text{BrO}$) was obtained from TCI America Co.

N-Bromosuccinimide (NBS) was obtained from Aldrich Chemical Co.

n-Butyllithium ($n\text{BuLi}$) was obtained from Aldrich Chemical Co.

Cesium fluoride (CsF) was obtained from Aldrich Chemical Co.

Copper (Cu) was obtained from Aldrich Chemical Co.

Copper (I) iodide (CuI) was obtained from Alfa Aesar Chemical Co.

1,4-Cyclohexadiene (C_6H_8) was obtained from Aldrich Chemical Co.

1,8-Diazabicyclo[5.4.0]undec-7-ene (DBU) was obtained from Alfa Aesar Chemical Co.

1,2-Dibromoethane ($\text{C}_2\text{H}_4\text{Br}_2$) was obtained from Acros Organics Co.

Diethyl amine ($\text{C}_4\text{H}_{11}\text{N}$) was obtained from VWR International.

1,2-Diiodobenzene ($\text{C}_6\text{H}_4\text{I}_2$) was obtained from VWR International.

1-(3-Dimethylaminopropyl)-3-ethylcarbodiimide hydrochloride (EDC) was obtained from TCI America Co.

Dimethyl sulfate (Me_2SO_4) was obtained from Aldrich Chemical Co.

Hexamethyldisilazane (HMDS) was obtained from Fluka Co.

Hydrochloric acid (HCl) was obtained from EM Science.

1-Hydroxybenzotriazole monohydrate (HOBT) was obtained from TCI America Co.

3-Hydroxy-2-naphthoic acid (C₁₁H₈O₃) was obtained from Aldrich Chemical Co.

Iodine (I₂) was obtained from Aldrich Chemical Co.

Lithium aluminum hydride (LAH) was obtained from Aldrich Chemical Co.

Lithium diisopropylamide (LDA) was obtained from Aldrich Chemical Co.

Mercuric acetate (Hg(OAc)₂) was obtained from J.T. Baker Chemical Co.

2,3-Naphthalenedicarboxylic acid (C₁₀H₆(CO₂H)₂) was obtained from TCI America Co.

2-Naphthol (C₁₀H₈O) was obtained from Aldrich Chemical Co.

Phenylboronic acid (C₆H₇BO₂) was obtained from Aldrich Chemical Co.

Phenyllithium (C₆H₅Li) was obtained from Aldrich Chemical Co.

Potassium iodide (KI) was obtained from Aldrich Chemical Co.

Pyridine (C₅H₅N) was obtained from Aldrich Chemical Co.

Silver nitrate (AgNO₃) was obtained from Alfa Aesar Chemical Co.

Sodium bicarbonate (NaHCO₃) was obtained from Fisher Scientific Co.

Sodium bisulfite (NaHSO₃) was obtained from EM Science.

Sodium borohydride (NaBH₄) was obtained from Aldrich Chemical Co.

Sodium carbonate (Na₂CO₃) was obtained from Fisher Scientific Co.

Sodium chloride (NaCl) was obtained from J.T. Baker Chemical Co.

Sodium hydroxide (NaOH) was obtained from EM Science.

Sodium nitrite (NaNO₂) was obtained from Aldrich Chemical Co.

Tetrafluoroboric acid diethyl ether complex (HBF₄·Et₂O) was obtained from Aldrich Chemical Co.

2-Thionaphthol (C₁₀H₈S) was obtained from VWR International.

Triethylamine (C₆H₁₅N) was obtained from Aldrich Chemical Co.

Trifluoroacetic anhydride (Tf₂O) was obtained from Alfa Aesar Chemical Co.

(Trimethylsilyl)acetylene (C₅H₁₀Si) was obtained from GFS Chemicals.

1,1,1-Tris(acetyloxy)-1,1-dihydro-1,2-benziodoxol-3-(1H)-one (DMP) was obtained from VWR International.

Experimental Procedures

Synthesis of **54** followed the methods reported by Niimi and coworkers.⁶⁶ Synthesis of **55** followed the methods reported by Pena and coworkers.⁶⁷ Synthesis of **57** followed the methods reported by Lucas and coworkers.⁶⁸ Synthesis of **65** followed the methods reported by Wu and coworkers.⁶⁹ Synthesis of **67** followed the methods reported by Hashmi and coworkers.⁷⁰ Synthesis of **69** followed the methods reported by Bowles and coworkers.⁷¹ Synthesis of **76** followed the methods reported by Janz and coworkers.⁷²

3-(Naphthalen-2-yloxy)-2-naphthoic acid (45). 2-Iodo-3-naphthoic acid (1.9 g, 6.37 mmol) was dissolved in DMF (20 mL), followed by 2-naphthol (1.84 g, 12.74 mmol), 1,8-diazabicyclo[5.4.0]undec-7-ene (DBU) (2.9 mL, 19.44 mmol), pyridine (0.1 mL), copper (101 mg), copper(I) iodide (97 mg). The reaction was heated to 105 °C for 80 min. After the reaction mixture was cooled to room temperature, it was diluted with ethyl acetate (120 mL). Then the mixture was washed with 1N HCl (240 mL), the aqueous layer was further extracted with ethyl acetate (2x60 mL). The organic layers were combined and washed with water (3x160 mL), brine (140 mL) and dried over Na₂SO₄. The solvent was removed under vacuum and the residue was dissolved in CH₂Cl₂ (20 mL). Then sat. Na₂CO₃ aq. (10 mL) was added to the solution followed by

vigorous stirring. The resulting precipitates were collected by vacuum filtration and washed with CH_2Cl_2 , sat. Na_2CO_3 aq. and air dried. The resulting solid was dissolved in water (650 mL) followed by adding 2N HCl. The precipitate obtained was washed with water and air dried to give the product as a beige solid (1.423 g, 71% yield). ^1H NMR (CDCl_3 , 400 MHz) δ 10.80 (s, 1H), 8.85 (s, 1H), 7.96 (dd, J = 8.6, 4.4 Hz, 2H), 7.93-7.87 (m, 1H), 7.82-7.76 (m, 1H), 7.62-7.45 (m, 6H), 7.36 (dd, J = 8.9, 2.5 Hz, 1H), 7.22 (s, 1H). ^{13}C NMR (CDCl_3 , 101 MHz) δ 166.29, 153.82, 152.63, 136.47, 136.20, 134.31, 131.29, 130.80, 129.56, 129.49, 129.41, 128.07, 127.63, 127.19, 126.92, 126.14, 125.97, 120.32, 119.45, 116.94, 114.28. MALDI-MS m/z : 314.1 $[\text{M}]^+$. HRMS (ESI) m/z = 315.1013 $[\text{M}+\text{H}]^+$, calcd m/z = 315.1016 (Error = 0.9 ppm).

***N,N*-Diethyl-3-(naphthalen-2-yloxy)-2-naphthamide (46)** *N*-(3-Dimethylaminopropyl)-*N'*-ethylcarbodiimide hydrochloride (EDC) (124 mg, 0.64 mmol) and hydroxybenzotriazole monohydrate ($\text{HOBT}\cdot\text{H}_2\text{O}$) (104 mg, 0.68 mmol) were added to a solution of **45** (200 mg, 0.64 mmol) dissolved in CH_2Cl_2 (15 mL). The resulting mixture was stirred at room temperature for 15 min. Then it was treated with diethylamine (0.10 mL, 0.97 mmol) and triethyl amine (0.20 mL, 1.32 mmol). The reaction stood overnight under room temperature. CH_2Cl_2 (30 mL) was added and the solution was washed with 0.5 N HCl (4x40 mL), 0.5 N NaOH (3x40 mL), brine (40 mL) and dried over Na_2SO_4 . The solvent was removed under vacuum and the crude product was subjected to column chromatography (silica, ethyl acetate/hexanes, 1:4) to obtain the pure product as a colorless oil (206 mg, 88% yield). ^1H NMR (CDCl_3 , 400 MHz) δ 7.90-7.82 (m, 4H), 7.75 (dd, J = 7.8, 1.6 Hz, 1H), 7.65-7.60 (m, 1H), 7.51-7.41 (m, 5H), 7.34 (dd, J = 8.9, 2.4 Hz, 1H), 7.26 (s, 1H), 3.82-3.19 (m, 4H), 1.17 (t, J = 7.2 Hz, 3H), 1.13 (t, J = 7.1 Hz, 3H). ^{13}C NMR (CDCl_3 , 101 MHz) δ 167.83, 154.23, 151.81, 134.39, 134.16, 130.68, 130.14, 129.83, 128.05, 127.89, 127.84, 127.40, 127.18,

127.05, 126.69, 125.38, 125.14, 120.40, 115.56, 113.88, 43.08, 38.98, 14.23, 12.88. MALDI-MS m/z : 369.4 $[M]^+$. HRMS (ESI) m/z = 370.1801 $[M+H]^+$, calcd m/z = 370.1802 (Error = 0.1 ppm).

13H-Dibenzo[*b,i*]xanthen-13-one (38) and 14H-Dibenzo[*a,i*]xanthen-14-one (42) (Via LDA-mediated ring closure): To a solution of **46** (206 mg, 0.56 mmol) in THF (5 mL) was treated with LDA mono (tetrahydrofuran) solution (1.5 M in cyclohexane, 1.5 mL, 2.25 mmol) at 0 °C. The reaction mixture was allowed to warm to room temperature for 4.5 h. Sat. NH_4Cl aq. (5 mL) was added to quench the reaction, followed by water (10 mL). The resulting mixture was extracted with CH_2Cl_2 (2x20 mL). The organic layers were combined and washed with 1N HCl (3x20 mL), water (2x15 mL), brine (15 mL), dried over Na_2SO_4 . The solvent was removed under vacuum to obtain the crude mixture of **38** and **42** as an orange solid (163 mg, 99% yield). The crude mixture was directly used in the next step without further purification. Another small scale of the crude mixture was subjected to column chromatography (silica, chloroform/hexanes, 13:7) to obtain pure **38** and **42** both as yellow solids. **(38)**: ^1H NMR (CDCl_3 , 400 MHz) δ 8.97 (s, 2H), 8.10-8.05 (m, 2H), 7.92 (dd, J = 8.3, 1.1 Hz, 2H), 7.88 (s, 2H), 7.63 (ddd, J = 8.2, 6.7, 1.2 Hz, 2H), 7.50 (ddd, J = 8.1, 6.7, 1.2 Hz, 2H). ^{13}C NMR (CDCl_3 , 101 MHz) δ 178.88, 152.82, 137.25, 130.07, 129.51, 129.39, 129.05, 127.15, 125.53, 121.11, 113.39. MALDI-MS m/z : 296.4 $[M]^+$. HRMS (ESI) m/z = 297.0923 $[M+H]^+$, calcd m/z = 297.0910 (Error = -4.1 ppm). UV-Vis-NIR: λ_{max} (CHCl_3) = 293, 330, 354, 436 nm. **(42)**: ^1H NMR (CDCl_3 , 400 MHz) δ 10.09 (dt, J = 8.8, 1.0 Hz, 1H), 9.02 (s, 1H), 8.20-8.09 (m, 2H), 7.98-7.89 (m, 3H), 7.81 (ddt, J = 8.2, 6.9, 1.3 Hz, 1H), 7.65-7.57 (m, 3H), 7.52 (ddt, J = 7.9, 6.7, 1.2 Hz, 1H). ^{13}C NMR (CDCl_3 , 101 MHz) δ 179.38, 158.52, 151.35, 137.35, 136.31, 131.46, 130.15, 130.08, 129.92, 128.89, 128.60, 128.28, 127.19, 127.02, 126.12, 125.69,

123.06, 118.35, 113.77, 113.40. MALDI-MS m/z : 296.8 $[M]^+$. HRMS (ESI) m/z = 297.0935 $[MH]^+$, calcd m/z = 297.0910 (Error = -8.3 ppm). UV-Vis-NIR: λ_{\max} ($CHCl_3$) = 318, 344, 383, 399 nm.

13*H*-Dibenzo[*b,i*]xanthen-13-one (38) (Via naphthalene intermediate (58)): CsF (2.16 mmol), the salicylate (57) (0.54 mmol), and the silylaryl triflate 55 (0.59 mmol) in anhydrous THF (6 mL) were stirred at 65 °C for 24 h. The reaction mixture was allowed to cool to room temperature, diluted with CH_2Cl_2 (40 mL) and washed with brine (20 mL), dried over Na_2SO_4 . The solvent was removed under vacuum and the residue was subjected to column chromatography (silica, chloroform/hexanes, 13:7) to obtain the product as a yellow solid (29 mg, 18% yield).

3-((1-Phenylnaphthalen-2-yl)oxy)-2-naphthoic acid (72): A mixture of 2-iodo-3-naphthoic acid (813 mg, 2.73 mmol), 1-phenyl-2-naphthol (720 mg, 3.27 mmol), DBU (1.0 mL, 6.83 mmol), pyridine (0.05 mL, 0.546 mmol), copper (50 mg) and copper(I) iodide (50 mg) in DMF (10 mL) was kept at 105 °C for 2 h. The reaction mixture was cooled and diluted with EtOAc (70 mL). Then it was washed with 1N HCl (3x50 mL), H_2O (2x50 mL), brine (2x50 mL) and dried over Na_2SO_4 . The solvent was evaporated under vacuum and the residue was subjected to column chromatography (silica, ethyl acetate/hexanes, 2:3). The purified product ran through the column and the unpurified product left on the top of the column were combined (469 mg, 44%) and directly used in the next step. 1H NMR ($CDCl_3$, 400 MHz) δ 8.69 (s, 1H), 8.03 (d, J = 8.9 Hz, 1H), 7.99 (d, J = 8.2 Hz, 1H), 7.89 (d, J = 8.2 Hz, 1H), 7.65 (d, J = 8.4 Hz, 1H), 7.61-7.40 (m, 6H), 7.37-7.31 (m, 3H), 7.31-7.27 (m, 2H), 7.06 (s, 1H). ^{13}C NMR ($CDCl_3$, 101 MHz) δ 165.20, 154.26, 147.63, 136.27, 136.25, 134.20, 133.94, 132.03, 131.73, 130.20, 130.01, 129.51, 129.50, 128.97, 128.70, 128.32, 128.29, 127.24, 126.73, 126.49, 126.28, 125.83, 120.87, 118.25, 111.73. MALDI-

MS m/z : 390.6 $[M]^+$. HRMS (ESI) m/z = 413.1149 $[M+Na]^+$, calcd m/z = 413.1148 (Error = -0.1 ppm).

***N,N*-Diethyl-3-((1-phenylnaphthalen-2-yl)oxy)-2-naphthamide (73):** *N*-(3-Dimethylaminopropyl)-*N'*-ethyl-carbodiimide hydrochloride (EDC) (159 mg, 0.83 mmol) and hydroxybenzotriazole monohydrate (HOBT·H₂O) (127 mg, 0.83 mmol) were added to a solution of **72** (270 mg, 0.69 mmol) dissolved in CH₂Cl₂ (15 mL). The resulting mixture was stirred at room temperature for 15 min. Then it was treated with diethylamine (0.15 mL, 1.38 mmol) and triethyl amine (0.21 mL, 1.38 mmol). The reaction stood under room temperature for 5 h. CH₂Cl₂ (30 mL) was added and the solution was washed with 0.5 N HCl (3x40 mL), 0.5 N NaOH (2x40 mL), brine (40 mL) and dried over Na₂SO₄. The solvent was removed under vacuum and the crude product was subjected to column chromatography (silica, ethyl acetate/hexanes, 1:3) to obtain the pure product as a white solid (251 mg, 81% yield). ¹H NMR (CD₂Cl₂, 400 MHz) δ 7.98-7.91 (m, 2H), 7.80 (d, J = 7.9 Hz, 1H), 7.69 (s, 1H), 7.57 (t, J = 8.2 Hz, 2H), 7.53-7.25 (m, 10H), 7.04 (s, 1H), 3.79-3.59 (m, 1H), 3.28-3.13 (m, 1H), 2.77-2.62 (m, 1H), 2.61-2.39 (m, 1H), 1.12 (t, J = 7.2 Hz, 3H), 0.76 (t, J = 7.3 Hz, 3H). ¹³C NMR (CD₂Cl₂, 101 MHz) δ 167.76, 153.32, 149.71, 136.16, 134.50, 134.46, 131.81, 131.25, 131.13, 130.53, 130.23, 129.77, 129.67, 128.71, 128.57, 128.31, 127.99, 127.59, 127.43, 127.27, 127.09, 126.44, 125.80, 125.31, 121.43, 111.39, 42.61, 39.27, 14.07, 13.11. MALDI-MS m/z : 445.8 $[M]^+$. HRMS (ESI) m/z = 446.2117 $[M+H]^+$, calcd m/z = 446.2115 (Error = -0.6 ppm).

5-Phenyl-13*H*-dibenzo[*b,i*]xanthen-13-one (74): To a solution of **73** (231 mg, 0.52 mmol) in THF (6 mL) was treated with LDA mono (tetrahydrofuran) solution (1.5 M in cyclohexane, 1.4 mL, 2.08 mmol) at 0 °C. The reaction mixture was allowed to warm to room temperature for 1 h. Sat.

NH₄Cl aq. (10 mL) was added to quench the reaction, followed by water (10 mL). The resulting mixture was extracted with CH₂Cl₂ (70 mL). The organic layers were combined and washed with water (2x25 mL), brine (25 mL), dried over Na₂SO₄. The solvent was removed under vacuum to obtain the crude product which was subjected to column chromatography (silica, chloroform/hexanes, 1:2) to obtain the pure product as a yellow solid (188 mg, 97%). ¹H NMR (CDCl₃, 400 MHz) δ 9.02 (s, 1H), 8.95 (s, 1H), 8.11 (dd, J = 7.6, 1.8 Hz, 1H), 8.05 (d, J = 8.3 Hz, 1H), 7.79 (d, J = 8.4 Hz, 1H), 7.74-7.67 (m, 1H), 7.66-7.61 (m, 3H), 7.60-7.41 (m, 7H). ¹³C NMR (CDCl₃, 101 MHz) δ 179.11, 152.72, 149.25, 137.18, 136.32, 134.80, 131.30, 130.29, 130.03, 129.47, 129.41, 129.31, 129.28, 128.82, 128.59, 128.57, 127.99, 127.03, 126.00, 125.82, 125.45, 125.30, 120.84, 120.71, 113.67. MALDI-MS m/z: 372.7 [M]⁺. HRMS (ESI) m/z = 373.1208 [M+H]⁺, calcd m/z = 373.1223 (Error = 4.1 ppm). UV-Vis: λ_{max} (CHCl₃) = 298, 332, 358, 445 nm.

3-(Naphthalen-2-ylthio)-2-naphthoic acid (78): 2-Iodo-3-naphthoic acid (2822 mg, 9.47 mmol) was dissolved in DMF (30 mL), followed by 2-thionaphthol (3034 mg, 18.93 mmol), 1,8-diazabicyclo[5.4.0]undec-7-ene (DBU) (4.25 mL, 28.41 mmol), pyridine (0.15 mL), copper (166 mg), copper(I) iodide (166 mg). The reaction was heated to 105 °C for 2 h. After the reaction mixture was cooled to room temperature, it was diluted with ethyl acetate (120 mL). Then the mixture was washed with 1N HCl (120 mL), the resulting suspension was filtered through the celite pad to get rid of the precipitate. The aqueous layer was extracted with EtOAc (2x75 mL). The organic layers were combined and washed with brine (2x70 mL) and dried over Na₂SO₄. The solvent was removed under vacuum. The residue was washed with cold EtOAc/Hexanes (2:5) to yield the crude product as a brown solid (3357 mg, 107%) which was used in the next step without further purification. Another small scale of the residue was purified through column

chromatography (silica, hexanes/ethyl acetate/acetic acid = 5:2:0.08) to obtain the pure product as an off-white solid. ^1H NMR (CDCl_3 , 400 MHz) δ 8.74 (s, 1H), 8.18 (s, 1H), 7.96-7.82 (m, 4H), 7.61-7.51 (m, 3H), 7.48-7.41 (m, 3H), 7.31 (s, 1H). ^{13}C NMR (Acetone- d_6 , 101 MHz) δ 167.04, 137.71, 135.27, 134.46, 134.39, 133.45, 132.53, 131.49, 131.36, 130.52, 129.74, 129.03, 128.96, 128.07, 127.26, 126.99, 126.89, 126.87, 126.46. MALDI-MS m/z : 330.6 $[\text{M}]^+$. HRMS (ESI) m/z = 331.0794 $[\text{M}+\text{H}]^+$, calcd m/z = 331.0787 (Error = -1.9 ppm).

***N,N*-Diethyl-3-(naphthalen-2-ylthio)-2-naphthamide (79)**: *N*-(3-Dimethylaminopropyl)-*N'*-ethylcarbodiimide hydrochloride (EDC) (2339 mg, 12.20 mmol) and hydroxybenzotriazole monohydrate (HOBT· H_2O) (1869 mg, 12.20 mmol) were added to a solution of **78** (3357 mg, 10.17 mmol) dissolved in CH_2Cl_2 (70 mL). The resulting mixture was stirred at room temperature for 15 min. Then it was treated with diethylamine (2.10 mL, 20.34 mmol) and triethyl amine (3.1 mL, 20.34 mmol). The reaction stood under room temperature for 10 h. CH_2Cl_2 (50 mL) was added and the solution was washed with 0.5 N HCl (2x150 mL), 0.5 N NaOH (2x100 mL), brine (50 mL) and dried over Na_2SO_4 . The solvent was removed under vacuum and the crude product was subjected to column chromatography (silica, ethyl acetate/hexanes, 1:3) to obtain the pure product as an off-white solid (3365 mg, 86% yield). ^1H NMR (CDCl_3 , 400 MHz) δ 7.99 (s, 1H), 7.86-7.73 (m, 5H), 7.61 (dd, J = 7.4, 1.9 Hz, 1H), 7.54-7.40 (m, 5H), 3.63 (s, 2H), 3.19 (q, J = 7.1 Hz, 2H), 1.30 (t, J = 7.2 Hz, 3H), 1.09 (t, J = 7.1 Hz, 3H). ^{13}C NMR (CDCl_3 , 101 MHz) δ 169.03, 136.57, 133.91, 133.57, 132.68, 131.87, 131.78, 131.42, 131.23, 130.73, 129.56, 129.17, 127.93, 127.88, 127.67, 127.31, 127.15, 126.78, 126.74, 126.58, 125.87, 43.09, 39.08, 14.17, 12.83. MALDI-MS m/z : 385.1 $[\text{M}]^+$. HRMS (ESI) m/z = 386.1550 $[\text{M}+\text{H}]^+$, calcd m/z = 386.1573 (Error = 6.0 ppm).

13H-Dibenzo[*b,j*]thioxanthen-13-one (80): To a solution of **79** (3355 mg, 8.70 mmol) in THF (25 mL) was treated with LDA solution (2.0 M in THF/heptane/ethylbenzene, 21.8 mL, 43.50 mmol) at 0 °C. The reaction mixture was allowed to warm to room temperature for 4 h. Sat. NH₄Cl aq. (20 mL) was added to quench the reaction, followed by water (20 mL). The suspension was filtered and the yellow solid was washed with water and air-dried. The remaining solid was washed with CH₂Cl₂ several times to get rid of isomer **81** and other impurities to obtain pure **80** as a light yellow solid (1160 mg, 43%). ¹H NMR (CDCl₃, 400 MHz) δ 9.20 (s, 2H), 8.09 (d, J = 8.3 Hz, 2H), 8.03 (s, 2H), 7.85 (d, J = 8.3 Hz, 2H), 7.64 (t, J = 7.5 Hz, 2H), 7.54 (t, J = 7.3 Hz, 2H). ¹³C NMR (CDCl₃, 101 MHz, 55 °C) δ 135.44, 132.34, 132.05, 131.41, 130.29, 129.59, 127.33, 126.67, 126.31, 123.80, the signal for the carbonyl group was missing due to the poor solubility. MALDI-MS m/z: 312.6 [M]⁺. HRMS (ESI) m/z = 313.0689 [M+H]⁺, calcd m/z = 313.0682 (Error = -2.2 ppm). UV-Vis: λ_{max} (CHCl₃) = 360, 467 nm.

13-Phenyl-dibenzo[*b,j*]xanthen-13-ol (83) and **14-Phenyl-dibenzo[*a,i*]xanthen-14-ol (82):** To a solution of the crude mixture of **38** and **42** (163 mg, 0.55 mmol) in THF (10 mL) was treated with phenyllithium solution (1.8 M in dibutyl ether, 0.60 mL, 1.08 mmol) under ice bath. The reaction mixture was allowed to rise to room temperature and stood for 4 h. The reaction was quenched with sat. NH₄Cl aq. (10 mL), followed by water (20 mL). The mixture was extracted with CH₂Cl₂ (3x20 mL). The organic layers were combined and washed with water (2x15 mL), brine (15 mL), dried over Na₂SO₄. The solvent was removed under vacuum and the crude product was subjected to column chromatography (silica, ethyl acetate/hexanes, 1:20 to 1:15) to obtain **83** as a yellow solid (74 mg, 35% yield) and **82** as a yellowish green solid (57 mg, 27% yield). (**83**): ¹H NMR (CD₂Cl₂, 400 MHz) δ 8.13 (s, 2H), 7.84 (ddd, J = 10.3, 8.2, 1.2 Hz, 4H), 7.69

(s, 2H), 7.49 (ddd, $J = 8.2, 6.8, 1.3$ Hz, 2H), 7.40 (tdd, $J = 8.1, 7.0, 1.4$ Hz, 4H), 7.28-7.22 (m, 2H), 7.20-7.15 (m, 1H), 3.10 (s, 1H). ^{13}C NMR (CD_2Cl_2 , 101 MHz) δ 149.53, 147.99, 134.39, 131.11, 130.85, 128.76, 128.55, 127.72, 127.66, 127.45, 127.29, 126.22, 125.19, 112.43, 72.33. MALDI-MS m/z : 374.1 $[\text{M}]^+$. HRMS (ESI) $m/z = 357.1268$ $[\text{M-OH}]^+$, calcd $m/z = 357.1274$ (Error = 1.7 ppm). (**82**): ^1H NMR (CD_2Cl_2 , 400 MHz) δ 8.46-8.38 (m, 1H), 8.11 (s, 1H), 7.88 (d, $J = 8.9$ Hz, 1H), 7.83-7.74 (m, 3H), 7.63-7.55 (m, 3H), 7.49-7.40 (m, 2H), 7.37-7.22 (m, 5H), 7.16-7.09 (m, 1H), 3.25 (s, 1H). ^{13}C NMR (CD_2Cl_2 , 101 MHz) δ 149.61, 149.04, 146.78, 133.96, 132.02, 131.71, 130.94, 130.44, 129.68, 129.11, 128.77, 128.48, 127.41, 127.38, 127.13, 126.99, 126.81, 125.71, 125.04, 124.63, 118.30, 117.67, 111.87, 71.88. MALDI-MS m/z : 374.2 $[\text{M}]^+$. HRMS (ESI) $m/z = 357.1271$ $[\text{M-OH}]^+$, calcd $m/z = 357.1274$ (Error = 0.8 ppm).

13-Mesityl-13H-dibenzo[*b,i*]xanthen-13-ol (85): To a solution of 2-bromomesitylene (0.083 mL, 0.54 mmol) in dry THF (3 mL) was added *n*-BuLi (2.5 M in hexane, 0.43 mL, 1.08 mmol) at -78 °C. The colorless solution was stirred for 40 min and a suspension of the crude mixture of **38** and **42** (80 mg, 0.27 mmol) in dry THF (4 mL) was added dropwise. The reaction mixture was warmed up to room temperature for 3 h. The reaction was quenched with sat. NH_4Cl aq. (5 mL), followed by Water (10 mL). The mixture was extracted with CH_2Cl_2 (2x25 mL). The organic layers were combined and washed with brine (15 mL), dried over Na_2SO_4 . The solvent was removed under vacuum and the crude product was subjected to column chromatography (silica, ethyl acetate/hexanes, 1:20) to obtain crude **85** which was further subjected to recrystallization with CHCl_3 and hexanes to obtain pure **85** as a colorless crystal (37 mg, 33%). ^1H NMR (CDCl_3 , 400 MHz) 7.83 (d, $J = 8.2$ Hz, 2H), 7.69 (t, $J = 4.1$ Hz, 4H), 7.62 (s, 2H), 7.46 (ddd, $J = 8.2, 6.8, 1.2$ Hz, 2H), 7.33 (ddd, $J = 8.1, 6.8, 1.2$ Hz, 2H), 6.91 (s, 2H), 2.35 (s, 3H), 2.28-2.03 (brs, 3H), 2.20 (s, 1H).

^{13}C NMR (CDCl_3 , 101 MHz) δ 148.43, 137.73, 137.71, 136.97, 134.15, 131.95, 130.33, 130.17, 128.28, 127.53, 127.00, 126.88, 124.46, 112.17, 75.77, 24.69, 20.83. MALDI-MS m/z : 416.5 $[\text{M}]^+$. HRMS (ESI) m/z = 399.1741 $[\text{M}-\text{OH}]^+$, calcd m/z = 399.1743 (Error = 0.6 ppm).

13-(4-(Dimethylamino)phenyl)-13H-dibenzo[*b,i*]xanthen-13-ol (87): To a solution of 4-bromo-N,N-dimethylaniline (108 mg, 0.54 mmol) in dry THF (2 mL) was added n-BuLi (2.5 M in hexane, 0.43 mL, 1.08 mmol) at $-78\text{ }^\circ\text{C}$. The colorless solution was stirred for 1 h and a suspension of the crude mixture of **38** and **42** (80 mg, 0.27 mmol) in dry THF (4 mL) was added dropwise. The reaction mixture was stirred at room temperature overnight. The reaction was quenched with sat. NH_4Cl aq. (5 mL), followed by Water (10 mL). The mixture was extracted with CH_2Cl_2 (2x25 mL). The organic layers were combined and washed with brine (15 mL), dried over Na_2SO_4 . The solvent was removed under vacuum and the crude product was subjected to TLC preparative plate (silica, ethyl acetate/hexanes, 1:5) to obtain **87** (10 mg, 9%). ^1H NMR (CDCl_3 , 400 MHz) 8.16 (s, 2H), 7.86-7.78 (m, 4H), 7.64 (s, 2H), 7.46 (ddd, J = 8.3, 6.8, 1.2 Hz, 2H), 7.37 (ddd, J = 8.0, 6.8, 1.2 Hz, 2H), 7.25-7.16 (m, 2H), 6.62-6.53 (m, 2H), 2.88 (brs, 1H), 2.87 (s, 6H). ^{13}C NMR (CDCl_3 , 101 MHz) δ 149.69, 149.52, 134.77, 133.86, 131.26, 130.44, 128.29, 127.07, 126.93, 126.90, 126.79, 124.58, 112.11, 112.07, 72.18, 40.57. MALDI-MS m/z : 417.7 $[\text{M}]^+$. HRMS (ESI) m/z = 418.1783 $[\text{M}+\text{H}]^+$, calcd m/z = 418.1802 (Error = 4.3 ppm).

5,13-Diphenyl-13H-dibenzo[*b,i*]xanthen-13-ol (88): To a solution of **74** (69 mg, 0.19 mmol) in THF (10 mL) was treated with phenyllithium solution (1.8 M in dibutyl ether, 0.21 mL, 0.38 mmol) under ice bath. The reaction mixture was allowed to rise to room temperature and stood for 4 h. The reaction was quenched with sat. NH_4Cl aq. (10 mL), followed by water (10 mL). The mixture was extracted with CH_2Cl_2 (2x25 mL). The organic layers were combined and washed

with brine (15 mL), dried over Na₂SO₄. The solvent was removed under vacuum and the crude product was subjected to column chromatography (silica, ethyl acetate/hexanes, 1:10) to obtain pure **88** as a light yellow solid (58 mg, 70% yield). ¹H NMR (CD₂Cl₂, 400 MHz) δ 8.21 (s, 1H), 8.14 (s, 1H), 7.89-7.83 (m, 1H), 7.80 (d, J = 8.2 Hz, 1H), 7.75 (d, J = 8.2 Hz, 1H), 7.68-7.49 (m, 6H), 7.49-7.33 (m, 7H), 7.31-7.24 (m, 2H), 7.23-7.15 (m, 1H), 3.21 (s, 1H). ¹³C NMR (CD₂Cl₂, 126 MHz) δ 149.67, 147.67, 146.20, 135.98, 134.34, 133.47, 131.89, 131.75, 131.33, 131.27, 130.90, 130.80, 128.86, 128.83, 128.80, 128.57, 128.09, 127.79, 127.40, 127.35, 127.27, 127.26, 127.03, 126.36, 125.93, 125.25, 125.20, 125.06, 72.82. MALDI-MS m/z: 450.7 [M]⁺. HRMS (ESI) m/z = 433.1579 [M-OH]⁺, calcd m/z = 433.1587 (Error = 1.7 ppm).

13-Mesityl-5-phenyl-13H-dibenzo[*b,i*]xanthen-13-ol (89): To a solution of 2-bromomesitylene (0.017 mL, 0.113 mmol) in dry THF (1 mL) was added n-BuLi (2.5 M in hexane, 0.09 mL, 0.224 mmol) at -78 °C. The colorless solution was stirred for 40 min and a solution of **74** (21 mg, 0.056 mmol) in dry THF (2 mL) was added dropwise. The reaction mixture was stirred under room temperature overnight. The reaction was quenched with sat. NH₄Cl aq. (5 mL), followed by water (10 mL). The mixture was extracted with CH₂Cl₂ (2x15 mL). The organic layers were combined and washed with brine (15 mL), dried over Na₂SO₄. The solvent was removed under vacuum and the crude product was subjected to column chromatography (silica, ethyl acetate/hexanes, 1:20) to obtain crude **89** as a yellow oil which was further subjected to trituration with cold hexanes to obtain pure **89** as a light yellow solid (20 mg, 71%). ¹H NMR (CD₂Cl₂, 500 MHz) δ 7.77-7.70 (m, 2H), 7.70-7.52 (m, 9H), 7.45-7.28 (m, 5H), 6.94 (s, 2H), 2.39 (s, 1H), 2.35 (s, 3H), 2.26-2.11 (m, 6H). ¹³C NMR (CD₂Cl₂, 126 MHz) δ 148.41, 144.97, 137.79, 137.63, 136.99, 135.71, 134.06, 133.31, 131.97, 131.50, 131.43, 130.29, 130.19, 130.11, 129.97,

129.24, 128.49, 128.39, 128.33, 128.24, 127.56, 127.18, 127.13, 126.91, 126.88, 126.76, 125.54, 124.69, 124.40, 124.28, 112.44, 76.17, 24.76, 20.84. HRMS (ESI) $m/z = 475.2043 [M-OH]^+$, calcd $m/z = 475.2056$ (Error = 2.9 ppm).

13-Phenyl-13H-dibenzo[*b,j*]thioxanthen-13-ol (90): To a suspension of **80** (50 mg, 0.16 mmol) in THF (5 mL) was treated with phenyllithium solution (1.8 M in dibutyl ether, 0.27 mL, 0.48 mmol) under ice bath. The reaction mixture was allowed to rise to room temperature and stood for 4 h. The reaction was quenched with sat. NH_4Cl aq. (5 mL), followed by water (20 mL). The mixture was extracted with CH_2Cl_2 (40 mL). The organic layers were combined and washed with brine (10 mL), dried over Na_2SO_4 . The solvent was removed under vacuum and the crude product was subjected to column chromatography (silica, ethyl acetate/hexanes, 1:10) to obtain pure **90** as an off-white solid (57 mg, 90% yield). 1H NMR ($CDCl_3$, 400 MHz) δ 8.61 (s, 2H), 7.97 (m, 4H), 7.85-7.75 (m, 2H), 7.56-7.47 (m, 4H), 7.24-7.17 (m, 1H), 7.17-7.09 (m, 2H), 7.01-6.92 (m, 2H), 2.99 (s, 1H). ^{13}C NMR ($CDCl_3$, 101 MHz) δ 143.09, 139.35, 132.72, 132.16, 130.27, 128.53, 128.36, 128.33, 127.51, 126.95, 126.88, 126.14, 125.86, 124.97, 78.46. MALDI-MS m/z : 390.0 $[M]^+$. HRMS (ESI) $m/z = 373.1052 [M-OH]^+$, calcd $m/z = 373.1045$ (Error = -1.6 ppm).

13-Mesityl-13H-dibenzo[*b,j*]thioxanthen-13-ol (91): To a solution of 2-bromomesitylene (0.07 mL, 0.45 mmol) in dry THF (2 mL) was added *n*-BuLi (2.5 M in hexane, 0.36 mL, 0.90 mmol) at -78 °C. The colorless solution was stirred for 40 min and a suspension of **80** (47 mg, 0.15 mmol) in dry THF (4 mL) was added dropwise. The reaction mixture was warmed to room temperature for 4 h. The reaction was quenched with sat. NH_4Cl aq. (5 mL), followed by water (10 mL). The mixture was extracted with EtOAc (2x20 mL). The organic layers were combined and washed with brine, dried over Na_2SO_4 . The solvent was removed under vacuum and the crude product

was subjected to column chromatography (silica, ethyl acetate/hexanes, 1:20) to obtain crude **91** which was further subjected to trituration with cold hexanes to obtain pure **91** as an off-white solid (47 mg, 72%). ¹H NMR (CDCl₃, 400 MHz) δ 7.96 (s, 2H), 7.76 (d, J = 8.3 Hz, 2H), 7.63 (d, J = 8.2 Hz, 2H), 7.57 (s, 2H), 7.46 (ddd, J = 8.2, 6.8, 1.3 Hz, 2H), 7.35 (ddd, J = 8.2, 6.7, 1.2 Hz, 2H), 6.96 (s, 2H), 2.61 (s, 1H), 2.42 (s, 3H), 2.12 (brs, 6H). ¹³C NMR (CDCl₃, 101 MHz) δ 138.48, 138.18, 137.12, 136.86, 132.84, 132.08, 131.94, 128.64, 127.98, 127.88, 127.20, 126.44, 125.52, 124.05, 81.45, 24.84, 20.91. MALDI-MS m/z: 431.8 [M]⁺. HRMS (ESI) m/z = 415.1537 [M-OH]⁺, calcd m/z = 415.1515 (Error = -5.4 ppm).

13-(2,6-Dimethylphenyl)-13H-dibenzo[*b*,*j*]thioxanthen-13-ol (92): To a solution of 2-bromo-1,3-dimethylbenzene (0.04 mL, 0.29 mmol) in dry THF (2 mL) was added n-BuLi (2.5 M in hexane, 0.13 mL, 0.32 mmol) at -78 °C. The colorless solution was stirred for 50 min and a suspension of **80** (60 mg, 0.19 mmol) in dry THF (3 mL) was added dropwise. The reaction mixture was warmed to room temperature for 3 h. The reaction was quenched with sat. NH₄Cl aq. (5 mL), followed by water (10 mL). The mixture was extracted with EtOAc (2x20 mL). The organic layers were combined and washed with brine, dried over Na₂SO₄. The solvent was removed under vacuum and the crude product was subjected to column chromatography (silica, ethyl acetate/hexanes, 1:15) to obtain crude **92** which was further subjected to trituration with cold hexanes to obtain pure **92** as a light brown solid (44 mg, 55%). ¹H NMR (CDCl₃, 400 MHz) δ 7.96 (s, 2H), 7.76 (d, J = 8.3 Hz, 2H), 7.61 (d, J = 8.2 Hz, 2H), 7.53 (s, 2H), 7.47 (ddd, J = 8.2, 6.8, 1.3 Hz, 2H), 7.36 (ddd, J = 8.1, 6.8, 1.2 Hz, 2H), 7.27 (t, J = 7.9 Hz, 1H), 7.14 (d, J = 7.5 Hz, 2H), 2.53 (s, 1H), 2.16 (brs, 6H). ¹³C NMR (CDCl₃, 101 MHz) δ 140.25, 138.39, 138.31, 132.86, 132.07,

131.17, 128.63, 127.90, 127.87, 127.60, 127.27, 126.46, 125.59, 124.08, 81.53, 24.99. MALDI-MS m/z: 417.8 [M]⁺.

13-(4-Methylphenyl)-13H-dibenzo[*b,i*]thioxanthen-13-ol (93): To a solution of 1-bromo-4-methylbenzene (50 mg, 0.29 mmol) in dry THF (2 mL) was added n-BuLi (1 M in hexane, 0.32 mL, 0.32 mmol) at -78 °C. The colorless solution was stirred for 1 h and a suspension of **80** (60 mg, 0.19 mmol) in dry THF (3 mL) was added dropwise. The reaction mixture was warmed to room temperature for 4 h. The reaction was quenched with sat. NH₄Cl aq. (5 mL), followed by water (10 mL). The mixture was extracted with EtOAc (20 mL). The organic layers were washed with brine, dried over Na₂SO₄. The solvent was removed under vacuum and the crude product was subjected to column chromatography (silica, ethyl acetate/hexanes, 1:10) to obtain crude **93** which was further subjected to trituration with cold hexanes to obtain pure **93** as a white solid (31 mg, 40%). ¹H NMR (CDCl₃, 400 MHz) δ 8.60 (s, 2H), 8.04-7.91 (m, 4H), 7.87-7.75 (m, 2H), 7.59-7.44 (m, 4H), 6.99 (d, J = 8.1, 2H), 6.88-6.78 (m, 2H), 2.97 (s, 1H), 2.23 (s, 3H). ¹³C NMR (CDCl₃, 101 MHz) δ 140.19, 139.47, 138.19, 132.68, 132.15, 130.24, 129.06, 128.52, 127.43, 126.88, 126.87, 126.09, 125.83, 124.88, 78.25, 21.20. MALDI-MS m/z: 404.2 [M]⁺.

13-(4-Methoxyphenyl)-13H-dibenzo[*b,i*]thioxanthen-13-ol (94): To a solution of 4-bromoanisole (0.08 mL, 0.64 mmol) in dry THF (2 mL) was added n-BuLi (2.5 M in hexane, 0.51 mL, 1.28 mmol) at -78 °C. The colorless solution was stirred for 1 h and a suspension of **80** (50 mg, 0.16 mmol) in dry THF (2.5 mL) was added dropwise. The reaction mixture was warmed to room temperature for 6 h. The reaction was quenched with sat. NH₄Cl aq. (3 mL), followed by water (10 mL). The resulting suspension was filtered to recover 25 mg of **80**. The filtrate was extracted with EtOAc (2x20 mL). The organic layers were combined and washed with brine,

dried over Na₂SO₄. The solvent was removed under vacuum and the crude product was subjected to column chromatography (silica, ethyl acetate/hexanes, 1:6) to obtain **94** as a white solid (15 mg, 22%). ¹H NMR (CDCl₃, 400 MHz) δ 8.60 (s, 2H), 7.99-7.94 (m, 4H), 7.84-7.75 (m, 2H), 7.57-7.46 (m, 4H), 6.90-6.81 (m, 2H), 6.67-6.59 (m, 2H), 3.69 (s, 3H), 2.96 (s, 1H). ¹³C NMR (CDCl₃, 101 MHz) δ 159.40, 139.52, 135.16, 132.66, 132.14, 130.22, 128.91, 128.51, 126.89, 126.87, 126.10, 125.82, 124.81, 113.57, 78.05, 55.29. MALDI-MS m/z: 419.9 [M]⁺. HRMS (ESI) m/z = 403.1137 [M-OH]⁺, calcd m/z = 403.1151 (Error = 3.5 ppm).

13-(4-(Trifluoromethyl)phenyl)-13H-dibenzo[*b,i*]thioxanthen-13-ol (95): To a solution of 1-bromo-4-(trifluoromethyl)benzene (0.04 mL, 0.29 mmol) in dry THF (2 mL) was added n-BuLi (1.1 M in hexane, 0.29 mL, 0.32 mmol) at -40 °C. The colorless solution was stirred for 50 min and a suspension of **80** (60 mg, 0.19 mmol) in dry THF (3 mL) was added dropwise. The reaction mixture was warmed to room temperature for 2 h. The reaction was quenched with sat. NH₄Cl aq. (5 mL), followed by water (10 mL). The mixture was extracted with EtOAc (2x20 mL). The organic layers were combined and washed with brine, dried over Na₂SO₄. The solvent was removed under vacuum and the crude product was subjected to column chromatography (silica, ethyl acetate/hexanes, 1:10) to obtain crude **95** which was further subjected to trituration with cold hexanes to obtain pure **95** as a white solid (60 mg, 68%). ¹H NMR (CDCl₃, 500 MHz) δ 8.57 (s, 2H), 8.00-7.93 (m, 4H), 7.85-7.78 (m, 2H), 7.58-7.48 (m, 4H), 7.38 (d, J = 8.4 Hz, 2H), 7.16-7.10 (m, 2H), 3.02 (s, 1H). ¹³C NMR (CDCl₃, 126 MHz) δ 146.93, 138.76, 132.87, 129.88, 128.54, 127.93, 127.26, 126.94, 126.37, 126.00, 125.27 (q, J = 3.7 Hz, CF₃), 125.04, 124.81, 78.02. LDI-MS m/z: 457.8 [M]⁺.

13*H*-dibenzo[*b,i*]thioxanthen-13-ol (98): To a suspension of **80** (42 mg, 0.13 mmol) in 95% ethanol (5 mL) was treated with sodium borohydride (50 mg, 1.34 mmol). The reaction mixture was refluxed for 6 h under argon. Then it was cooled to room temperature and water (5 mL) was added to quench the reaction. The resulting precipitate was washed with water to yield **98** as a white solid (26 mg, 62%). ¹H NMR (CDCl₃, 500 MHz) δ 8.15 (s, 2H), 8.01 (s, 2H), 7.93-7.85 (m, 2H), 7.82-7.76 (m, 2H), 7.55-7.42 (m, 4H), 5.88 (d, *J* = 7.0 Hz, 1H), 2.79 (d, *J* = 7.0 Hz, 1H). ¹³C NMR (CDCl₃, 101 MHz) δ 136.50, 132.77, 132.35, 129.73, 128.17, 127.03, 126.91, 126.18, 125.88, 124.92, 72.56. MALDI-MS *m/z*: 314.1 [M]⁺.

13-Phenyldibenzo[*b,i*]xanthen-6-ium tetrafluoroborate (99): To a solution of **83** (41 mg, 0.11 mmol) in CH₂Cl₂ (5 mL) was added HBF₄·Et₂O (0.09 mL, 0.66 mmol) under room temperature. The reaction mixture immediately turned from yellow to deep red and was further stirred for 5 h. Ether (12 mL) was carefully placed on the reaction mixture. Slow diffusion (12 h) led to the formation of the precipitate which was filtered and washed with ether. The resulting solid was dried in the vacuum oven (65 °C, 6h) to give the product as a dark purple solid (48 mg, 99% yield). ¹H NMR (CD₃CN, 400 MHz) δ 8.97 (s, 2H), 8.62 (s, 2H), 8.30-8.22 (m, 4H), 8.06-7.98 (m, 3H), 7.96-7.91 (m, 2H), 7.88 (dt, *J* = 7.2, 1.5 Hz, 2H), 7.72 (ddd, *J* = 8.0, 6.8, 1.1 Hz, 2H). ¹³C NMR (CD₃CN, 101 MHz) δ 181.34, 153.02, 143.46, 140.54, 136.91, 133.69, 132.75, 132.56, 132.42, 130.10, 128.87, 128.57, 123.35, 115.38. MALDI-MS *m/z*: 357.3 [M-BF₄]⁺. HRMS (ESI) *m/z* = 357.1260 [M-BF₄]⁺, calcd *m/z* = 357.1274 (Error = 4.0 ppm). UV-Vis-NIR: λ_{max} (CH₂Cl₂) = 233, 299, 451, 519, 555, 730, 804 nm.

14-Phenyldibenzo[*α,i*]xanthen-7-ium tetrafluoroborate (100): To a solution of **82** (37 mg, 0.10 mmol) in CH₂Cl₂ (5 mL) was added HBF₄·Et₂O (0.09 mL, 0.65 mmol) under room temperature.

The reaction mixture immediately turned from yellow to deep red and was further stirred for 5 h. Ether (12 mL) was carefully placed on the reaction mixture. Slow diffusion (12 h) led to the formation of the precipitate which was filtered and washed with ether. The resulting solid was dried in the vacuum oven (65 °C, 6h) to give the product as a dark green solid (41 mg, 93% yield). ^1H NMR (CD_3CN , 400 MHz) δ 9.00 (d, J = 9.2 Hz, 1H), 8.87 (s, 1H), 8.76 (s, 1H), 8.36 (d, J = 8.6 Hz, 1H), 8.29-8.19 (m, 3H), 8.03-7.86 (m, 4H), 7.84-7.73 (m, 2H), 7.66-7.59 (m, 2H), 7.55 (ddd, J = 8.7, 7.2, 1.5 Hz, 1H), 7.37 (d, J = 8.6 Hz, 1H). ^{13}C NMR (101 MHz, CD_3CN) δ 172.12, 166.67, 152.79, 150.10, 140.18, 136.07, 135.22, 134.32, 133.15, 133.11, 132.59, 132.50, 132.46, 131.56, 131.47, 130.57, 130.49, 129.23, 129.06, 128.70, 128.55, 124.08, 122.69, 119.53, 115.90. MALDI-MS m/z : 357.4 $[\text{M}-\text{BF}_4]^+$. HRMS (ESI) m/z = 357.1270 $[\text{M}-\text{BF}_4]^+$, calcd m/z = 357.1274 (Error = 1.7 ppm). UV-Vis-NIR: λ_{max} (CH_2Cl_2) = 247, 305, 406, 500 nm.

13-Mesityldibenzo[*b,j*]xanthen-6-ium tetrafluoroborate (101): To a solution of **85** (29 mg, 0.07 mmol) in CH_2Cl_2 (4 mL) was added $\text{HBF}_4 \cdot \text{Et}_2\text{O}$ (0.05 mL, 0.35 mmol) under room temperature. The reaction mixture immediately turned from yellow to deep red and was further stirred for 5 h. Ether (10 mL) was carefully placed on the reaction mixture. Slow diffusion (5 h) led to the formation of the precipitate which was filtered and washed with ether. The resulting solid was dried in the vacuum oven (60 °C, 3 h) to give the product as a dark purple solid (26 mg, 77% yield). ^1H NMR (CD_3CN , 400 MHz) δ 9.00-7.20 (broad and indiscernible aromatic signals), 2.56 (s, 3H), 1.91 (s, 6H). ^{13}C NMR (CD_3CN , 101 MHz) δ 142.47, 129.87, 21.43, 20.40. MALDI-MS m/z : 399.8 $[\text{M}-\text{BF}_4]^+$. HRMS (ESI) m/z = 399.1734 $[\text{M}-\text{BF}_4]^+$, calcd m/z = 399.1743 (Error = 2.4 ppm). UV-Vis-NIR: λ_{max} (CH_2Cl_2) = 231, 299, 451, 521, 558, 723, 807 nm.

13-(4-(Dimethylamino)phenyl)dibenzo[*b,i*]xanthen-6-ium (102): To a solution of **87** (10 mg, 0.024 mmol) in CH₂Cl₂ (1 mL) was added HBF₄·Et₂O (0.02 mL, 0.12 mmol) under room temperature. The reaction mixture immediately turned from yellow to deep red and was further stirred overnight. Ether (3 mL) was carefully placed on the reaction mixture. Slow diffusion (12 h) led to the formation of the precipitate which was filtered and washed with ether. The resulting solid was dried in the vacuum oven (60 °C, 4 h) to give the product as a black solid which was not pure and contained lots of starting materials.

5,13-Diphenyldibenzo[*b,i*]xanthen-6-ium tetrafluoroborate (103): To a solution of **88** (49 mg, 0.11 mmol) in CH₂Cl₂ (4 mL) was added HBF₄·Et₂O (0.08 mL, 0.55 mmol) under room temperature. The reaction mixture immediately turned from yellow to deep red and was further stirred for 5 h. Ether (12 mL) was slowly added to the reaction mixture. The formed dark purple precipitate was collected by vacuum filtration and washed with ether. The resulting solid was dried in the vacuum oven (60 °C, 3h) to give the product as a dark purple solid (25 mg, 44% yield). ¹H NMR (CD₂Cl₂, 500 MHz) δ 8.96 (s, 1H), 8.89 (s, 1H), 8.34 (s, 1H), 8.26 (d, *J* = 8.5 Hz, 1H), 8.19 (d, *J* = 8.6 Hz, 1H), 8.13 (d, *J* = 8.5 Hz, 1H), 8.07-7.92 (m, 6H), 7.91-7.86 (m, 2H), 7.78-7.71 (m, 5H), 7.69-7.64 (m, 2H). ¹³C NMR (126 MHz, CD₂Cl₂) δ 180.31, 152.56, 149.18, 143.31, 142.33, 139.38, 139.11, 136.84, 136.69, 133.75, 132.78, 132.58, 132.40, 132.34, 132.01, 131.94, 131.46, 130.04, 129.86, 129.75, 128.87, 128.61, 128.28, 127.12, 122.39, 115.58. MALDI-MS *m/z*: 433.9 [M-BF₄]⁺. HRMS (ESI) *m/z* = 433.1610 [M-BF₄]⁺, calcd *m/z* = 433.1587 (Error = -5.3 ppm). UV-Vis-NIR: λ_{max} (CH₂Cl₂) = 232, 303, 453, 531, 565, 746, 818 nm.

13-Mesityl-5-phenyldibenzo[*b,i*]xanthen-6-ium tetrafluoroborate (104): To a solution of **89** (18 mg, 0.037 mmol) in ether (1 mL) was added HBF₄·Et₂O (0.05 mL, 0.37 mmol) under room

temperature. The reaction mixture immediately turned from yellow to deep red and was further stirred for 6 h. Due to good solubility, **102** could not be precipitated out by either using hexanes or benzene. The solvent was removed under vacuum to obtain the crude product as a viscose oil which was washed with hexanes and dried in the vacuum oven (55 °C, 6 h) to give the unpurified product as a dark purple solid (21 mg, quantitative yield). ^1H NMR (CD_2Cl_2 , 500 MHz) δ 9.10-7.90 (broad and indiscernible aromatic signals), 7.84-7.73 (m, 5H), 7.72-7.65 (m, 2H), 7.35 (s, 2H), 2.60 (s, 3H), 1.96 (s, 6H). ^{13}C NMR (CD_2Cl_2 , 126 MHz) δ 142.81, 132.36, 131.42, 129.98, 129.90, 129.79, 21.73, 20.72. MALDI-MS m/z : 475.5 $[\text{M-BF}_4]^+$. HRMS (ESI) m/z = 475.2081 $[\text{M-BF}_4]^+$, calcd m/z = 475.2056 (Error = -5.1 ppm). UV-Vis-NIR: λ_{max} (CH_2Cl_2) = 230, 304, 452, 533, 568, 748, 820 nm.

13-Phenyldibenzo[*b,i*]thioxanthen-6-ium tetrafluoroborate (105): To a solution of **90** (50 mg, 0.13 mmol) in CH_2Cl_2 (3 mL) was added $\text{HBF}_4 \cdot \text{Et}_2\text{O}$ (0.09 mL, 0.65 mmol) under room temperature. The reaction mixture immediately turned from yellow to deep red and was further stirred for 5 h. Ether (10 mL) was carefully placed on the reaction mixture. Slow diffusion (14 h) led to the formation of the precipitate which was filtered and washed with ether. The resulting solid was dried in the vacuum oven (55 °C, 8 h) to give the product as a dark purple solid (41 mg, 68% yield). ^1H NMR (CD_2Cl_2 , 400 MHz) δ 9.06 (d, J = 6.0 Hz, 4H), 8.25 (d, J = 8.5 Hz, 2H), 8.15 (d, J = 8.6 Hz, 2H), 8.08 (ddd, J = 8.3, 6.7, 1.2 Hz, 2H), 8.00-7.93 (m, 1H), 7.93-7.85 (m, 2H), 7.79 (ddd, J = 8.2, 6.7, 1.1 Hz, 2H), 7.74-7.64 (m, 2H). ^{13}C NMR (101 MHz, CD_2Cl_2) δ 179.05, 143.79, 138.85, 138.78, 136.84, 135.31, 133.14, 132.21, 132.03, 130.91, 129.53, 127.90, 127.39, 126.17. MALDI-MS m/z : 373.4 $[\text{M-BF}_4]^+$. HRMS (ESI) m/z = 373.1069 $[\text{M-BF}_4]^+$, calcd m/z

= 373.1045 (Error = -6.2 ppm). UV-Vis-NIR: λ_{\max} (CH₂Cl₂) = 240, 324, 449, 523, 557, 745, 822 916 nm.

13-Mesityldibenzo[*b,i*]thioxanthen-6-ium tetrafluoroborate (106): To a solution of **91** (41 mg, 0.095 mmol) in CH₂Cl₂ (3 mL) was added HBF₄·Et₂O (0.07 mL, 0.48 mmol) under room temperature. The reaction mixture immediately turned from yellow to deep red and was further stirred for 6 hours. Ether (12 mL) was carefully placed on the reaction mixture. Slow diffusion (11 h) led to the formation of the precipitate which was filtered and washed with ether. The resulting solid was dried in the vacuum oven (60 °C, 8 h) to give the product as dark purple crystals (36 mg, 76% yield). ¹H NMR (CD₂Cl₂, 400 MHz) δ 9.80-7.00 (broad and indiscernible aromatic signals), 2.61 (s, 3H), 1.83 (s, 6H). ¹³C NMR (CD₂Cl₂, 101 MHz) δ 142.07, 129.87, 21.72, 20.48. ¹H NMR (CD₂Cl₂, 500 MHz, after rise to room temperature from -27 °C (**Figure 26**) in VT-NMR) δ 9.13 (s, 2H), 8.97 (s, 2H), 8.28 (d, *J* = 8.5 Hz, 2H), 8.15 (d, *J* = 8.6 Hz, 2H), 8.13-8.05 (m, 2H), 7.80 (ddd, *J* = 8.4, 6.8, 1.0 Hz, 2H), 7.32 (s, 2H), 2.61 (s, 3H), 1.82 (s, 6H). ¹³C NMR (CD₂Cl₂, 126 MHz, after rise to room temperature from -27 °C (**Figure 26**) in VT-NMR) δ 181.96, 142.06, 141.48, 139.24, 138.62, 136.77, 136.42, 133.74, 132.10, 131.96, 129.83, 129.59, 128.05, 127.05, 126.68, 21.73, 20.50. LDI-MS *m/z*: 415.3 [M-BF₄]⁺. HRMS (ESI) *m/z* = 415.1540 [M-BF₄]⁺, calcd *m/z* = 415.1515 (Error = -6.0 ppm). UV-Vis-NIR: λ_{\max} (CH₂Cl₂) = 242, 324, 448, 525, 558, 736, 819 916 nm.

13-(2,6-Dimethylphenyl)dibenzo[*b,i*]thioxanthen-6-ium tetrafluoroborate (107): To a solution of **92** (32 mg, 0.076 mmol) in CH₂Cl₂ (4 mL) was added HBF₄·Et₂O (0.052 mL, 0.38 mmol) under room temperature. The reaction mixture immediately turned from yellow to deep red and was further stirred for 5 hours. Ether (12 mL) was carefully placed on the reaction mixture. Slow

diffusion (17 h) led to the formation of the precipitate which was filtered and washed with ether. The resulting solid was dried in the vacuum oven (60 °C, 10 h) to give the product as dark purple crystal flakes (32 mg, 86% yield). ^1H NMR (CD_2Cl_2 , 400 MHz) δ 9.50-7.40 (broad and indiscernible aromatic signals), 7.72 (t, $J = 7.6$ Hz, 1H), 1.86 (s, 6H). ^{13}C NMR (CD_2Cl_2 , 101 MHz) δ 131.69, 129.14, 20.58. LDI-MS m/z : 401.8 $[\text{M-BF}_4]^+$. UV-Vis-NIR: λ_{max} (CH_2Cl_2) = 242, 324, 450, 520, 560, 734, 822 919 nm.

13-(4-Methylphenyl)dibenzo[*b,i*]thioxanthen-6-ium tetrafluoroborate (108): To a solution of **93** (31 mg, 0.077 mmol) in CH_2Cl_2 (4 mL) was added $\text{HBF}_4 \cdot \text{Et}_2\text{O}$ (0.05 mL, 0.39 mmol) under room temperature. The reaction mixture immediately turned from yellow to deep red and was further stirred for 5 hours. Ether (12 mL) was carefully placed on the reaction mixture. Slow diffusion (12 h) led to the formation of the precipitate which was filtered and washed with ether. The resulting solid was dried in the vacuum oven (60 °C, 10 h) to give the product as a dark purple solid (22 mg, 61% yield). ^1H NMR (CD_2Cl_2 , 400 MHz) δ 9.09 (s, 2H), 9.02 (s, 2H), 8.24 (d, $J = 8.5$ Hz, 2H), 8.15 (d, $J = 8.6$ Hz, 2H), 8.07 (t, $J = 7.6$ Hz, 2H), 7.84-7.75 (m, 2H), 7.69 (d, $J = 7.7$ Hz, 2H), 7.60 (d, $J = 7.7$ Hz, 2H), 2.71 (s, 3H). ^{13}C NMR (CD_2Cl_2 , 101 MHz) δ 179.81, 144.01, 143.42, 138.75, 138.58, 136.70, 133.08, 132.50, 132.02, 131.29, 130.18, 129.43, 127.86, 127.50, 126.07, 22.08. LDI-MS m/z : 387.7 $[\text{M-BF}_4]^+$. UV-Vis-NIR: λ_{max} (CH_2Cl_2) = 239, 324, 447, 520, 555, 757, 815, 909 nm.

13-(4-Methoxyphenyl)dibenzo[*b,i*]thioxanthen-6-ium tetrafluoroborate (109): To a solution of **94** (13 mg, 0.031 mmol) in CH_2Cl_2 (2 mL) was added $\text{HBF}_4 \cdot \text{Et}_2\text{O}$ (0.043 mL, 0.31 mmol) under room temperature. The reaction mixture immediately turned from yellow to deep red and was further stirred for 5 h. Ether (6 mL) was carefully placed on the reaction mixture. Slow diffusion

(12 h) led to the formation of the precipitate which was filtered and washed with ether. The resulting solid was dried in the vacuum oven (55 °C, 10 h) to give the product as dark purple solid (7 mg, 47% yield) which contained lots of starting material. ^1H NMR (CD_2Cl_2 , 400 MHz) δ 9.15 (s, 2H), 8.98 (s, 2H), 8.23 (d, J = 8.5 Hz, 2H), 8.18 (d, J = 8.6 Hz, 2H), 8.07 (t, J = 7.6 Hz, 2H), 7.79 (t, J = 7.5 Hz, 2H), 7.69 (d, J = 8.1 Hz, 2H), 7.41 (d, J = 8.0 Hz, 2H), 4.11 (s, 3H). MALDI-MS m/z : 403.3 $[\text{M-BF}_4]^+$. HRMS (ESI) m/z = 403.1131 $[\text{M-BF}_4]^+$, calcd m/z = 403.1151 (Error = 4.9 ppm). UV-Vis-NIR: λ_{max} (CH_2Cl_2) = 235, 324, 444, 522, 551, 743, 810, 906 nm.

13-(4-(Trifluoromethyl)phenyl)dibenzo[*b,i*]thioxanthen-6-ium tetrafluoroborate (110): To a solution of **95** (51 mg, 0.11 mmol) in CH_2Cl_2 (4 mL) was added $\text{HBF}_4 \cdot \text{Et}_2\text{O}$ (0.08 mL, 0.55 mmol) under room temperature. The reaction mixture immediately turned from yellow to deep red and was further stirred for 5 h. Ether (12 mL) was carefully placed on the reaction mixture. Slow diffusion (12 h) led to the formation of the precipitate which was filtered and washed with ether. The resulting solid was dried in the vacuum oven (60 °C, 9 h) to give the product as a dark purple solid (54 mg, 92% yield). ^1H NMR (CD_2Cl_2 , 400 MHz) δ 9.12 (s, 2H), 8.92 (s, 2H), 8.26 (d, J = 8.5 Hz, 2H), 8.17 (d, J = 8.3 Hz, 4H), 8.09 (t, J = 7.7 Hz, 2H), 7.89 (d, J = 7.9 Hz, 2H), 7.80 (t, J = 7.7 Hz, 2H). ^{13}C NMR (101 MHz, CD_2Cl_2) δ 175.99 (C-13), 126.74 (q, J = 3.6 Hz, CF_3). LDI-MS m/z : 441.7 $[\text{M-BF}_4]^+$. UV-Vis-NIR: λ_{max} (CH_2Cl_2) = 243, 324, 455, 530, 565, 764, 837 945 nm.

CHAPTER 3

Summary and conclusions

3.1 Summary

3.1.1 Summary of syntheses

Linearly extended pyrylium salts (LEPS) and linearly extended thiopyrylium salts (LETS) were synthesized within six steps in moderate to high yields in each step.

An LDA-mediated ring closure reaction was successfully applied in the syntheses of dibenzoxanthone intermediate **38** and dibenzothioxanthone intermediate **80**. In this way, linear dibenzoxanthone **38** and its bent isomer **42** were generated in a 1:1 molar ratio. The separation is difficult due to their similar polarities and poor solubilities. However, linear dibenzothioxanthone **80** and its bent isomer **81** were generated in a 4:1 molar ratio and they were readily separated because of their highly different solubilities.

Two regiospecific synthetic routes were attempted for dibenzoxanthone intermediate **38**. Synthesis through tandem intermolecular nucleophilic coupling involving a naphthalene intermediate was successful to generate **38** regiospecifically in low yield. Synthesis through Pd-catalyzed annulation was not successful due to difficulties in synthesizing and purifying the 2,3-dibromonaphthalene intermediate.

Through an LDA-mediated ring closure reaction, linear dibenzoxanthone **74** was synthesized from α -phenyl blocked amide intermediate **73** in high yield and without forming any bent isomer.

A series of dibenzoxanthenol and dibenzothioxanthenol intermediates for LEPS and LETS compounds were successfully synthesized either by hydride reduction or nucleophilic organolithium attack at the carbonyl groups of the corresponding dibenzoxanthenones and dibenzothioxanthenone. Lithium-halogen exchange for 4-dimethylamino phenyl bromide is low yielding, hindering formation of the corresponding dibenzoxanthenol intermediate **87**.

By treating the dibenzoxanthenols and dibenzothioxanthenols with non-oxidative fluoroboric acid, a series of LEPS and LETS compounds were generated in moderate to high yield.

3.1.2 Summary of properties

The LEPS and LETS compounds show moderate to good solubilities in organic solvents like acetonitrile and dichloromethane. The nature and number of phenyl substituents determine the solubility of LEPS and LETS compounds. LEPS **104** with one mesityl and one phenyl substituent shows excellent solubility in several organic solvents including diethyl ether which is typically applied to precipitate other pyrylium salts. Thus, purification by precipitation and solvent washing was difficult for **104**.

Depending on their substituents, LEPS and LETS compounds show variable sensitivity to moisture. Placing mesityl or 2',6'-dimethylphenyl substituents at the C-13 position of LEPS and LETS compounds improves their resistance to moisture compared to other LEPS and LETS compounds. This is due to the steric shielding of the C-13 position by the *o*-methyl groups.

LEPS and LETS compounds all have a formal positive charge delocalized in their extended π -systems. Likewise, a downfield shifting of aromatic ^1H NMR signals is observed

compared to those of their alcohol precursors. This highly delocalized, electron deficient π -system may be ideal for some n-type organic semiconductor applications.

LEPS **99** showed reversible electrochemical behavior in its cyclic voltammograms. A redox wave centered at approximately +270 mV (vs. Ag/AgCl) was found, indicating that its reduction is remarkably easy. The observed reversibility is necessary for high-performance organic semiconductor application.

All synthesized dibenzoxanthone and dibenzothioxanthone intermediates have strong absorptions and emissions in the UV-Vis region. Dibenzothioxanthone has obviously red-shifted absorptions and emissions compared to the corresponding dibenzoxanthone. Dibenzoxathone with phenyl substituent has only a slightly red-shifted absorptions and emissions compared to the dibenzoxathone without, indicating that the phenyl substituent is twisted relative to the backbone thus minimizing conjugation.

The synthesized LEPS and LETS compounds show broad and strong absorptions in the UV-Vis-NIR region. LETS compounds have red-shifted absorptions compared to the corresponding LEPS compounds, especially for the broad peak extended to the NIR region. The optical HOMO-LUMO gaps for LEPS **99** and LETS **105** are both approximately 2.1 eV. This value is also close to the HOMO-LUMO gap of pentacene. The absorptions of LEPS and LETS compounds are similar regardless of the phenyl substituents, indicating that the phenyl substituents sit far from co-planar with respect to the backbone. Thus, the phenyl substituents contribute very little to the overall conjugation.

Single crystal X-ray diffraction studies indicate that several LEPS and LETS compounds show slight curvature in their backbones, particularly those with 2',6'-dimethylphenyl or mesityl or multiple phenyl substituents. Also, intermolecular face to face π - π stacking was observed in the crystal packing of LEPS and LETS compounds, which is essential for intermolecular electron transfer in solid state devices.

Broad NMR signals were observed for mesityl and 2',6'-dimethylphenyl substituted LEPS and LETS compounds indicating paramagnetic character. Strong ESR signals were detected for mesityl substituted LEPS and LETS compounds, while weak to moderate ESR signals were observed for other LEPS and LETS compounds that showed sharp NMR signals. VT-NMR studies for LETS **106** in CD₂Cl₂ revealed that **106** likely has a low lying triplet excited state that is readily accessed at room temperature.

3.2 Conclusions and outlook

With broad absorption in the UV-Vis-NIR region, low HOMO-LUMO gap, delocalized electron-deficient backbone and face to face π - π stacking, both LEPS and LETS compounds show promise as a new category of high-performance n-type organic semiconductors. Also, since LEPS and LETS compounds show good solubilities in organic solvents, economic and highly efficient solution-based manufacturing processes (e.g., high speed printing) for organic electronic devices could be achieved. The paramagnetic character for some LEPS and LETS compounds is exciting and potentially advantageous for some applications. However, advanced ESR techniques should be utilized in the future to fully elucidate their electronic structures.

By combining LEPS and LETS compounds as n-type organic semiconductors with high-performance p-type organic semiconductors like polythiophene, pentacene and their derivatives. High-performance organic electronics could potentially be fabricated at high rates and over large areas.

References

1. Yacobi, B. G., *Semiconductor Materials: An Introduction to Basic Principles*. Springer: 2003.
2. Facchetti, A., Semiconductors for organic transistors. *Materials Today* **2007**, *10*, 28-37.
3. Usta, H.; Facchetti, A.; Marks, T. J., n-Channel Semiconductor Materials Design for Organic Complementary Circuits. *Acc. Chem. Res.* **2011**, *44*, 501-510.
4. Mishra, A.; Bauerle, P., Small molecule organic semiconductors on the move: promises for future solar energy technology. *Angew. Chem. Int. Ed.* **2012**, *51*, 2020-2067.
5. Coropceanu, V.; Cornil, J.; Da Silva Filho, D. A.; Olivier, Y.; Silbey, R.; Bredas, J.-L., Charge Transport in Organic Semiconductors. *Chem. Rev.* **2007**, *107*, 926-952.
6. Klauk, H., Organic thin-film transistors. *Chem. Soc. Rev.* **2010**, *39*, 2643-2666.
7. McCulloch, I.; Heeney, M.; Chabinyc, M. L.; De Longchamp, D.; Kline, R. J.; Colle, M.; Duffy, W.; Fischer, D.; Gundlach, D.; Hamadani, B.; Hamilton, R.; Richter, L.; Salleo, A.; Shkunov, M.; Sparrowe, D.; Tierney, S.; Zhang, W., Semiconducting thienothiophene copolymers: design, synthesis, morphology, and performance in thin-film organic transistors. *Adv. Mater.* **2009**, *21*, 1091-1109.
8. Vernitskaya, T. V.; Efimov, O. N., Polypyrrole: a conducting polymer; its synthesis, properties and applications. *Russ. Chem. Rev.* **1997**, *66*, 443-457.
9. Chiang, C. K.; Gau, S. C.; Fincher, C. R. J.; Park, Y. W.; MacDiarmid, A. G.; Heeger, A. J., Polyacetylene (CH)_x: n-type and p-type doping and compensation. *Appl. Phys. Lett.* **1978**, *33*, 18-20.
10. Loewe, R. R.; Khersonsky, S. M.; McCullough, R. D., A simple method to prepare head-to-tail coupled, regioregular poly(3-alkylthiophenes) using Grignard metathesis. *Adv. Mater.* **1999**, *3*, 250-253.
11. Burroughes, J. H.; Bradley, D. D. C.; Brown, A. R.; Marks, R. N.; Mackay, K.; Friend, R. H.; Burns, P. L.; Holmes, A. B., Light-emitting diodes based on conjugated polymers. *Nature* **1990**, *347*, 539-541.
12. Wang, C.; Dong, H.; Hu, W.; Liu, Y.; Zhu, D., Semiconducting pi-conjugated systems in field-effect transistors: a material odyssey of organic electronics. *Chem. Rev.* **2012**, *112*, 2208-2267.
13. (a) Anthony, J. E., Functionalized acenes and heteroacenes for organic electronics. *Chem. Rev.* **2006**, *106*, 5028-5048; (b) Anthony, J. E., The larger acenes: versatile organic semiconductors. *Angew. Chem., Int. Ed.* **2008**, *47*, 452-483.
14. (a) Tsumura, A.; Koezuka, H.; Ando, T., Macromolecular electronic device: field-effect transistor with a polythiophene thin film. *Appl. Phys. Lett.* **1986**, *49*, 1210-1212; (b) Garnier, F.; Hajlaoui, R.; Yassar, A.; Srivastava, P., All-polymer field-effect transistor realized by printing techniques. *Science* **1994**, *265*, 1684-1686; (c) Garnier, F., Materials research in France. *Adv. Mater.* **1990**, *2*, 277.
15. Che, C.-M.; Xiang, H.-F.; Chui, S. S.-Y.; Xu, Z.-X.; Roy, V. A. L.; Yan, J. J.; Fu, W.-F.; Lai, P. T.; Williams, I. D., A high-performance organic field-effect transistor based on platinum(II) porphyrin: peripheral substituents on porphyrin ligand significantly affect film structure and charge mobility. *Chem. - Asian J.* **2008**, *3*, 1092-1103.
16. Paloheimo, J.; Isotalo, H.; Kastner, J.; Kuzmany, H., Conduction mechanisms in undoped thin films of C₆₀ and C_{60/70}. *Synth. Met.* **1993**, *56*, 3185-3190.
17. Jones, B. A.; Facchetti, A.; Wasielewski, M. R.; Marks, T. J., Tuning Orbital Energetics in Arylene Diimide Semiconductors. Materials Design for Ambient Stability of n-Type Charge Transport. *J. Am. Chem. Soc.* **2007**, *129*, 15259-15278.
18. (a) Clar, E.; John, F., Polynuclear aromatic hydrocarbons and their derivatives. V. Naphthoanthracenes, their oxidation products and a new class of deeply colored hydrocarbons. *Ber. Dtsch. Chem. Ges. B* **1929**, *62B*, 3021-3029; (b) Clar, E.; John, F., Polynuclear aromatic hydrocarbons and their derivatives. VII. A new class of deeply colored radical hydrocarbons and the supposed pentacene of E. Philippi; also a reply to remarks of Roland Scholl and Oskar B. ovrddot.ottger. *Ber. Dtsch. Chem. Ges. B* **1930**, *63B*, 2967-2977.

19. Kaur, I.; Jia, W.; Kopreski, R. P.; Selvarasah, S.; Dokmeci, M. R.; Pramanik, C.; McGruer, N. E.; Miller, G. P., Substituent Effects in Pentacenes: Gaining Control over HOMO-LUMO Gaps and Photooxidative Resistances. *J. Am. Chem. Soc.* **2008**, *130*, 16274-16286.
20. Reese, C.; Chung, W.-J.; Ling, M.-m.; Roberts, M.; Bao, Z., High-performance microscale single-crystal transistors by lithography on an elastomer dielectric. *Appl. Phys. Lett.* **2006**, *89*, 202108/1-202108/3.
21. (a) Tang, M. L.; Okamoto, T.; Bao, Z., High-Performance Organic Semiconductors: Asymmetric Linear Acenes Containing Sulphur. *J. Am. Chem. Soc.* **2006**, *128*, 16002-16003; (b) Valiyev, F.; Hu, W.-S.; Chen, H.-Y.; Kuo, M.-Y.; Chao, I.; Tao, Y.-T., Synthesis and Characterization of Anthra[2,3-*b*]thiophene and Tetraceno[2,3-*b*]thiophenes for Organic Field-Effect Transistor Applications. *Chem. Mater.* **2007**, *19*, 3018-3026.
22. (a) Ohki, K.; Inokuchi, H.; Maruyama, Y., Charge mobility in pyrene crystals. *Bull. Chem. Soc. Jpn.* **1963**, *36*, 1512-1515; (b) Suzuki, A.; Inokuchi, H.; Maruyama, Y., Charge-carrier drift mobility in pyrene single crystals. *Bull. Chem. Soc. Jpn.* **1976**, *49*, 3347-3348.
23. (a) Choi, T. Y.; Kang, H. S.; Park, D. H.; Koo, J. M.; Lee, J. K.; Ahn, S. D.; Joo, J., Trap distribution and field effect transistor (FET) of perylene by organic molecular beam deposition (OMBD). *Synth. Met.* **2003**, *137*, 929-930; (b) Ohta, T.; Nagano, T.; Ochi, K.; Kubozono, Y.; Fujiwara, A., Field-effect transistors with thin films of perylene on SiO₂ and polyimide gate insulators. *Appl. Phys. Lett.* **2006**, *88*, 103506/1-103506/3; (c) Kotani, M.; Kakinuma, K.; Yoshimura, M.; Ishii, K.; Yamazaki, S.; Kobori, T.; Okuyama, H.; Kobayashi, H.; Tada, H., Charge carrier transport in high purity perylene single crystal studied by time-of-flight measurements and through field effect transistor characteristics. *Chem. Phys.* **2006**, *325*, 160-169.
24. (a) Waldauf, C.; Schilinsky, P.; Perisutti, M.; Hauch, J.; Brabec, C. J., Solution-processed organic n-type thin-film transistors. *Adv. Mater.* **2003**, *15*, 2084-2088; (b) Anthopoulos, T. D.; Tanase, C.; Setayesh, S.; Meijer, E. J.; Hummelen, J. C.; Blom, P. W. M.; de Leeuw, D. M., Ambipolar organic field-effect transistors based on a solution-processed methanofullerene. *Adv. Mater.* **2004**, *16*, 2174-2179; (c) Singh, T. B.; Marjanovic, N.; Stadler, P.; Auinger, M.; Matt, G. J.; Gunes, S.; Sariciftci, N. S.; Schwodiauer, R.; Bauer, S., Fabrication and characterization of solution-processed methanofullerene-based organic field-effect transistors. *J. Appl. Phys.* **2005**, *97*, 083714/1-083714/5.
25. Sakamoto, Y.; Suzuki, T.; Kobayashi, M.; Gao, Y.; Fukai, Y.; Inoue, Y.; Sato, F.; Tokito, S., Perfluoropentacene: High-Performance p-n Junctions and Complementary Circuits with Pentacene. *J. Am. Chem. Soc.* **2004**, *126*, 8138-8140.
26. (a) Brown, A. R.; de Leeuw, D. M.; Lous, E. J.; Havinga, E. E., Organic n-type field-effect transistor. *Synth. Met.* **1994**, *66*, 257-262; (b) Briseno, A. L.; Mannsfeld, S. C. B.; Ling, M. M.; Liu, S.; Tseng, R. J.; Reese, C.; Roberts, M. E.; Yang, Y.; Wudl, F.; Bao, Z., Patterning organic single-crystal transistor arrays. *Nature* **2006**, *444*, 913-917; (c) Menard, E.; Podzorov, V.; Hur, S.-H.; Gaur, A.; Gershenson, M. E.; Rogers, J. A., High-performance n- and p-type single-crystal organic transistors with free-space gate dielectrics. *Adv. Mater.* **2004**, *16*, 2097-2101.
27. (a) Katz, H. E.; Lovinger, A. J.; Johnson, J.; Kloc, C.; Slegrist, T.; Li, W.; Lin, Y. Y.; Dodabalapur, A., A soluble and air-stable organic semiconductor with high electron mobility. *Nature* **2000**, *404*, 478-481; (b) Katz, H. E.; Johnson, J.; Lovinger, A. J.; Li, W., Naphthalenetetracarboxylic Diimide-Based n-Channel Transistor Semiconductors: Structural Variation and Thiol-Enhanced Gold Contacts. *J. Am. Chem. Soc.* **2000**, *122*, 7787-7792; (c) Shukla, D.; Nelson, S. F.; Freeman, D. C.; Rajeswaran, M.; Ahearn, W. G.; Meyer, D. M.; Carey, J. T., Thin-Film Morphology Control in Naphthalene-Diimide-Based Semiconductors: High Mobility n-Type Semiconductor for Organic Thin-Film Transistors. *Chem. Mater.* **2008**, *20*, 7486-7491; (d) Gawrys, P.; Boudinet, D.; Zagorska, M.; Djurado, D.; Verilhac, J.-M.; Horowitz, G.; Pecaud, J.; Pouget, S.; Pron, A., Solution processible naphthalene and perylene bisimides: Synthesis, electrochemical characterization and application to organic field effect transistors (OFETs) fabrication. *Synth. Met.* **2009**, *159*, 1478-1485.

28. von Baeyer, A.; Villiger, V., Basic properties of oxygen. *Ber. Dtsch. Chem. Ges.* **1901**, *34*, 2679-2698.
29. Balaban, T. S.; Balaban, A. T., Product class 1: pyrylium salts. *Sci. Synth.* **2003**, *14*, 11-200.
30. (a) Balaban, A. T.; Dinculescu, A.; Dorofeenko, G. N.; Fischer, G. V.; Kablik, A. V.; Mezheritskii, V. V.; Schroth, W., *Advances in Heterocyclic Chemistry, Supplement 2: Pyrylium Salts: Synthesis, Reactions, and Physical Properties*. Academic Press: 1982; (b) Balaban, A. T.; Oniciu, D. C.; Katritzky, A. R., Aromaticity as a Cornerstone of Heterocyclic Chemistry. *Chem. Rev.* **2004**, *104*, 2777-2812.
31. Alvarez-Builla, J.; Vaquero, J. J.; Barluenga, J.; Editors, *Modern Heterocyclic chemistry, Volume 3*. Wiley: New York, 2011.
32. Rudolf, W. D., Product class 6: thiopyrylium salts. *Sci. Synth.* **2003**, *14*, 649-718.
33. Valentino, M. R.; Boyd, M. K., Quenching behavior of singlet excited 9-arylxanthylium cations. *J. Org. Chem.* **1993**, *58*, 5826-5831.
34. Hagel, M.; Liu, J.; Muth, O.; Estevez Rivera, H. J.; Schwake, E.; Sripanom, L.; Henkel, G.; Dyker, G., *p*-Quinoid Compounds by Nucleophilic Aromatic Substitution with Hydride as Leaving Group. *Eur. J. Org. Chem.* **2007**, *72*, 3573-3582.
35. Zhu, X.-Q.; Dai, Z.; Yu, A.; Wu, S.; Cheng, J.-P., Driving Forces for the Mutual Conversions between Phenothiazines and Their Various Reaction Intermediates in Acetonitrile. *J. Phys. Chem. B* **2008**, *112*, 11694-11707.
36. Mueller, C.; Wasserberg, D.; Weemers, J. J. M.; Pidko, E. A.; Hoffmann, S.; Lutz, M.; Spek, A. L.; Meskers, S. C. J.; Janssen, R. A. J.; van Santen, R. A.; Vogt, D., Donor-functionalized polydentate pyrylium salts and phosphinines: synthesis, structural characterization, and photophysical properties. *Chem. - Eur. J.* **2007**, *13*, 4548-4559.
37. Mills, N. S.; Levy, A.; Plummer, B. F., Antiaromaticity in Fluorenylidene Dications. Experimental and Theoretical Evidence for the Relationship between the HOMO/LUMO Gap and Antiaromaticity. *J. Org. Chem.* **2004**, *69*, 6623-6633.
38. Kashefolgheta, S.; Razzaghi, M.; Hammann, B.; Eilers, J.; Roston, D.; Lu, Y., Computational Replication of the Abnormal Secondary Kinetic Isotope Effects in a Hydride Transfer Reaction in Solution with a Motion Assisted H-Tunneling Model. *J. Org. Chem.* **2014**, *79*, 1989-1994.
39. (a) El-Idreesy, T. T.; Clennan, E. L., Hydrolytic Stability of *N*-Methyl-2,6-dimesityl-4,4'-Pyrylogen Bis-tetrafluoroborate. *J. Org. Chem.* **2011**, *76*, 7175-7179; (b) Sheng, Y.; Ren, Y., Computational Study on a HS- Sensing Reaction Utilizing a Pyrylium Derivative. *J. Phys. Chem. A* **2012**, *116*, 5420-5427.
40. Grimme, S.; Steinmetz, M.; Korth, M., How to Compute Isomerization Energies of Organic Molecules with Quantum Chemical Methods. *J. Org. Chem.* **2007**, *72*, 2118-2126.
41. Familoni, O. B.; Ionica, I.; Bower, J. F.; Snieckus, V., Intramolecular anionic Friedel-Crafts equivalents. A general regioselective route to substituted and naturally occurring xanthen-9-ones. *Synlett* **1997**, 1081-1083.
42. Luis, S. V.; Gavina, F.; Ferrer, P.; Safont, V. S.; Torres, M. C.; Burguete, M. I., Nonconcerted pathways in the generation of dehydroarenes by thermal decomposition of diaryliodonium carboxylates. *Tetrahedron* **1989**, *45*, 6281-6296.
43. Uyanik, M.; Akakura, M.; Ishihara, K., 2-Iodoxybenzenesulfonic Acid as an Extremely Active Catalyst for the Selective Oxidation of Alcohols to Aldehydes, Ketones, Carboxylic Acids, and Enones with Oxone. *J. Am. Chem. Soc.* **2009**, *131*, 251-262.
44. (a) Li, J.; Jin, C.; Su, W., Microwave-assisted, Yb(OTf)₃/TfOH cocatalyzed synthesis of xanthenes and thioxanthenes by intramolecular Friedel-Crafts reaction under solvent-free conditions. *Heterocycles* **2011**, *83*, 855-866; (b) Nakano, T.; Saeki, Y., Daphniphyllum alkaloids. II. Isolation and the structures of the alkaloids from *Daphniphyllum macropodum*. *Tetrahedron Lett.* **1967**, 4791-4797.
45. Beak, P.; Meyers, A. I., Stereo- and regiocontrol by complex induced proximity effects: reactions of organolithium compounds. *Acc. Chem. Res.* **1986**, *19*, 356-363.

46. Snieckus, V., Directed ortho metalation. Tertiary amide and O-carbamate directors in synthetic strategies for polysubstituted aromatics. *Chem. Rev.* **1990**, *90*, 879-933.
47. Zhao, J.; Larock, R. C., Synthesis of Xanthenes, Thioxanthenes, and Acridones by the Coupling of Arynes and Substituted Benzoates. *J. Org. Chem.* **2007**, *72*, 583-588.
48. Wang, S.; Xie, K.; Tan, Z.; An, X.; Zhou, X.; Guo, C.-C.; Peng, Z., One-step preparation of xanthenes via Pd-catalyzed annulation of 1,2-dibromoarenes and salicylaldehydes. *Chem. Commun.* **2009**, 6469-6471.
49. Haneda, H.; Eda, S.; Aratani, M.; Hamura, T., Dibromoisobenzofuran as a Formal Equivalent of Didehydroisobenzofuran: Reactive Platform for Expedient Assembly of Polycycles. *Org. Lett.* **2014**, *16*, 286-289.
50. Albert, R.; Dax, K.; Pleschko, R.; Stuetz, A. E., Tetrafluoroboric acid, an efficient catalyst in carbohydrate protection and deprotection reactions. *Carbohydr. Res.* **1985**, *137*, 282-290.
51. Moss, R. A.; Platz, M. S.; Jones, M., Jr.; Editors, *Reactive Intermediate Chemistry*. John Wiley & Sons, Inc.: 2004.
52. Abe, M., Diradicals. *Chem. Rev.* **2013**, *113*, 7011-7088.
53. (a) Wang, J.; Hou, L.; Browne, W. R.; Feringa, B. L., Photoswitchable Intramolecular Through-Space Magnetic Interaction. *J. Am. Chem. Soc.* **2011**, *133*, 8162-8164; (b) Fairfull-Smith, K. E.; Blinco, J. P.; Keddie, D. J.; George, G. A.; Bottle, S. E., A Novel Profluorescent Dinitroxide for Imaging Polypropylene Degradation. *Macromolecules* **2008**, *41*, 1577-1580.
54. Usuki, T.; Kawai, M.; Nakanishi, K.; Ellestad, G. A., Calicheamicin γ 11 and phenyl tert-butyl nitrene (PBN): observation of a kinetic isotope effect by an ESR study. *Chem. Commun.* **2010**, *46*, 737-739.
55. Wang, S. R.; Qiu, Z.; Xie, Z., Regioselective Insertion of Carborynes into Etheral C-H Bond: Facile Synthesis of α -Carboranylated Ethers. *J. Am. Chem. Soc.* **2011**, *133*, 5760-5763.
56. Nozawa, T.; Nagata, M.; Ichinohe, M.; Sekiguchi, A., Isolable *p*- and *m*-[$(t\text{Bu}_2\text{MeSi})_2\text{Si}$] $_2\text{C}_6\text{H}_4$: Disilaquinodimethane vs triplet bis(silyl radical). *J. Am. Chem. Soc.* **2011**, *133*, 5773-5775.
57. Takahashi, T.; Matsuoka, K.; Takimiya, K.; Otsubo, T.; Aso, Y., Extensive Quinoidal Oligothiophenes with Dicyanomethylene Groups at Terminal Positions as Highly Amphoteric Redox Molecules. *J. Am. Chem. Soc.* **2005**, *127*, 8928-8929.
58. Tsuda, A.; Osuka, A., Fully conjugated porphyrin tapes with electronic absorption bands that reach into infrared. *Science* **2001**, *293*, 79-82.
59. Inoue, S.; Aso, Y.; Otsubo, T., Push-pull type of diphenoquinoid chromophores as novel near-infrared dyes. *Chem. Commun.* **1997**, 1105-1106.
60. (a) Fabian, J.; Nakazumi, H.; Matsuoka, M., Near-infrared absorbing dyes. *Chem. Rev.* **1992**, *92*, 1197-1226; (b) Fabian, J.; Zahradnik, R., The Search for Highly Colored Organic Compounds. *Angew. Chem., Int. Ed. Engl.* **1989**, *28*, 677-694.
61. (a) Bohnen, A.; Koch, K. H.; Luettker, W.; Muellen, K., Oligorylene as a Model for "Poly(perinaphthalene)". *Angew. Chem., Int. Ed. Engl.* **1990**, *29*, 525-527; (b) Koch, K. H.; Muellen, K., Polyarylenes and poly(arylenevinylene)s. V. Synthesis of tetraalkyl-substituted oligo(1,4-naphthylene)s and cyclization to soluble oligo(peri-naphthylene)s. *Chem. Ber.* **1991**, *124*, 2091-2100.
62. Konishi, A.; Hirao, Y.; Matsumoto, K.; Kurata, H.; Kishi, R.; Shigeta, Y.; Nakano, M.; Tokunaga, K.; Kamada, K.; Kubo, T., Synthesis and Characterization of Quarteranthenes: Elucidating the Characteristics of the Edge State of Graphene Nanoribbons at the Molecular Level. *J. Am. Chem. Soc.* **2013**, *135*, 1430-1437.
63. (a) Yao, J. H.; Chi, C.; Wu, J.; Loh, K. P., Bisanthracene bis(dicarboxylic imide)s as soluble and stable NIR dyes. *Chem. Eur. J.* **2009**, *15*, 9299-9302; (b) Li, J.; Chang, J.-J.; Tan, H. S.; Jiang, H.; Chen, X.; Chen, Z.; Zhang, J.; Wu, J., Disc-like 7, 14-dicyano-ovalene-3,4:10,11-bis(dicarboximide) as a solution-processible n-type semiconductor for air stable field-effect transistors. *Chem. Sci.* **2012**, *3*, 846-850; (c) Li,

J.; Zhang, K.; Zhang, X.; Huang, K.-W.; Chi, C.; Wu, J., *meso*-Substituted bisanthrenes as soluble and stable near-infrared dyes. *J. Org. Chem.* **2010**, *75*, 856-863.

64. Konishi, A.; Hirao, Y.; Nakano, M.; Shimizu, A.; Botek, E.; Champagne, B.; Shiomi, D.; Sato, K.; Takui, T.; Matsumoto, K.; Kurata, H.; Kubo, T., Synthesis and Characterization of Teranthene: A Singlet Biradical Polycyclic Aromatic Hydrocarbon Having Kekule Structures. *J. Am. Chem. Soc.* **2010**, *132*, 11021-11023.

65. (a) Rao, K. P.; Kondo, M.; Sakamoto, R.; Kusamoto, T.; Nishikawa, M.; Kume, S.; Nihei, M.; Oshio, H.; Nishihara, H., Benzo[*e*]pyrene Skeleton Dipyrilium Dication with a Strong Donor-Acceptor-Donor Interaction, and Its Two-Electron Reduced Molecule. *Chem. - Eur. J.* **2011**, *17*, 14010-14019; (b) Kondo, M.; Uchikawa, M.; Zhang, W.-W.; Namiki, K.; Kume, S.; Murata, M.; Kobayashi, Y.; Nishihara, H., Protonation-induced cyclocondensation of 1-aryl ethynylantraquinones: expanding the π conjugation. *Angew. Chem., Int. Ed.* **2007**, *46*, 6271-6274; (c) Kondo, M.; Uchikawa, M.; Namiki, K.; Zhang, W.-W.; Kume, S.; Nishibori, E.; Suwa, H.; Aoyagi, S.; Sakata, M.; Murata, M.; Kobayashi, Y.; Nishihara, H., Counterion-dependent valence tautomerization of ferrocenyl-conjugated pyrylium salts. *J. Am. Chem. Soc.* **2009**, *131*, 12112-12124; (d) Kondo, M.; Uchikawa, M.; Kume, S.; Nishihara, H., Alcohol- and acid-causing reversible switching of near-infrared absorption and luminescence in a donor-acceptor conjugated system. *Chem. Commun.* **2009**, 1993-1995; (e) Rao, K. P.; Kusamoto, T.; Sakamoto, R.; Yamamoto, Y.; Kume, S.; Nihei, M.; Oshio, H.; Nishihara, H., Platinadithiolene-conjugated pyrylium salt with strong intramolecular donor-acceptor interaction. *Chem. Commun.* **2011**, *47*, 2330-2332; (f) Rao, K. P.; Kondo, M.; Sakamoto, R.; Kusamoto, T.; Kume, S.; Nishihara, H., Protonation-induced cyclization of 1,8-bis(arylethynyl)anthraquinones: monopyrylium salt formation and intensification of donor-acceptor interaction. *Chem. Lett.* **2011**, *40*, 1456-1458; (g) Kondo, M.; Murata, M.; Nishihara, H.; Nishibori, E.; Aoyagi, S.; Yoshida, M.; Kinoshita, Y.; Sakata, M., Guest-induced instant and reversible crystal-to-crystal transformation of 1,4-bis(ferrocenylethynyl)anthraquinone. *Angew. Chem., Int. Ed.* **2006**, *45*, 5461-5464; (h) Sakamoto, R.; Rao, K. P.; Nishihara, H., Arylethynylantraquinone and bis(arylethynyl)anthraquinone: strong donor-acceptor interaction and proton-induced cyclization to form pyrylium and dipyrilium salts. *Chem. Lett.* **2011**, *40*, 1316-1326; (i) Rao, K. P.; Kusamoto, T.; Toshimitsu, F.; Inayoshi, K.; Kume, S.; Sakamoto, R.; Nishihara, H., Double Protonation of 1,5-Bis(triarylaminoethynyl)anthraquinone To Form a Paramagnetic Pentacyclic Dipyrilium Salt. *J. Am. Chem. Soc.* **2010**, *132*, 12472-12479.

66. Niimi, K.; Mori, H.; Miyazaki, E.; Osaka, I.; Kakizoe, H.; Takimiya, K.; Adachi, C., [2,2']Bi[naphtho[2,3-*b*]furanyl]: a versatile organic semiconductor with a furan-furan junction. *Chem. Commun.* **2012**, *48*, 5892-5894.

67. Pena, D.; Cobas, A.; Perez, D.; Guitian, E., An efficient procedure for the synthesis of ortho-trialkylsilylaryl triflates: easy access to precursors of functionalized arynes. *Synthesis* **2002**, 1454-1458.

68. Lucas, S.; Heim, R.; Negri, M.; Antes, I.; Ries, C.; Schewe, K. E.; Bisi, A.; Gobbi, S.; Hartmann, R. W., Novel Aldosterone Synthase Inhibitors with Extended Carbocyclic Skeleton by a Combined Ligand-Based and Structure-Based Drug Design Approach. *J. Med. Chem.* **2008**, *51*, 6138-6149.

69. Wu, K.-C.; Lin, Y.-S.; Yeh, Y.-S.; Chen, C.-Y.; Ahmed, M. O.; Chou, P.-T.; Hon, Y.-S., Design and synthesis of intramolecular hydrogen bonding systems. Their application in metal cation sensing based on excited-state proton transfer reaction. *Tetrahedron* **2004**, *60*, 11861-11868.

70. Hashmi, A. S. K.; Braun, I.; Rudolph, M.; Rominger, F., The role of gold acetylides as a selectivity trigger and the importance of gem-diaurated species in the gold-catalyzed hydroarylation-aromatization of arene-diyne. *Organometallics* **2012**, *31*, 644-661.

71. Bowles, D. M.; Anthony, J. E., A reiterative approach to 2,3-disubstituted naphthalenes and anthracenes. *Org. Lett.* **2000**, *2*, 85-87.

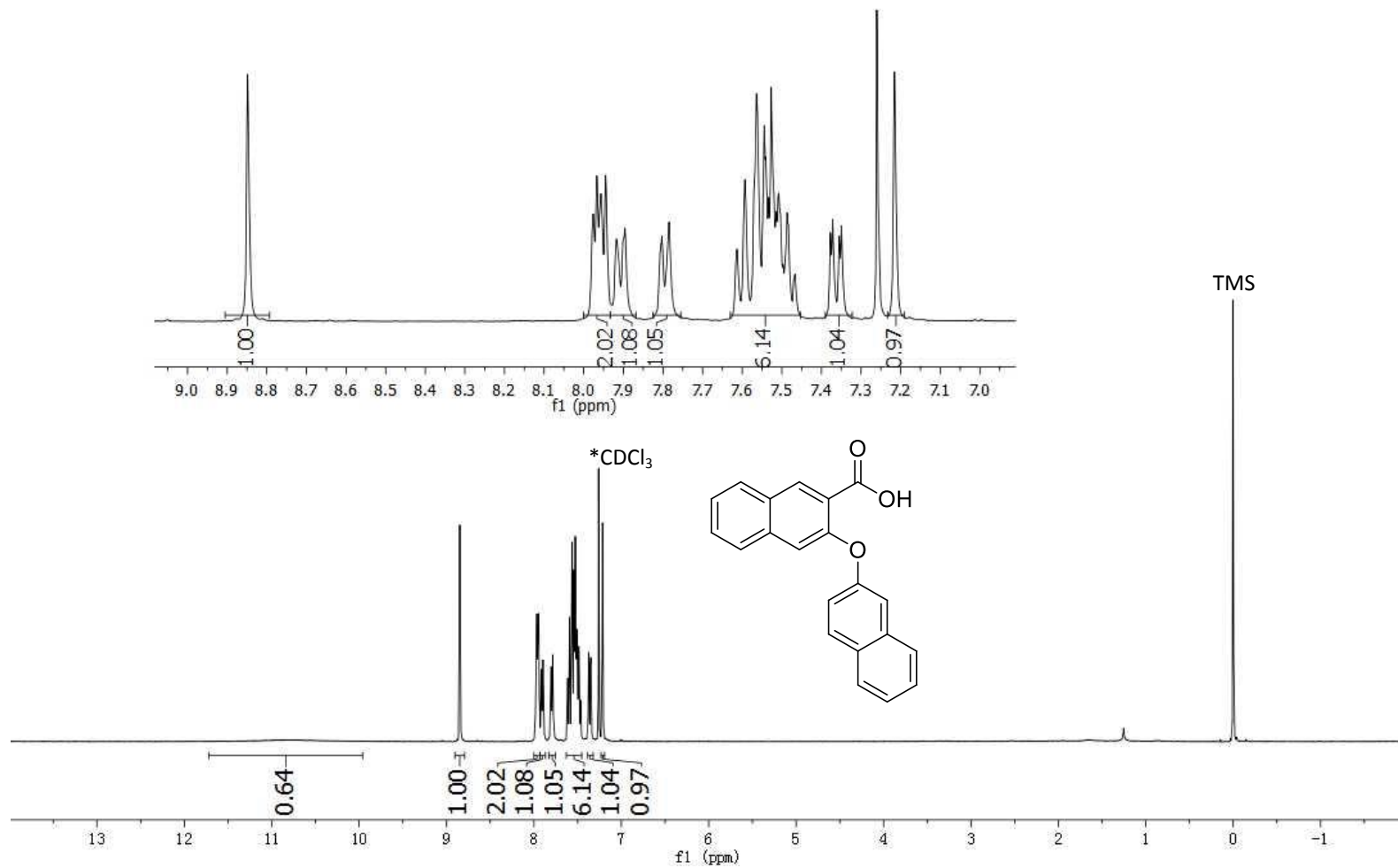
72. Janz, K.; Kaila, N., Bromodecarboxylation of Quinoline Salicylic Acids: Increasing the Diversity of Accessible Substituted Quinolines. *J. Org. Chem.* **2009**, *74*, 8874-8877.

Appendix

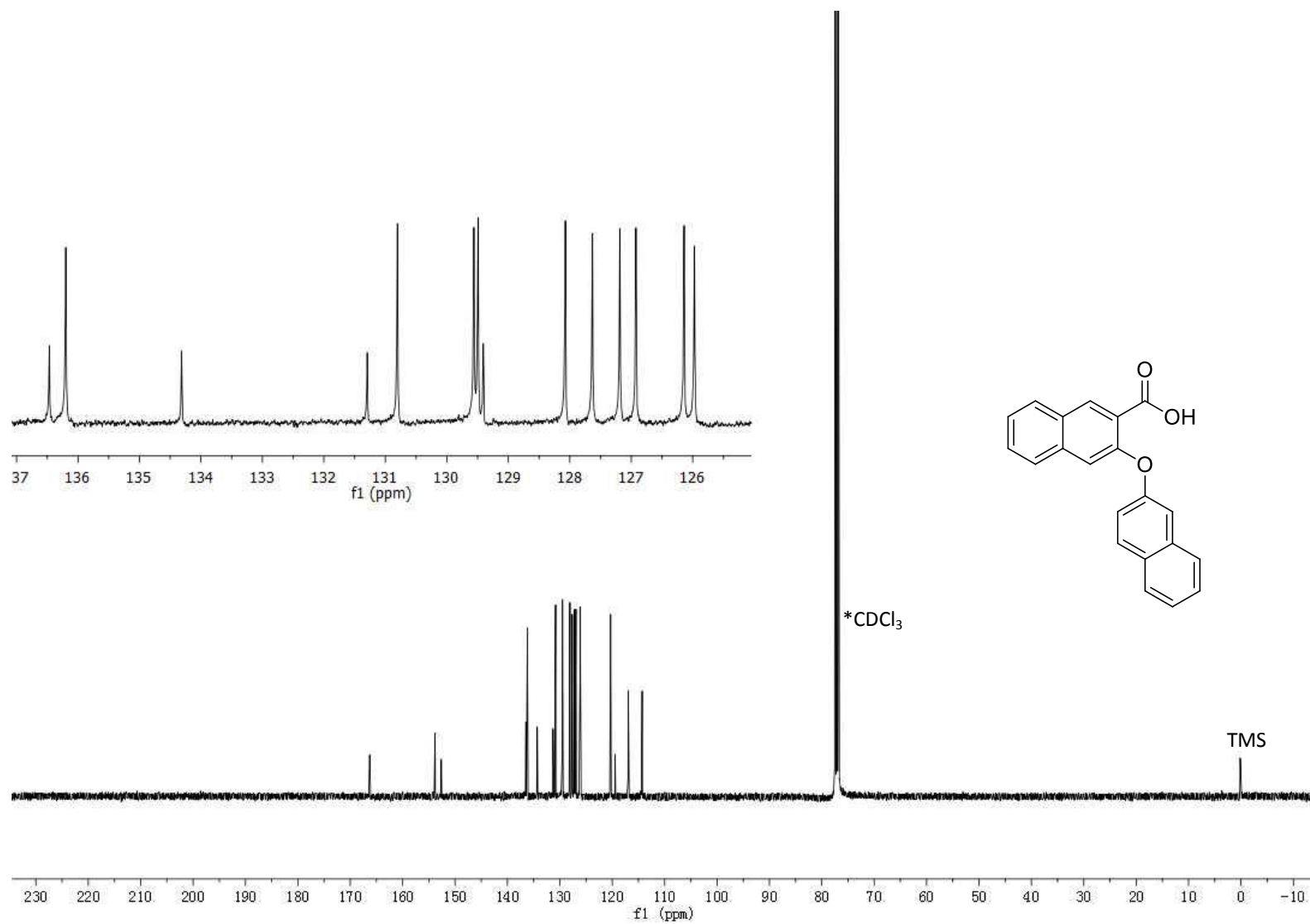
NMR spectra

Mass spectra

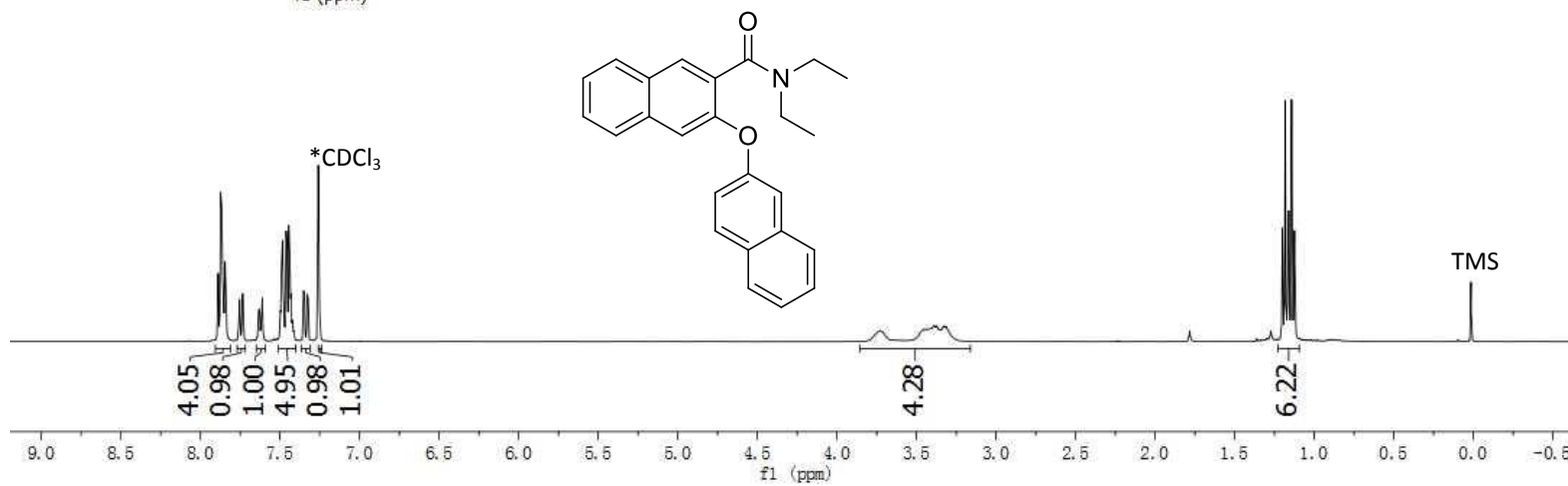
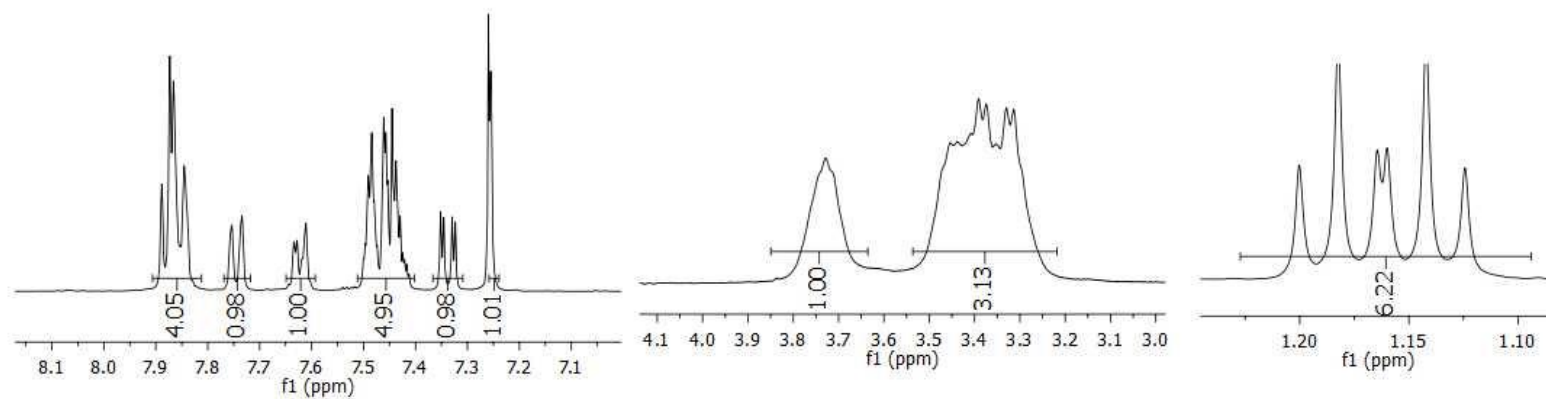
^1H NMR (CDCl_3 , 400 MHz) for **45**



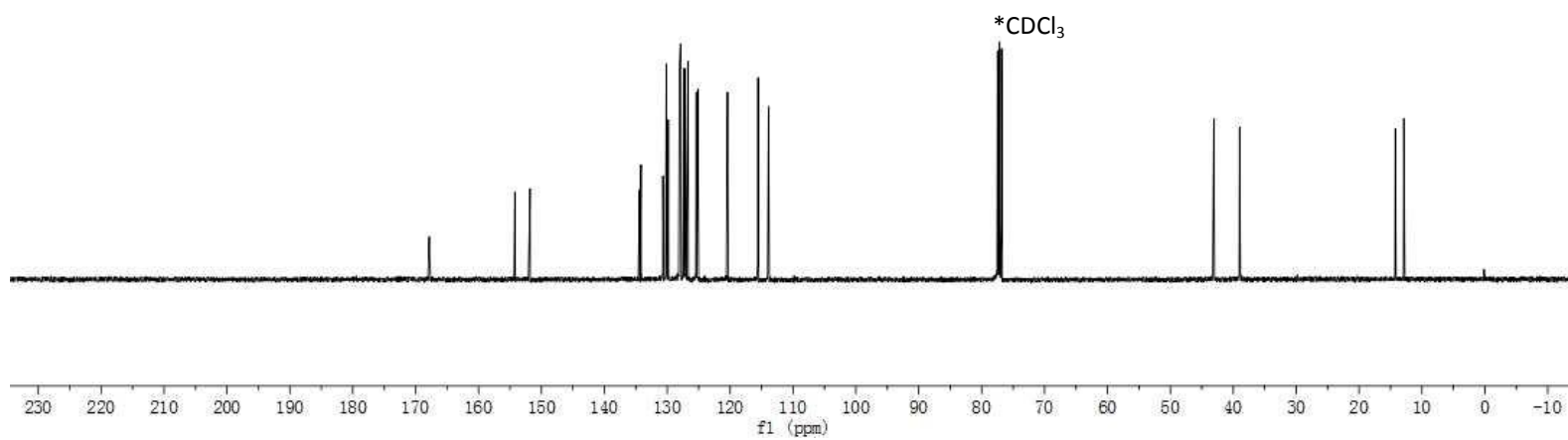
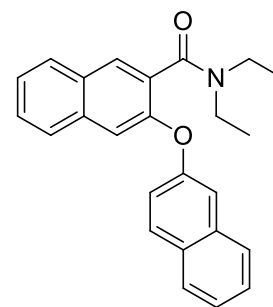
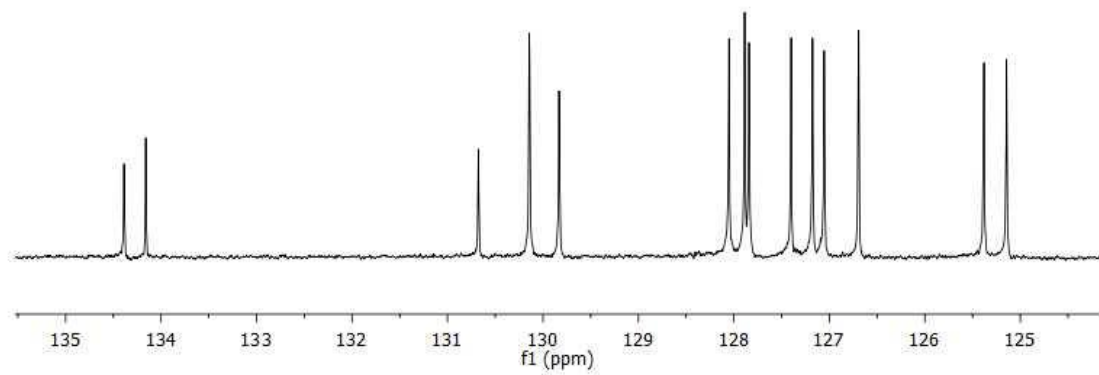
^{13}C NMR (CDCl_3 , 101 MHz) for 45



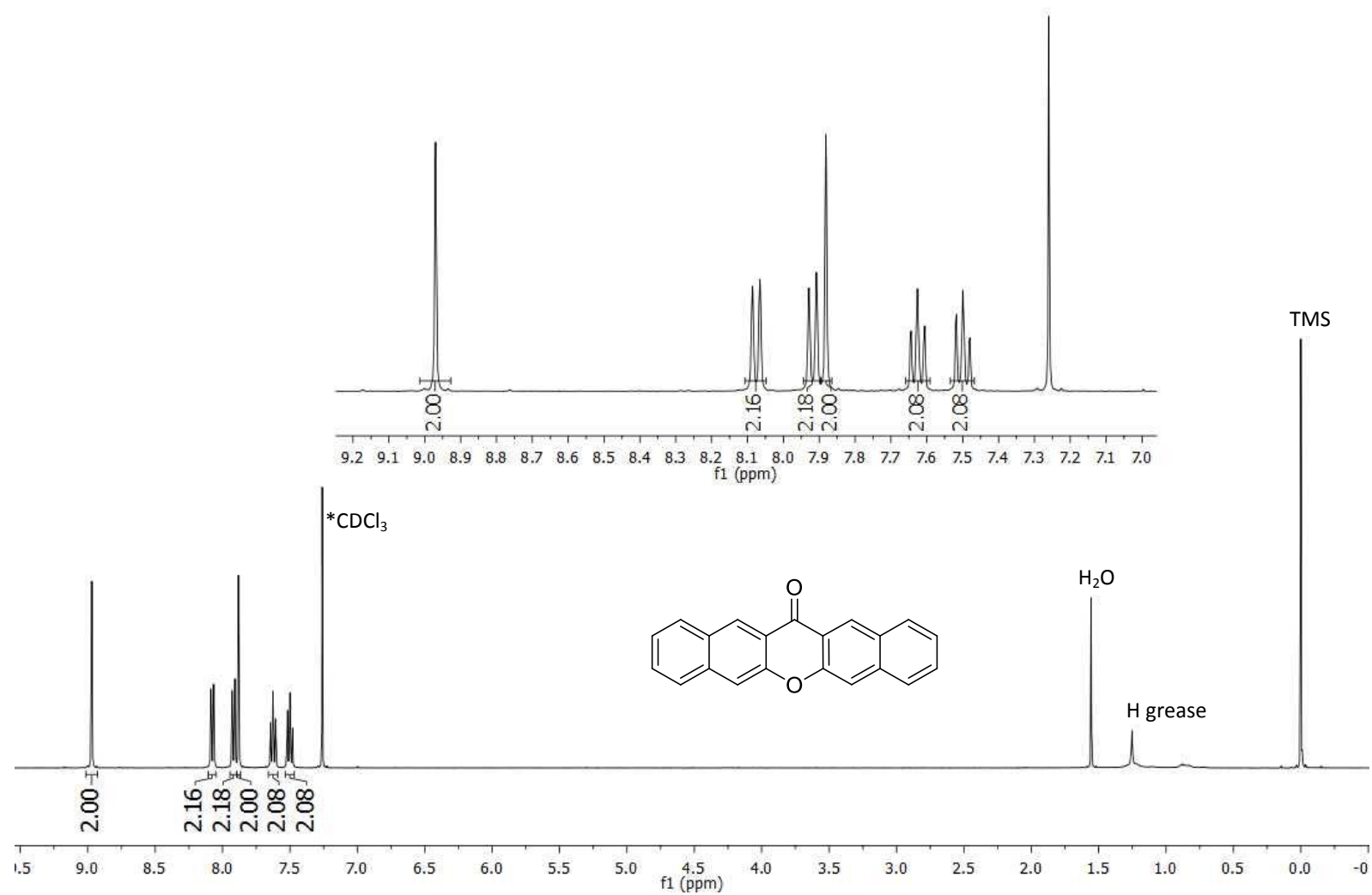
^1H NMR (CDCl_3 , 400 MHz) for **46**



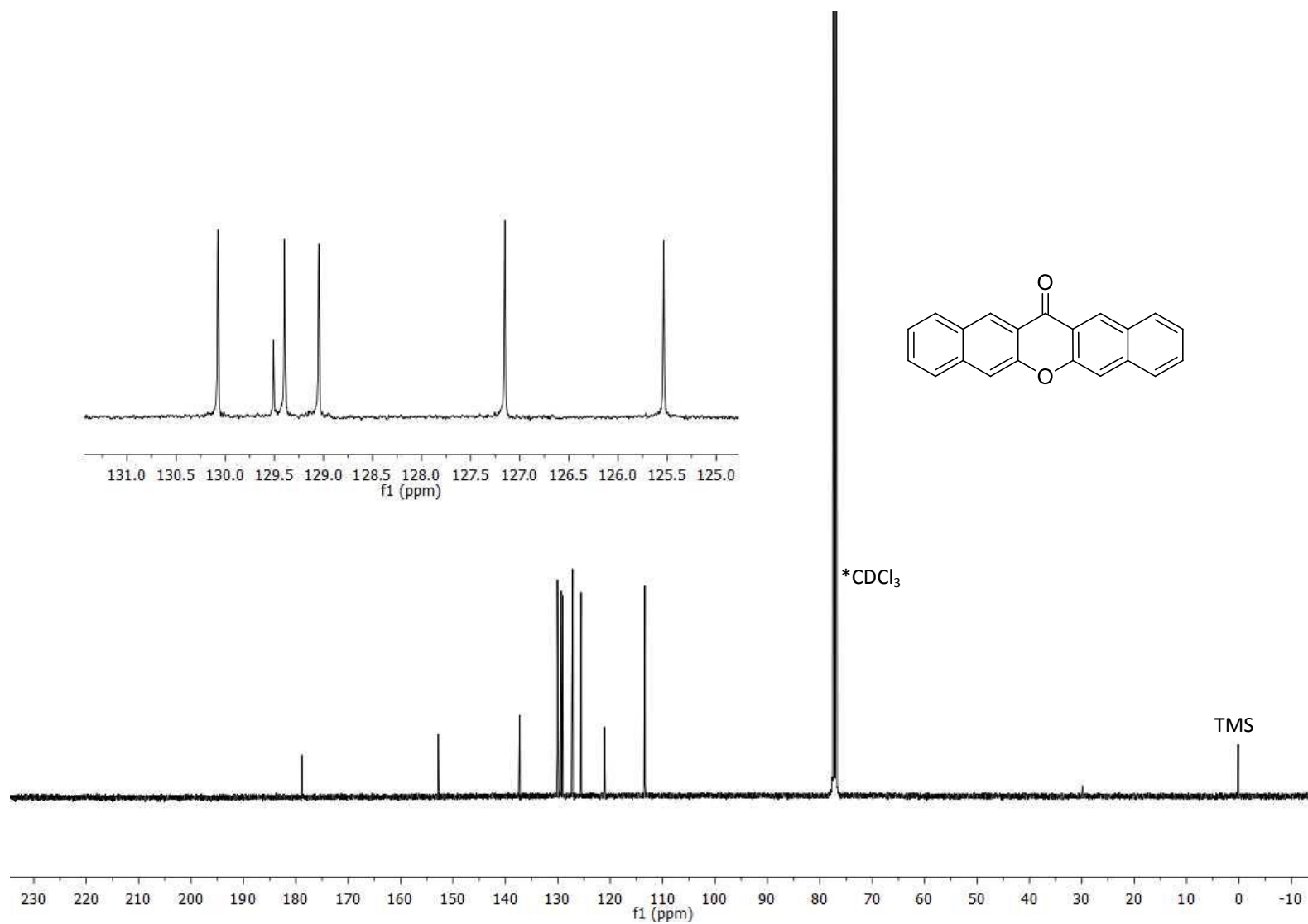
^{13}C NMR (CDCl_3 , 101 MHz) for **46**



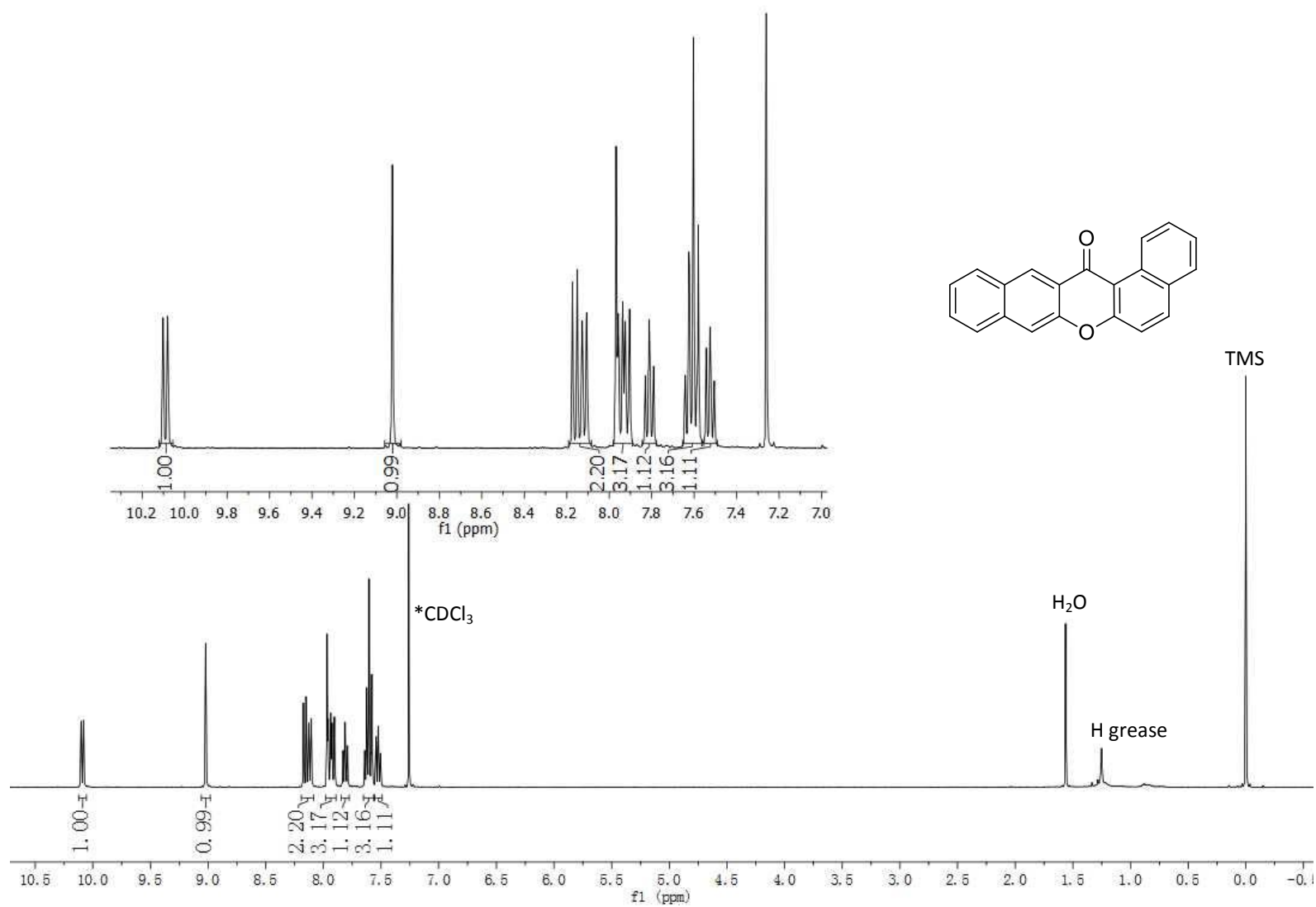
^1H NMR (CDCl_3 , 400 MHz) for **38**



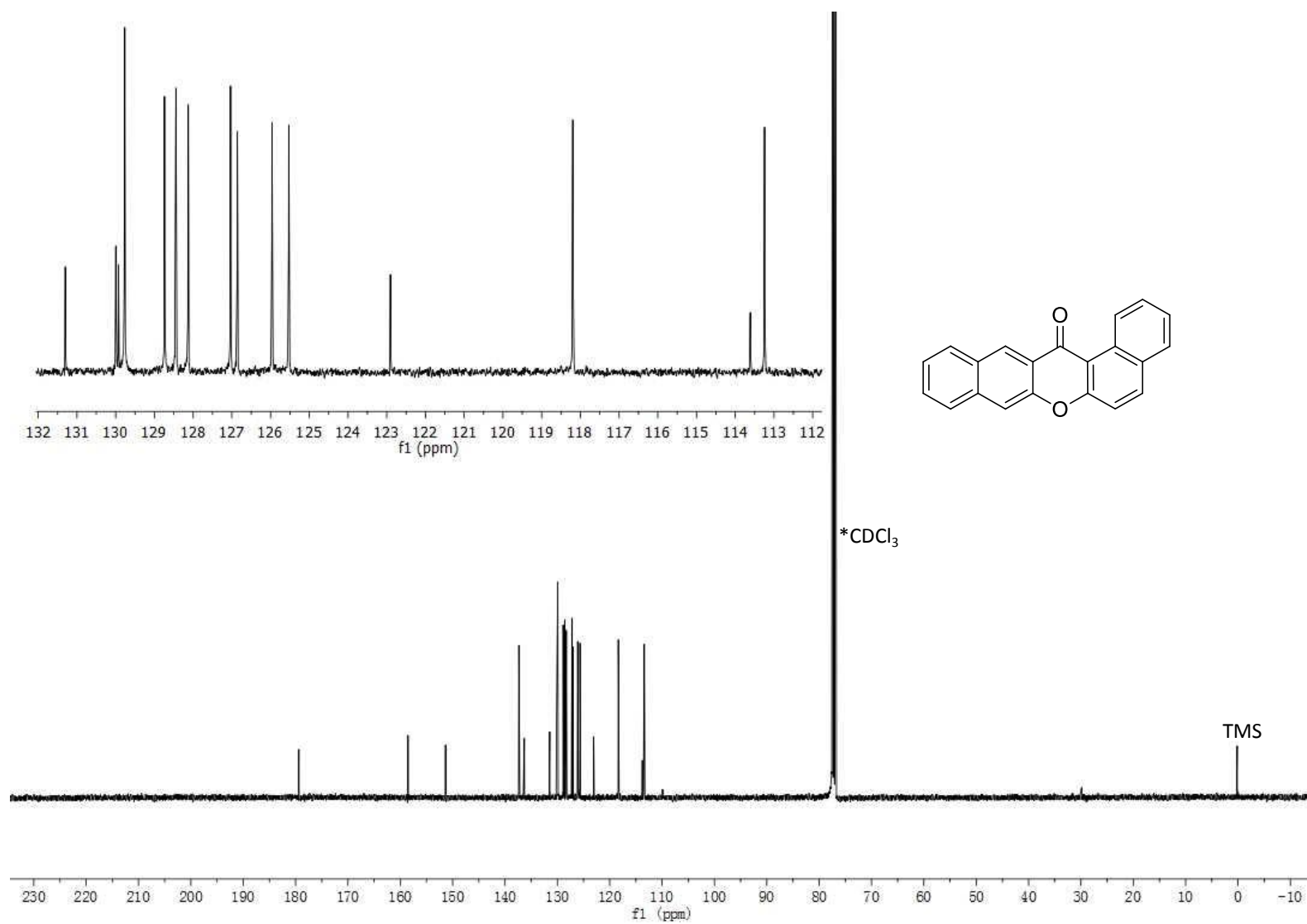
^{13}C NMR (CDCl_3 , 101 MHz) for **38**



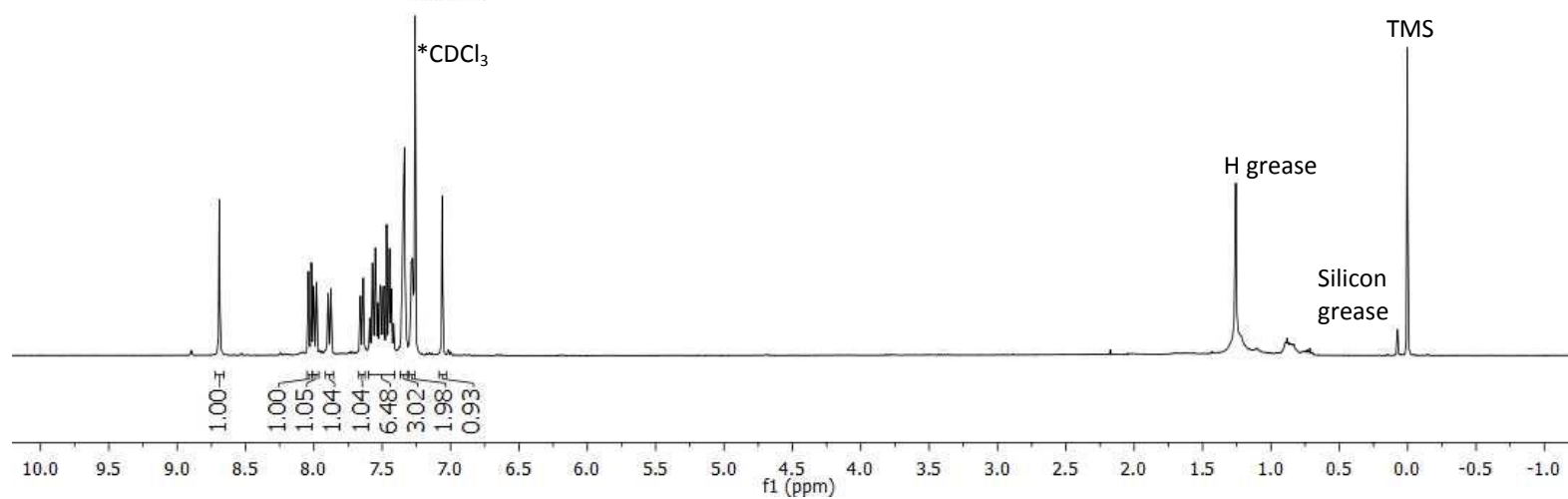
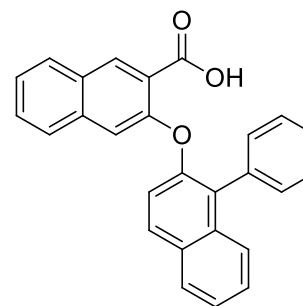
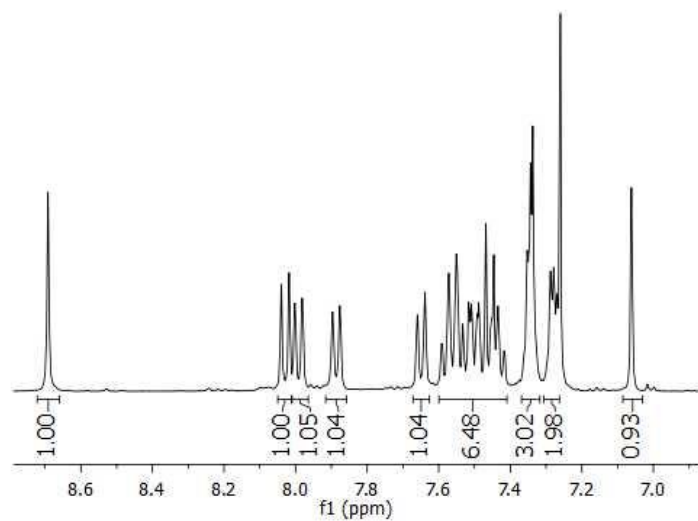
^1H NMR (CDCl_3 , 400 MHz) for **42**



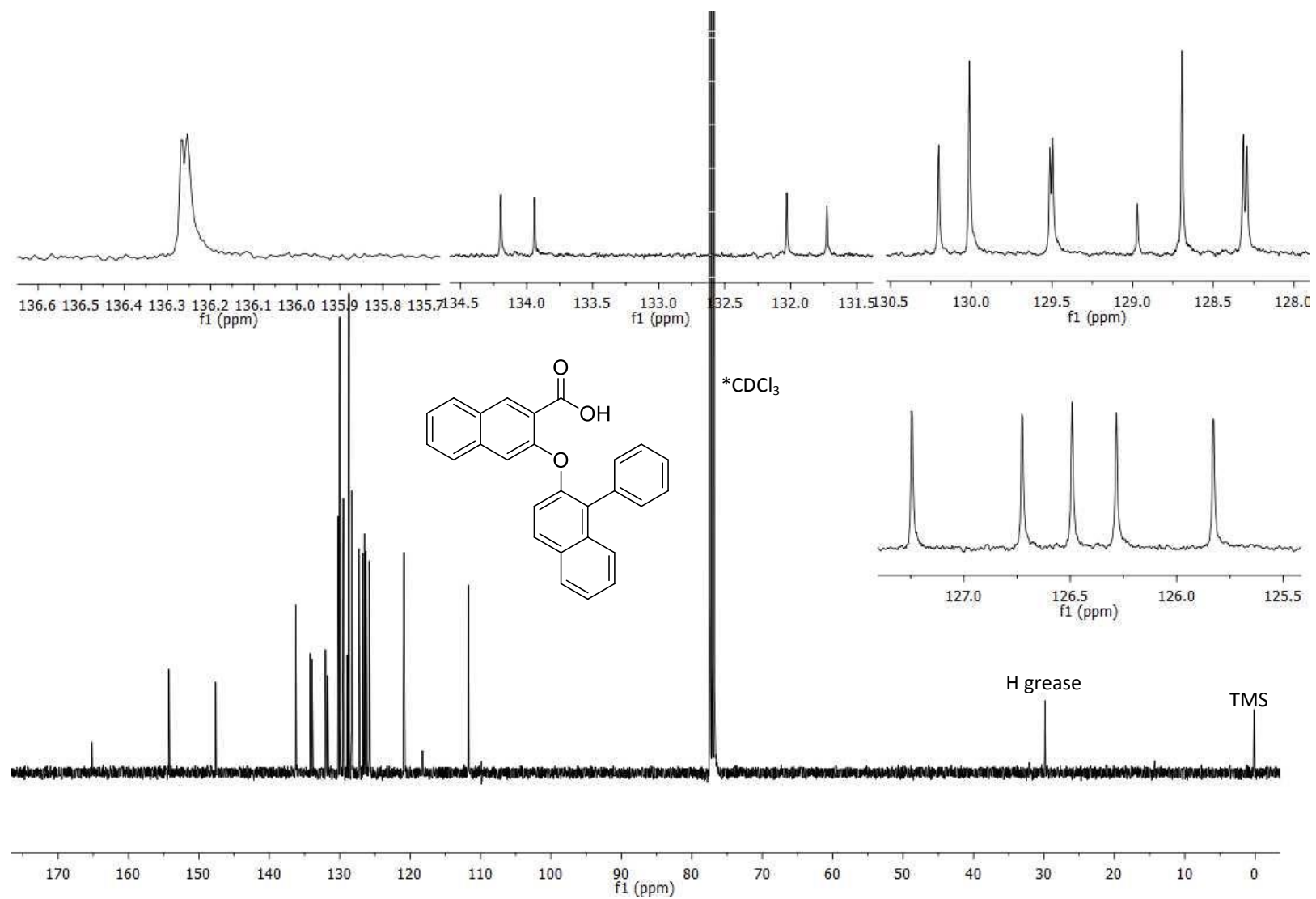
^{13}C NMR (CDCl_3 , 101 MHz) for **42**



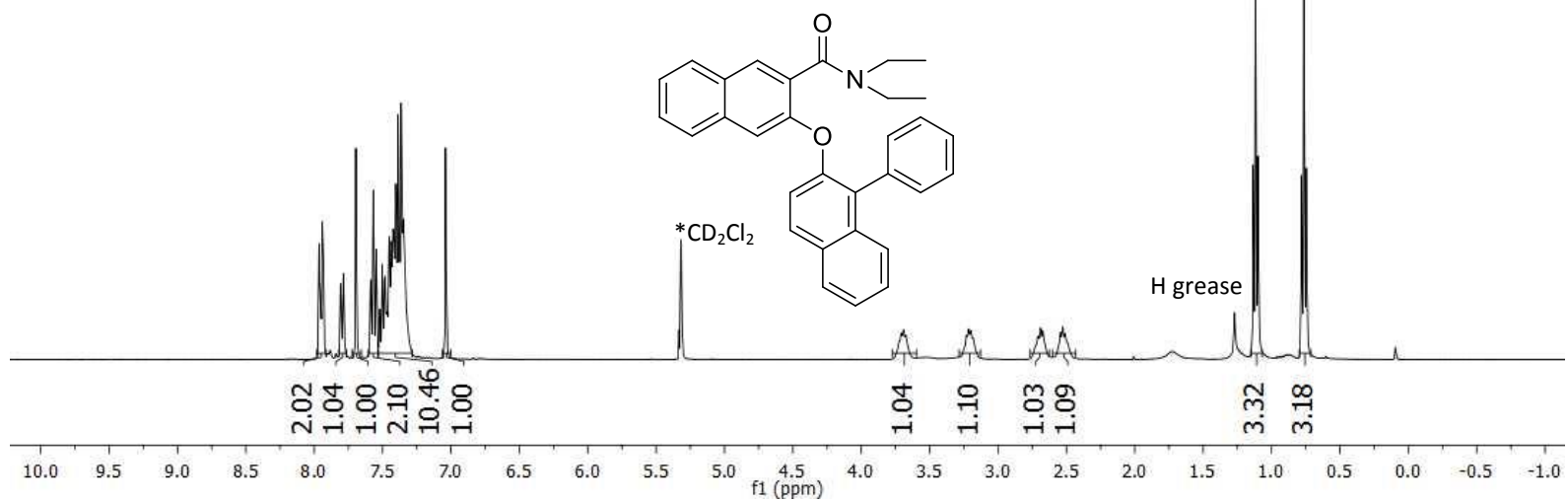
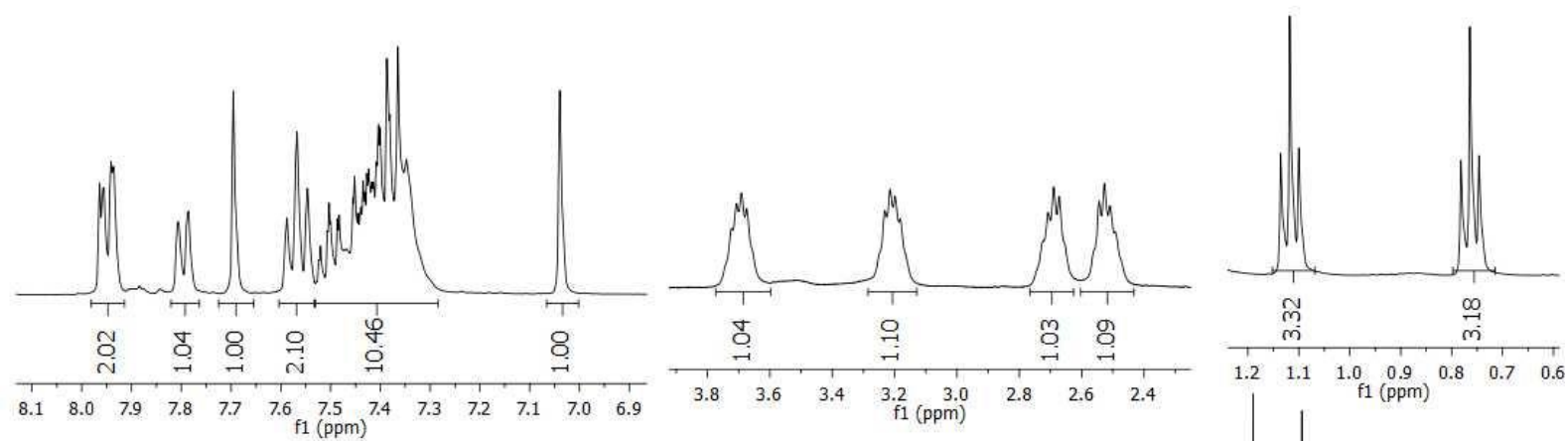
^1H NMR (CDCl_3 , 400 MHz) for **72**



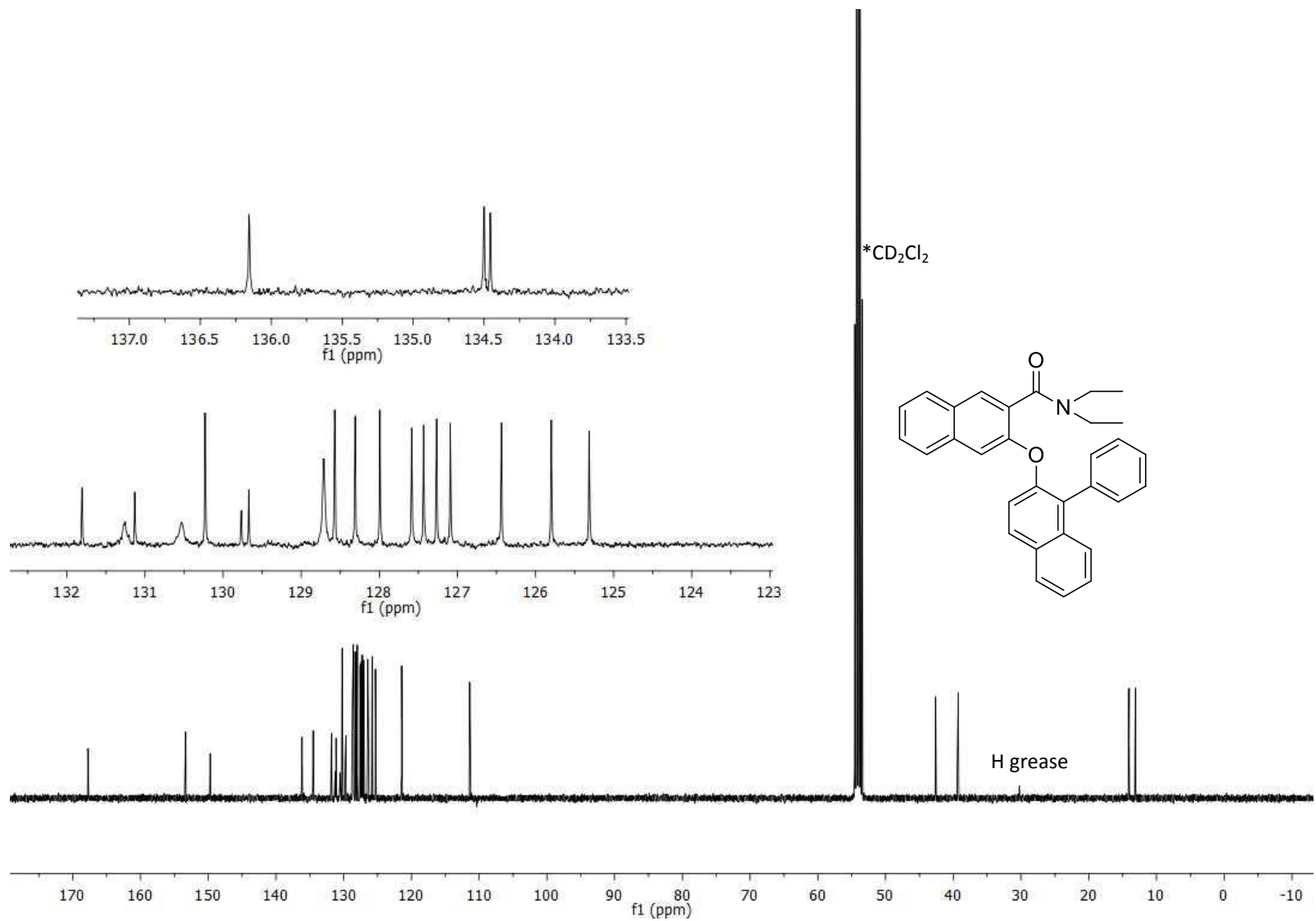
^{13}C NMR (CDCl_3 , 101 MHz) for **72**



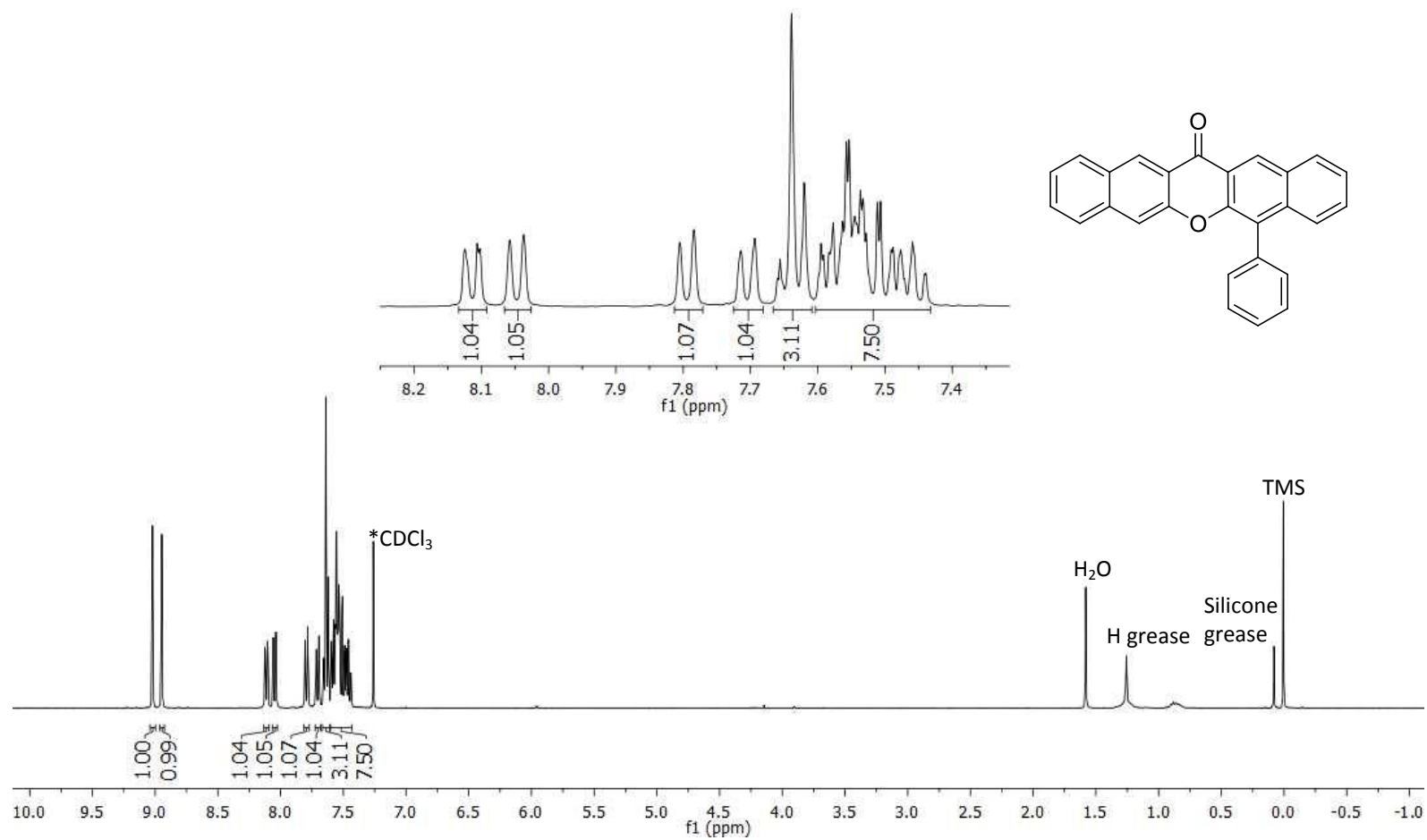
^1H NMR (CD_2Cl_2 , 400 MHz) for **73**



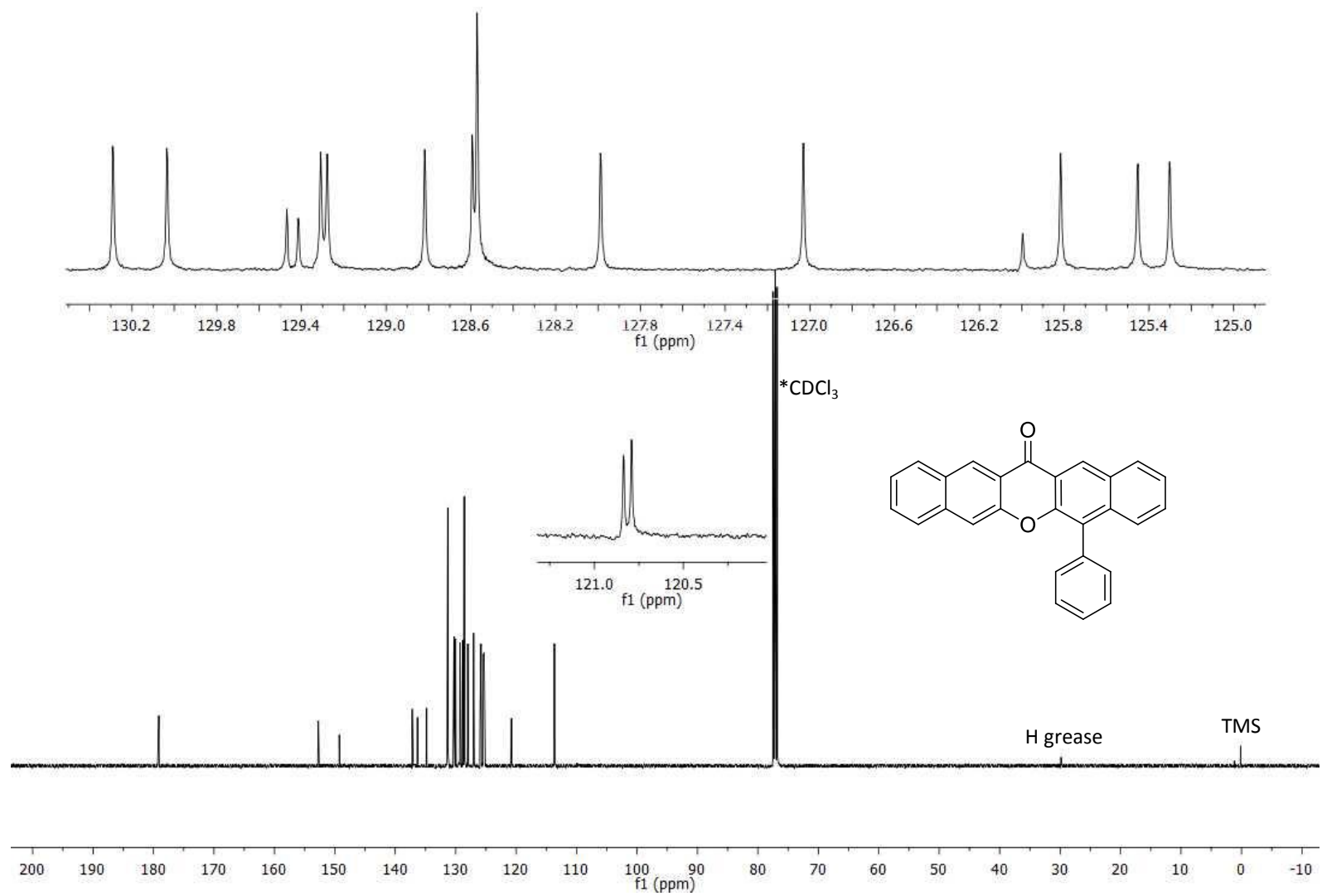
^{13}C NMR (CD_2Cl_2 , 101 MHz) for **73**



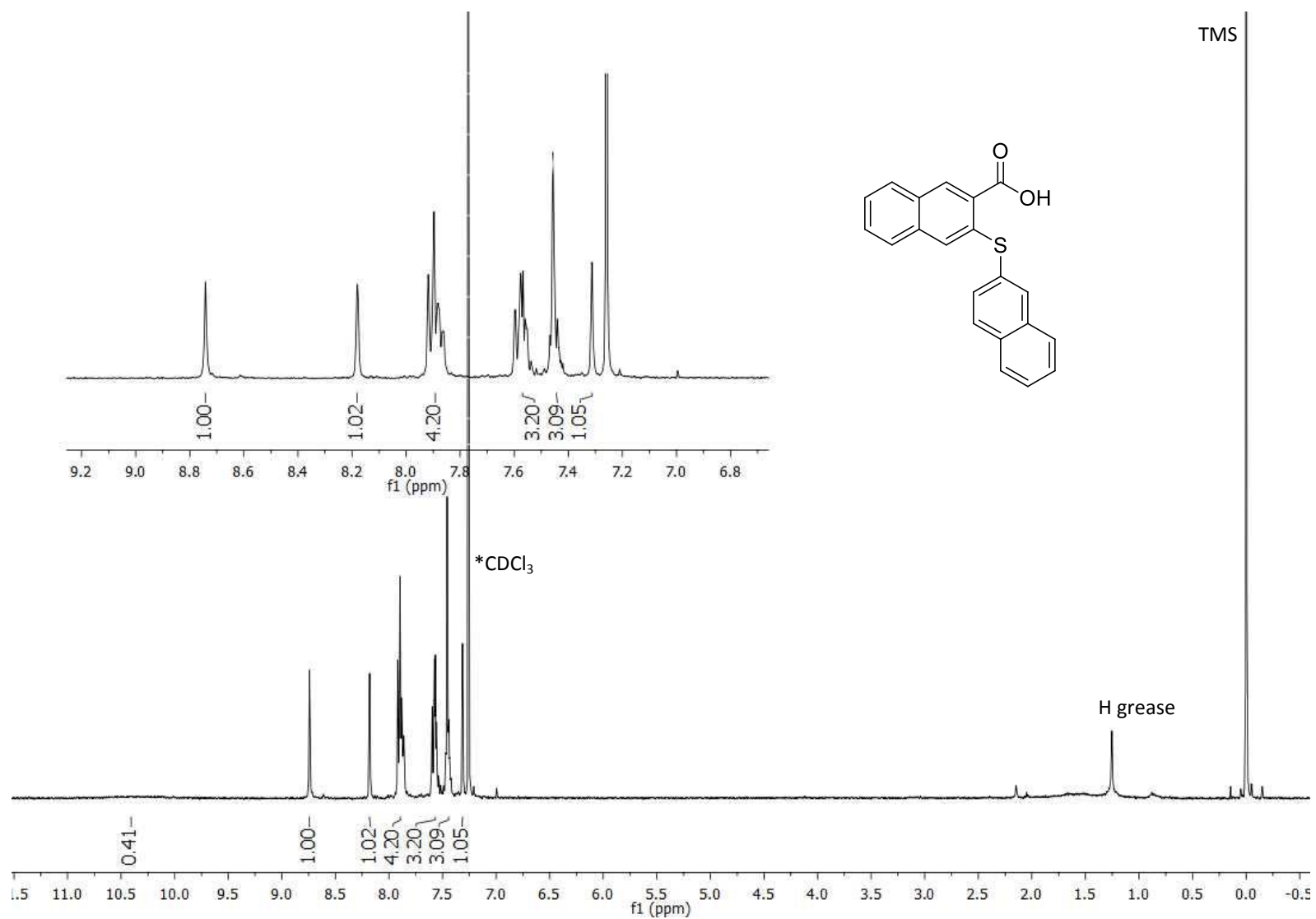
^1H NMR (CDCl_3 , 400 MHz) for **74**



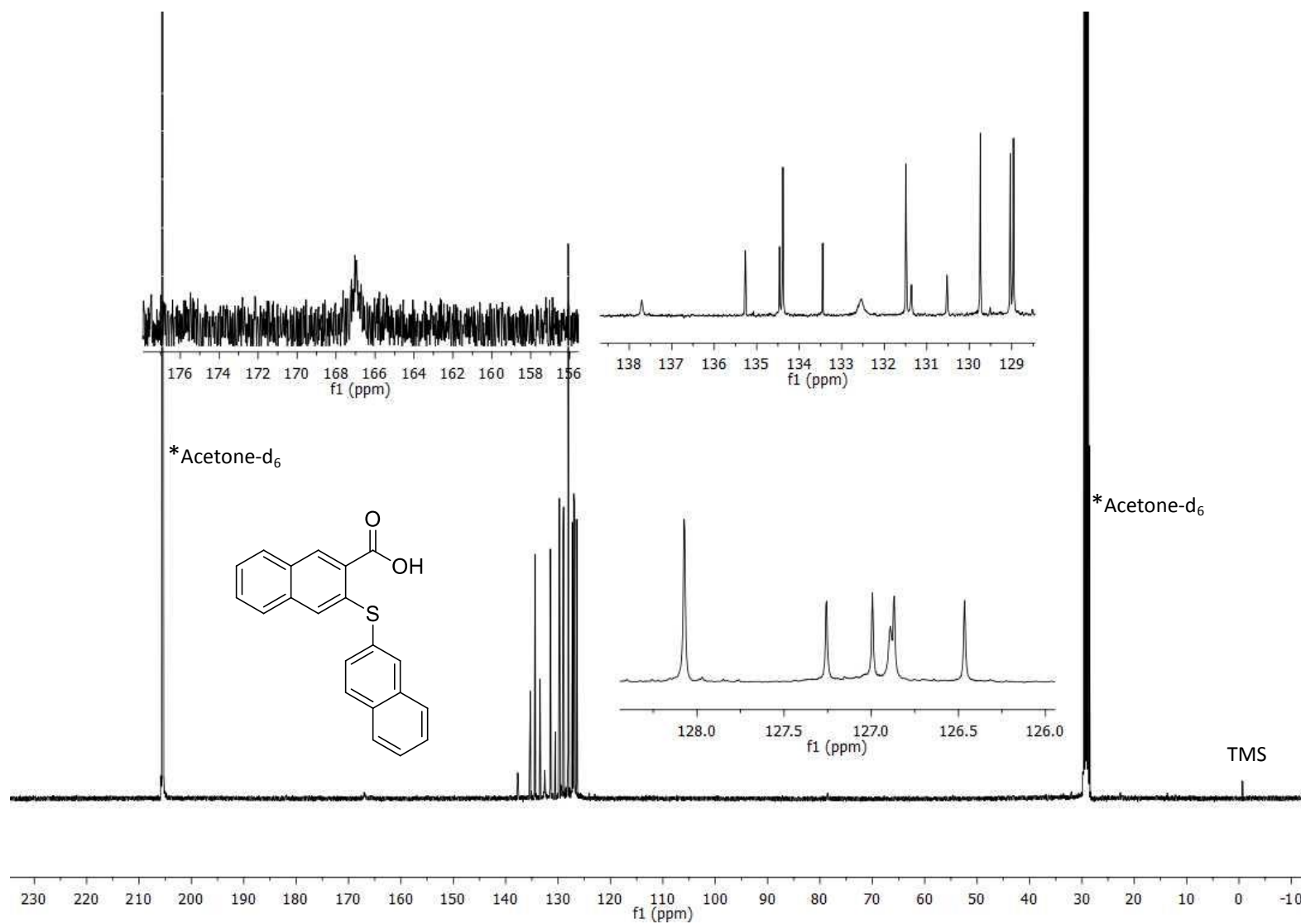
^{13}C NMR (CDCl_3 , 101 MHz) for **74**



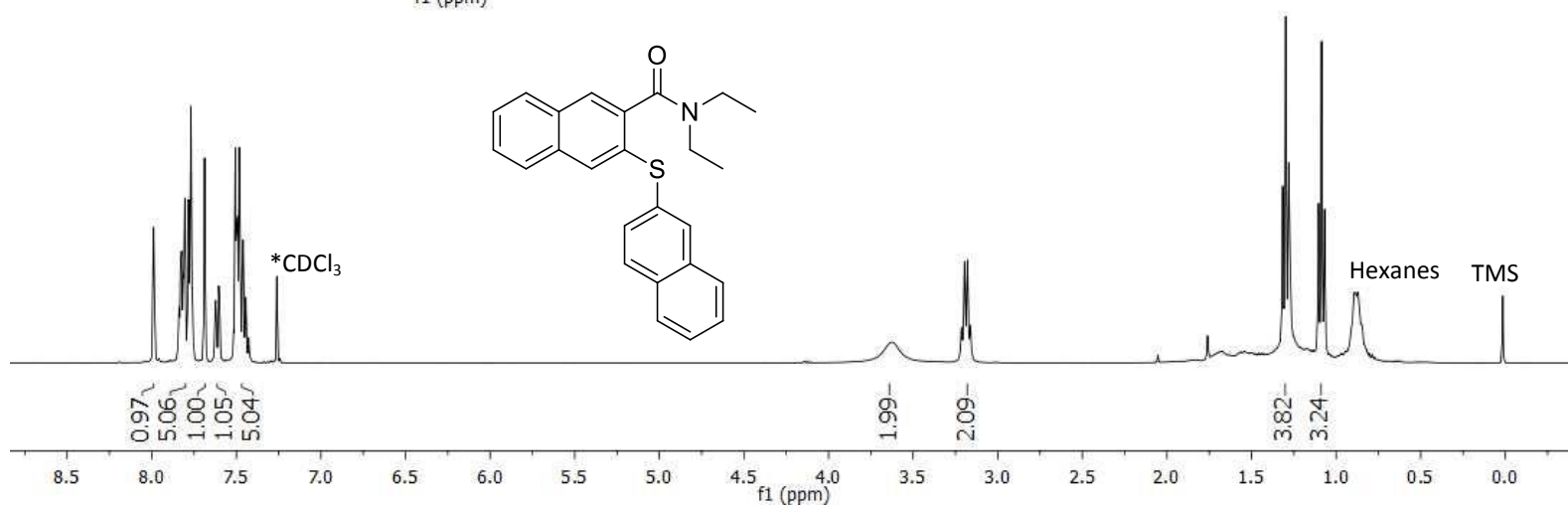
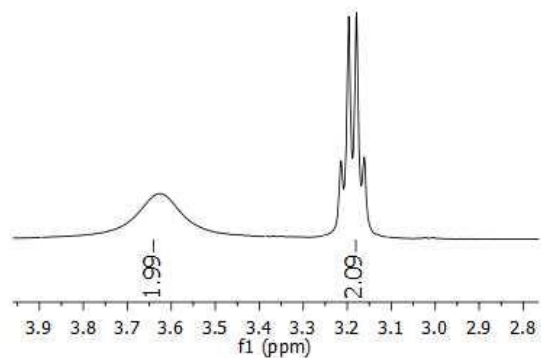
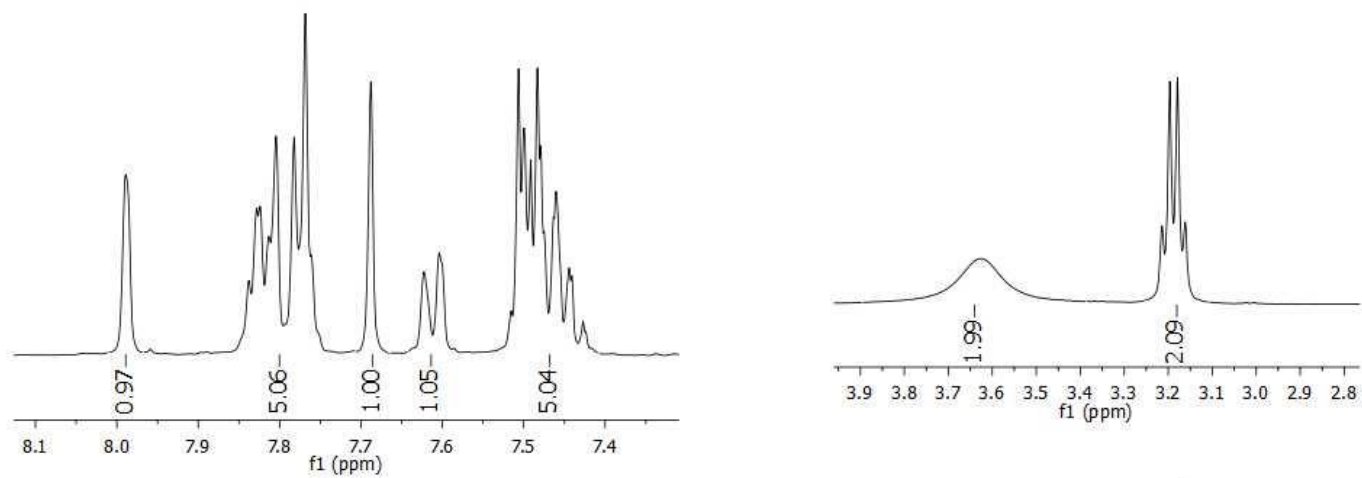
^1H NMR (CDCl_3 , 400 MHz) for **78**



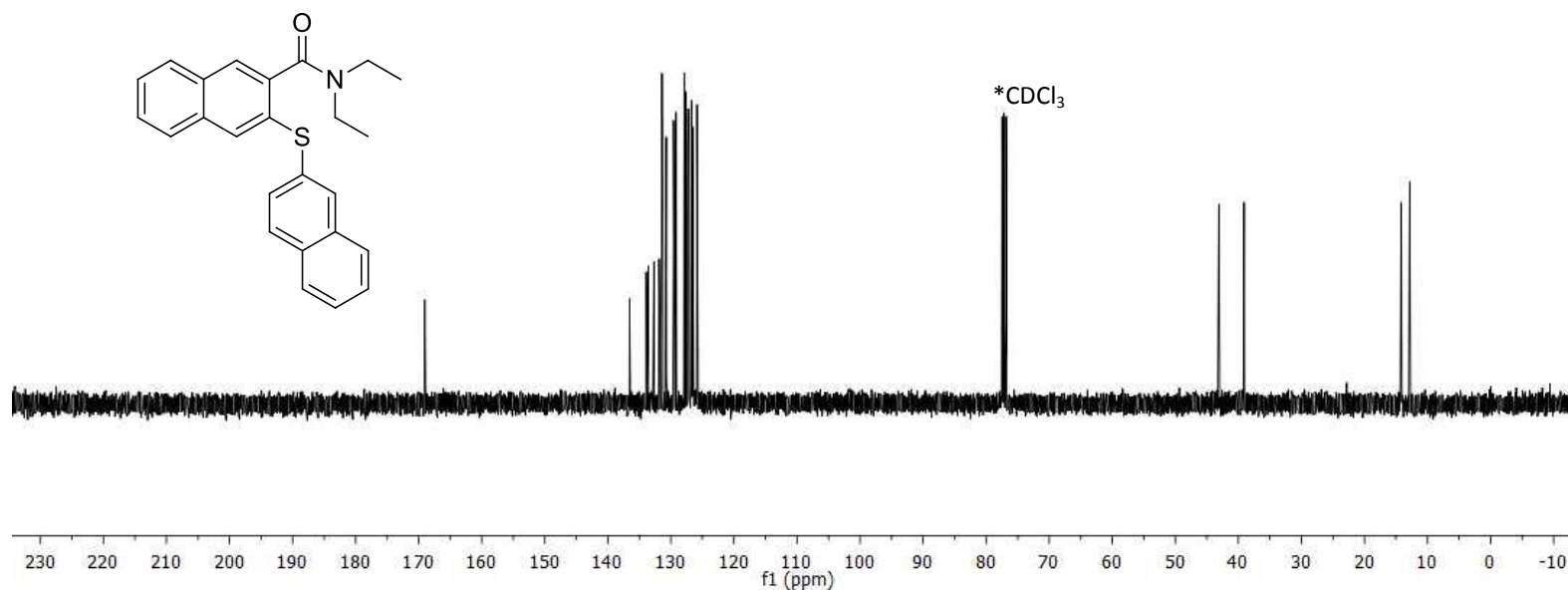
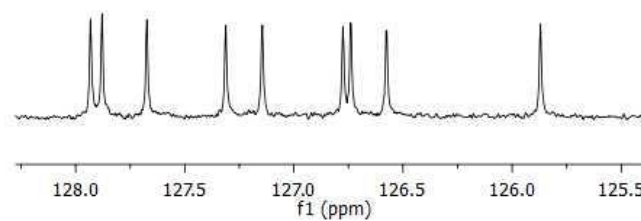
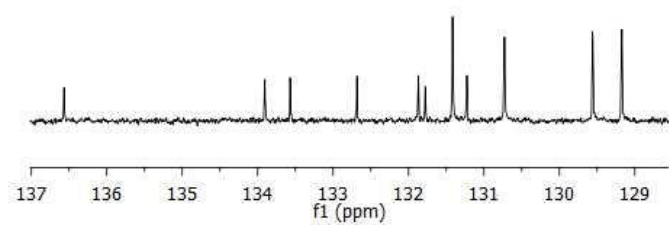
^{13}C NMR (Acetone- d_6 , 101 MHz) for **78**



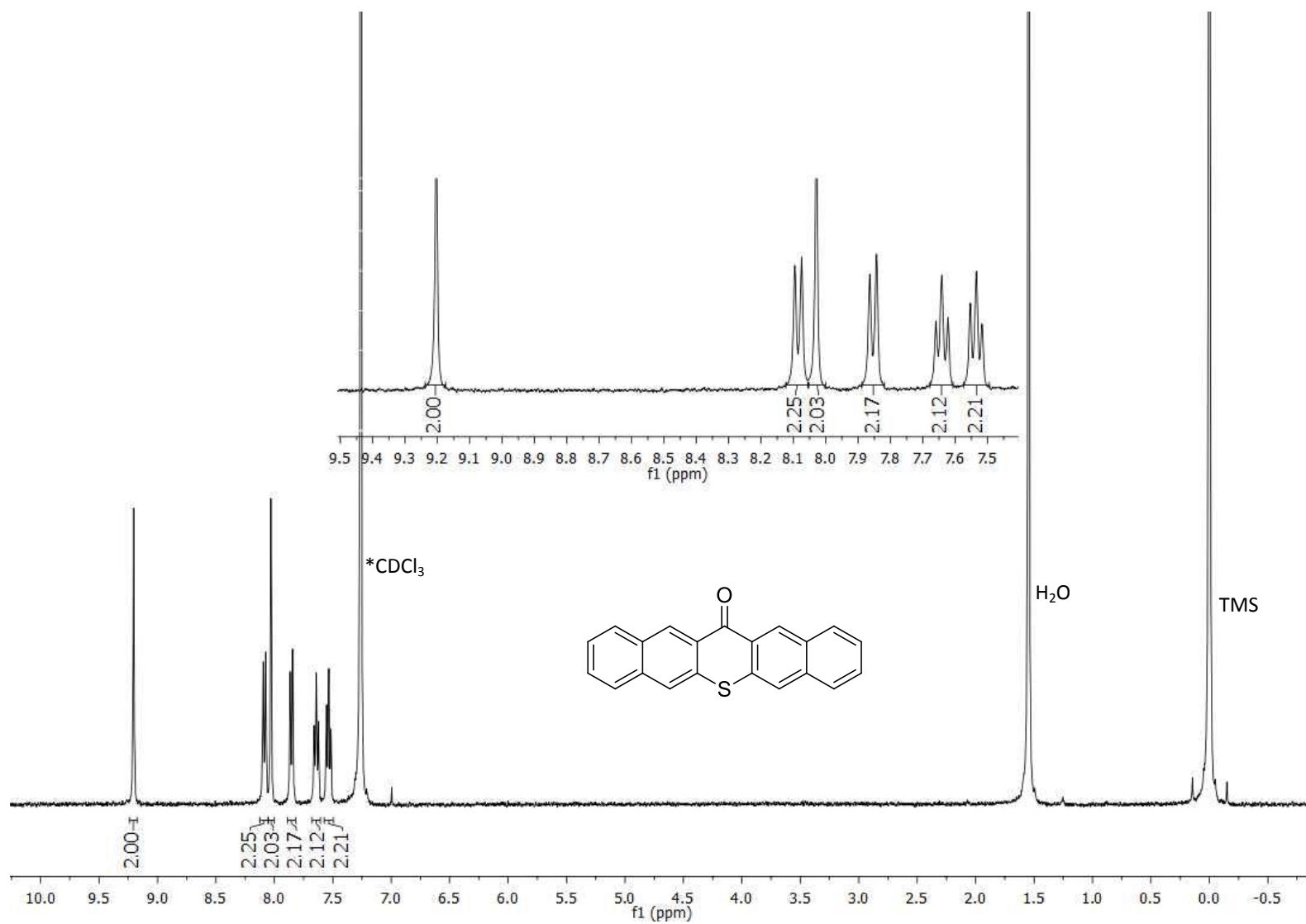
^1H NMR (CDCl_3 , 400 MHz) for **79**



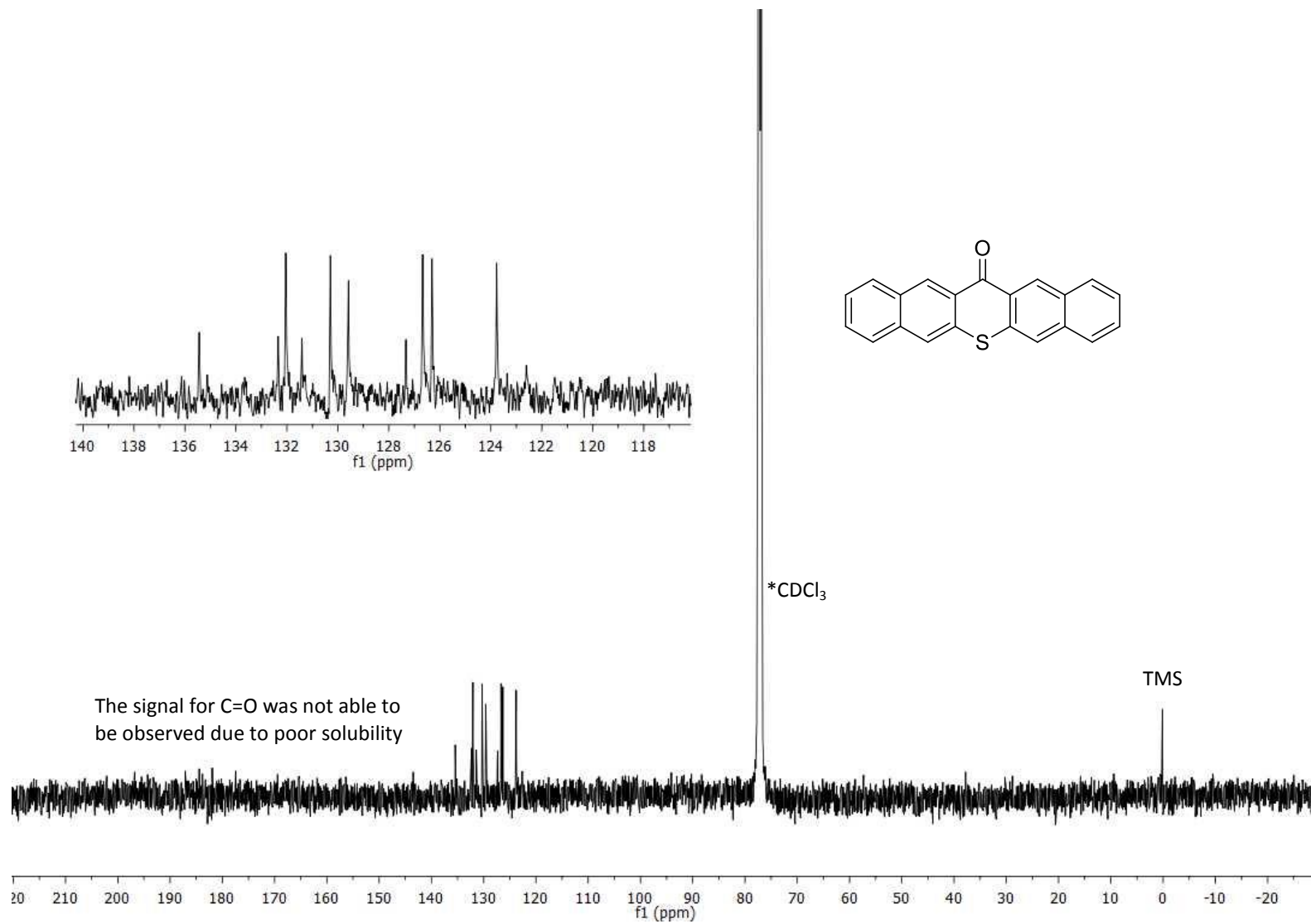
^{13}C NMR (CDCl_3 , 101 MHz) for **79**



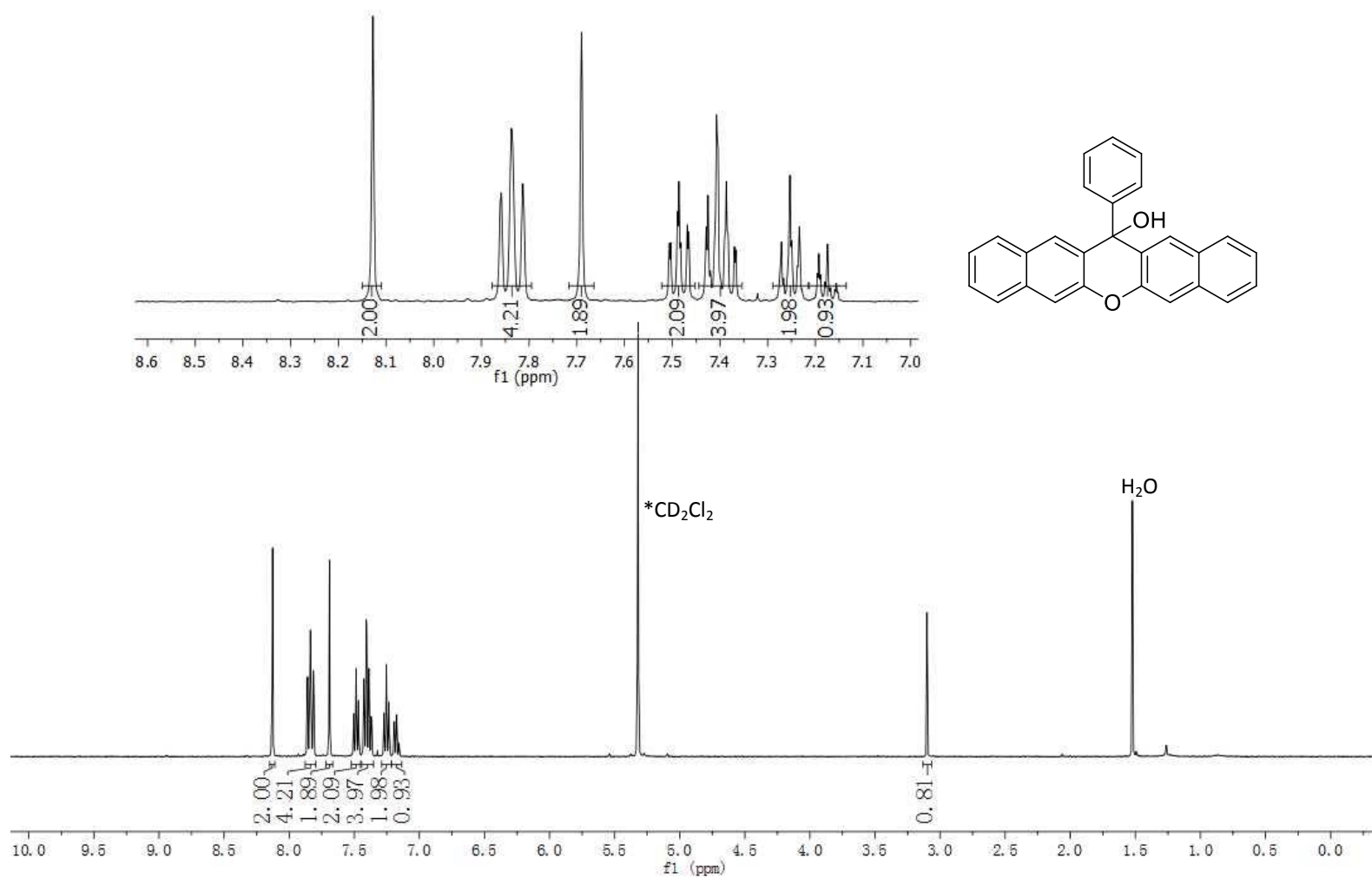
^1H NMR (CDCl_3 , 400 MHz) for **80**



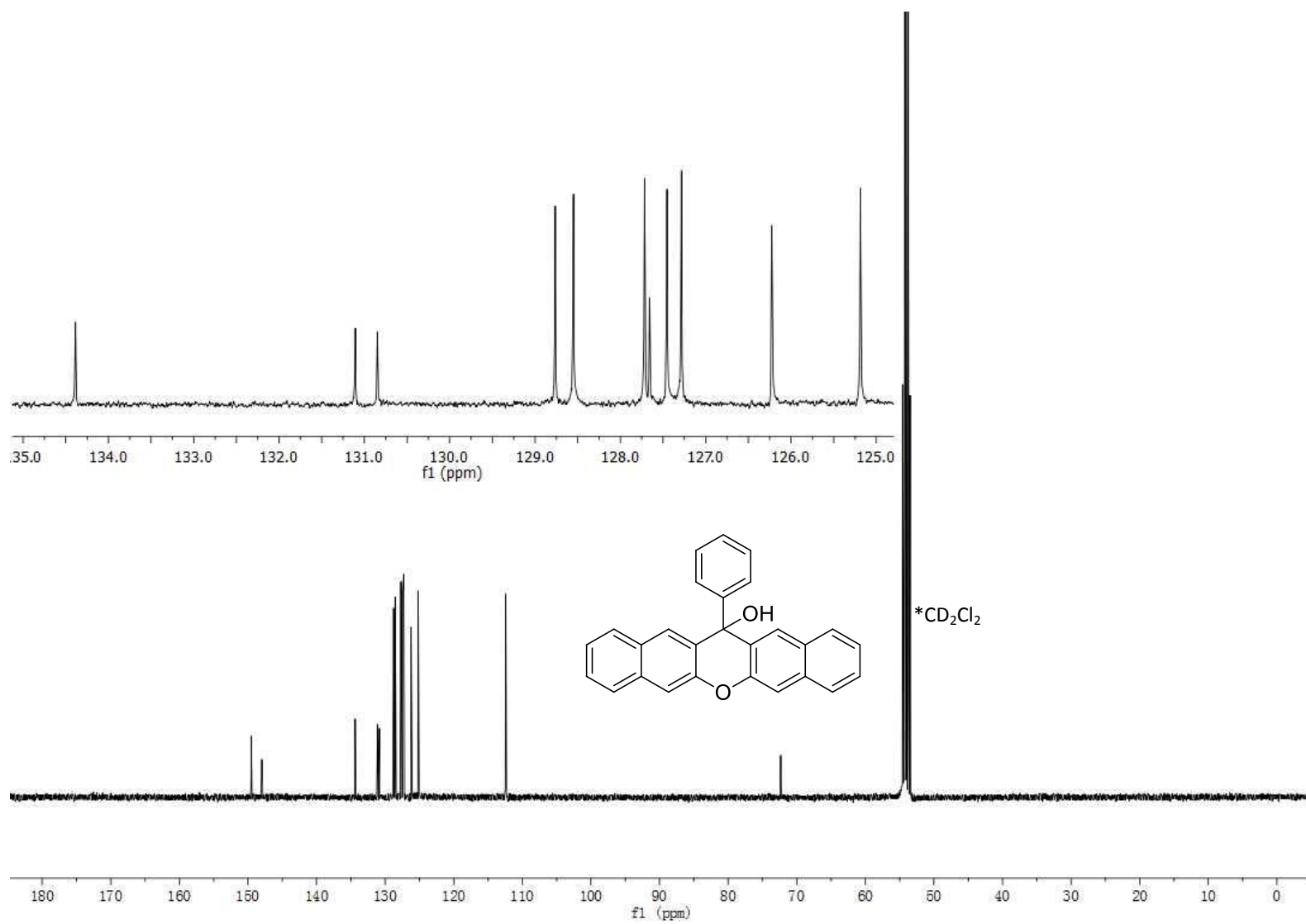
^{13}C NMR (CDCl_3 , 126 MHz, 55 °C) for **80**



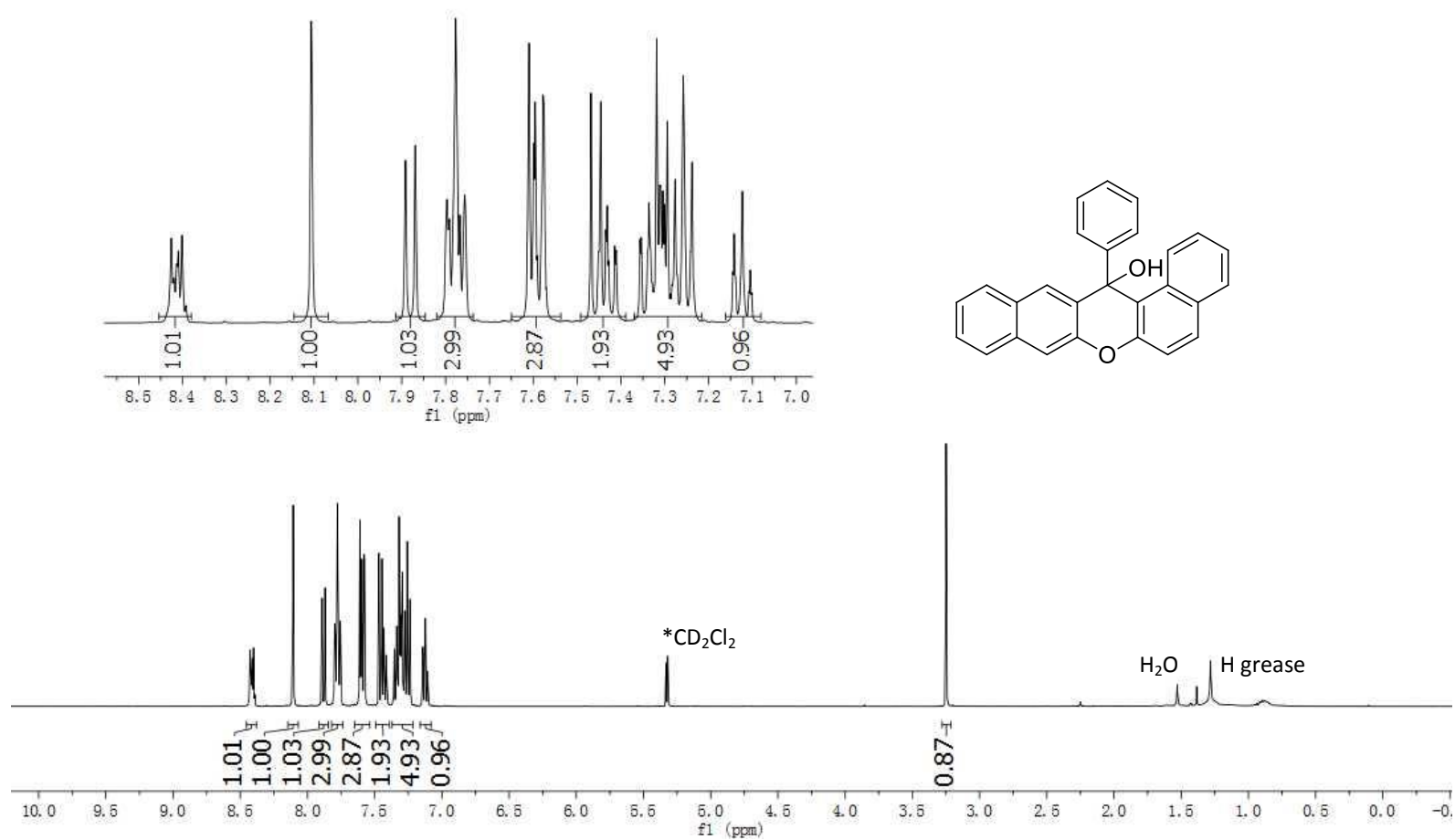
^1H NMR (CD_2Cl_2 , 400 MHz) for **83**



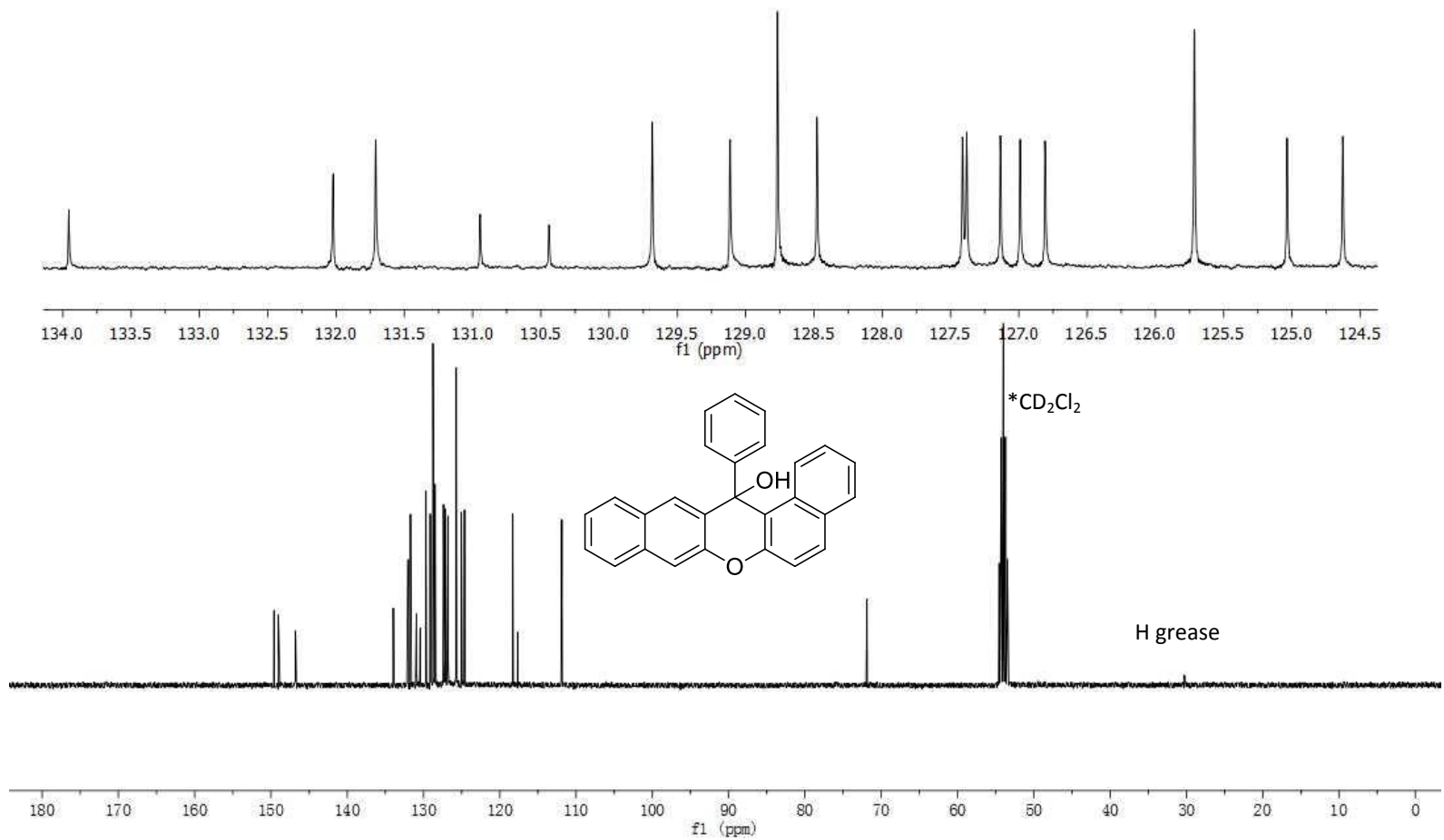
^{13}C NMR (CD_2Cl_2 , 101 MHz) for **83**



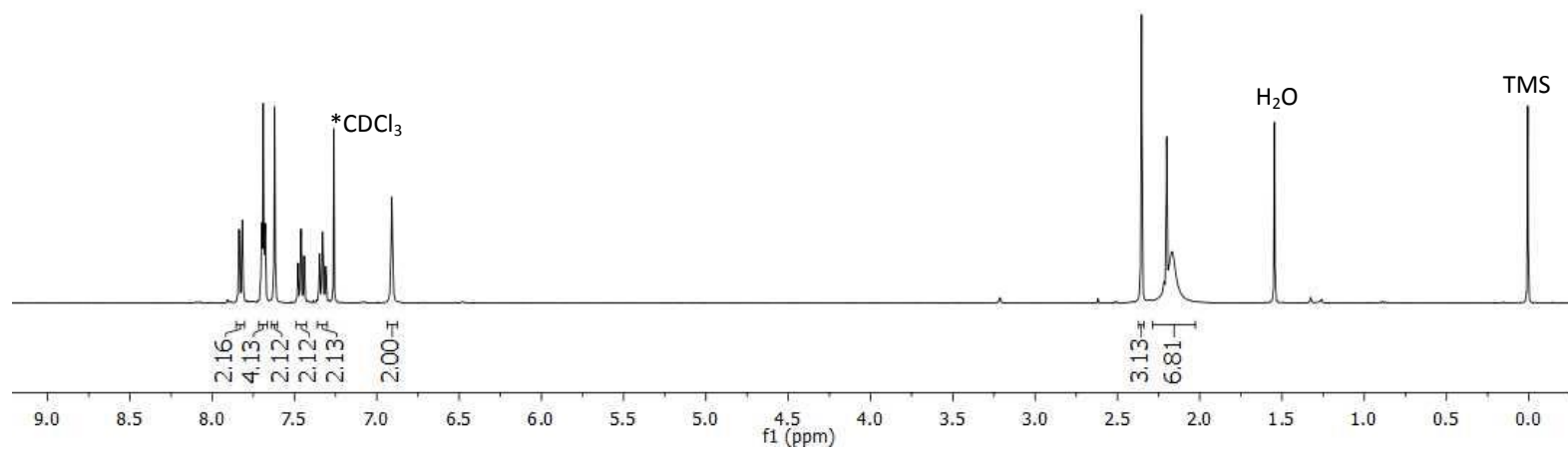
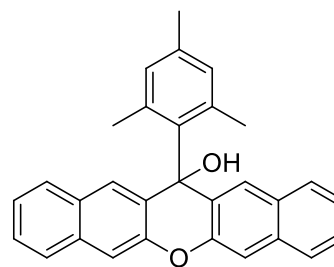
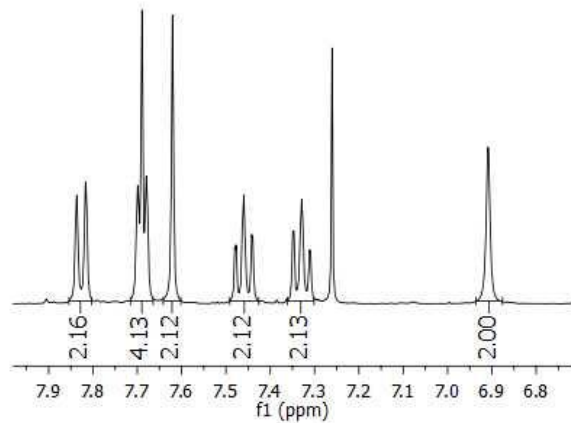
^1H NMR (CD_2Cl_2 , 400 MHz) for **82**



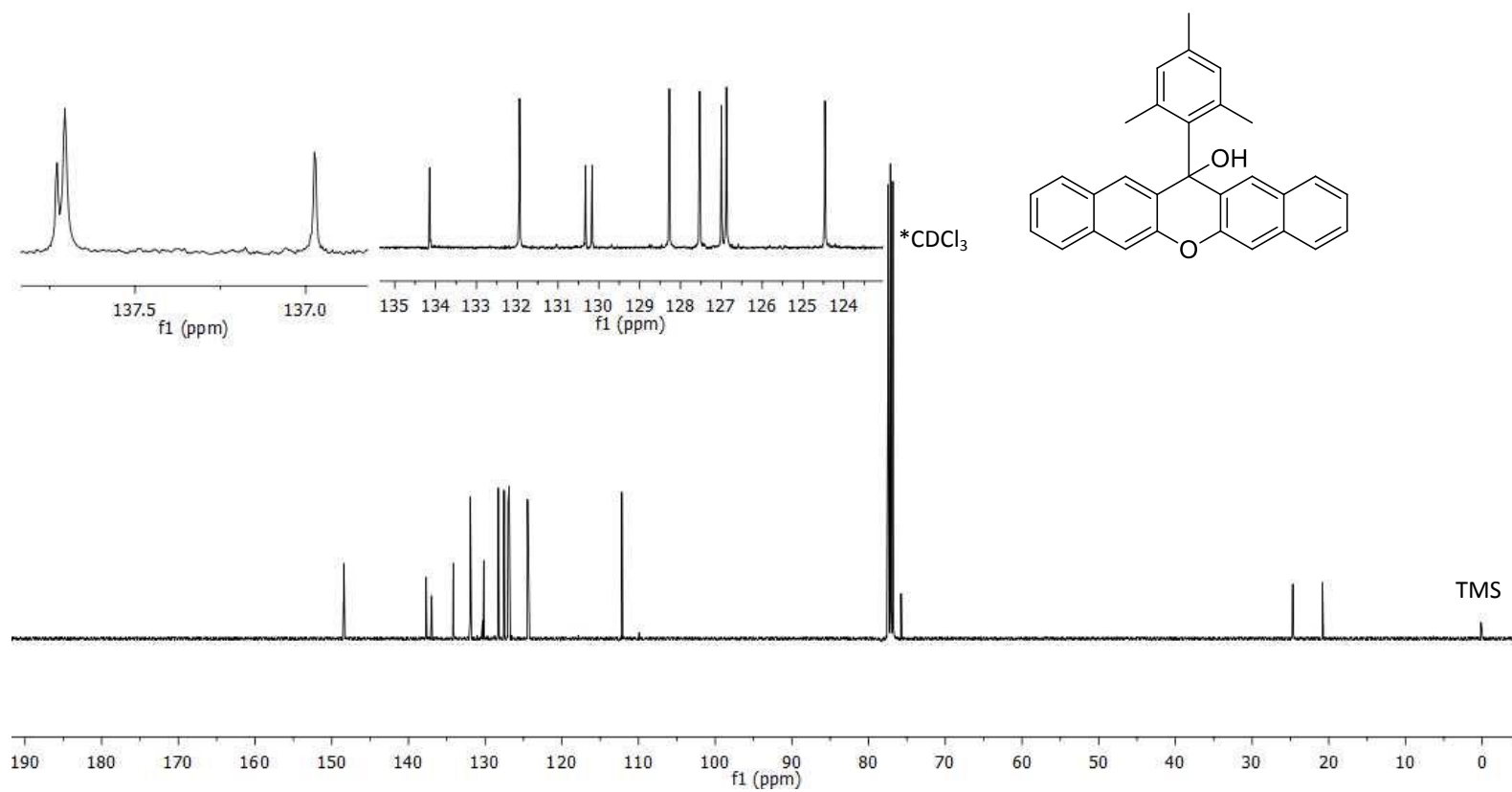
^{13}C NMR (CD_2Cl_2 , 101 MHz) for **82**



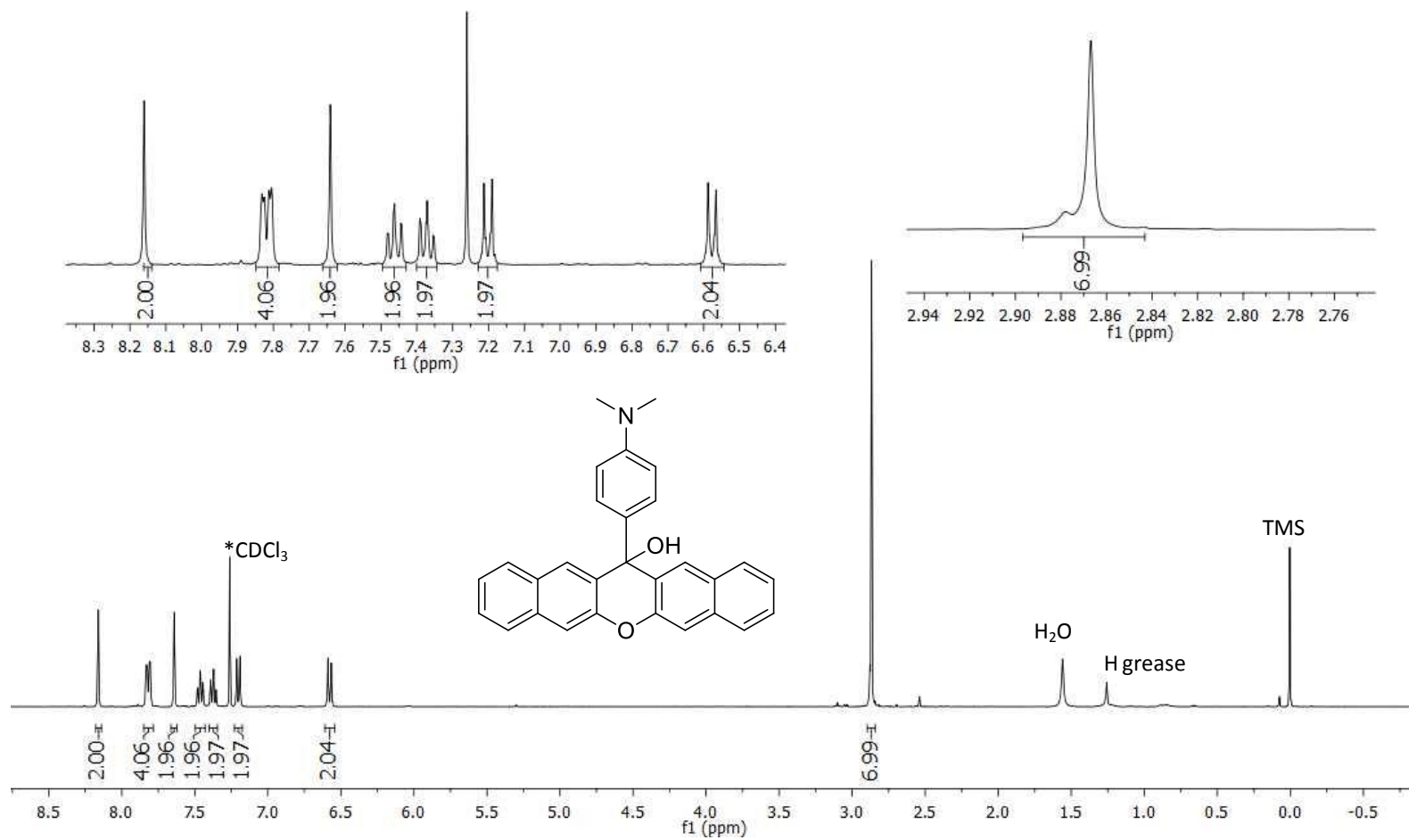
^1H NMR (CDCl_3 , 400 MHz) for **85**



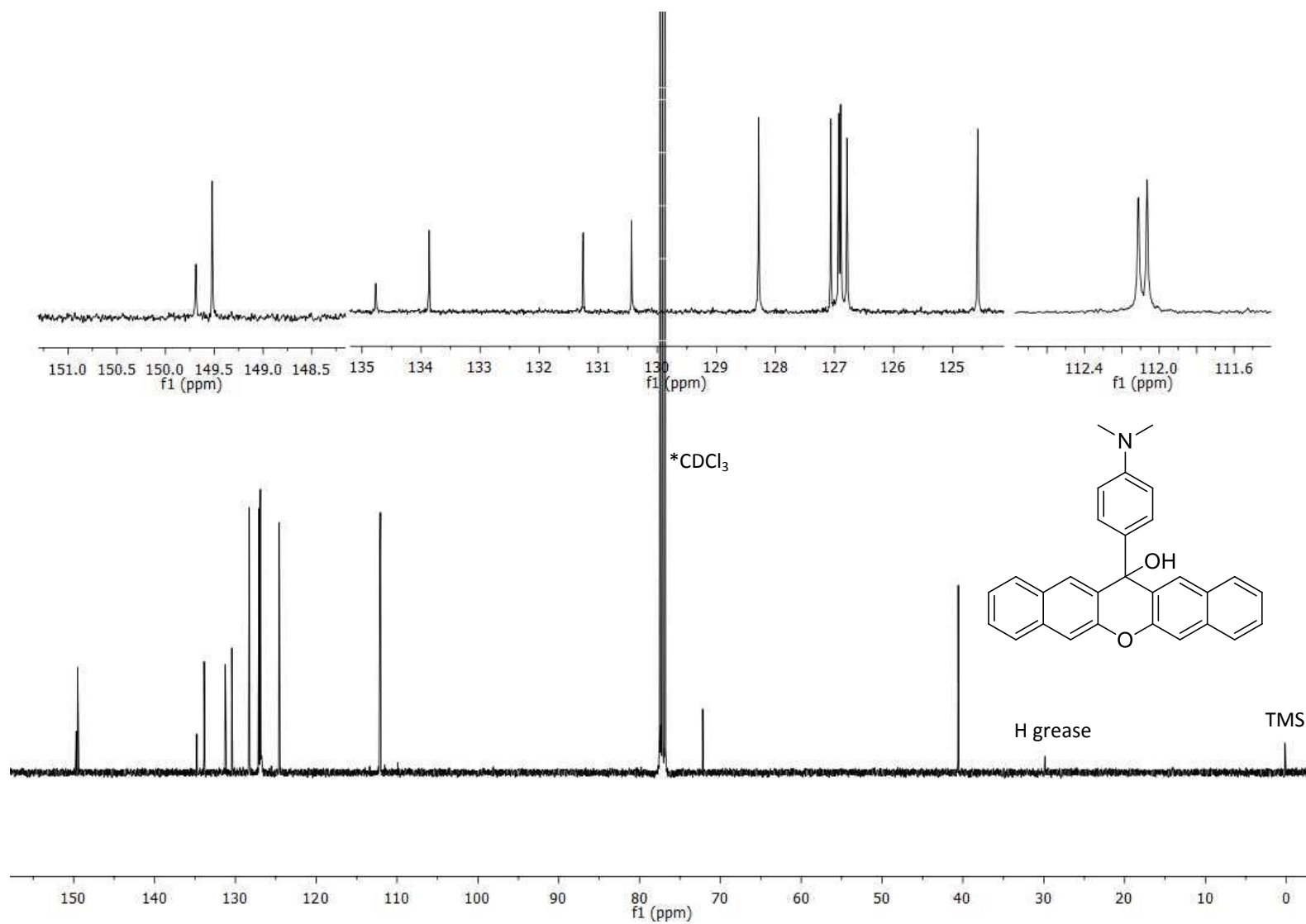
^{13}C NMR (CDCl_3 , 101 MHz) for **85**



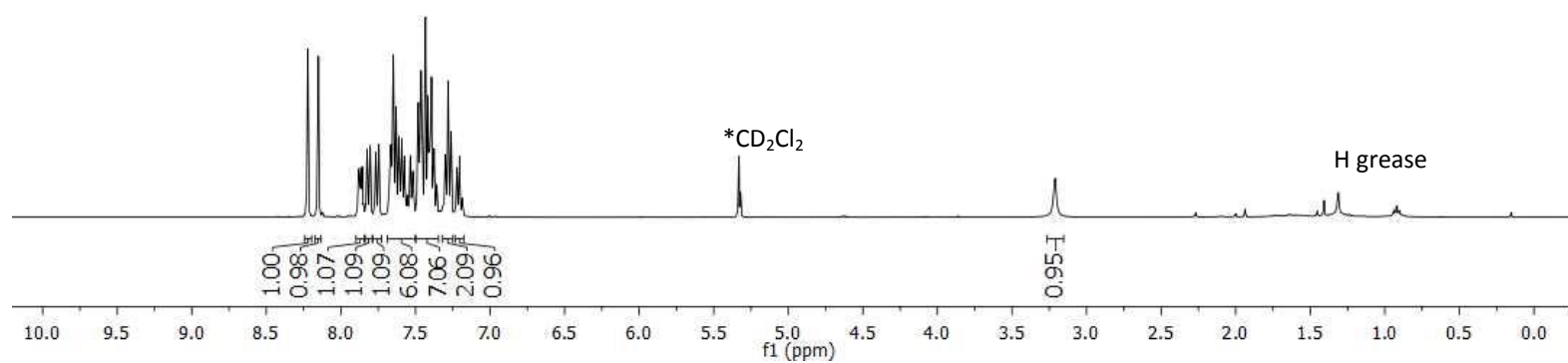
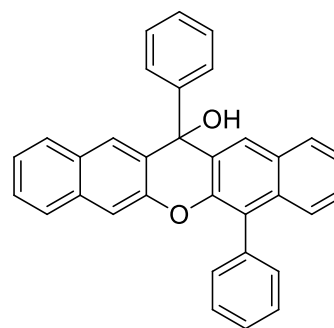
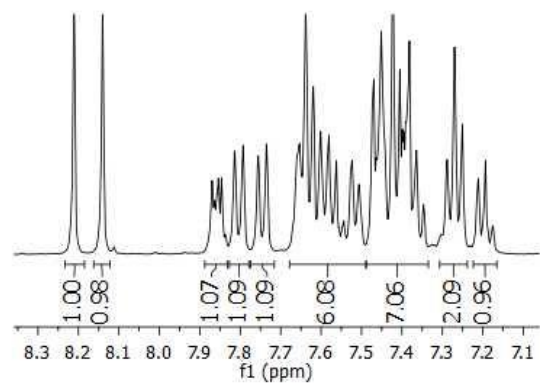
^1H NMR (CDCl_3 , 400 MHz) for **87**



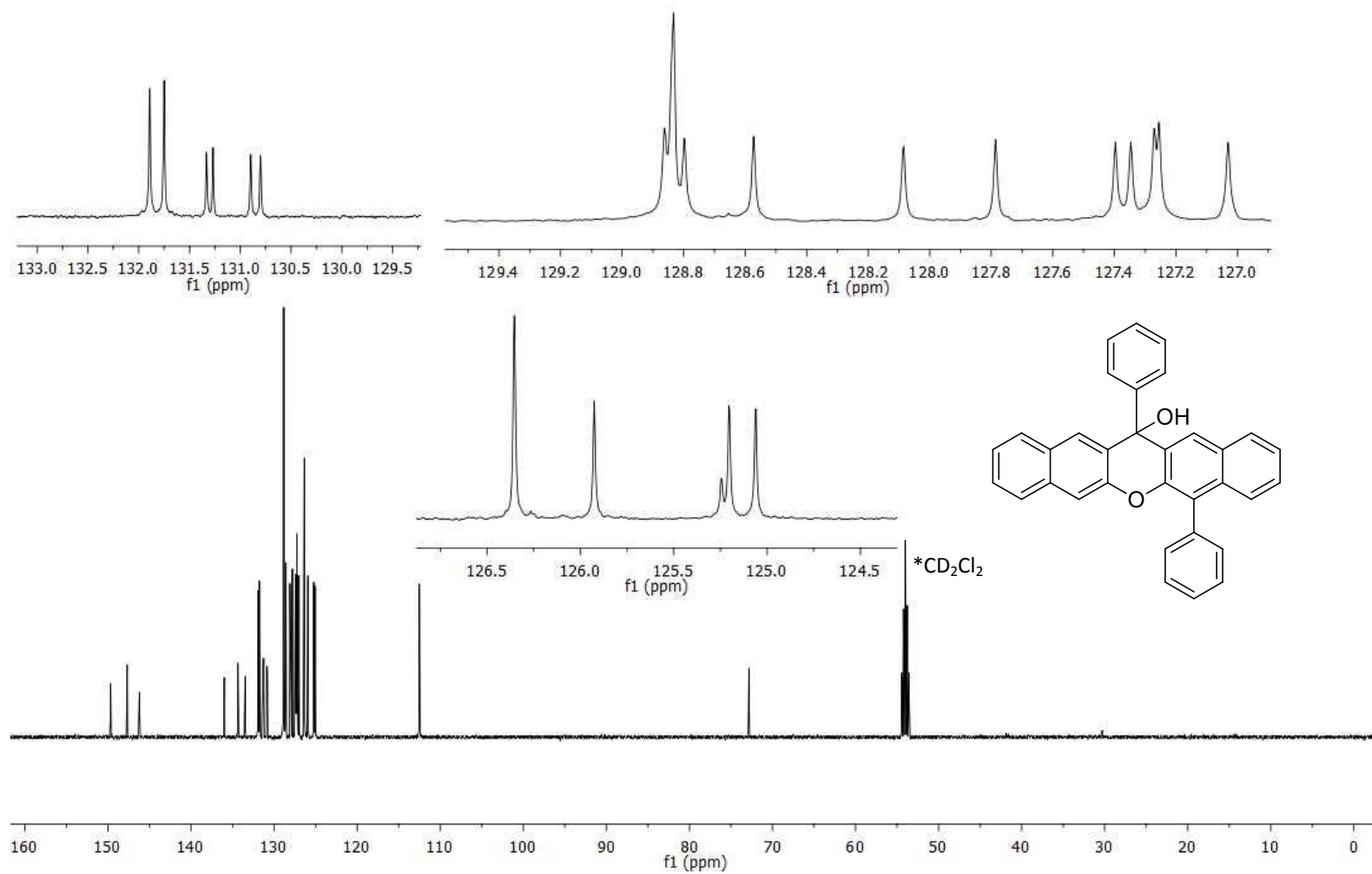
^{13}C NMR (CDCl_3 , 101 MHz) for **87**



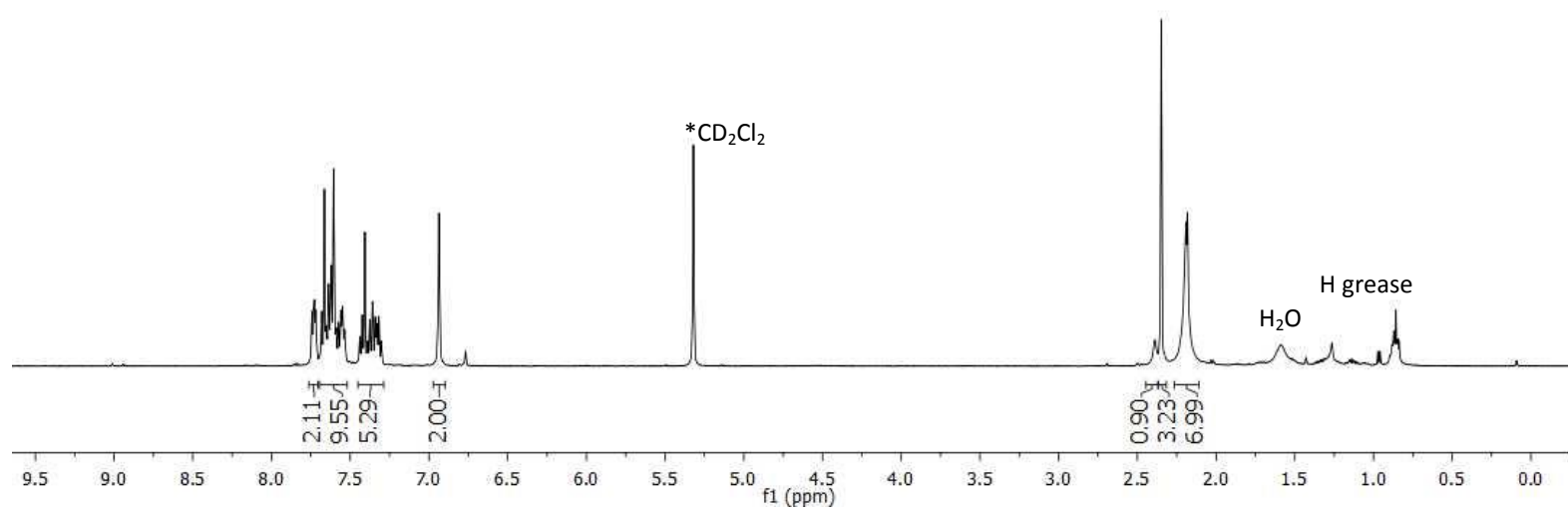
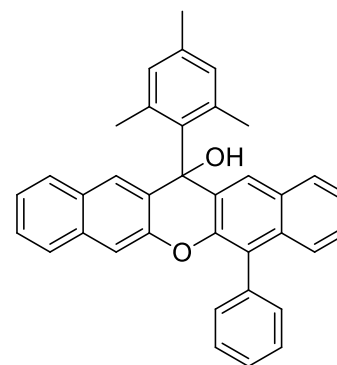
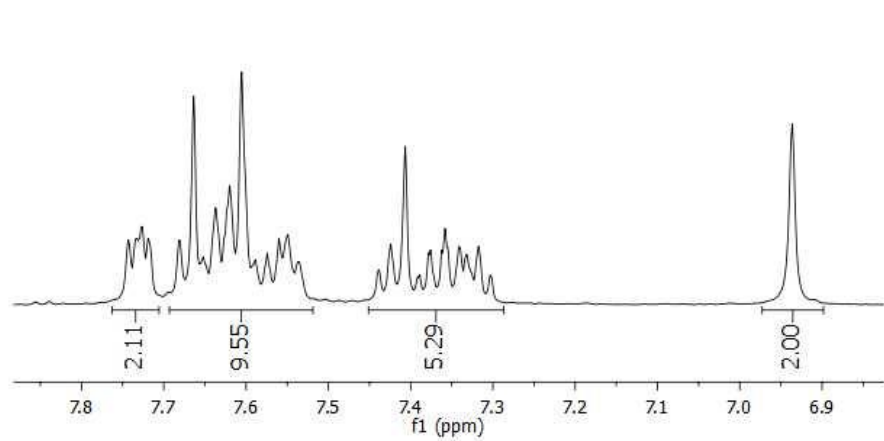
^1H NMR (CD_2Cl_2 , 400 MHz) for **88**



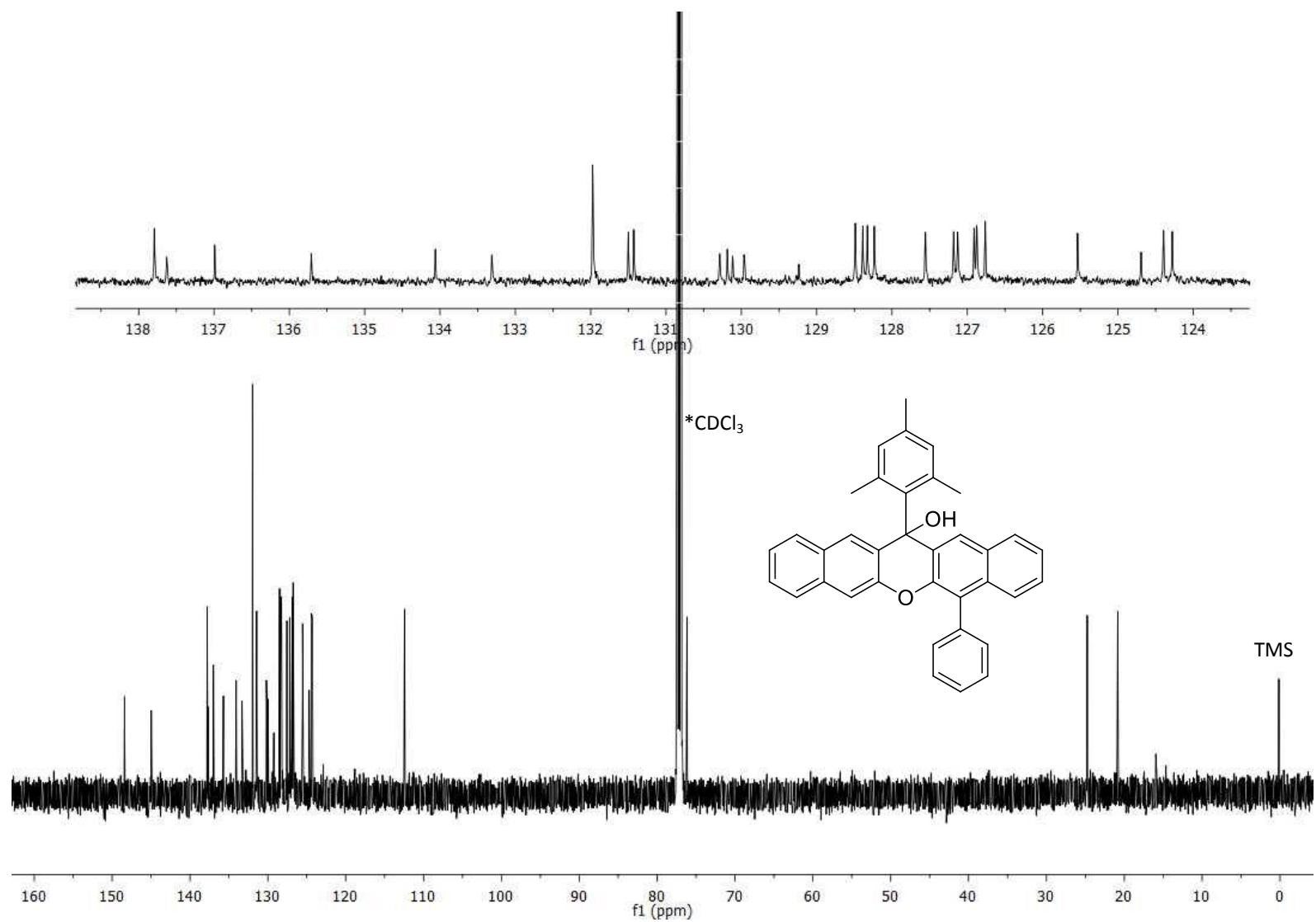
^{13}C NMR (CD_2Cl_2 , 126 MHz) for **88**



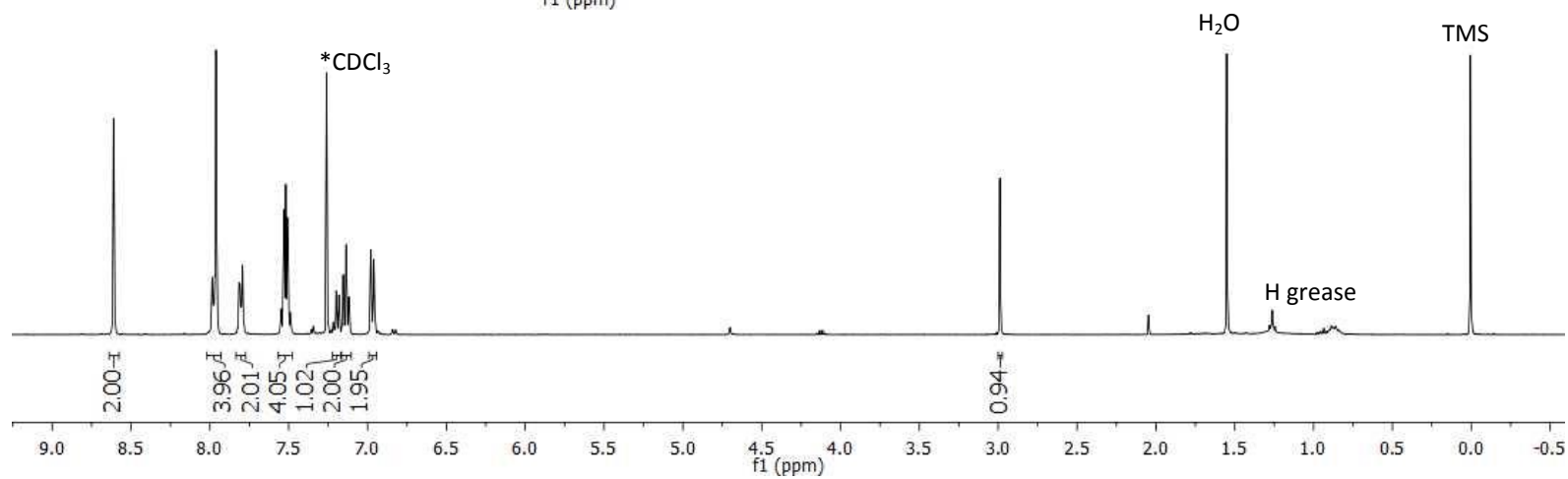
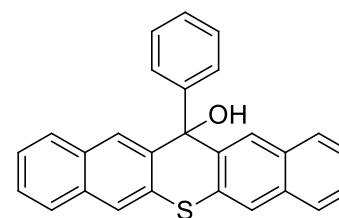
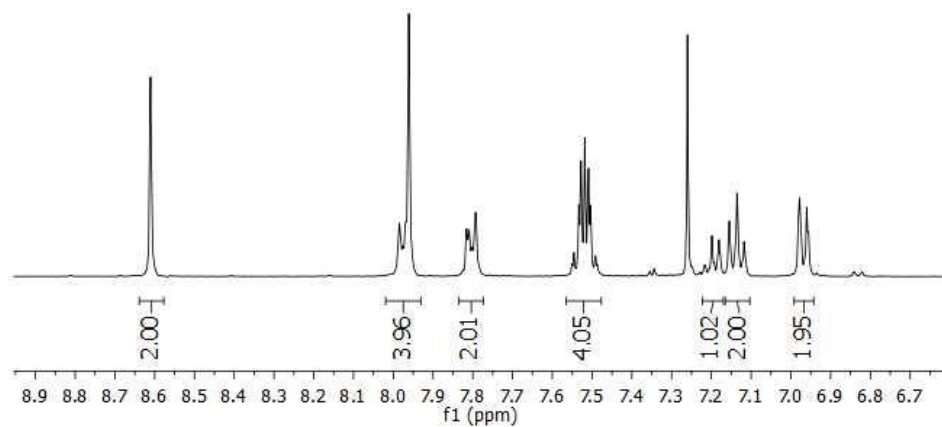
^1H NMR (CD_2Cl_2 , 500 MHz) for **89**



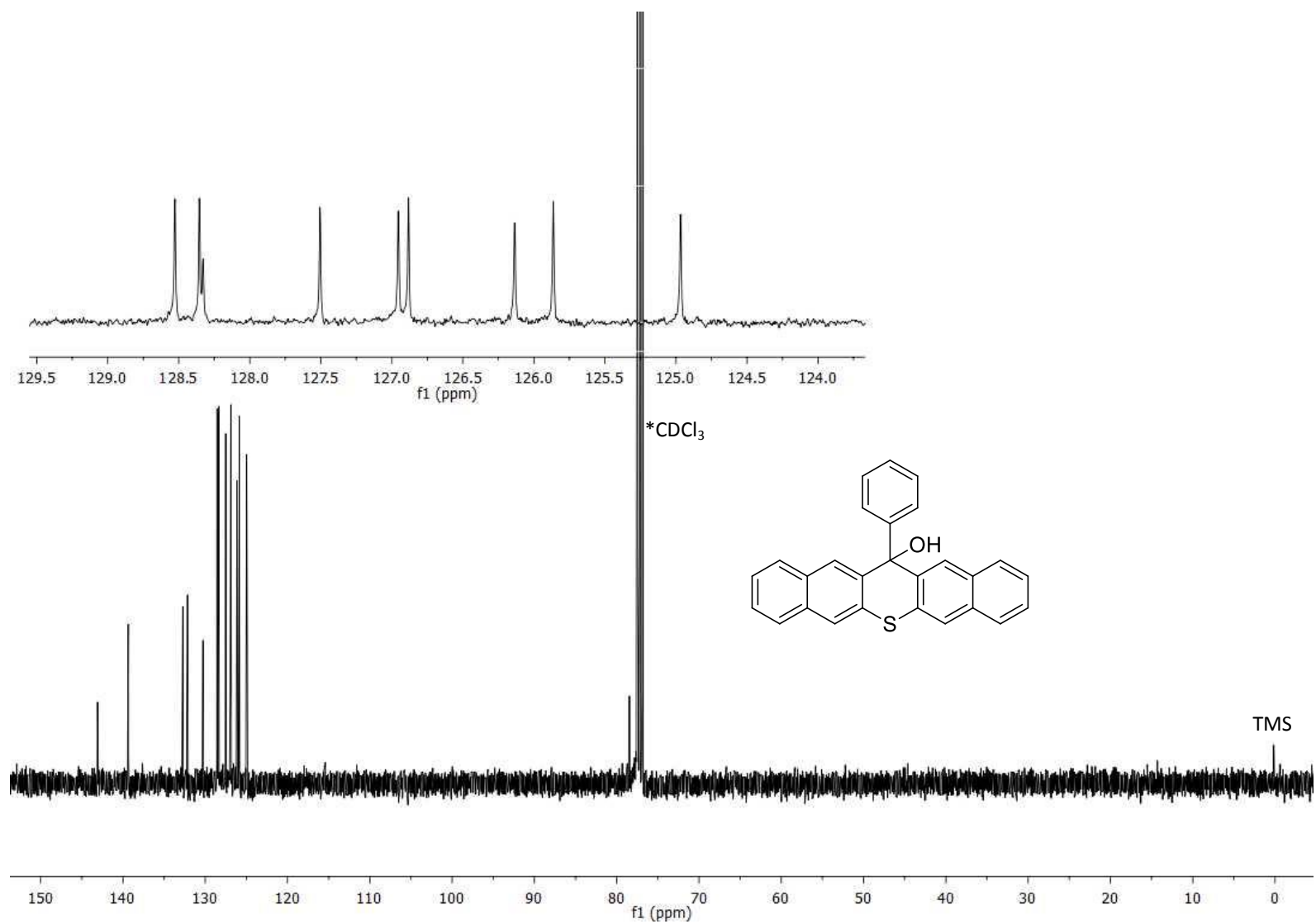
^{13}C NMR (CDCl_3 , 126 MHz) for **89**



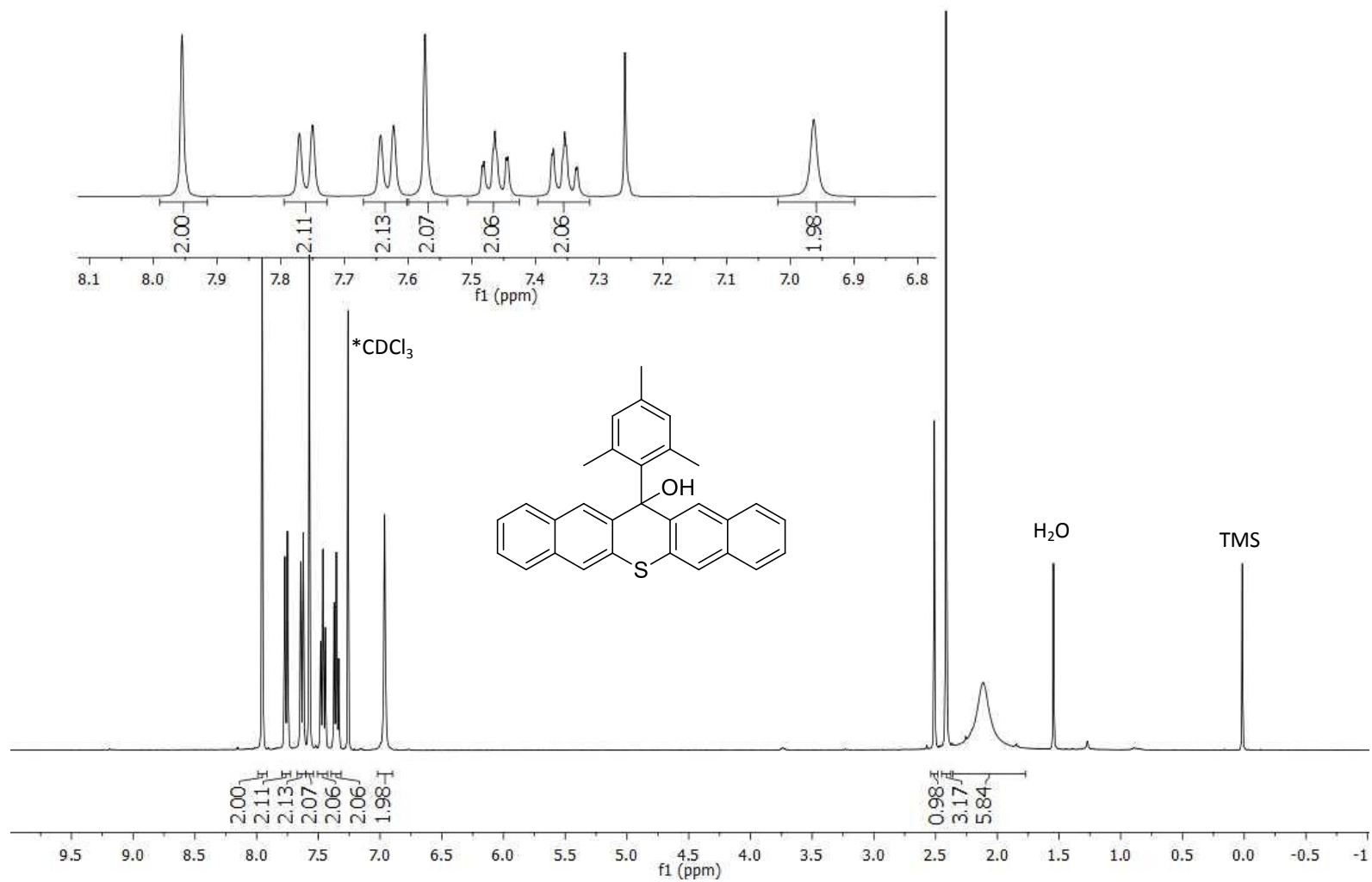
^1H NMR (CDCl_3 , 400 MHz) for **90**



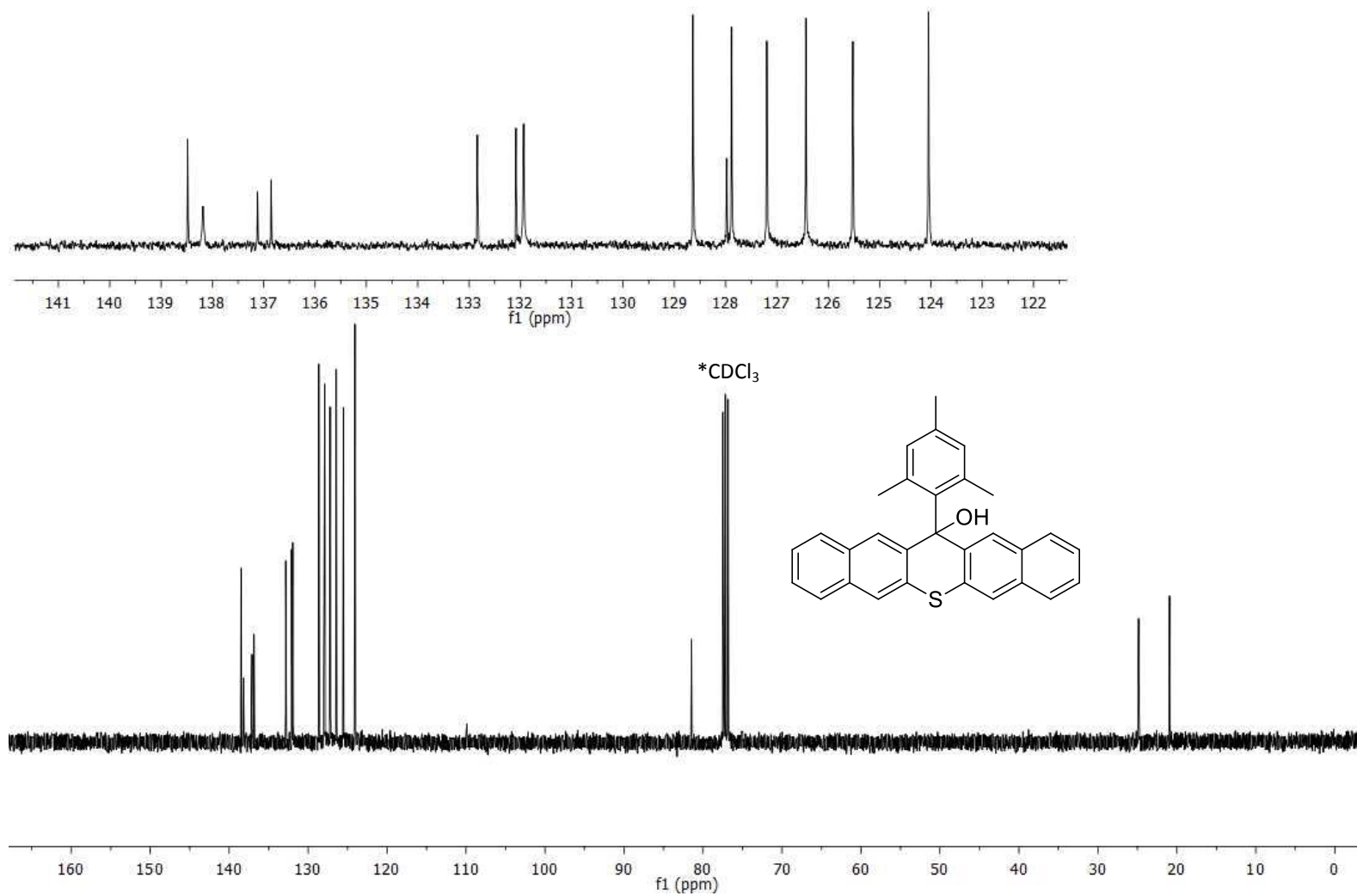
^{13}C NMR (CDCl_3 , 101 MHz) for **90**



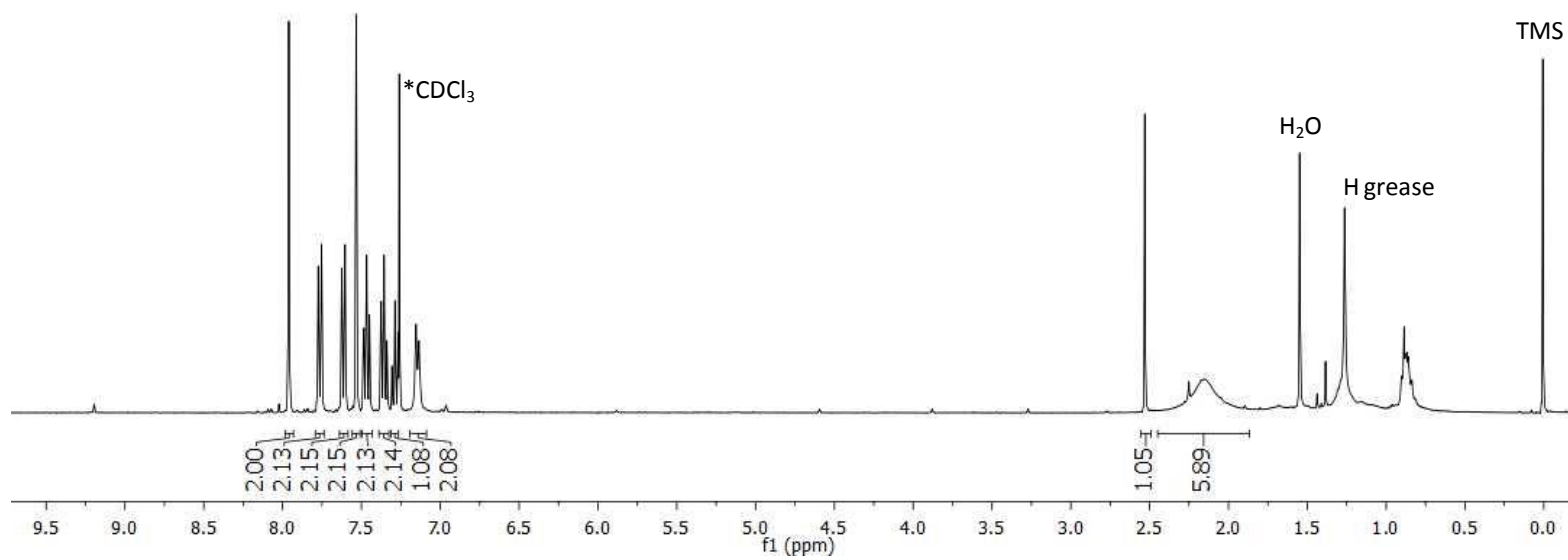
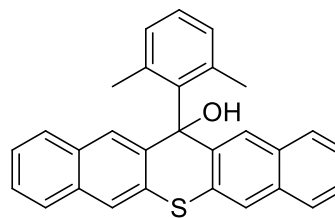
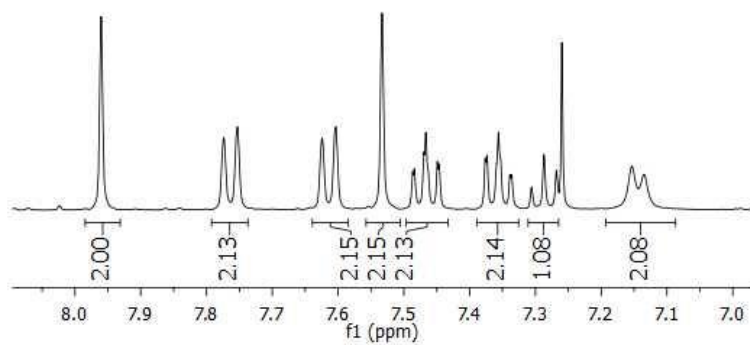
^1H NMR (CDCl_3 , 400 MHz) for **91**



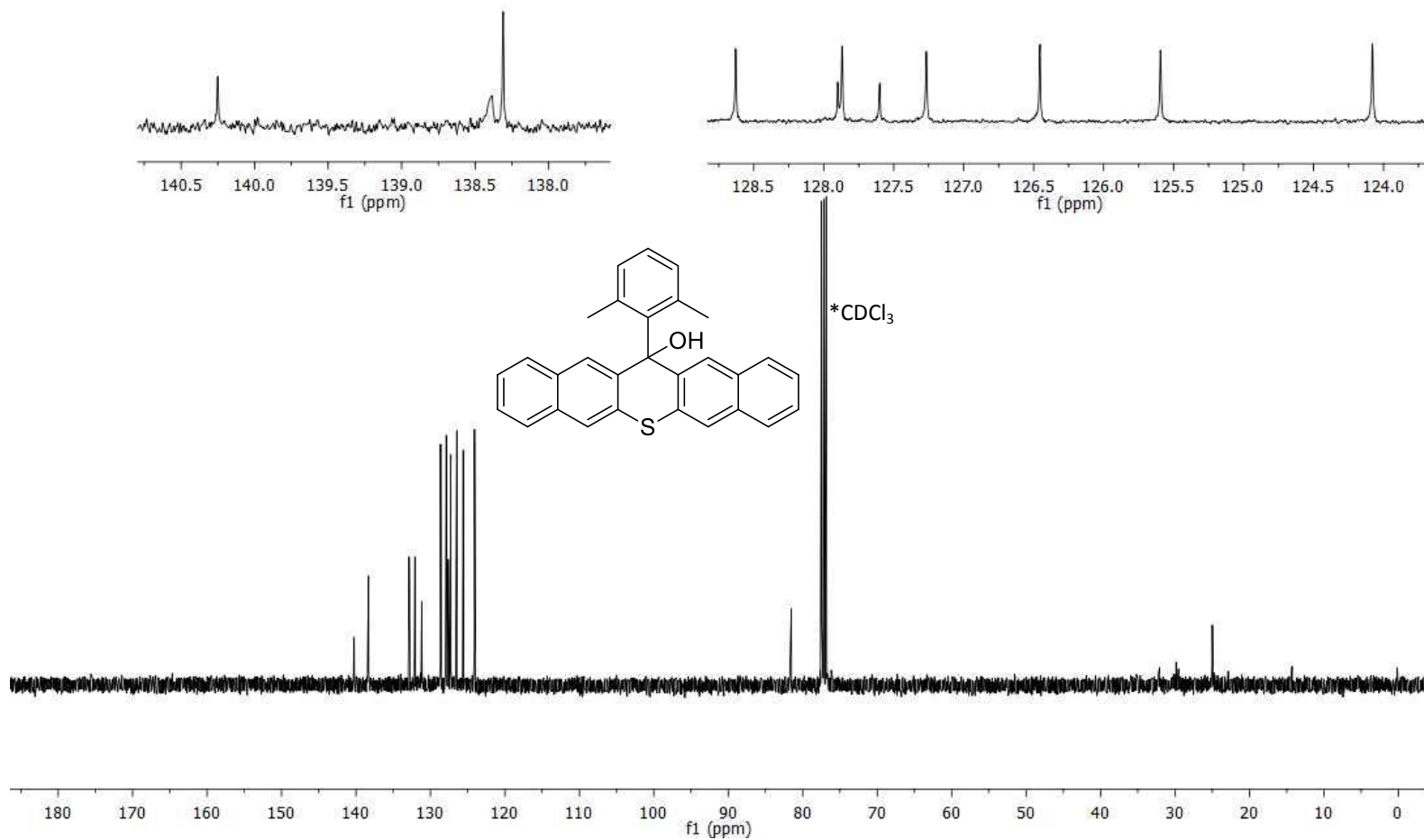
^{13}C NMR (CDCl_3 , 101 MHz) for **91**



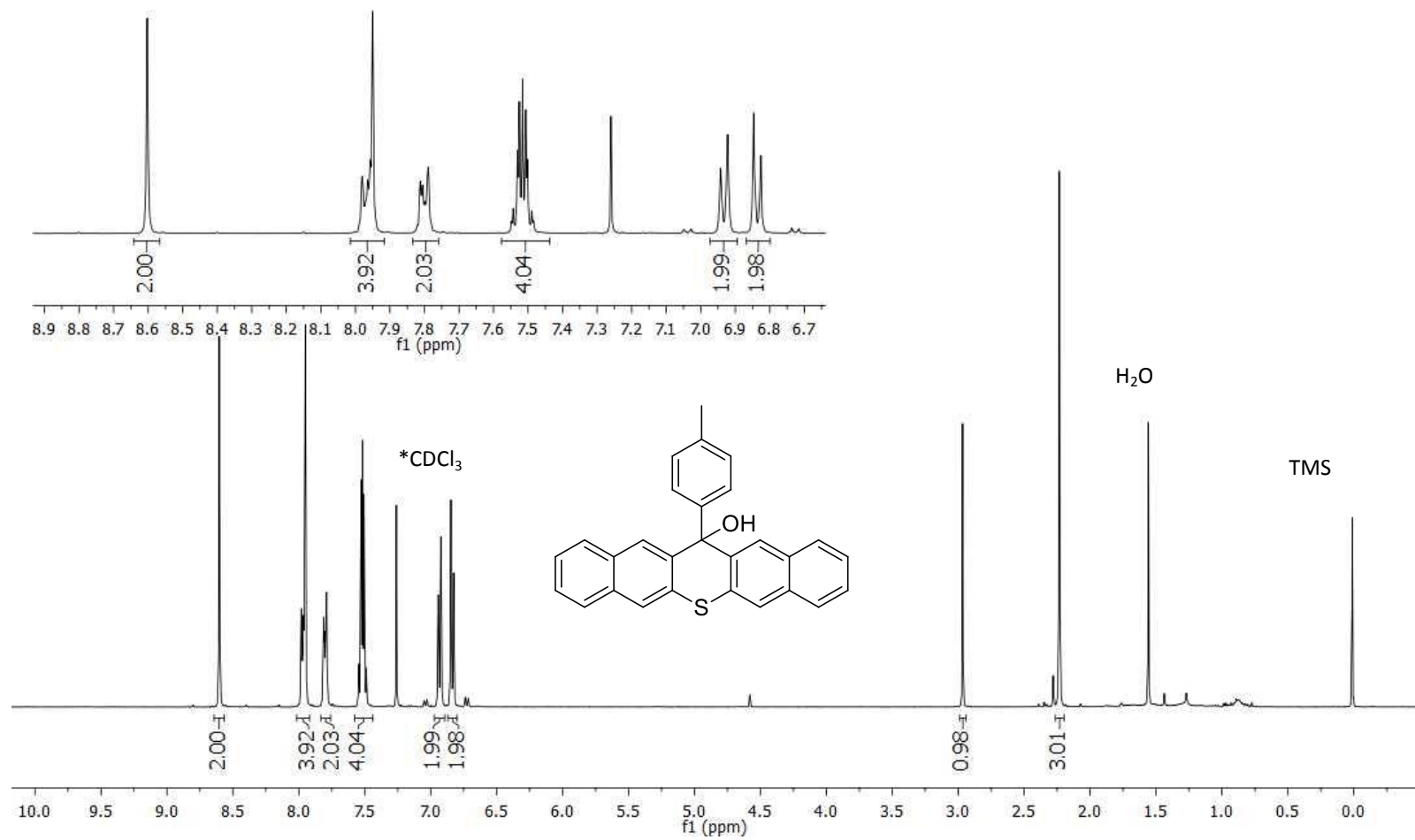
^1H NMR (CDCl_3 , 400 MHz) for **92**



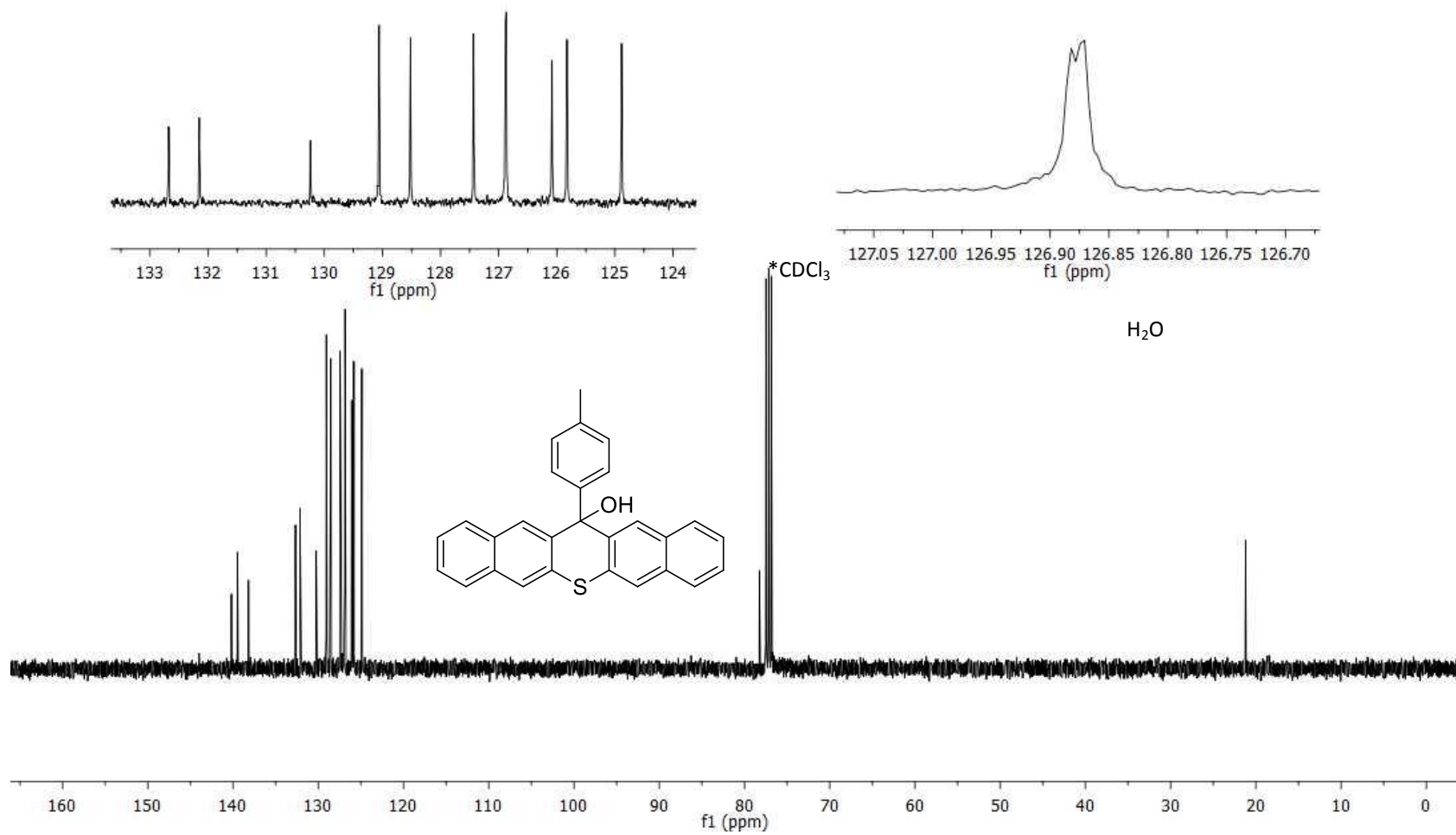
^{13}C NMR (CDCl_3 , 101 MHz) for **92**



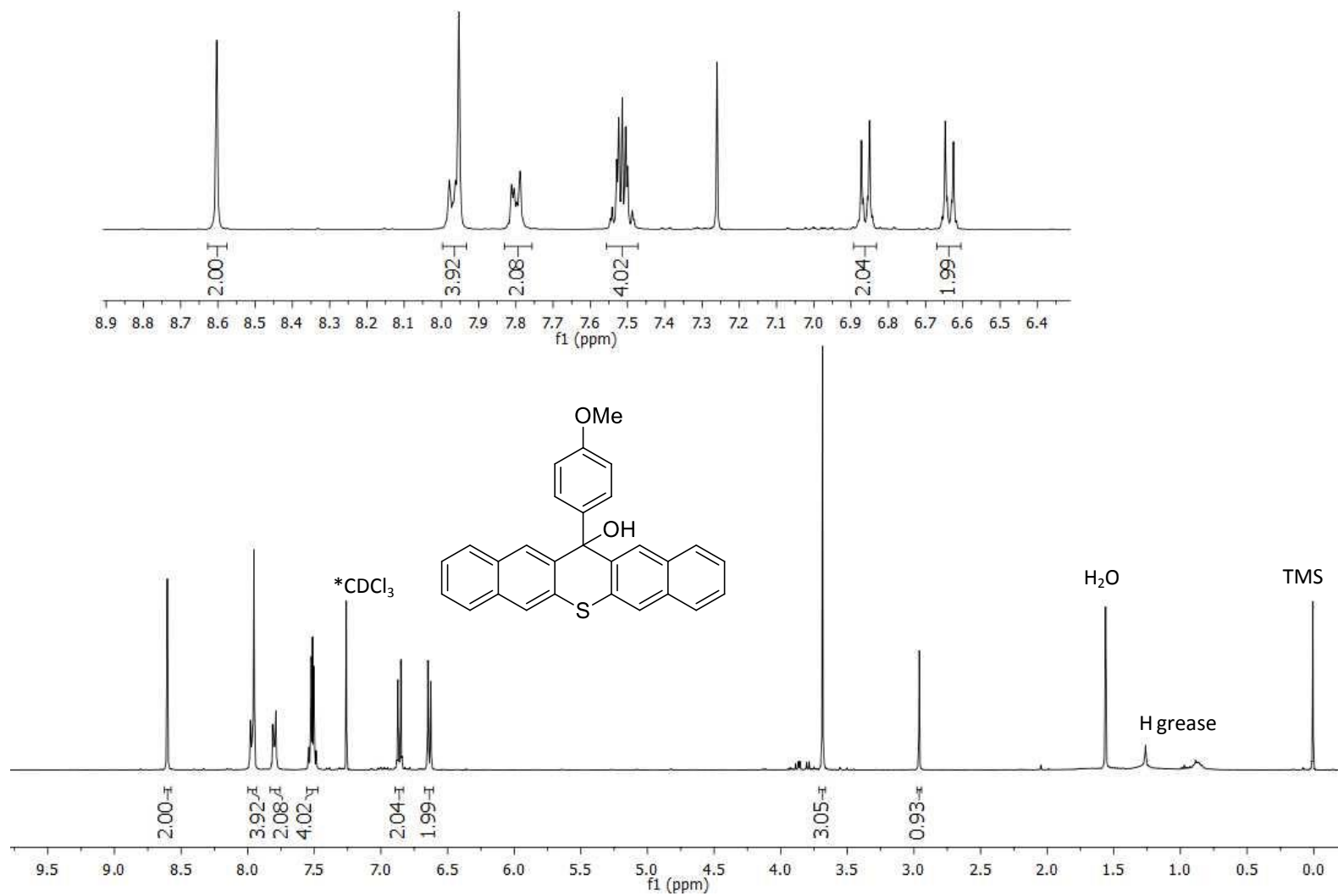
^1H NMR (CDCl_3 , 400 MHz) for **93**



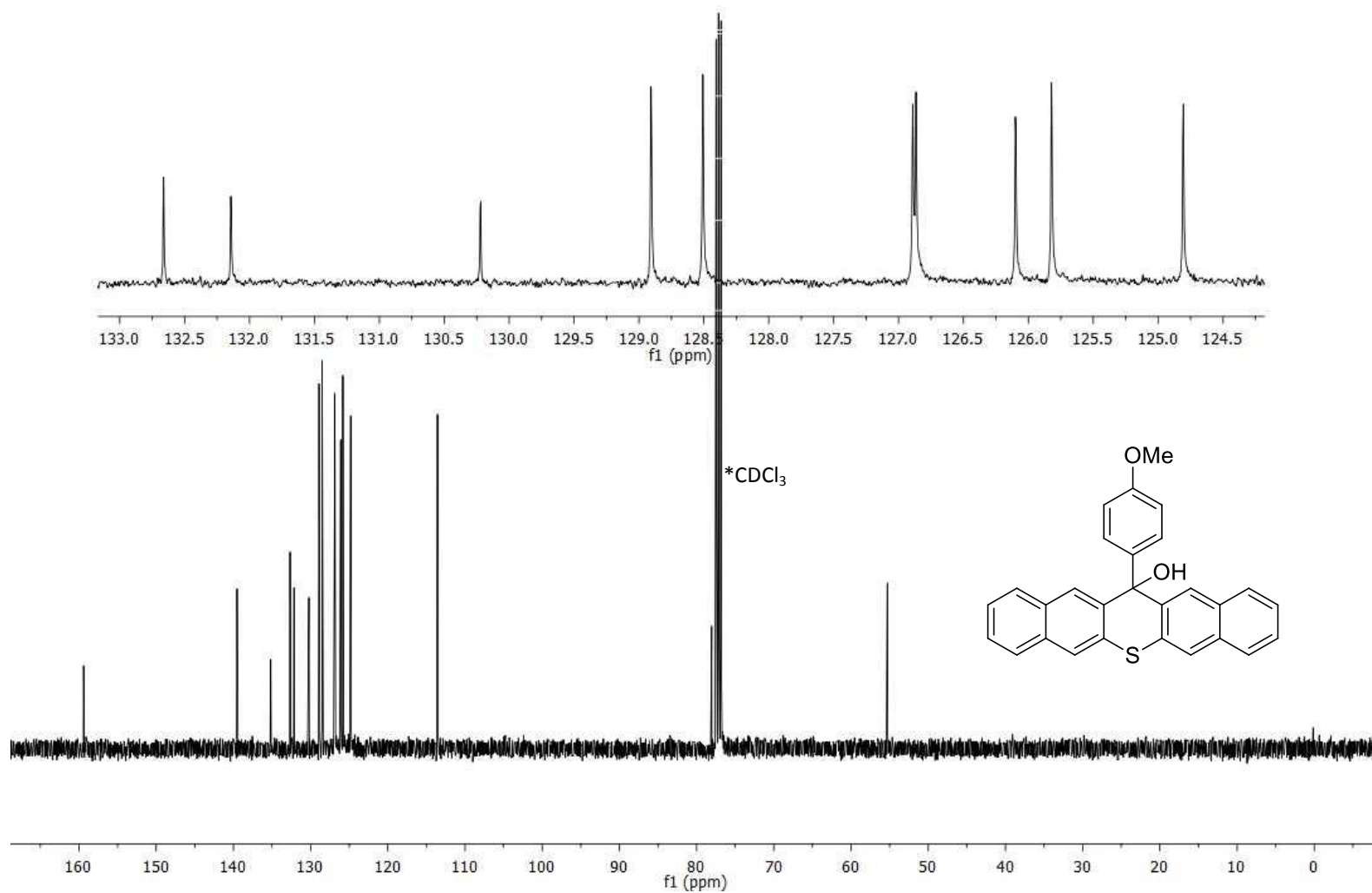
^{13}C NMR (CDCl_3 , 400 MHz) for **93**



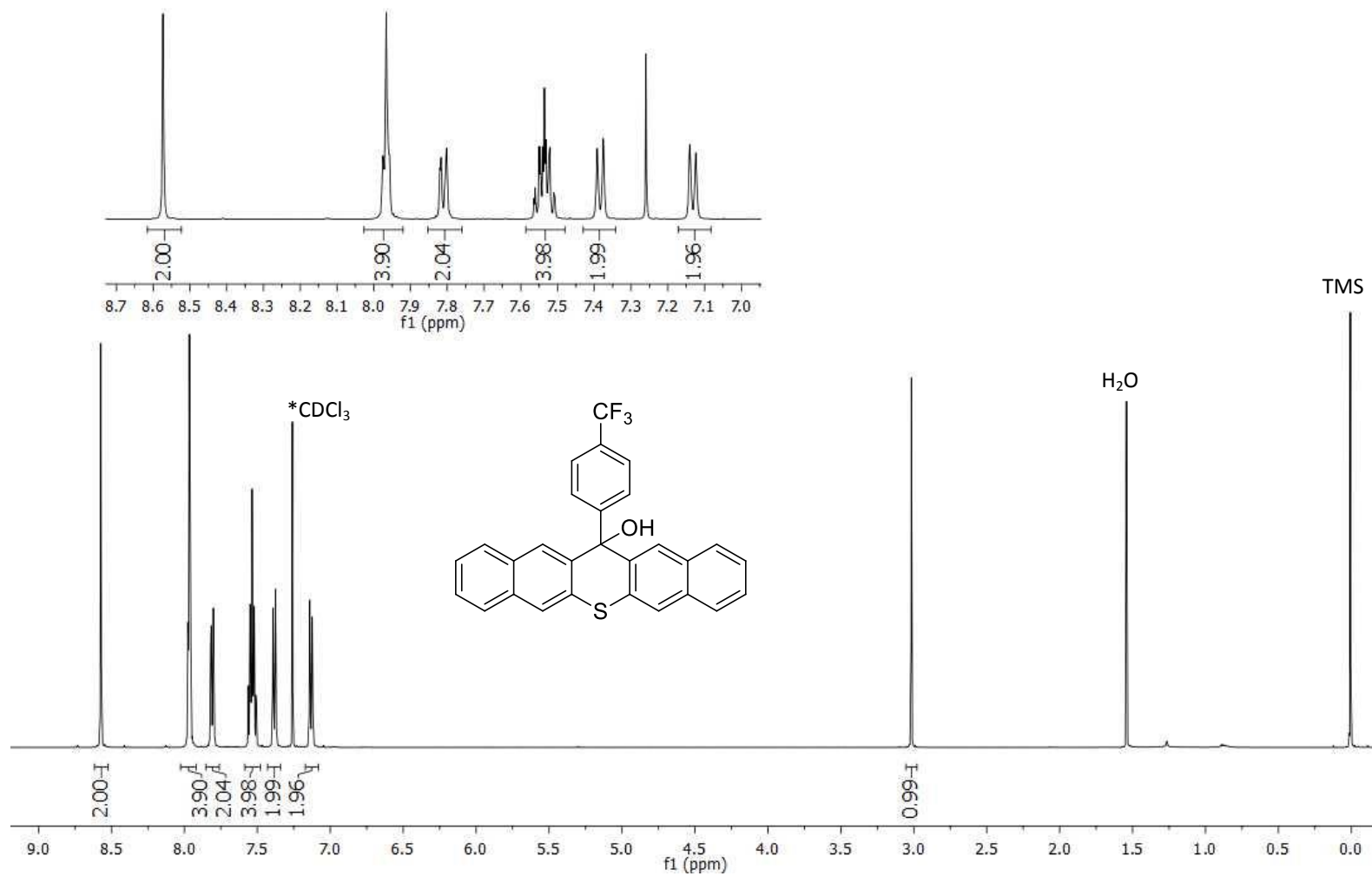
^1H NMR (CDCl_3 , 400 MHz) for **94**



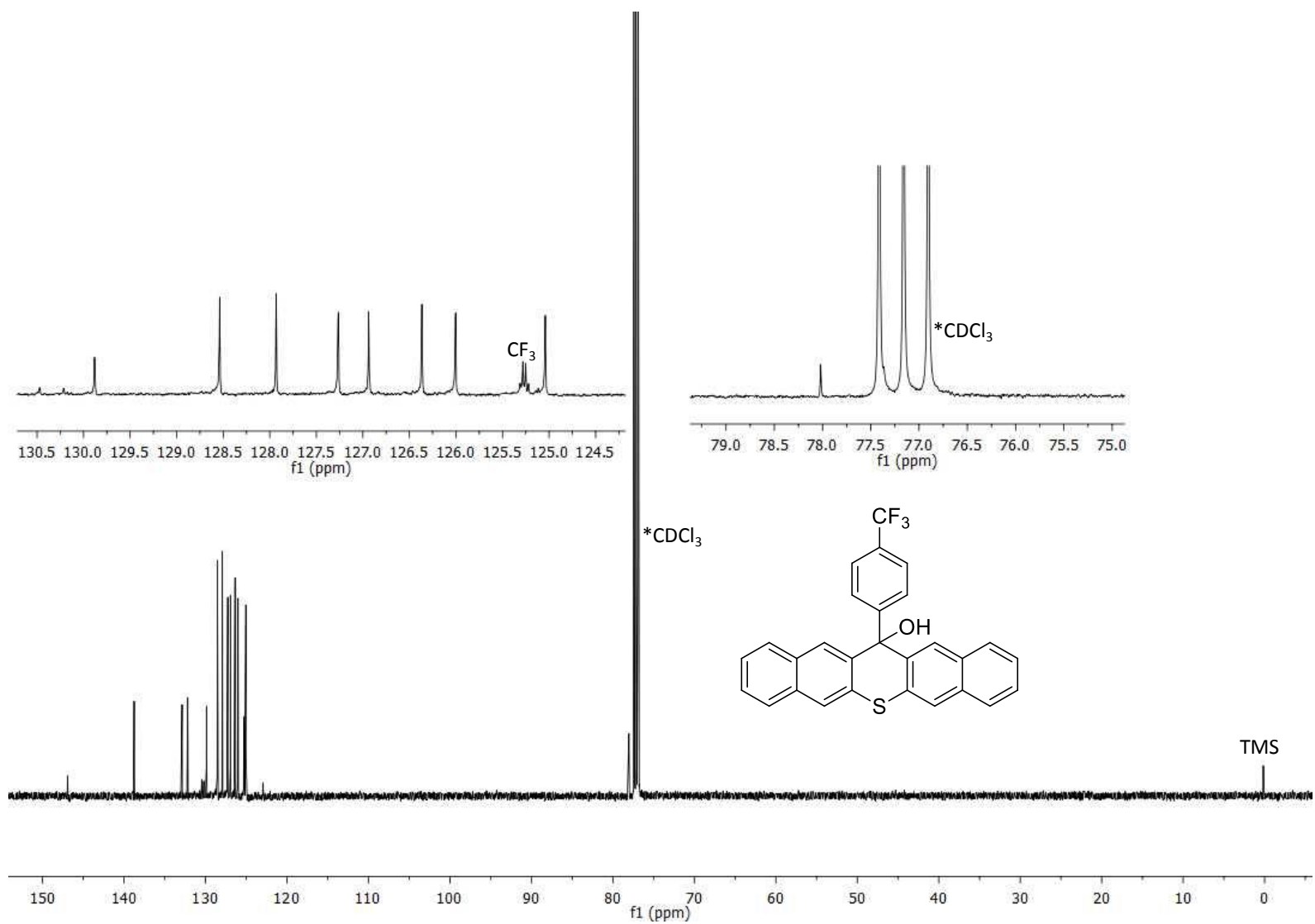
^{13}C NMR (CDCl_3 , 101 MHz) for **94**



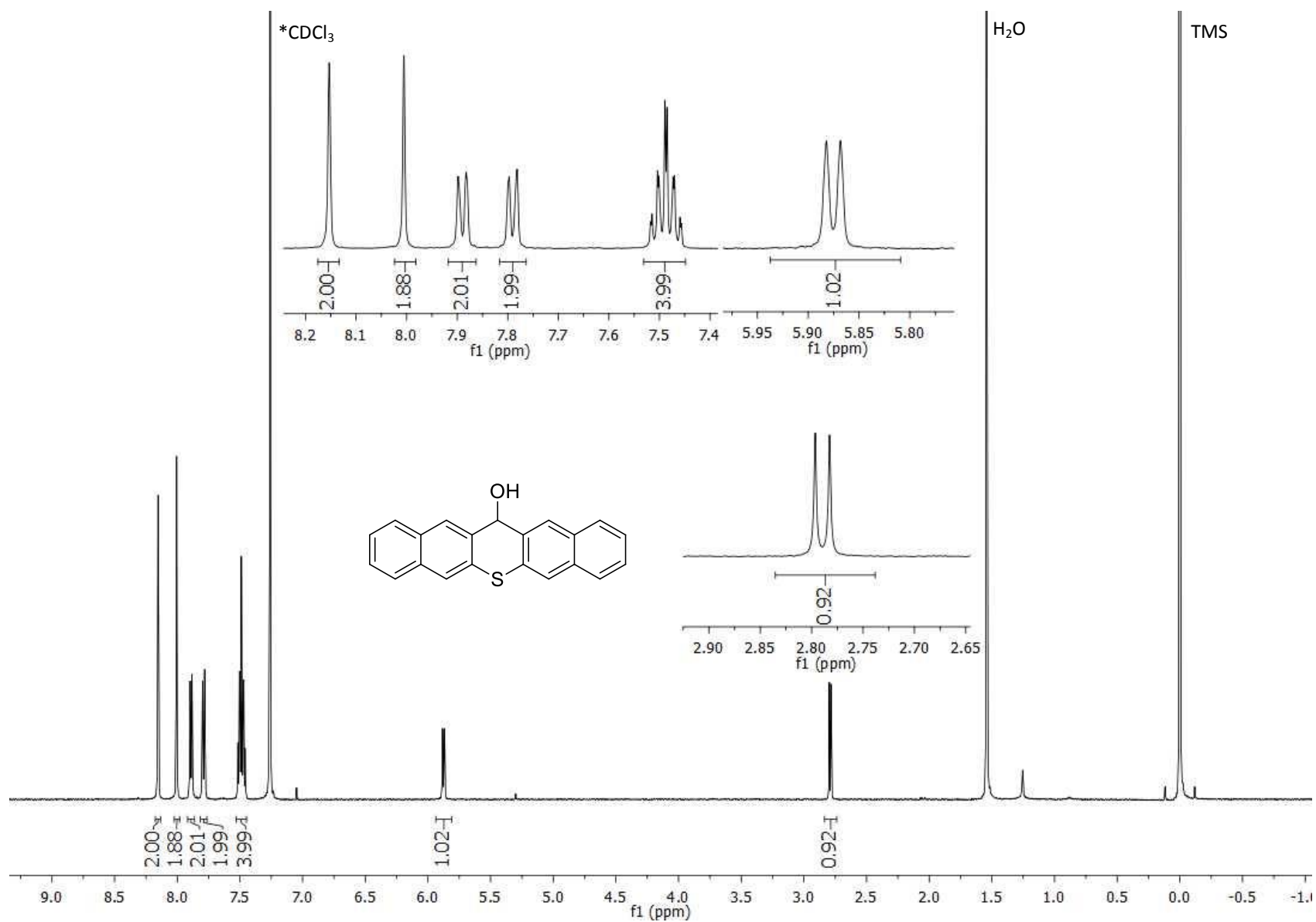
^1H NMR (CDCl_3 , 500 MHz) for **95**



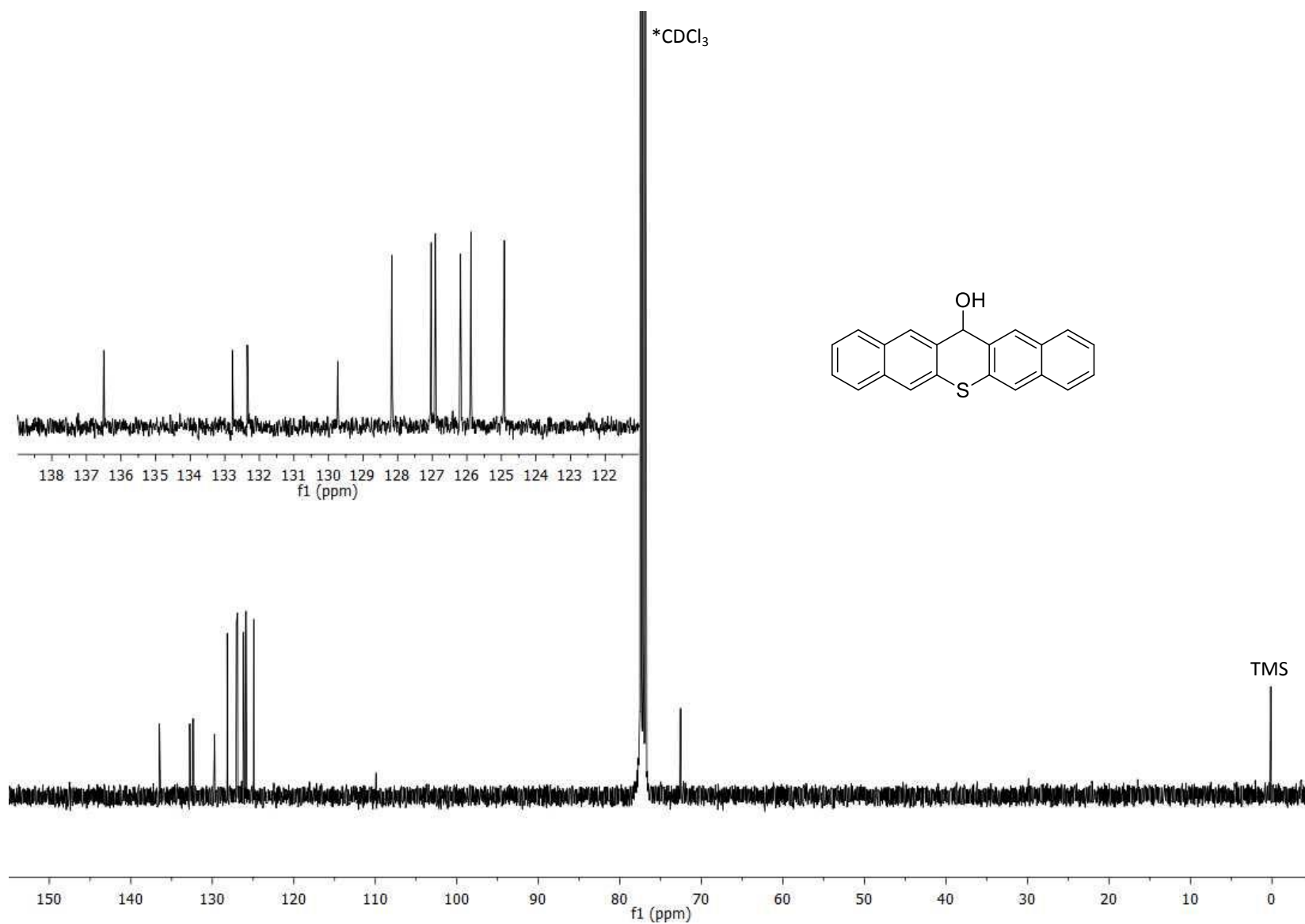
^{13}C NMR (CDCl_3 , 126 MHz) for **95**



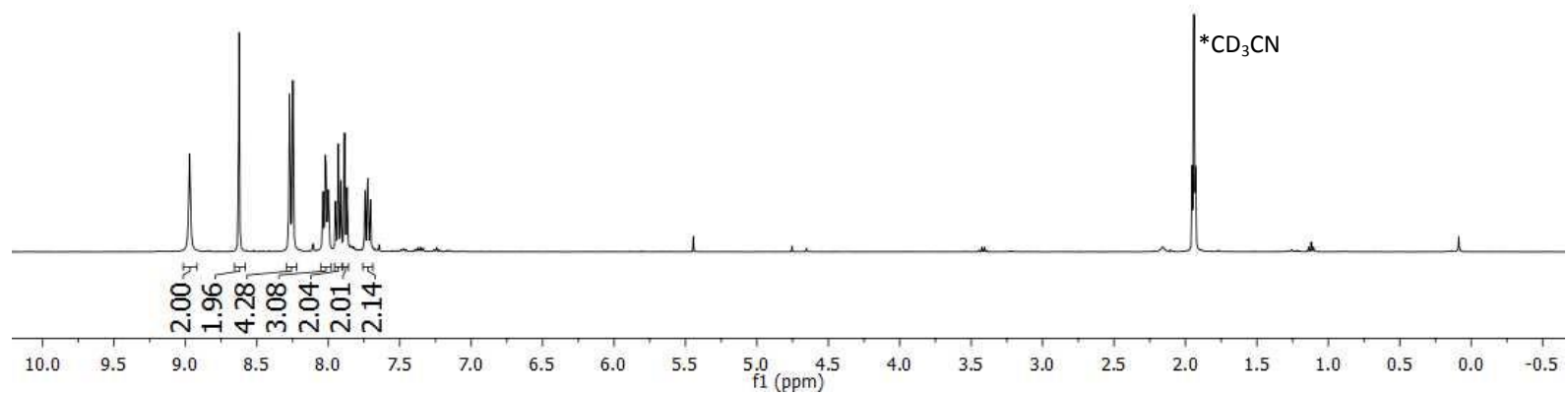
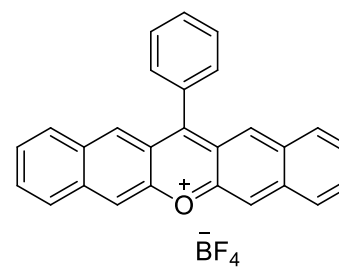
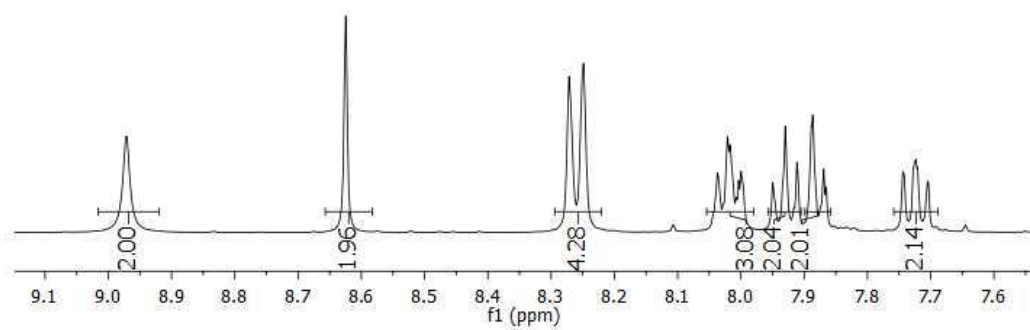
^1H NMR (CDCl_3 , 500 MHz) for **98**



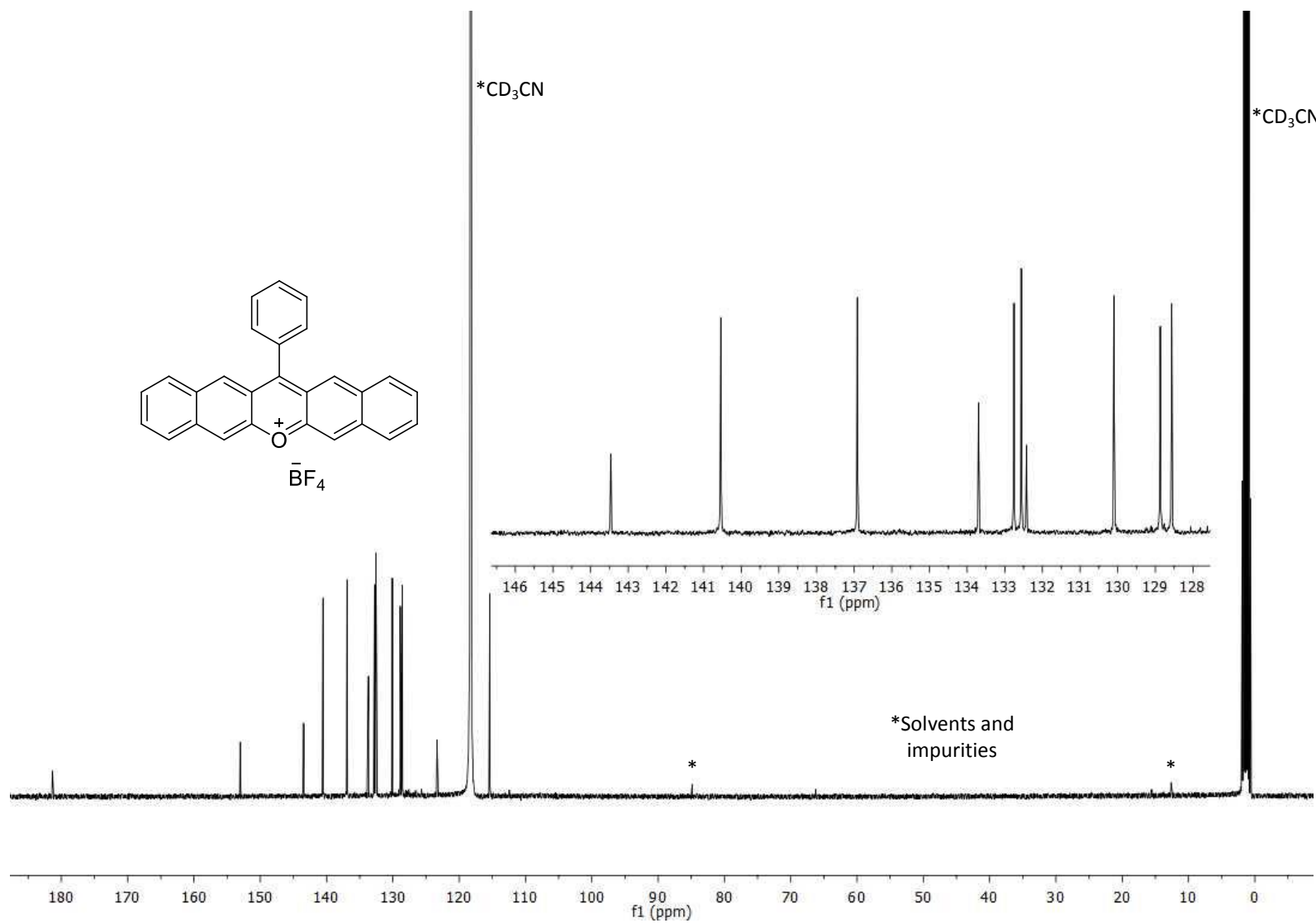
^{13}C NMR (CDCl_3 , 101 MHz) for **98**



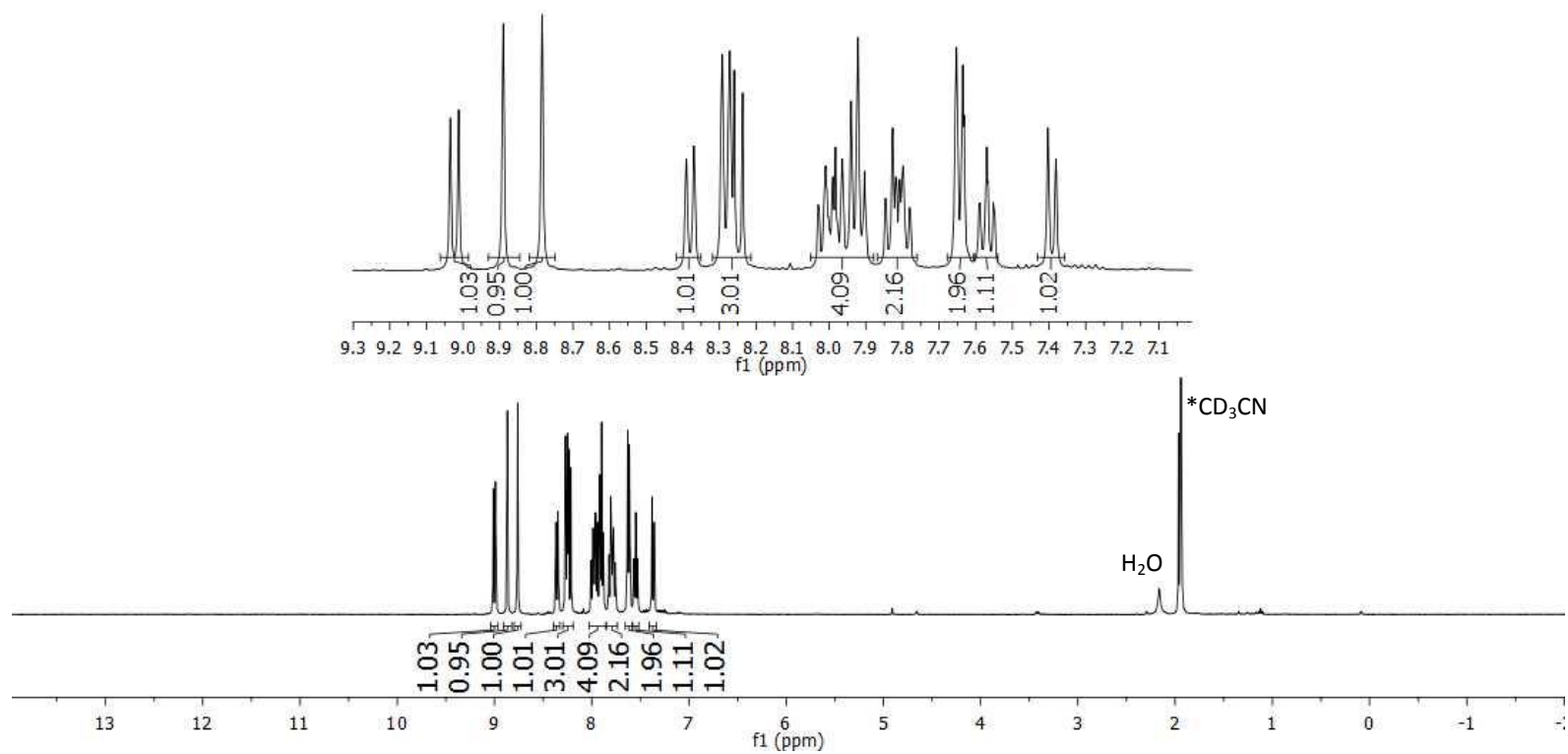
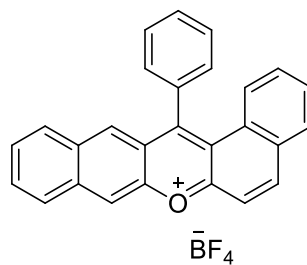
^1H NMR (CD_3CN , 400 MHz) for **99**



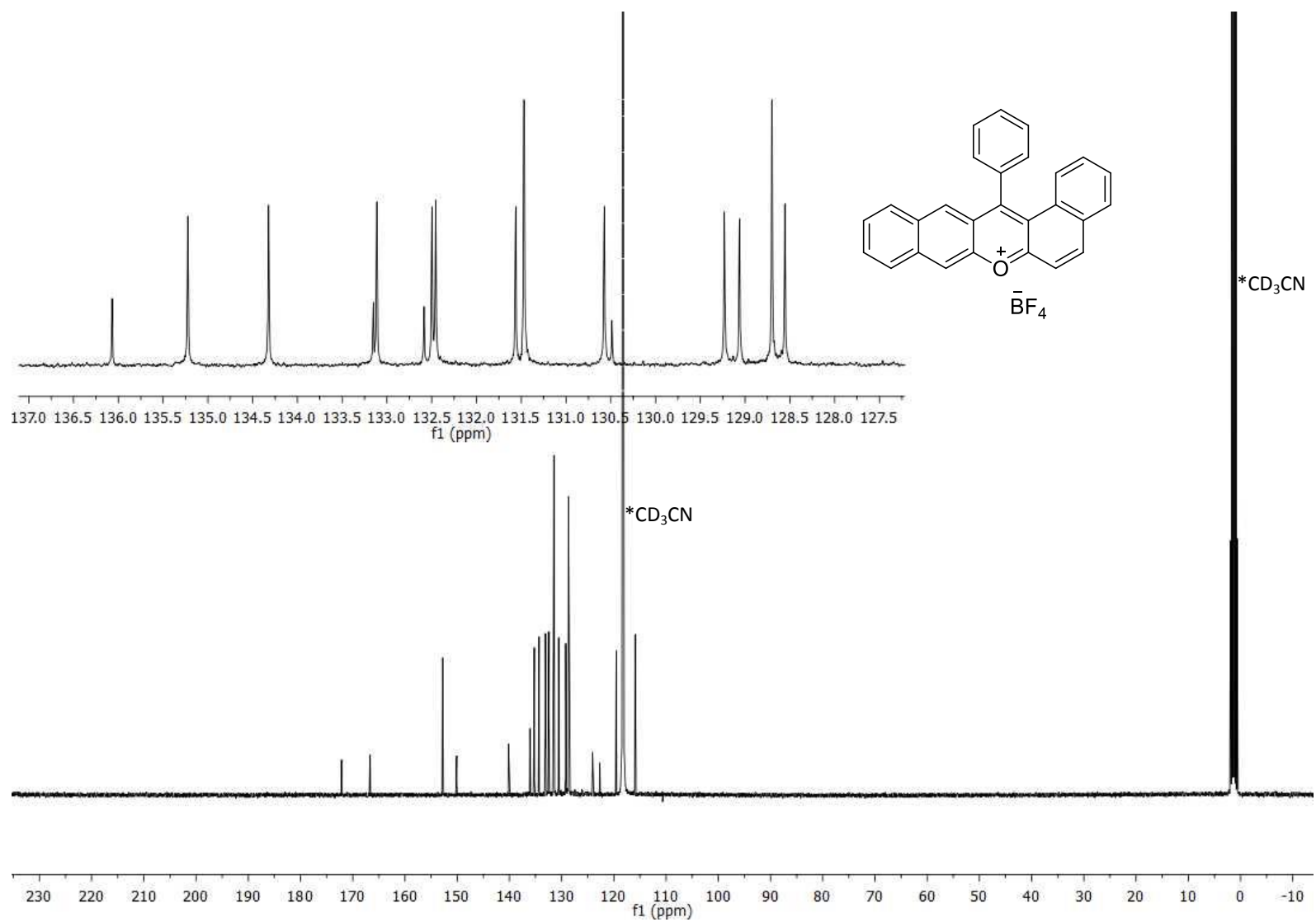
^{13}C NMR (CD_3CN , 101 MHz) for **99**



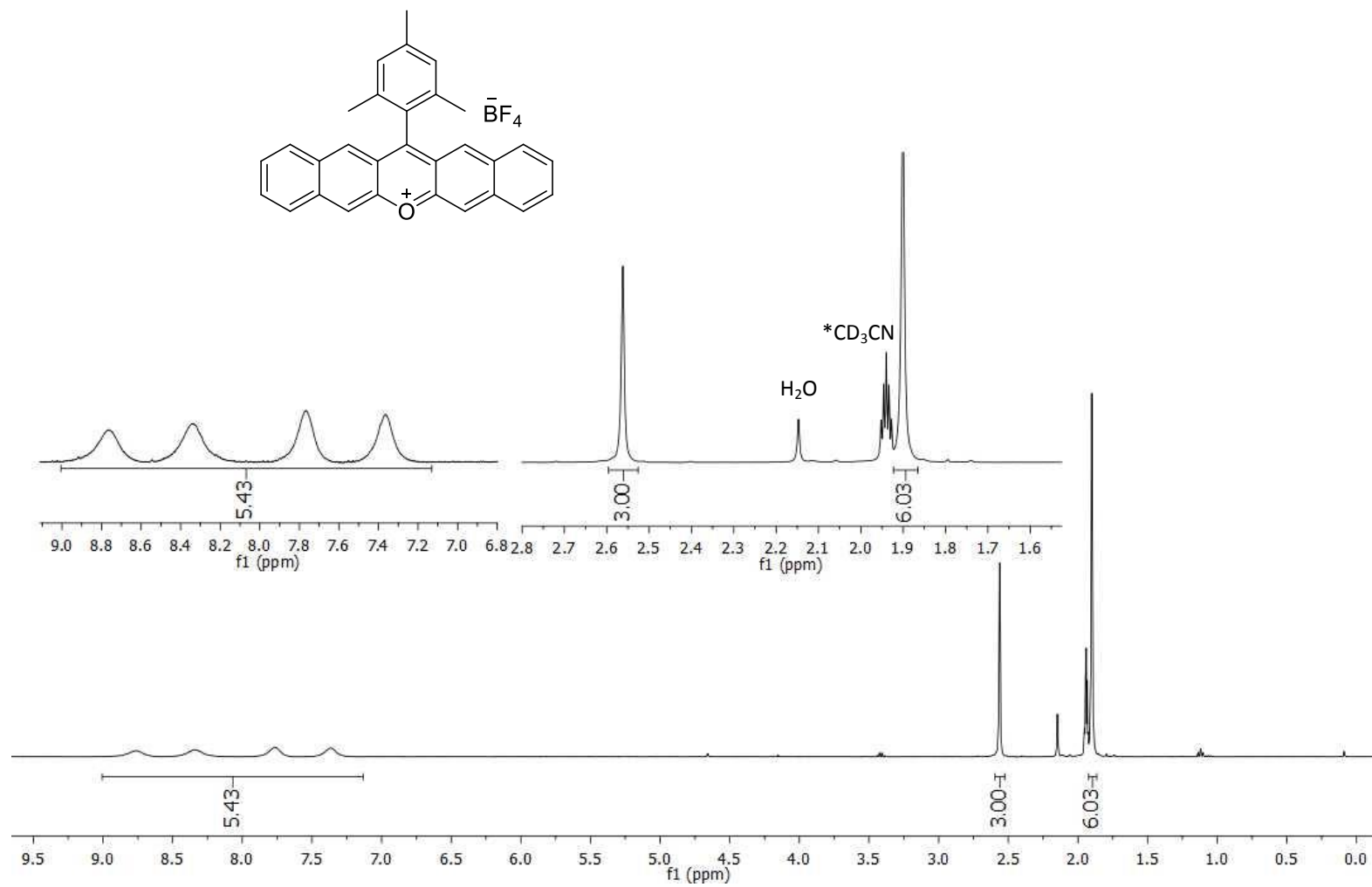
^1H NMR (CD_3CN , 400 MHz) for **100**



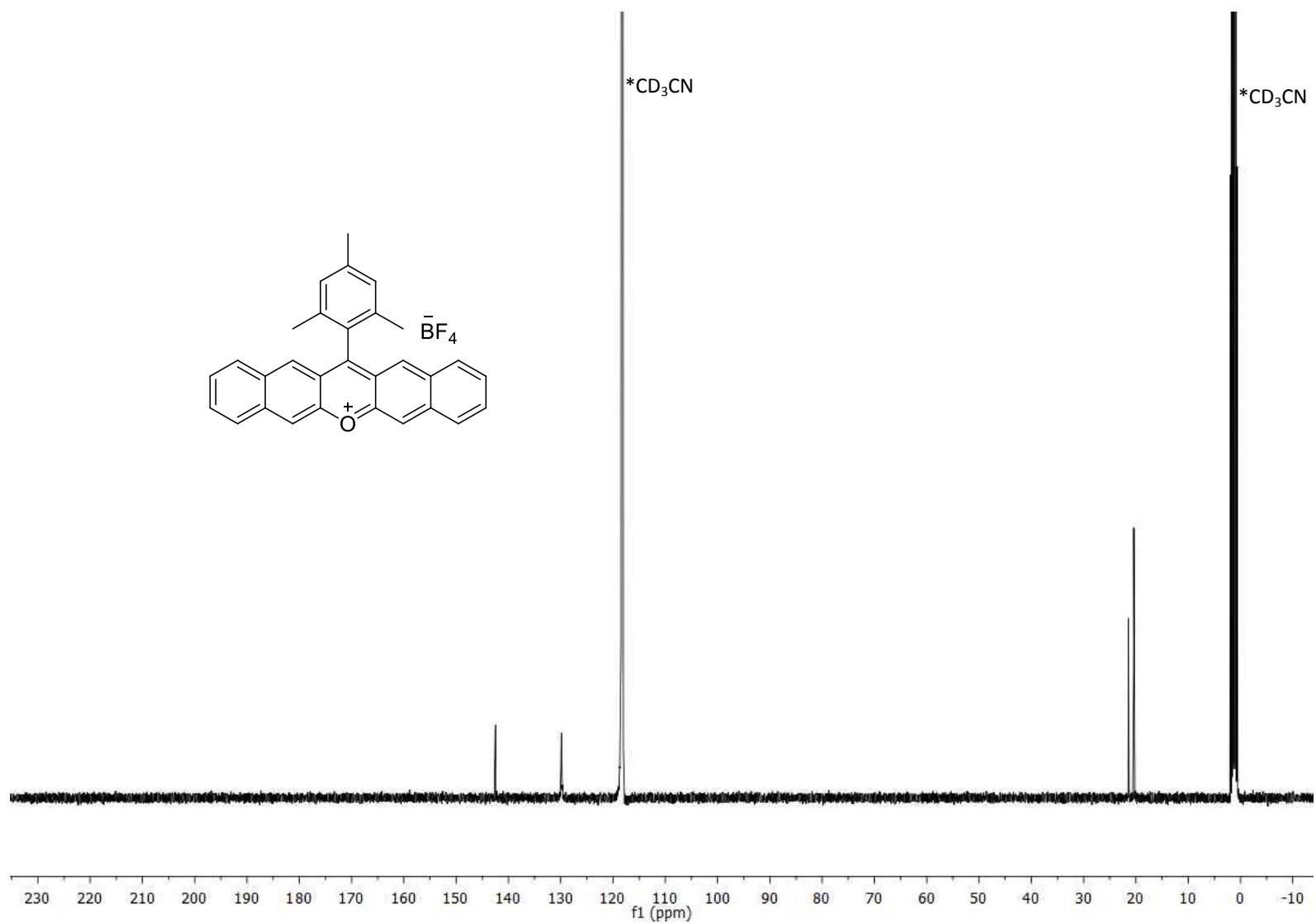
^{13}C NMR (CD_3CN , 101 MHz) for **100**



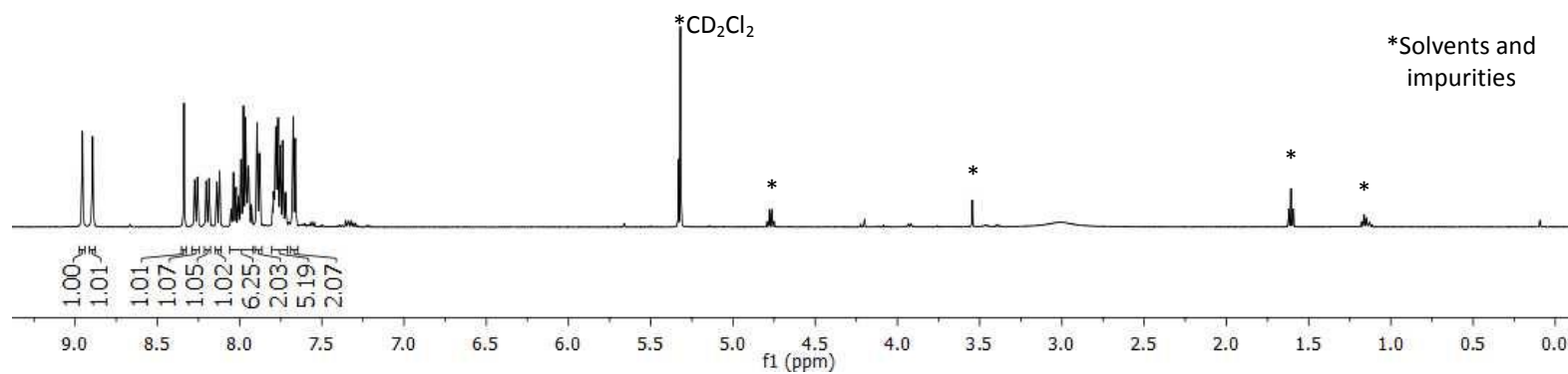
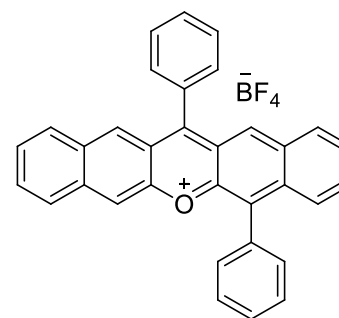
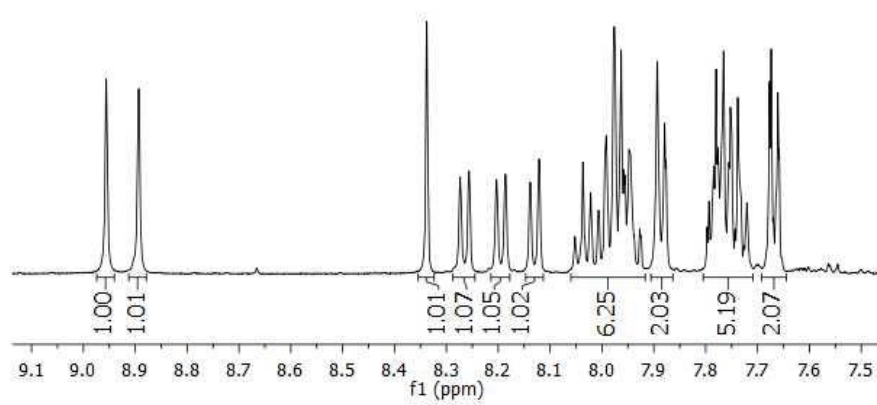
^1H NMR (CD_3CN , 400 MHz) for **101**



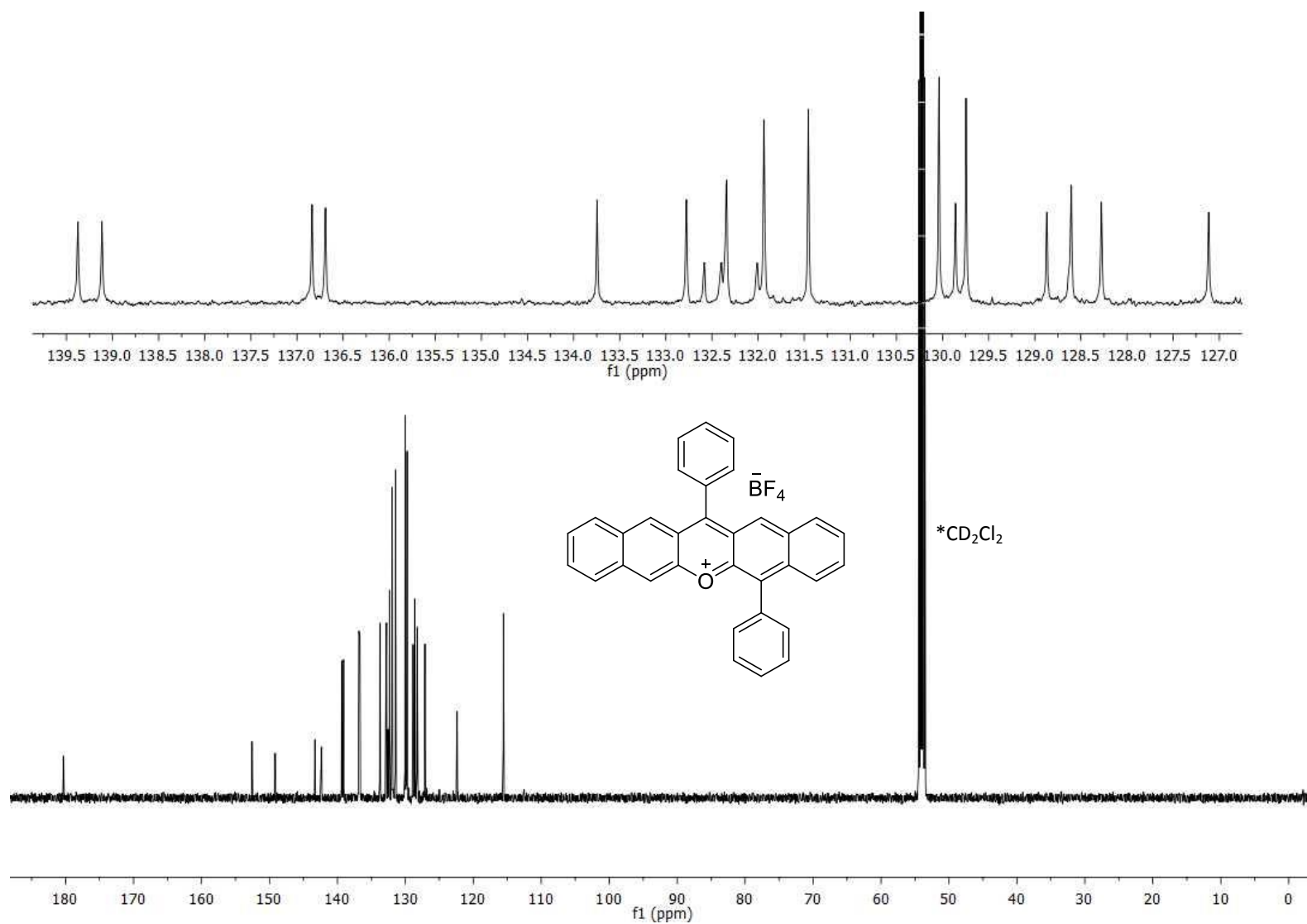
^{13}C NMR (CD_3CN , 101 MHz) for **101**



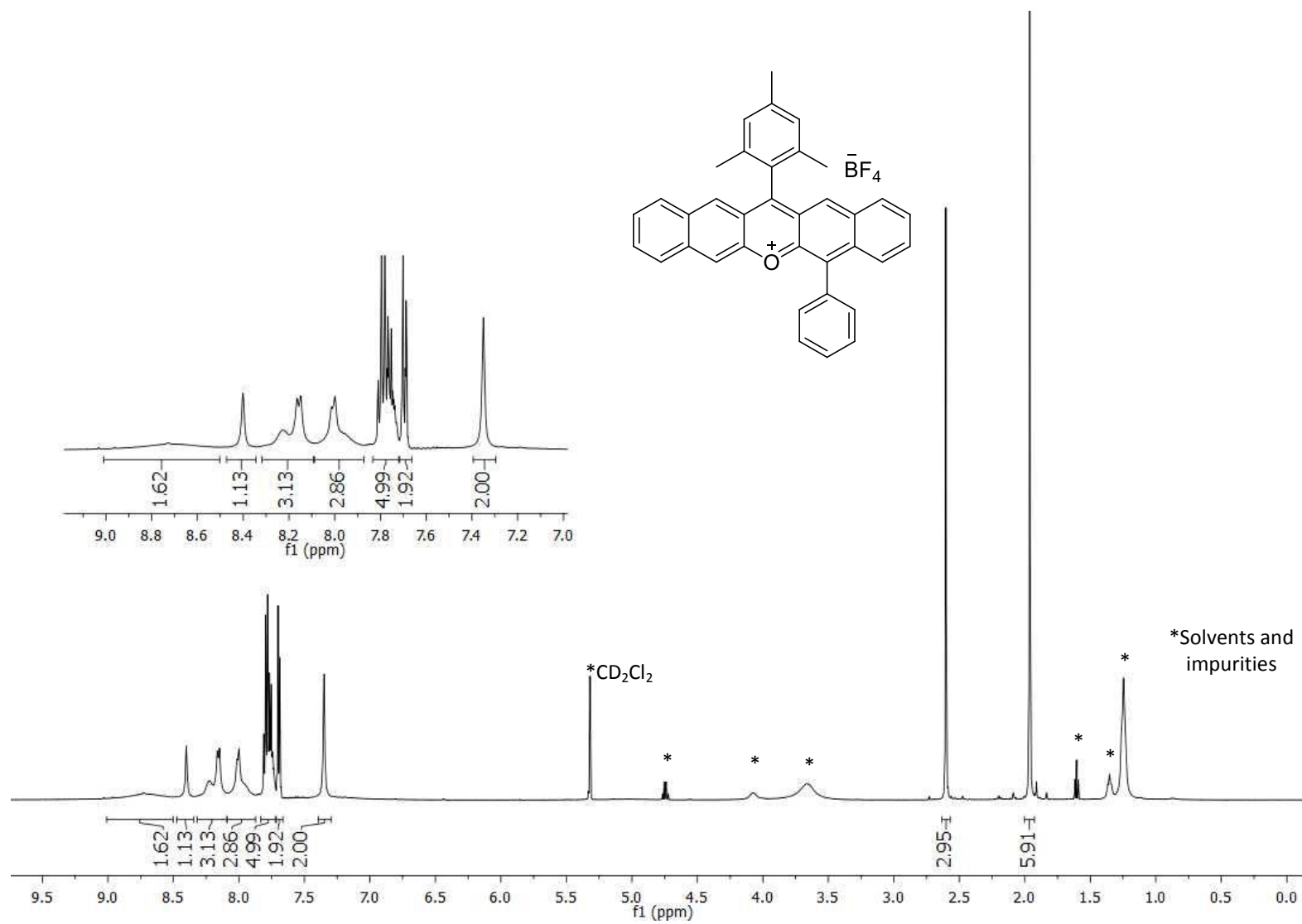
^1H NMR (CD_2Cl_2 , 500 MHz) for **103**



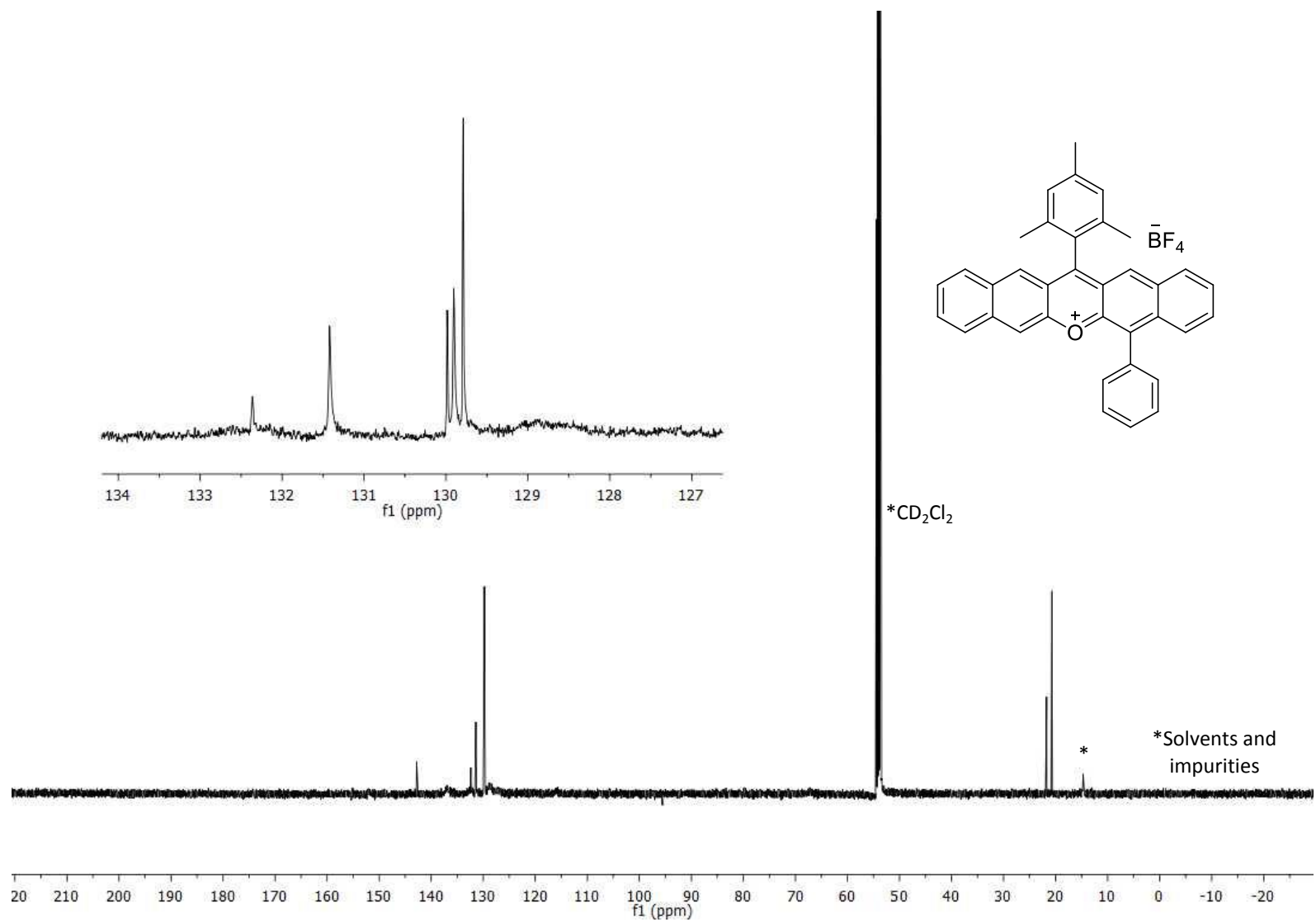
^{13}C NMR (CD_2Cl_2 , 126 MHz) for **103**



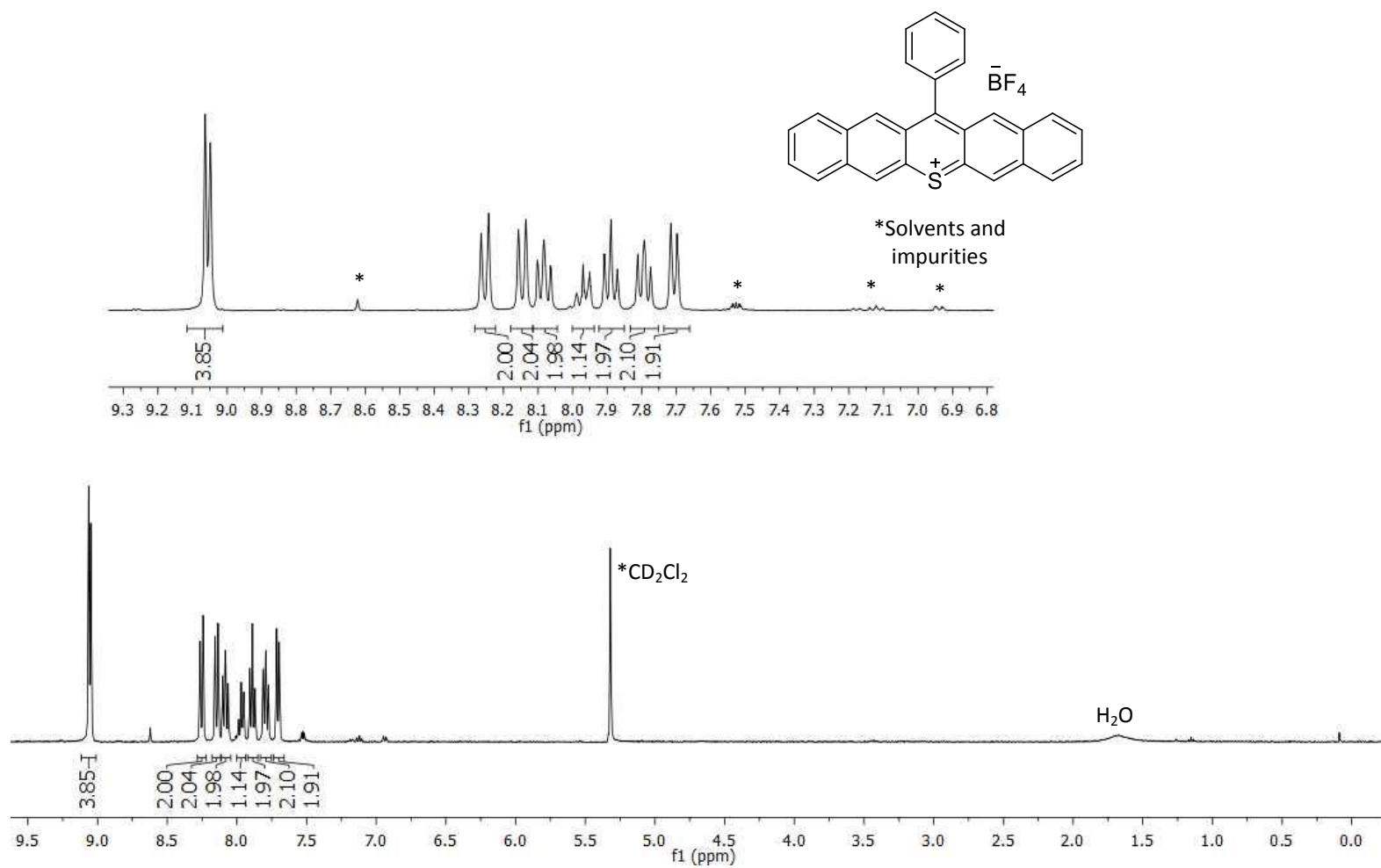
^1H NMR (CD_2Cl_2 , 500 MHz) for **104**



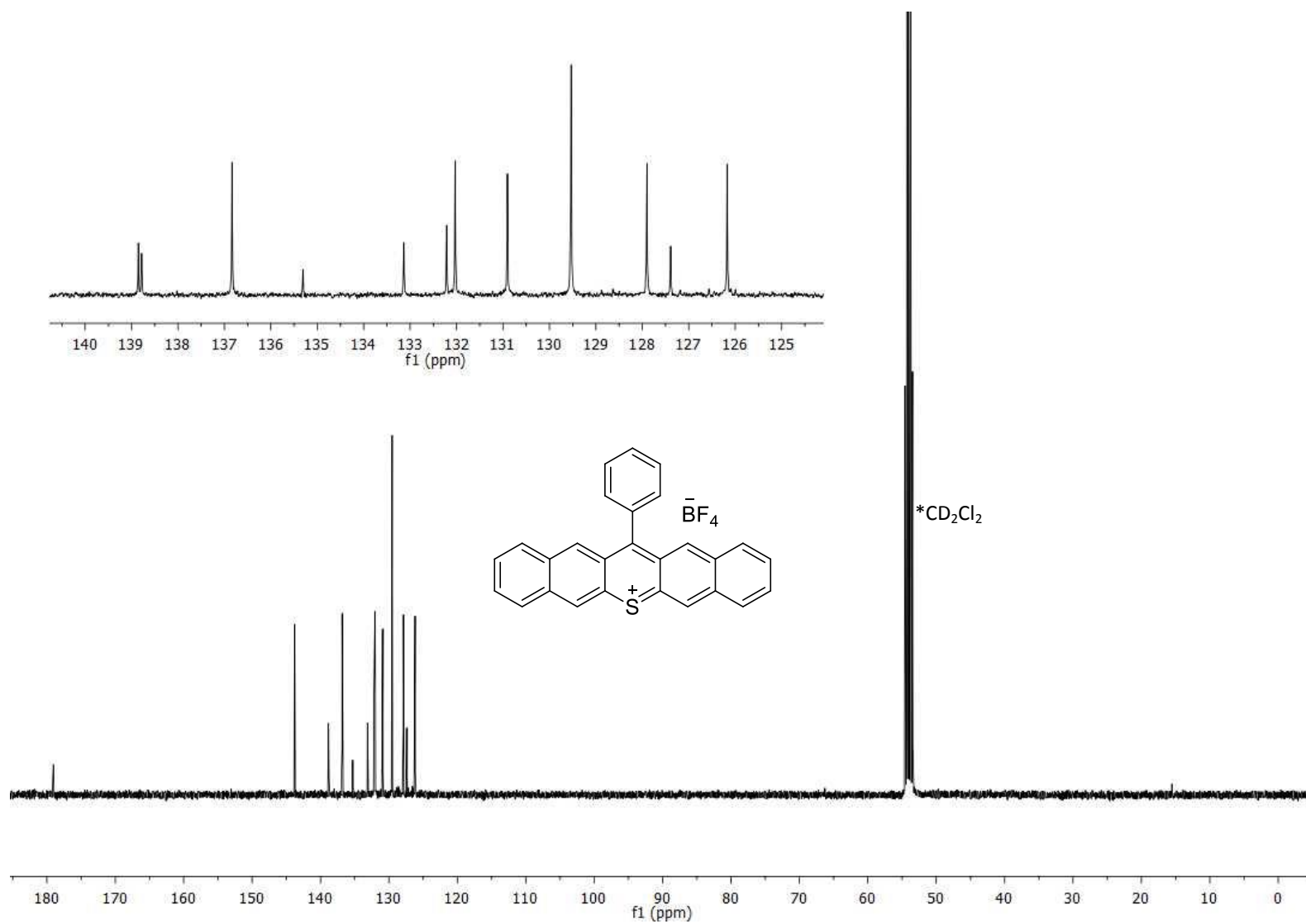
^{13}C NMR (CD_2Cl_2 , 126 MHz) for **104**



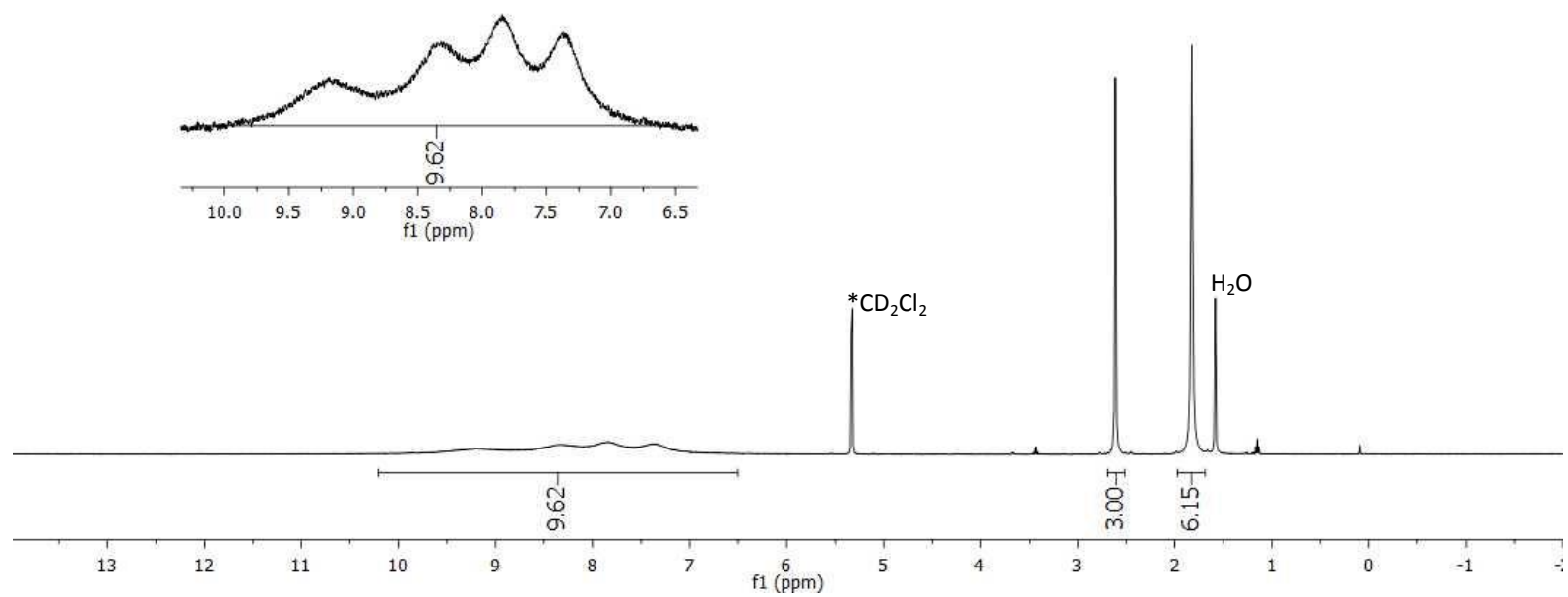
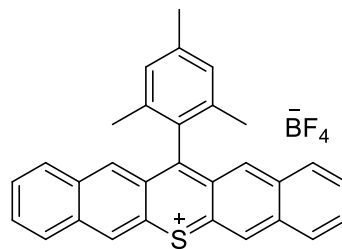
^1H NMR (CD_2Cl_2 , 400 MHz) for **105**



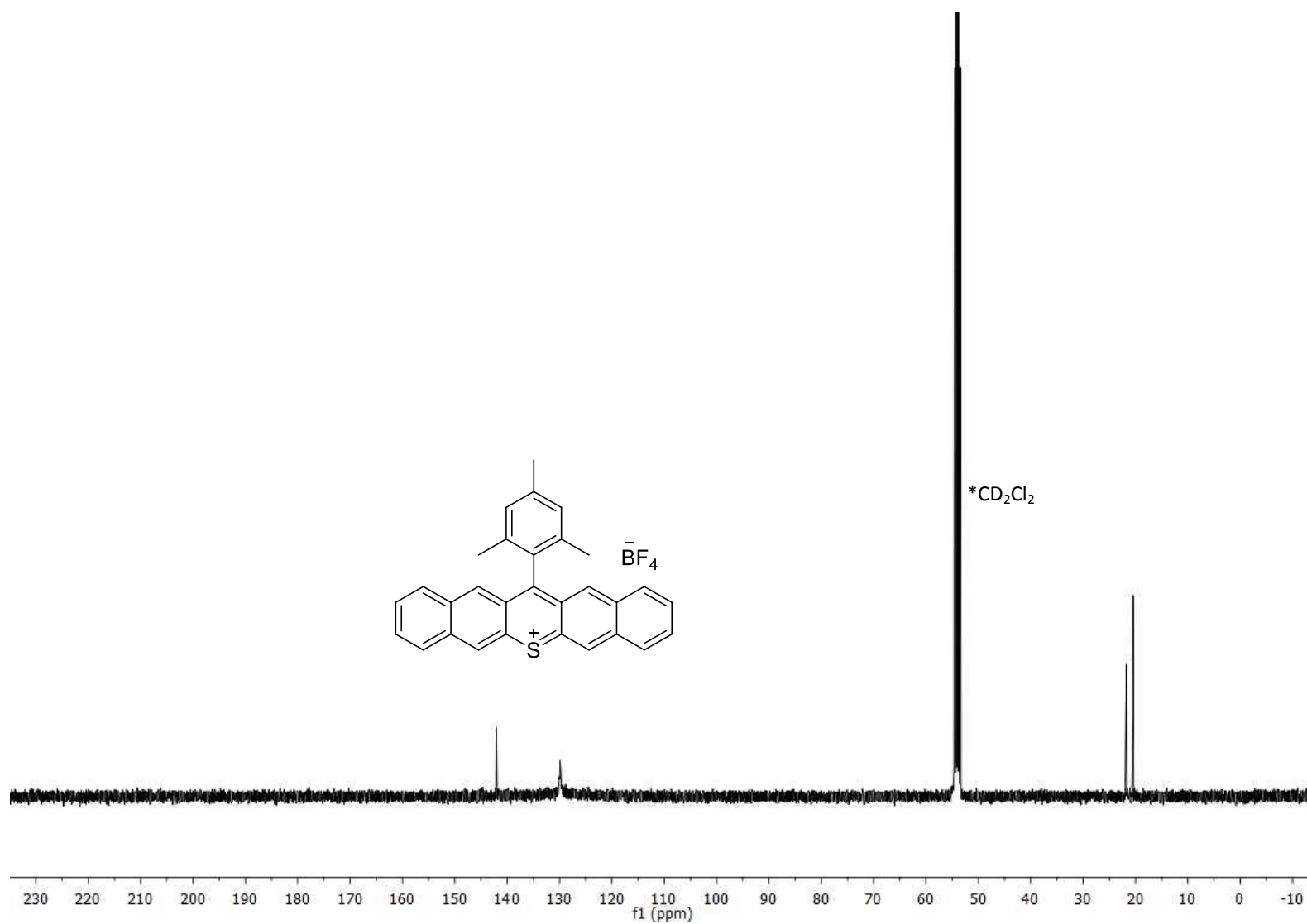
^{13}C NMR (CD_2Cl_2 , 101 MHz) for **105**



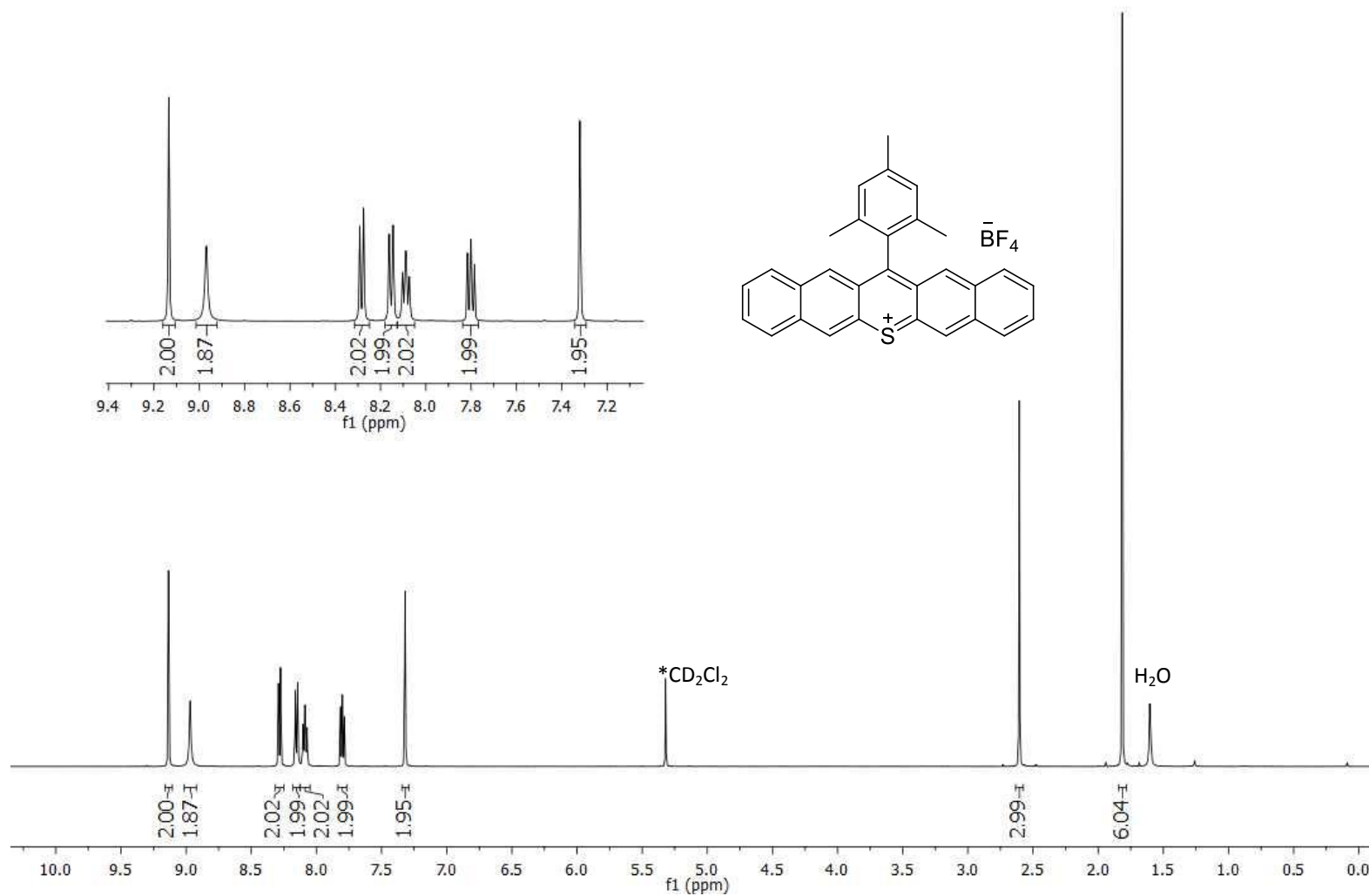
^1H NMR (CD_2Cl_2 , 400 MHz) for **106**



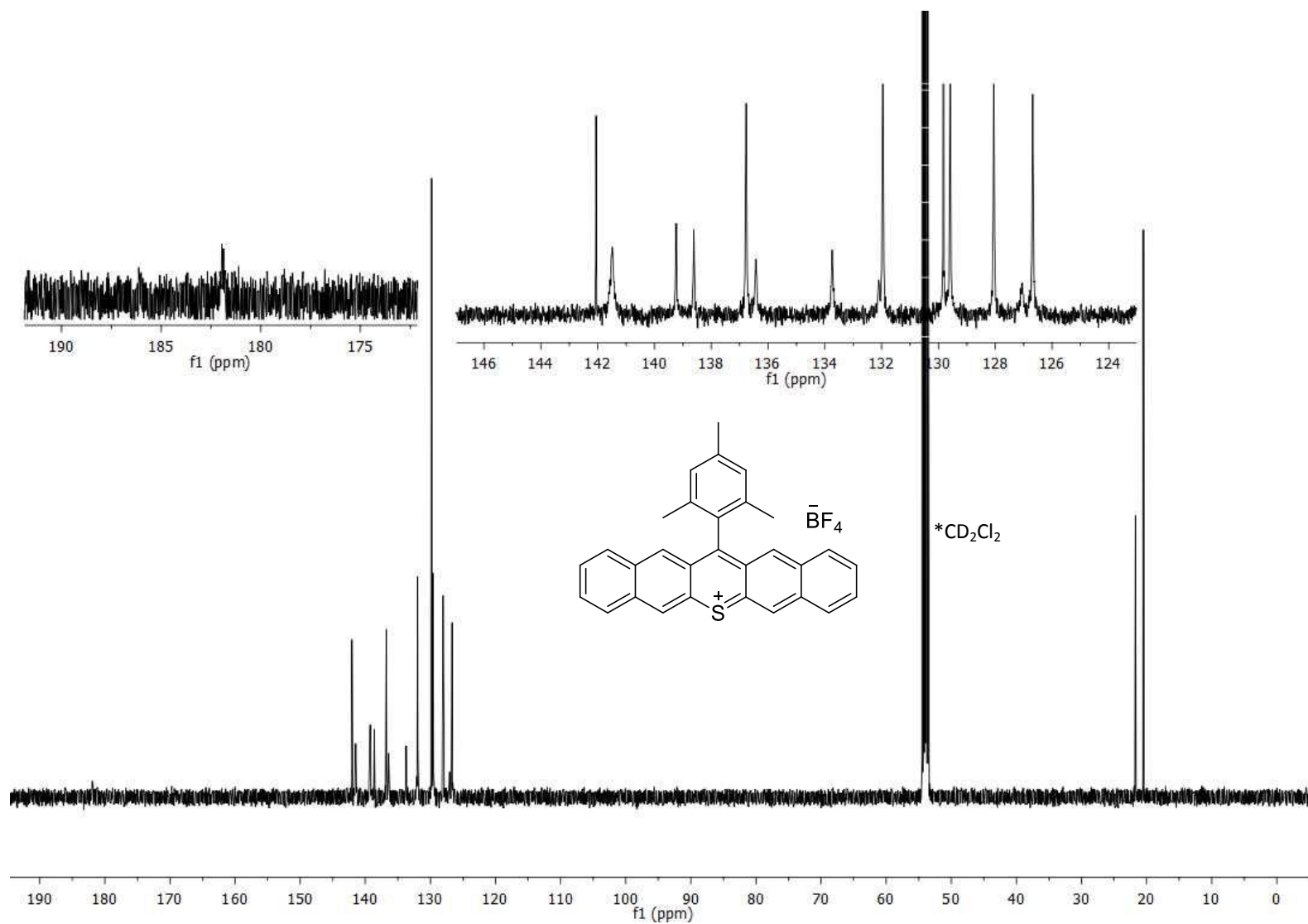
^{13}C NMR (CD_2Cl_2 , 101 MHz) for **106**



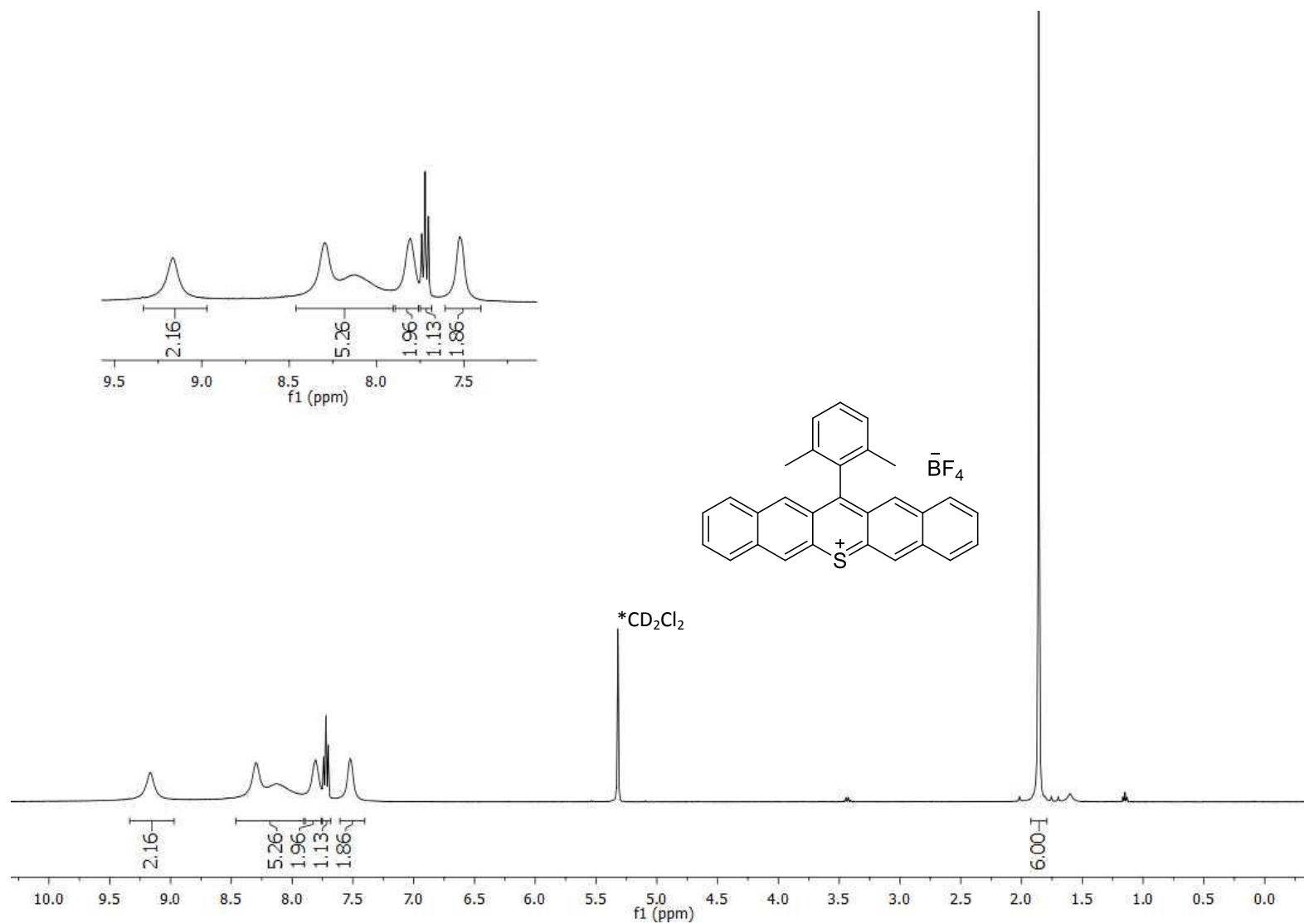
^1H NMR (CD_2Cl_2 , 500 MHz, after rise to room temperature from $-27\text{ }^\circ\text{C}$ (**Figure 26**) in VT-NMR) for **106**



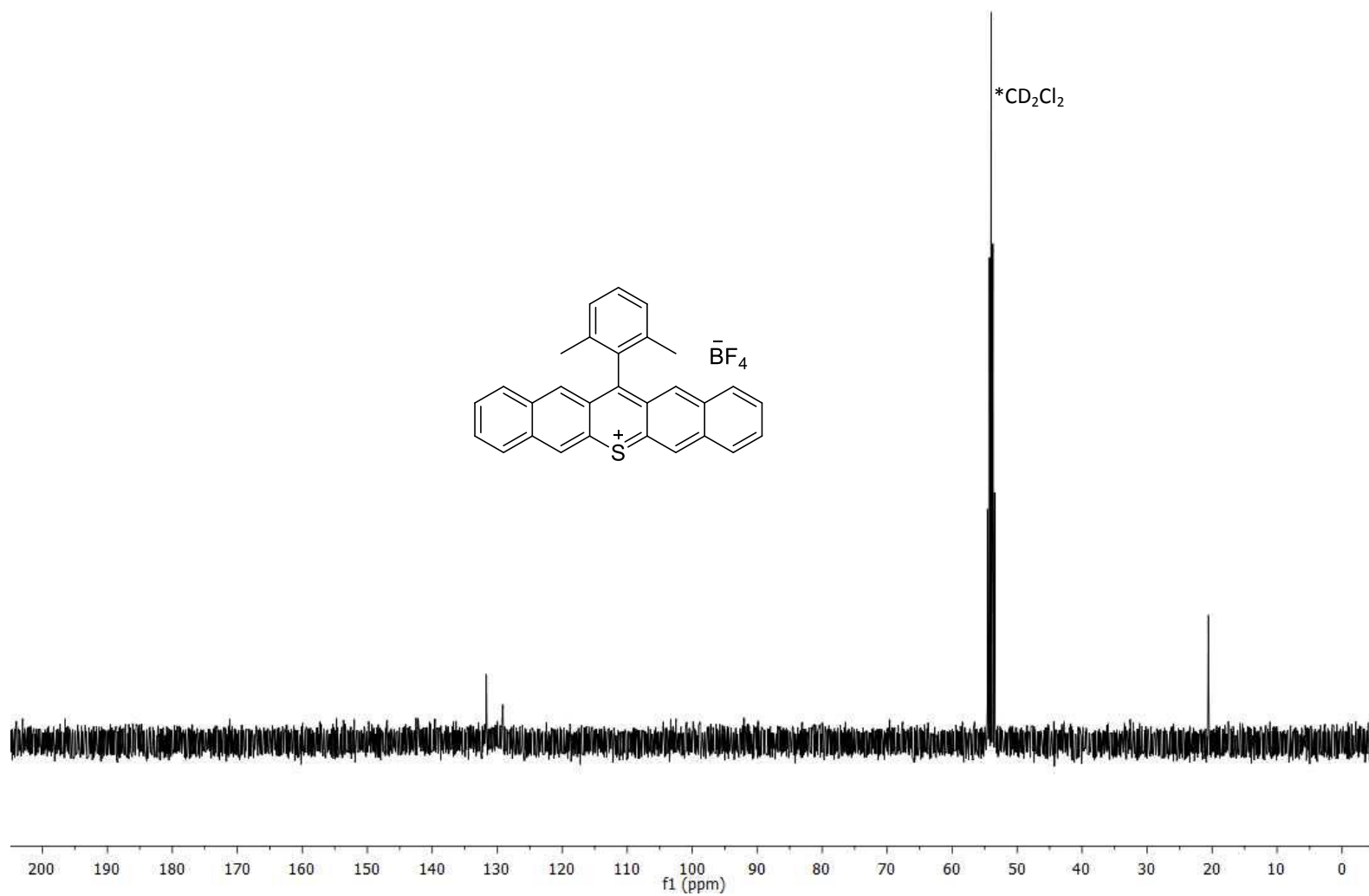
^{13}C NMR (CD_2Cl_2 , 126 MHz, after rise to room temperature from $-27\text{ }^\circ\text{C}$ (Figure 26) in VT-NMR) for **106**



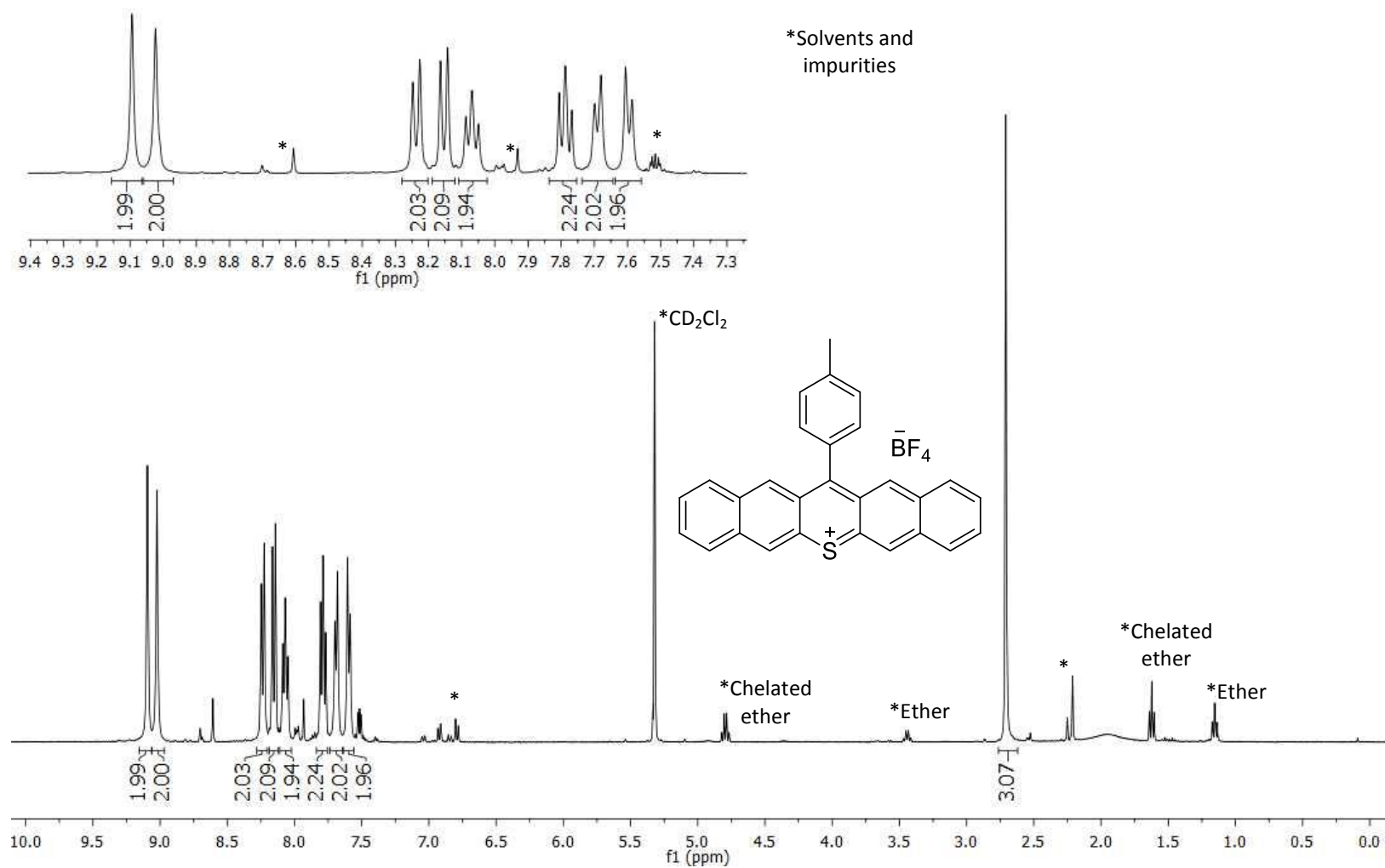
^1H NMR (CD_2Cl_2 , 400 MHz) for **107**



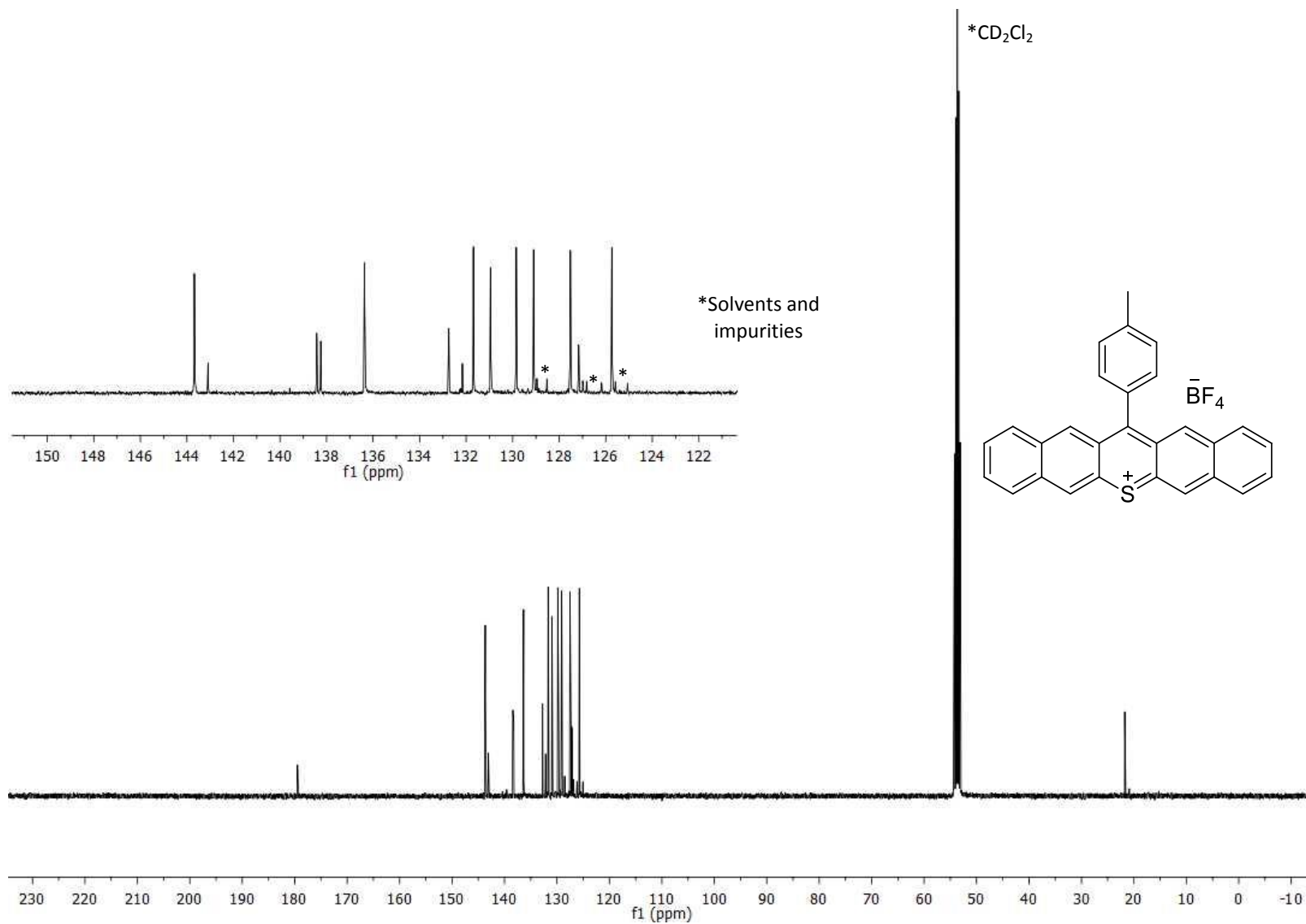
^{13}C NMR (CD_2Cl_2 , 101 MHz) for **107**



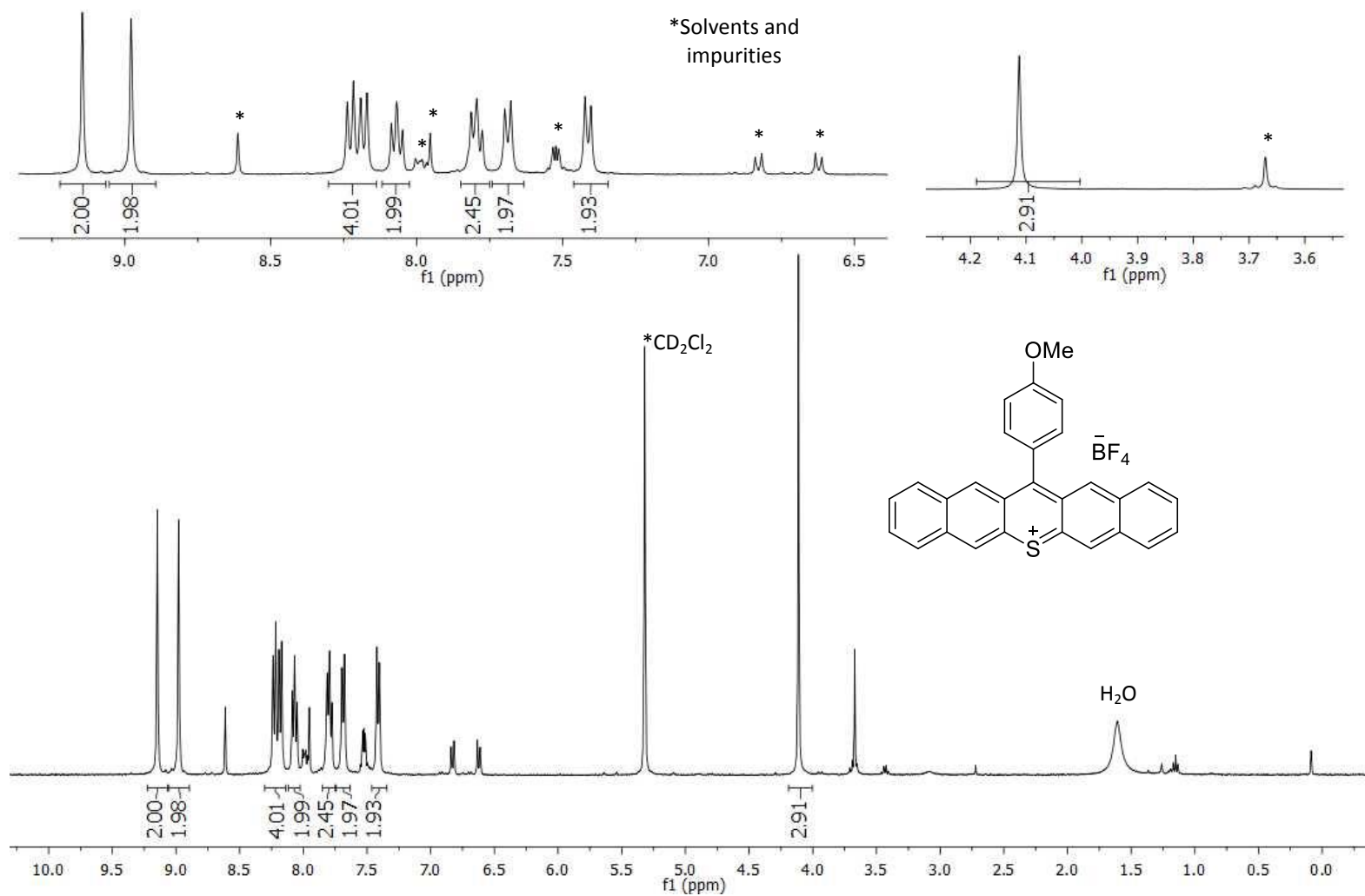
^1H NMR (CD_2Cl_2 , 400 MHz) for **108**



^{13}C NMR (CD_2Cl_2 , 400 MHz) for **108**

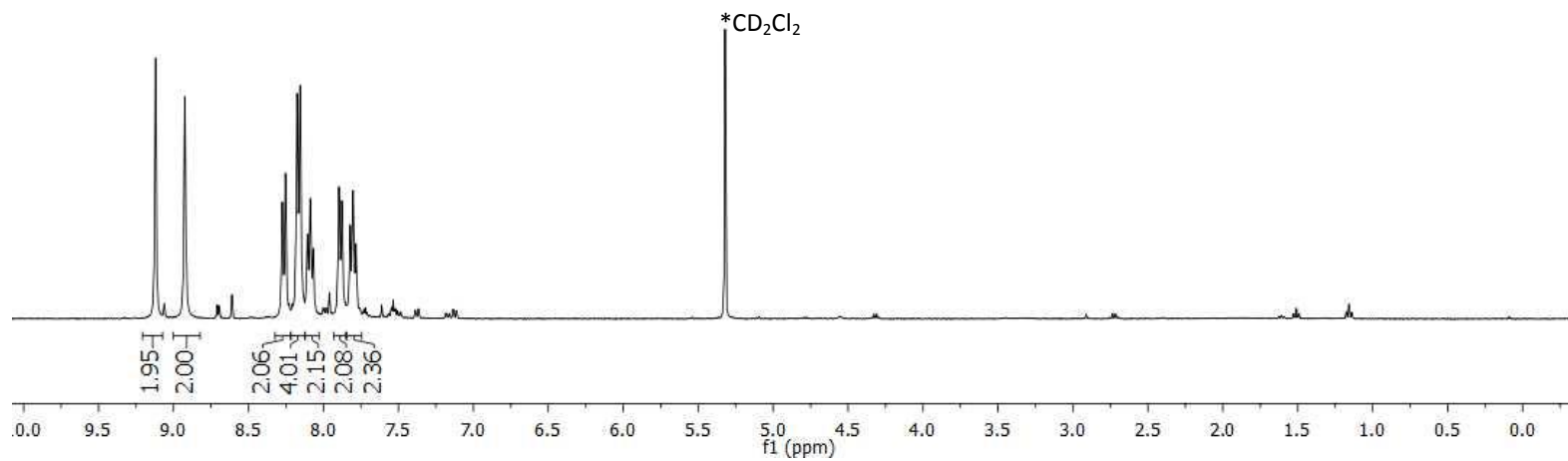
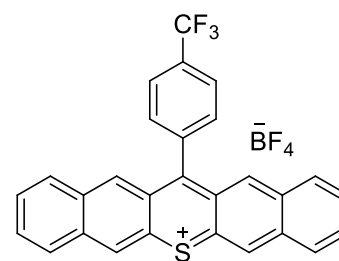
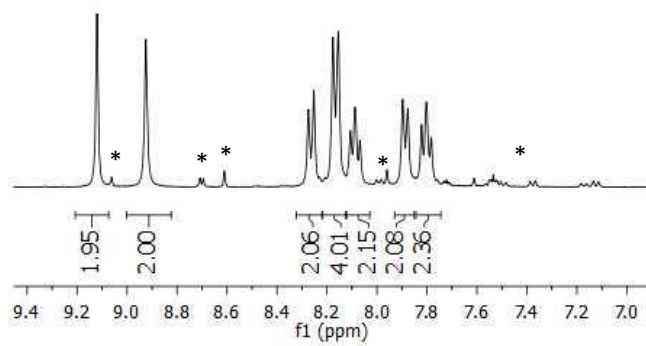


^1H NMR (CD_2Cl_2 , 400 MHz) for **109**

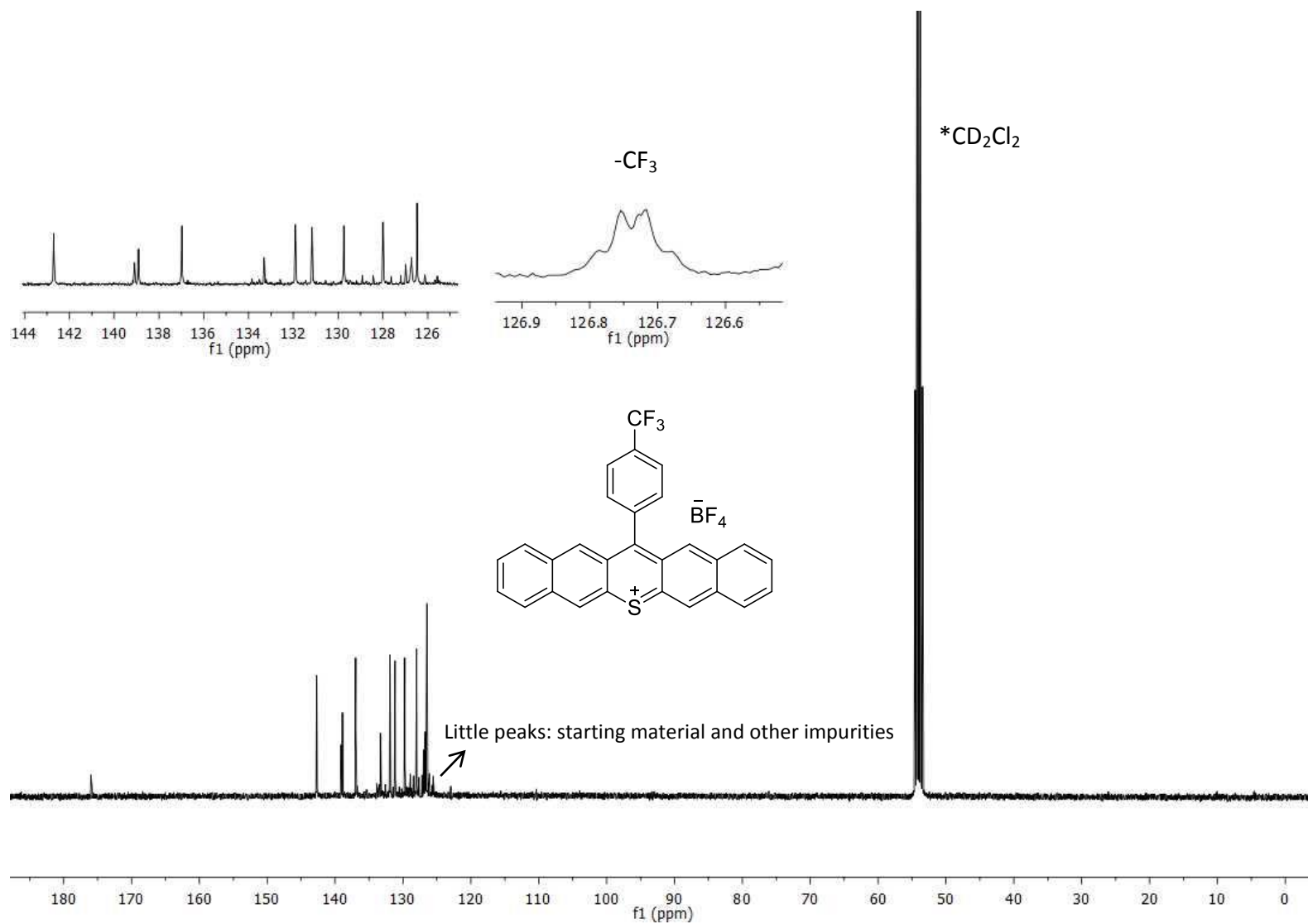


^1H NMR (CD_2Cl_2 , 400 MHz) for **110**

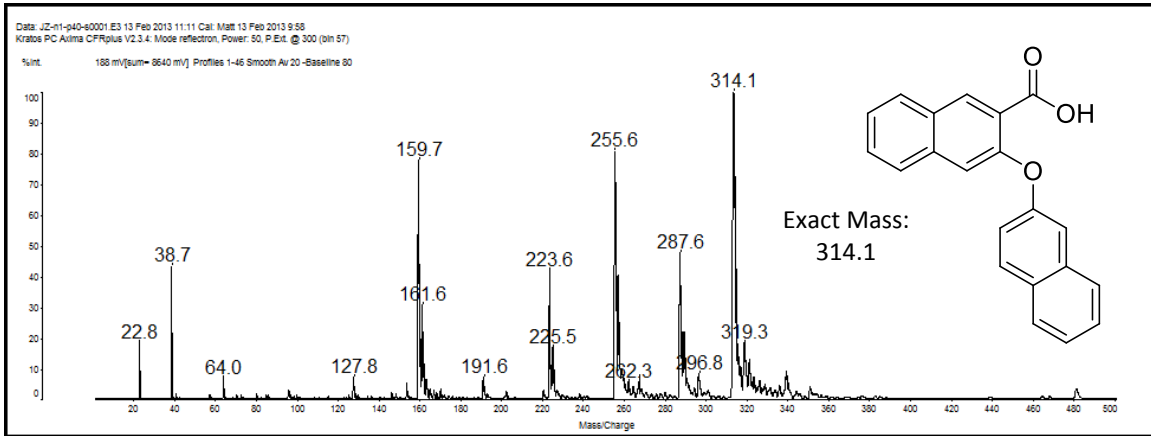
*Solvents and
impurities



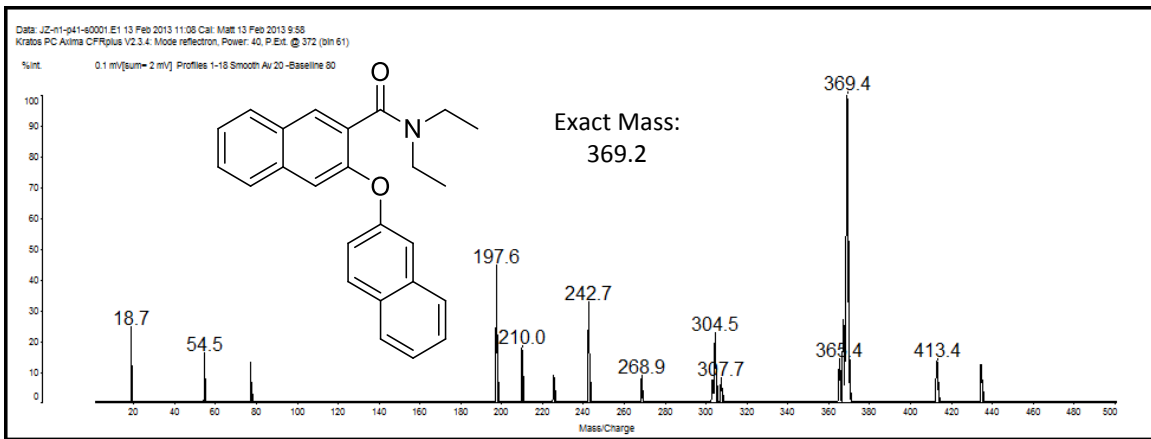
^{13}C NMR (CD_2Cl_2 , 101 MHz) for **110**



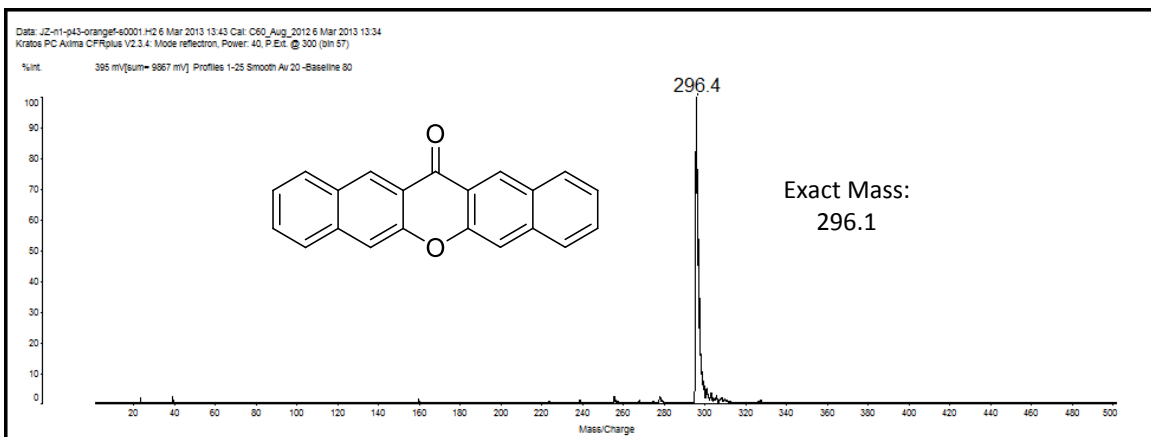
MALDI-TOF Mass Spectrum for 45



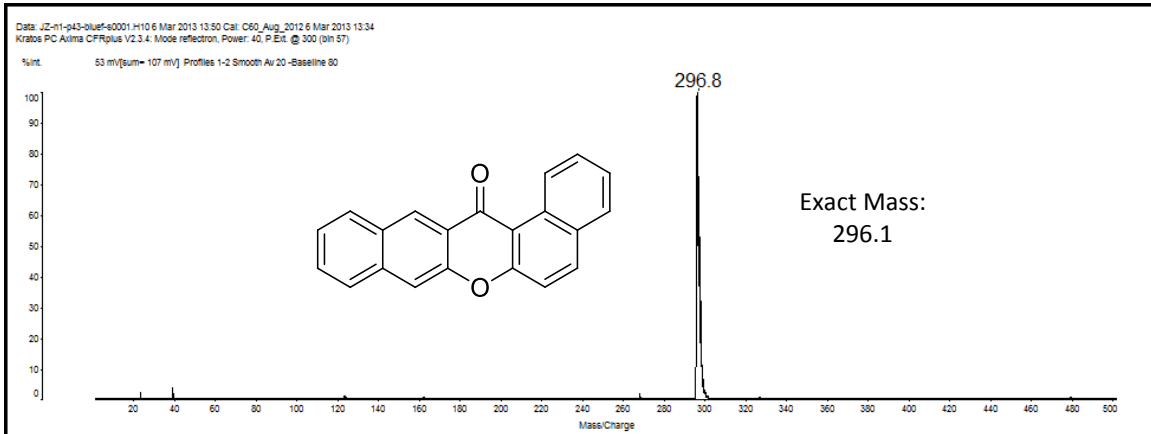
MALDI-TOF Mass Spectrum for 46



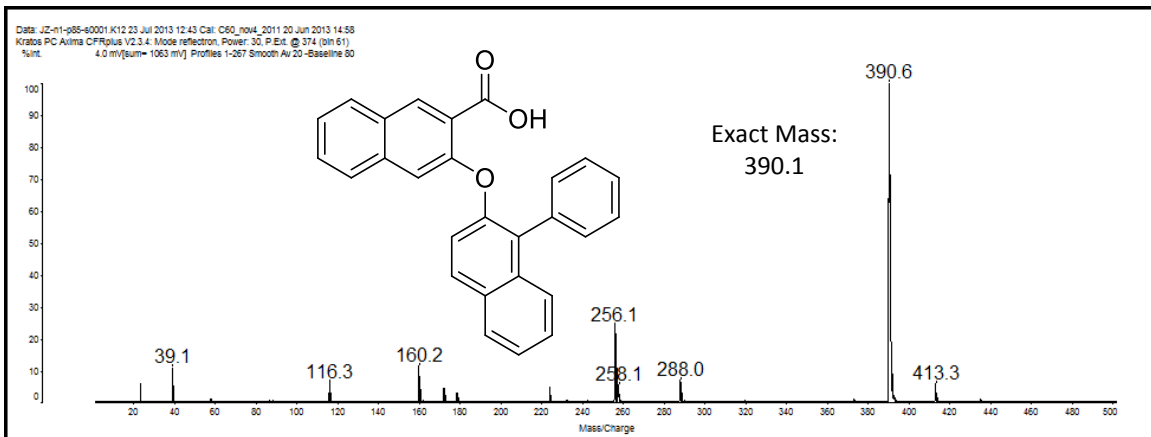
MALDI-TOF Mass Spectrum for 38



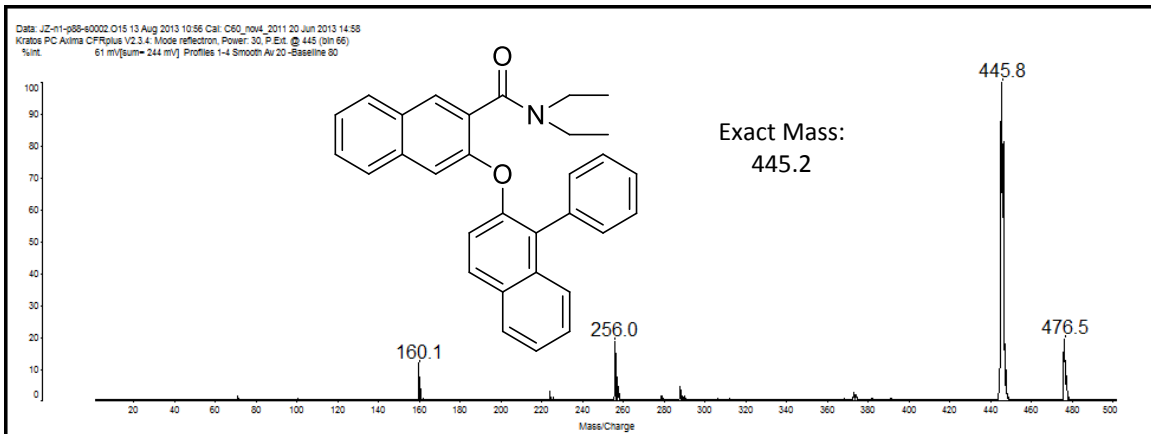
MALDI-TOF Mass Spectrum for **42**



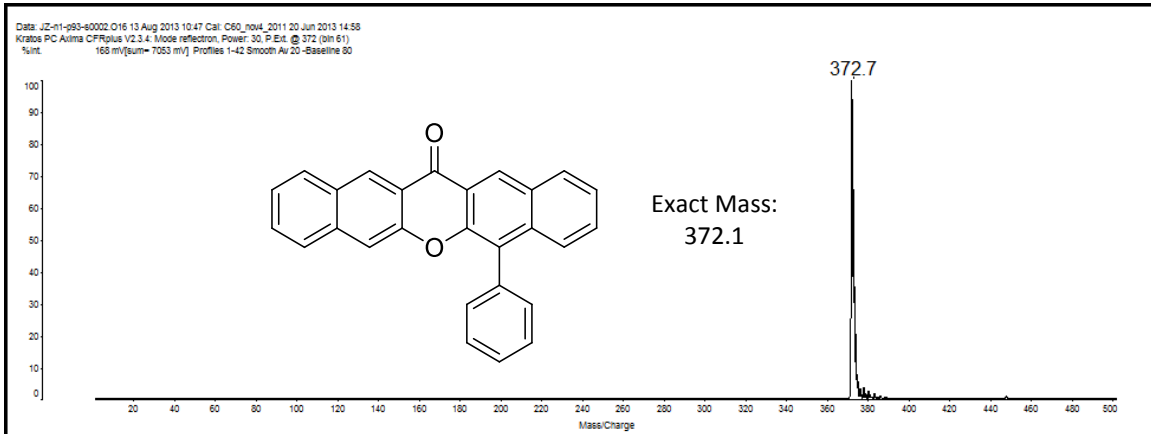
MALDI-TOF Mass Spectrum for **72**



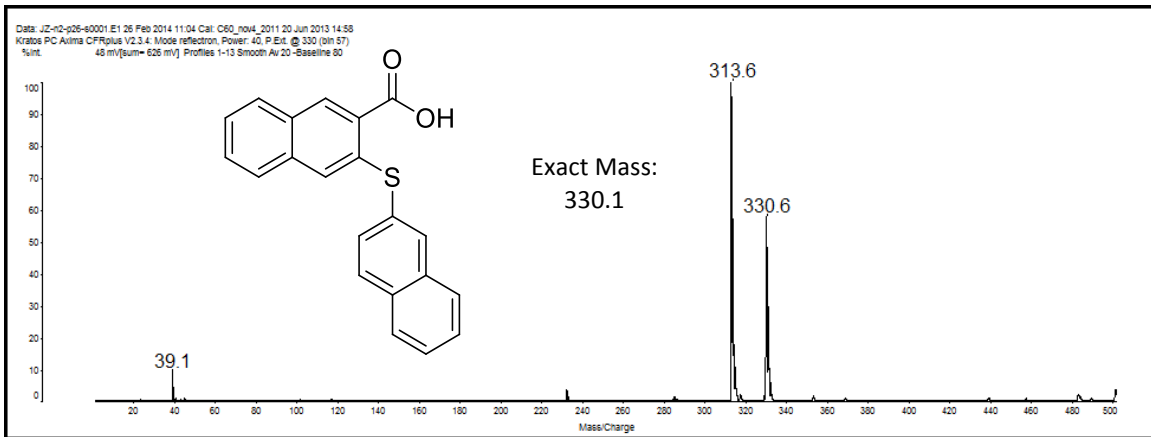
MALDI-TOF Mass Spectrum for **73**



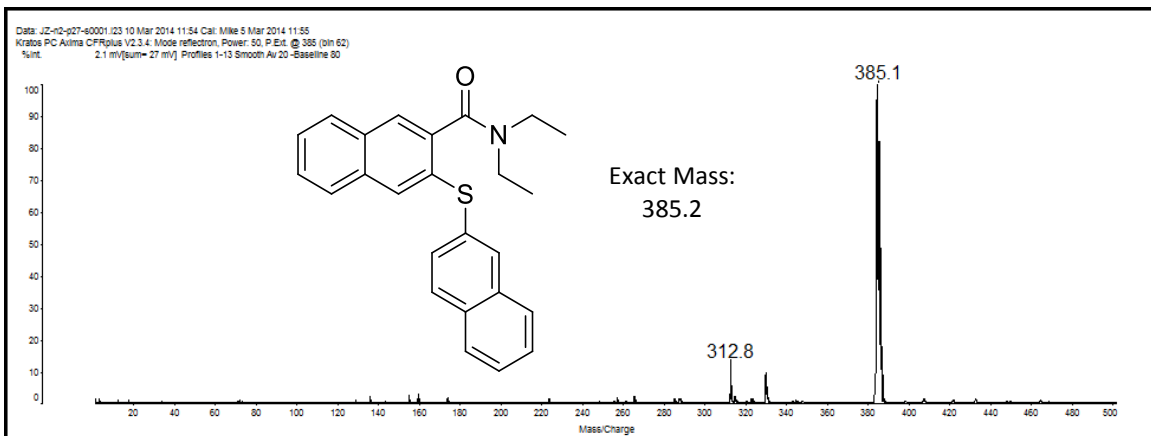
MALDI-TOF Mass Spectrum for 74



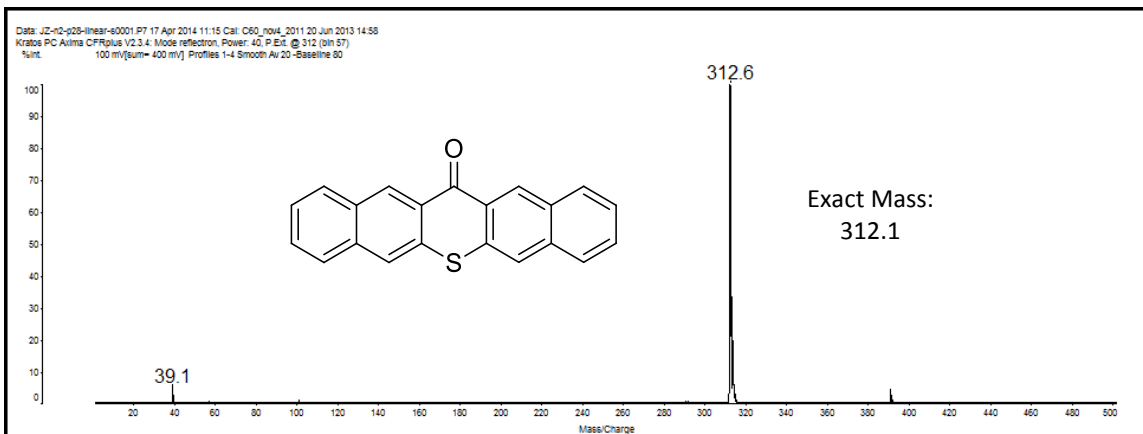
MALDI-TOF Mass Spectrum for 78



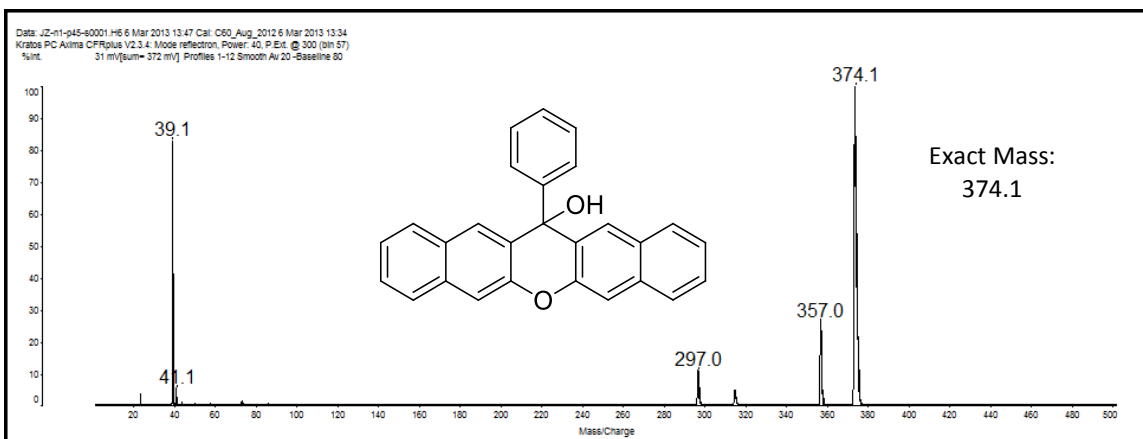
MALDI-TOF Mass Spectrum for 79



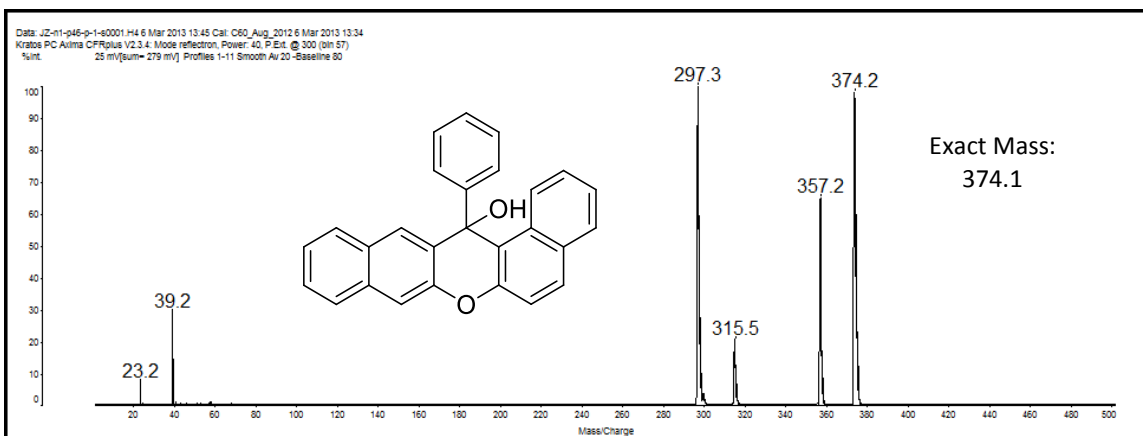
MALDI-TOF Mass Spectrum for **80**



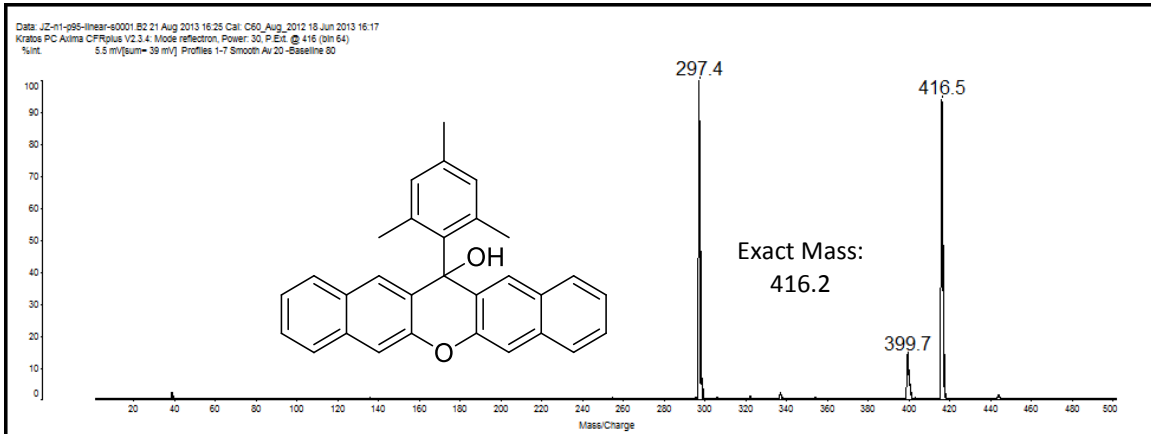
MALDI-TOF Mass Spectrum for **83**



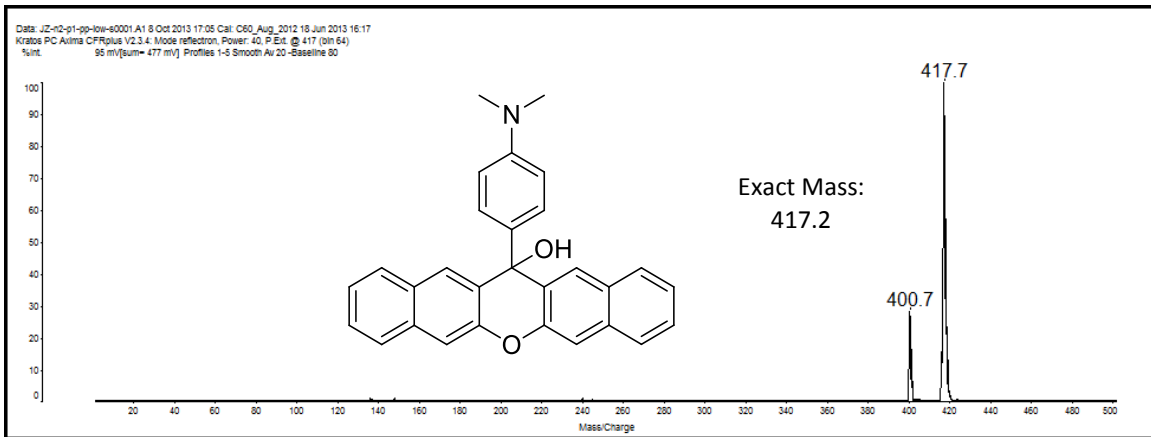
MALDI-TOF Mass Spectrum for **82**



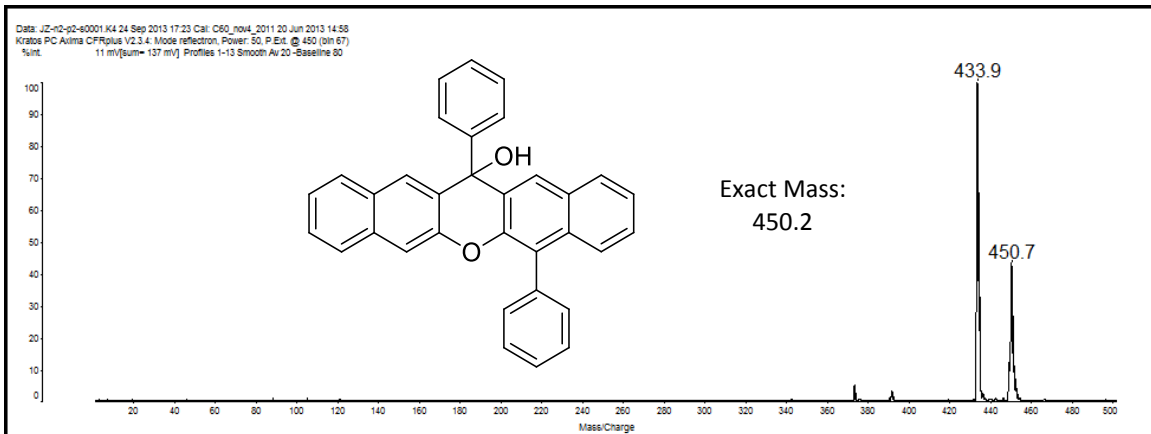
MALDI-TOF Mass Spectrum for **85**



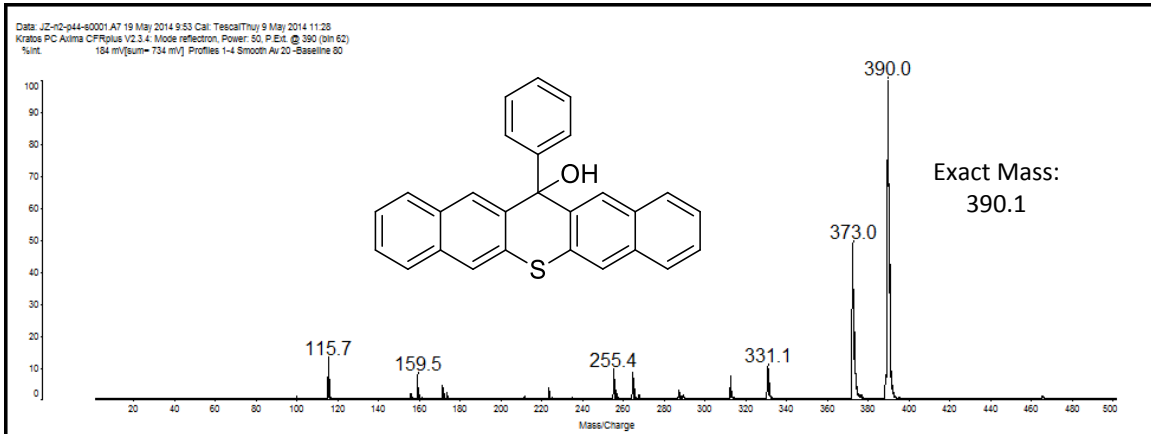
MALDI-TOF Mass Spectrum for **87**



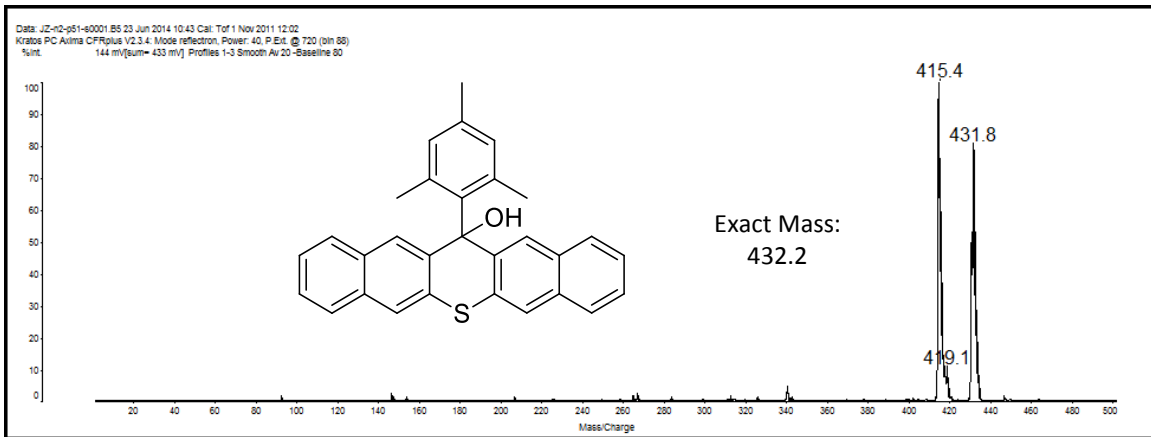
MALDI-TOF Mass Spectrum for **88**



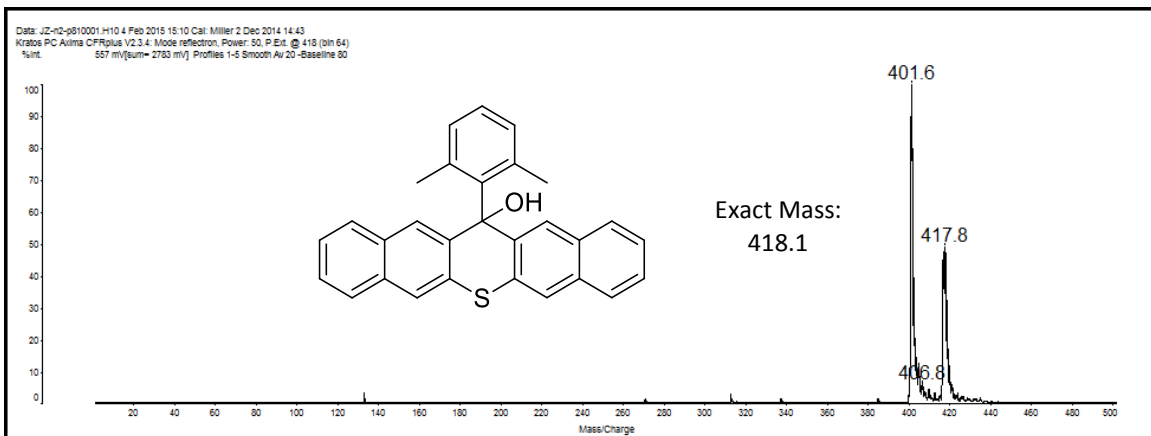
MALDI-TOF Mass Spectrum for 90



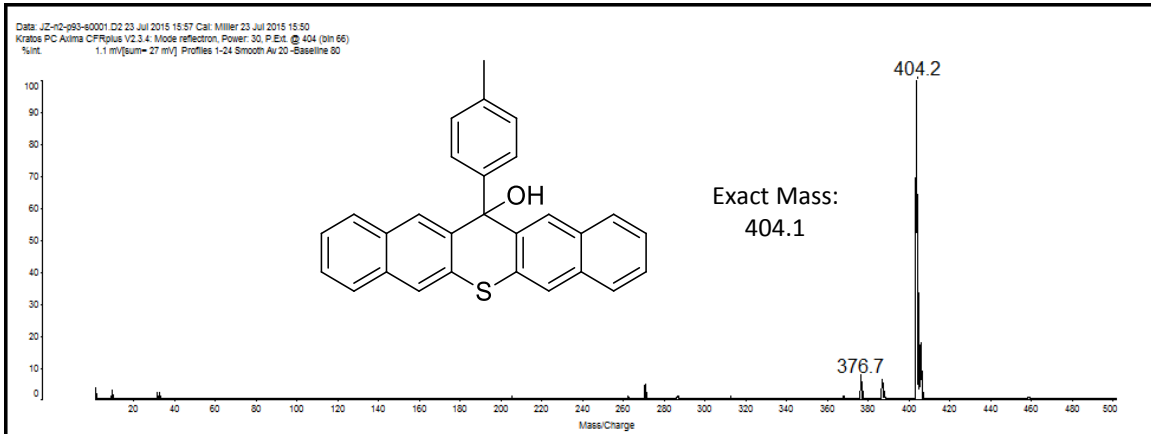
MALDI-TOF Mass Spectrum for 91



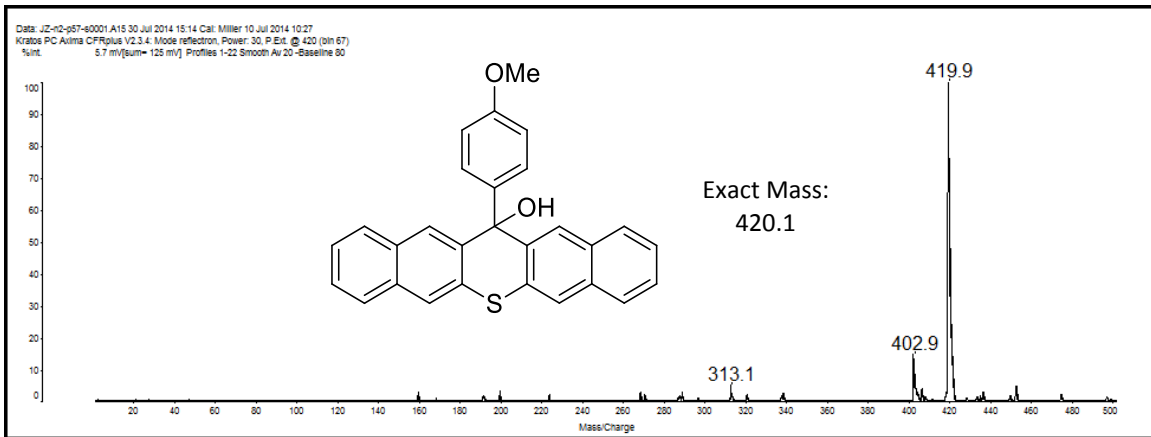
MALDI-TOF Mass Spectrum for 92



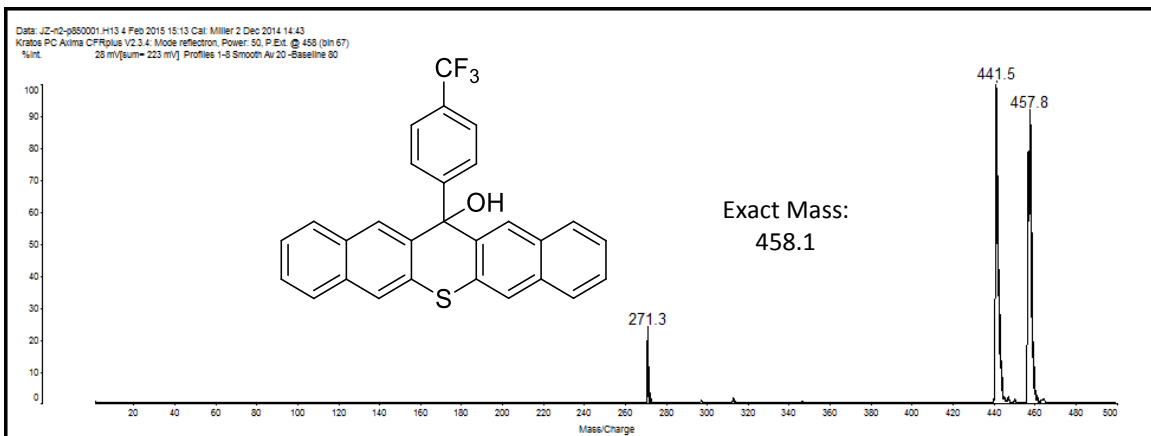
MALDI-TOF Mass Spectrum for 93



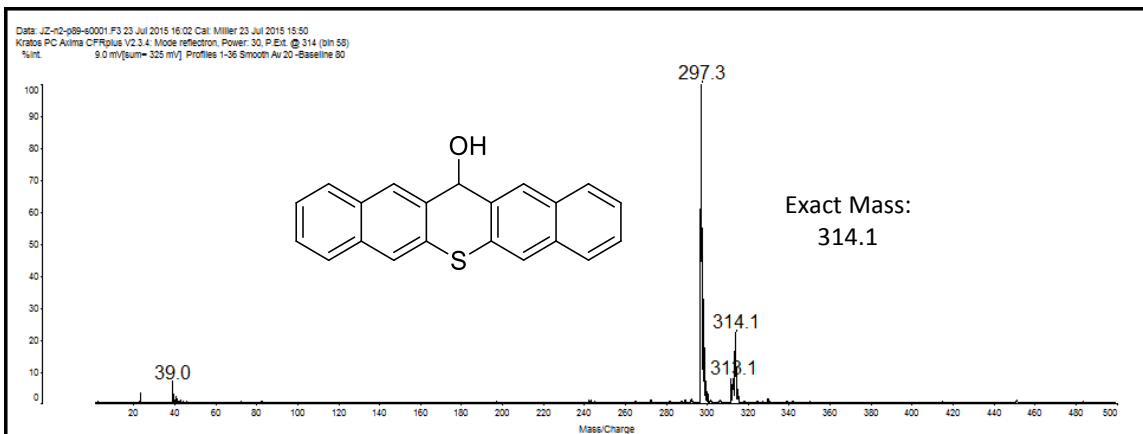
MALDI-TOF Mass Spectrum for 94



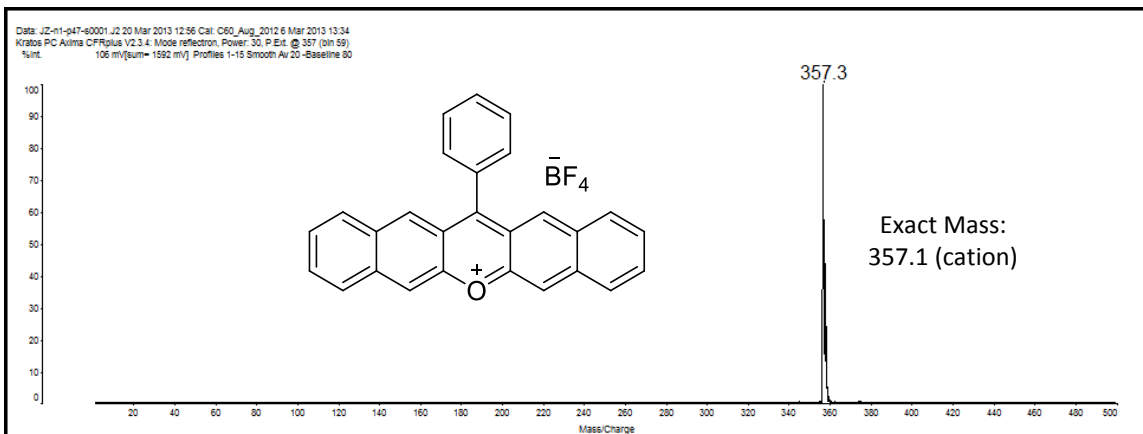
LDI-TOF Mass Spectrum for 95



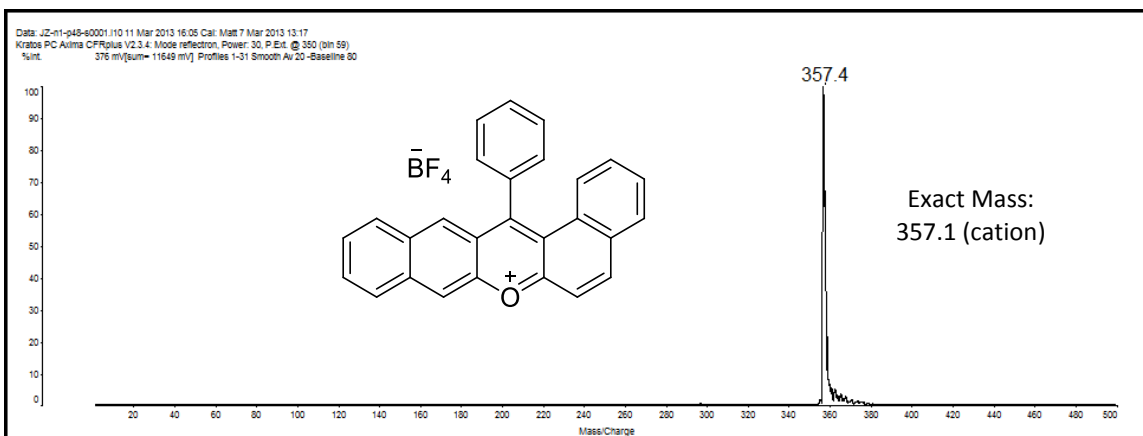
MALDI-TOF Mass Spectrum for 98



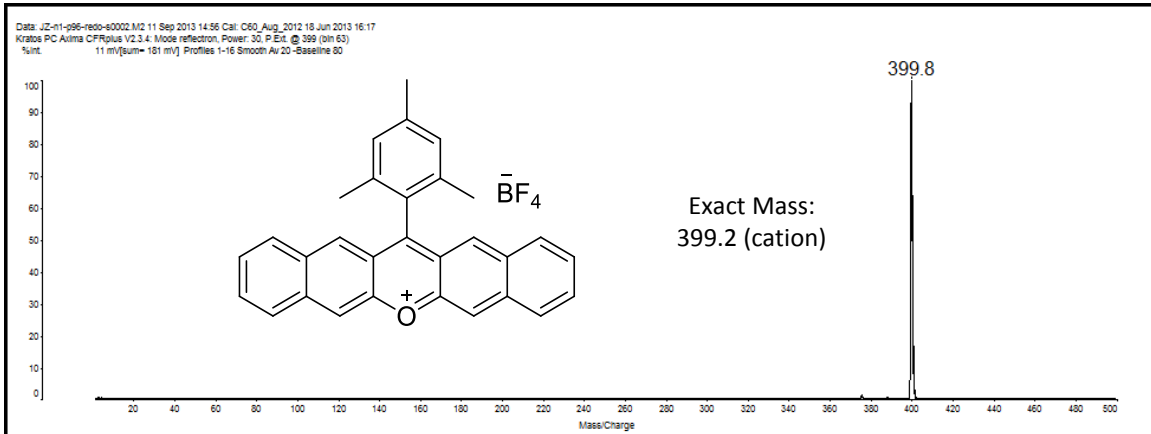
MALDI-TOF Mass Spectrum for 99



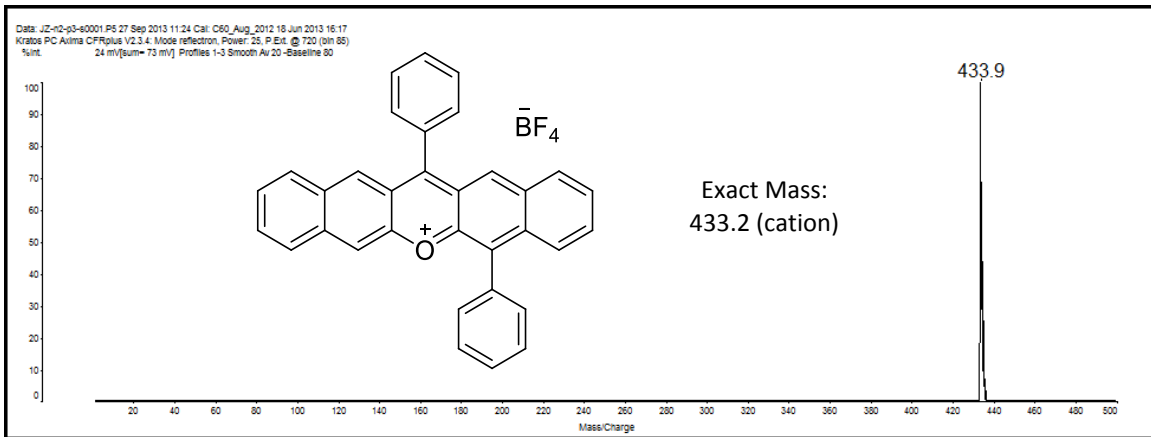
MALDI-TOF Mass Spectrum for 100



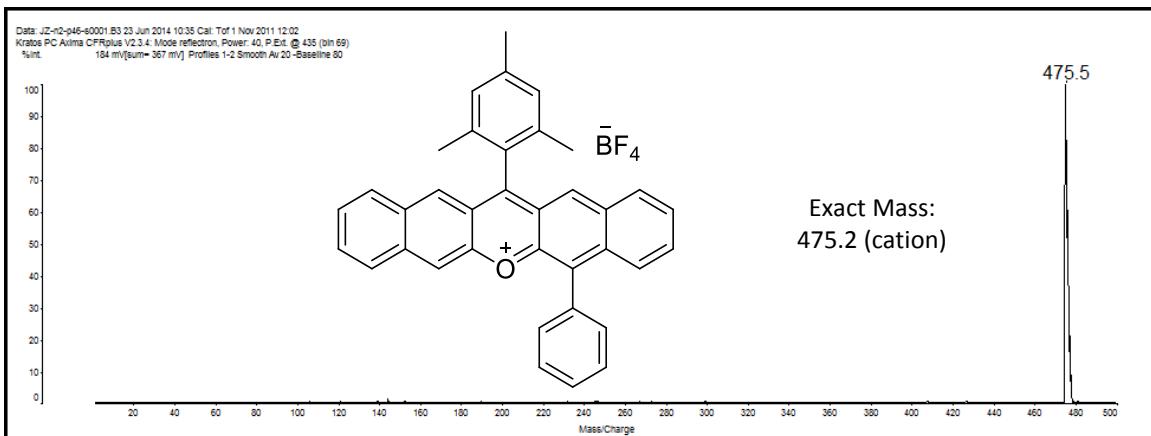
MALDI-TOF Mass Spectrum for 101



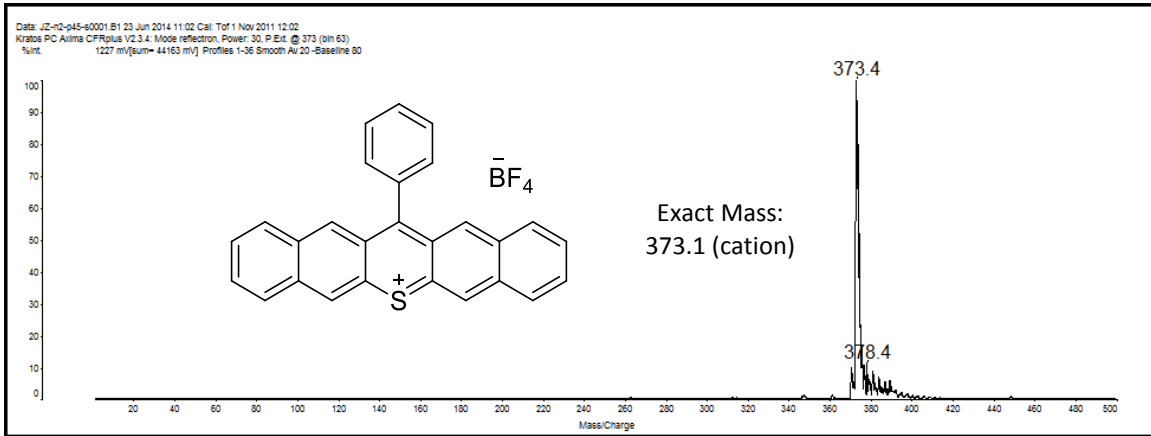
MALDI-TOF Mass Spectrum for 103



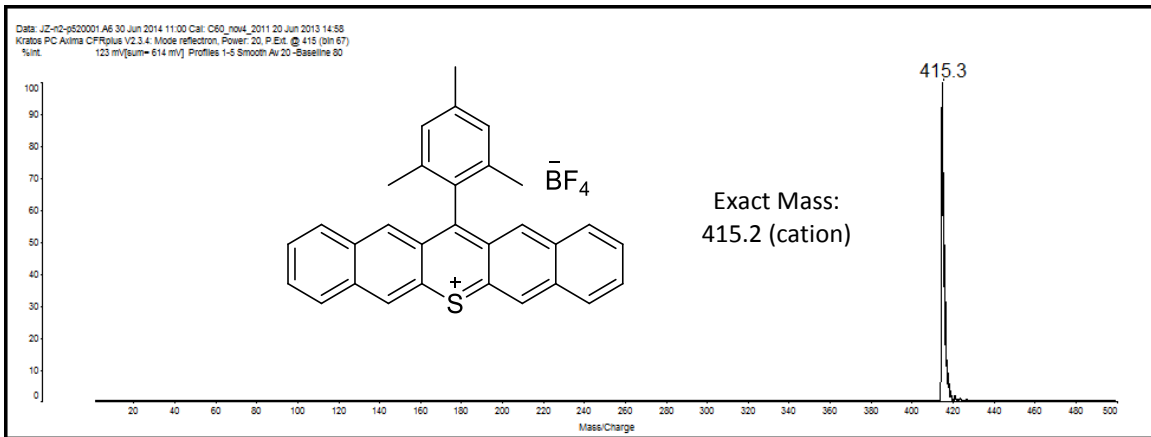
MALDI-TOF Mass Spectrum for 104



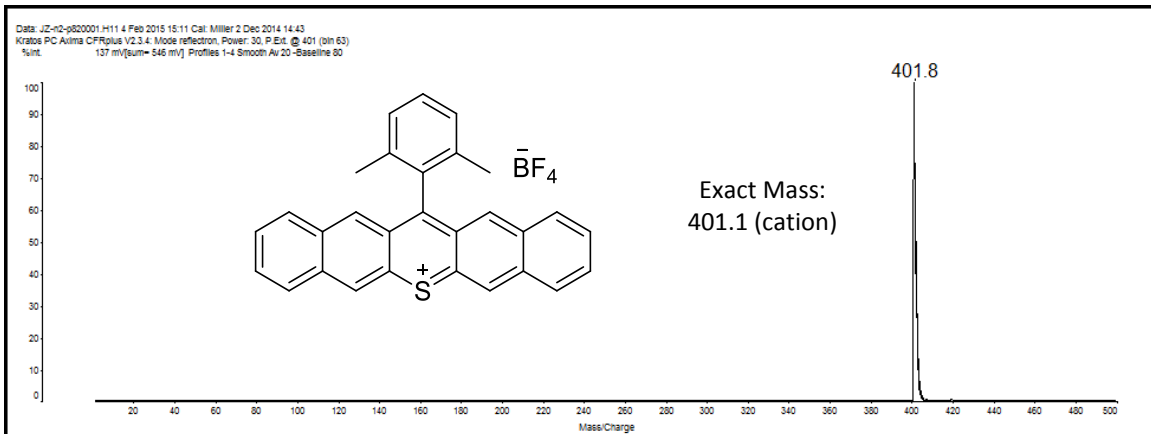
MALDI-TOF Mass Spectrum for 105



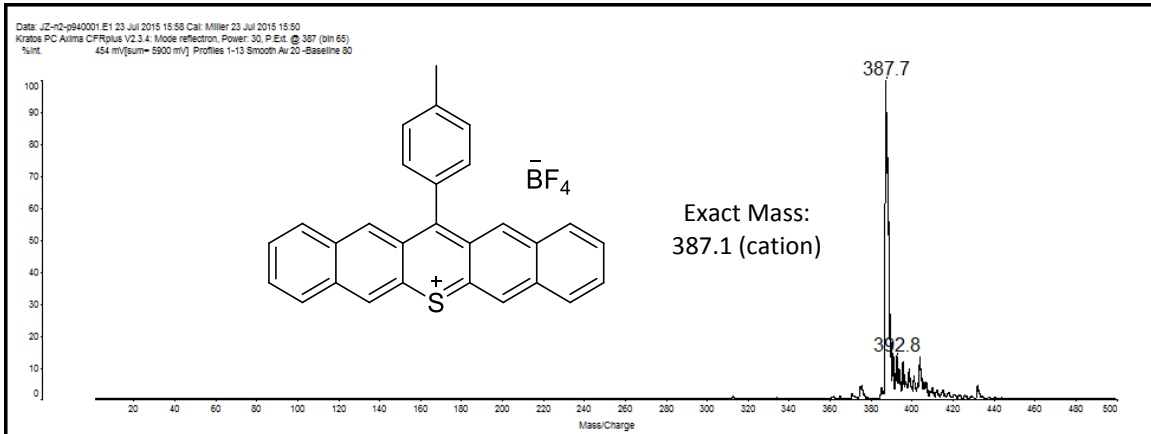
LDI-TOF Mass Spectrum for 106



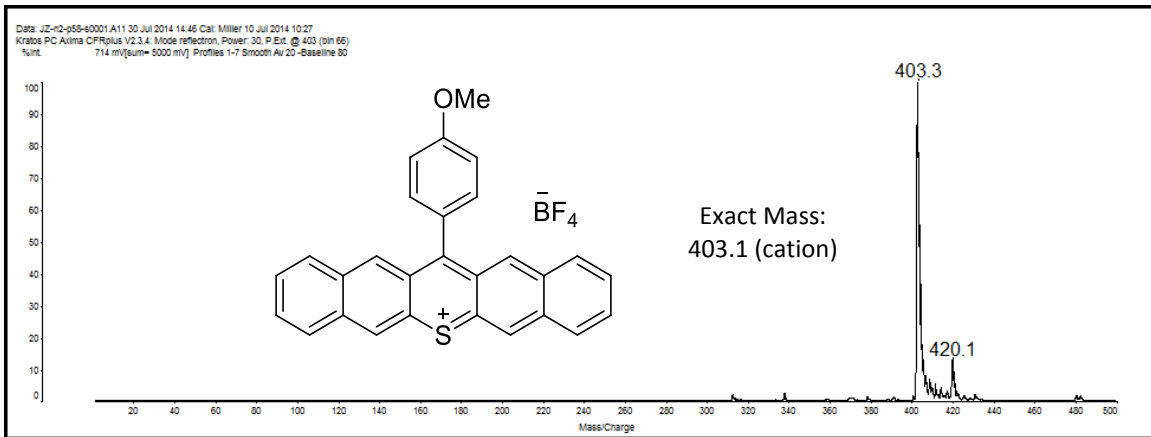
LDI-TOF Mass Spectrum for 107



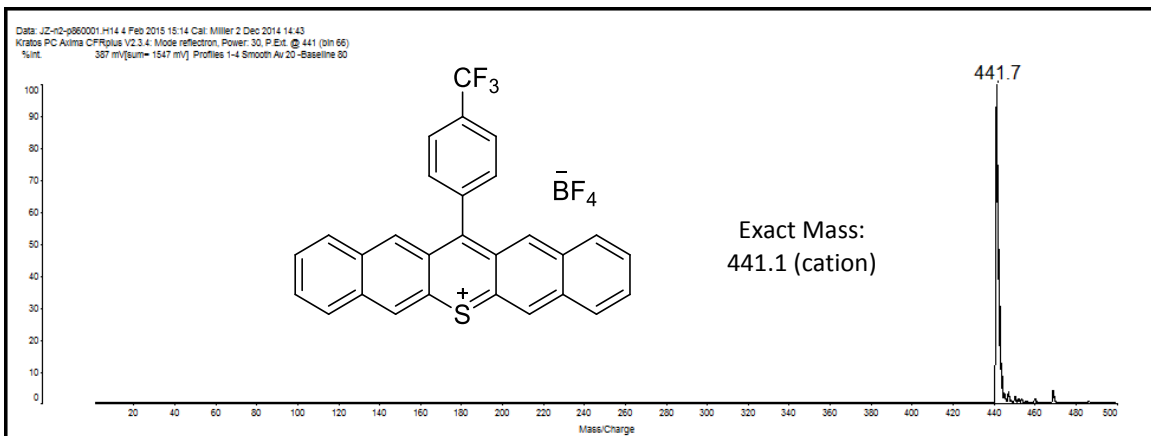
LDI-TOF Mass Spectrum for 108



MALDI-TOF Mass Spectrum for 109



LDI-TOF Mass Spectrum for 110



HRMS Spectrum for 45

Analysis Info

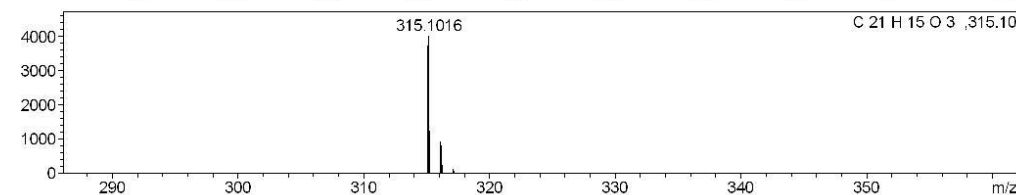
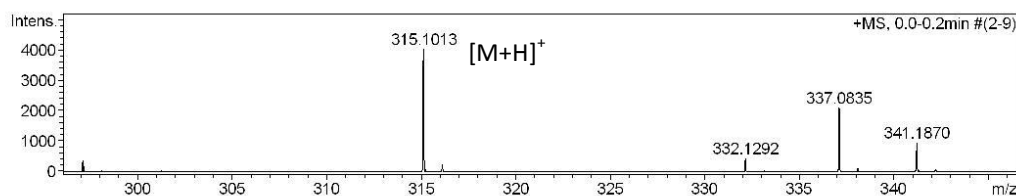
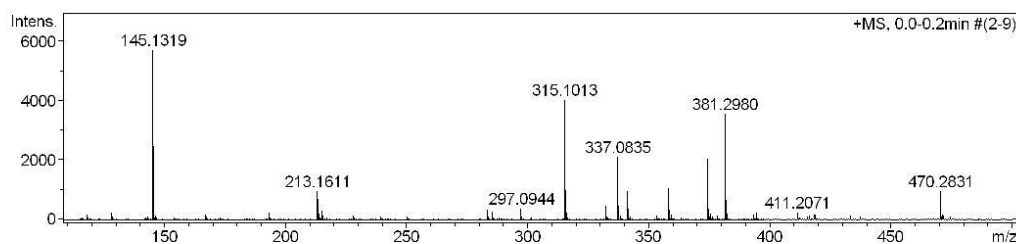
Analysis Name D:\Data\041213\3481-1.JZ-N1-P40.d
 Method cal80-1550.m
 Sample Name JZ-N1-P40
 Comment in CH3CN

Acquisition Date 4/12/2013 2:53:03 PM

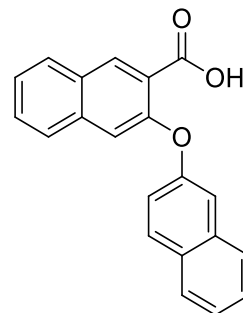
Operator Nonka Sevova
 Instrument / Ser# micrOTOF 10314

Acquisition Parameter

Source Type	ESI	Ion Polarity	Positive	Set Nebulizer	0.3 Bar
Focus	Not active	Set Capillary	4500 V	Set Dry Heater	180 °C
Scan Begin	50 m/z	Set End Plate Offset	-500 V	Set Dry Gas	4.0 l/min
Scan End	3000 m/z	n/a	n/a	Set Divert Valve	Source



Meas. m/z	#	Formula	m/z	err [ppm]	Mean err [ppm]	rdb	N-Rule
315.1013	1	C 21 H 15 O 3	315.1016	0.9	0.9	14.5	ok

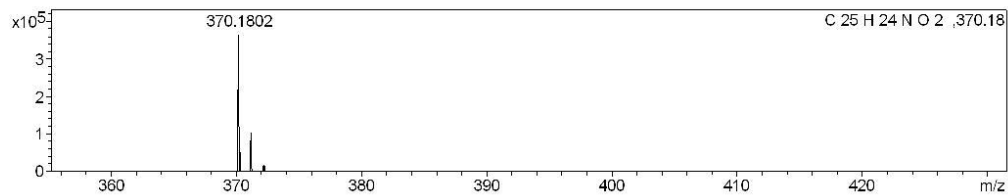
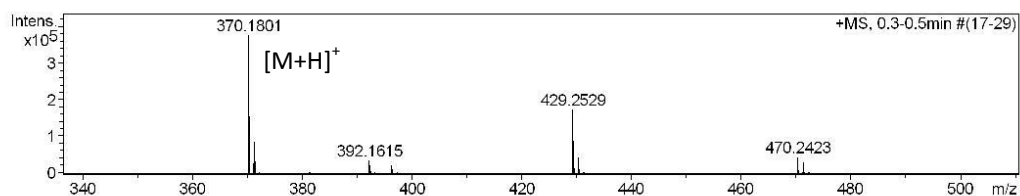
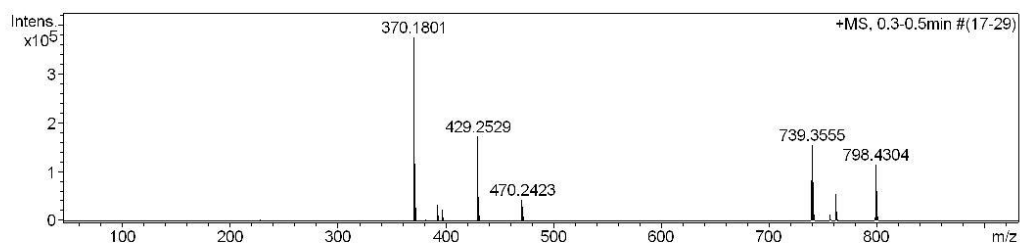


HRMS Spectrum for 46

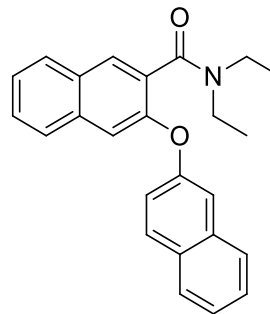
 Mass Spectrometry & Proteomics FacilityMass Spectrum SmartFormula Report

Analysis Info		Acquisition Date	4/12/2013 2:55:17 PM
Analysis Name	D:\Data\041213\3481-2.JZ-N1-P41.d	Operator	Nonka Sevova
Method	cal80-1550.m	Instrument / Ser#	micrOTOF 10314
Sample Name	JZ-N1-P41		
Comment	in CH3CN		

Acquisition Parameter					
Source Type	ESI	Ion Polarity	Positive	Set Nebulizer	0.3 Bar
Focus	Not active	Set Capillary	4500 V	Set Dry Heater	180 °C
Scan Begin	50 m/z	Set End Plate Offset	-500 V	Set Dry Gas	4.0 l/min
Scan End	3000 m/z	n/a	n/a	Set Divert Valve	Source



Meas. m/z	#	Formula	m/z	err [ppm]	Mean err [ppm]	rdb	N-Rule
370.1801	1	C 25 H 24 N O 2	370.1802	0.1	-0.1	14.5	ok



HRMS Spectrum for 38

Mass Spectrometry & Proteomics Facility

Mass Spectrum SmartFormula Report

Analysis Info

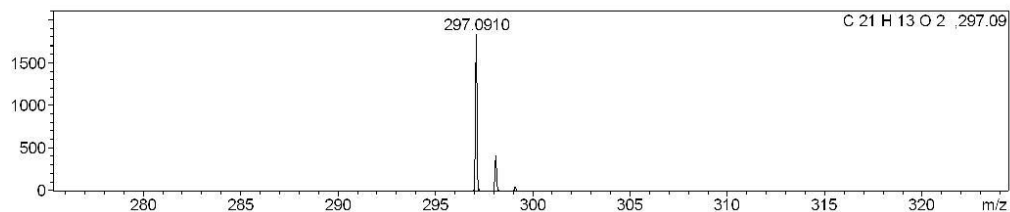
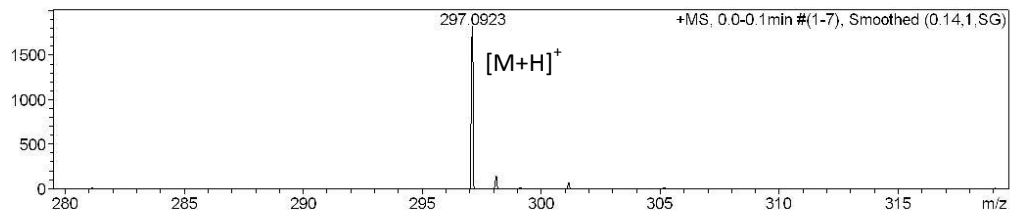
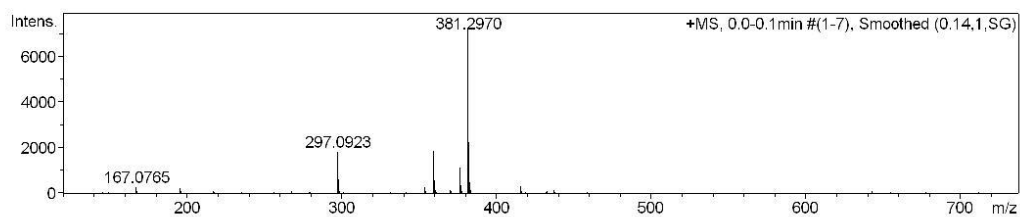
Analysis Name D:\Data\041213\3481-3.JZ-N1-P43A.d
 Method cal80-1550.m
 Sample Name JZ-N1-P43A
 Comment in CH3CN

Acquisition Date 4/12/2013 2:59:55 PM

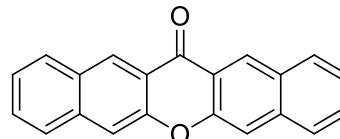
Operator Nonka Sevova
 Instrument / Ser# micrOTOF 10314

Acquisition Parameter

Source Type	ESI	Ion Polarity	Positive	Set Nebulizer	0.3 Bar
Focus	Not active	Set Capillary	4500 V	Set Dry Heater	180 °C
Scan Begin	50 m/z	Set End Plate Offset	-500 V	Set Dry Gas	4.0 l/min
Scan End	3000 m/z	n/a	n/a	Set Divert Valve	Source



Meas. m/z	#	Formula	m/z	err [ppm]	Mean err [ppm]	rdb	N-Rule
297.0923	1	C 21 H 13 O 2	297.0910	-4.3	-4.1	15.5	ok

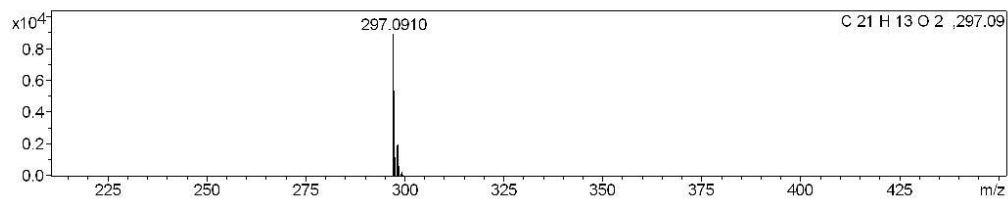
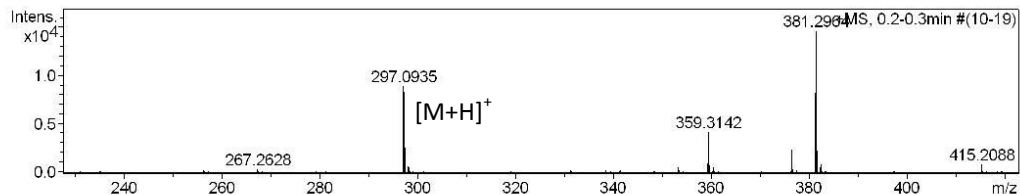
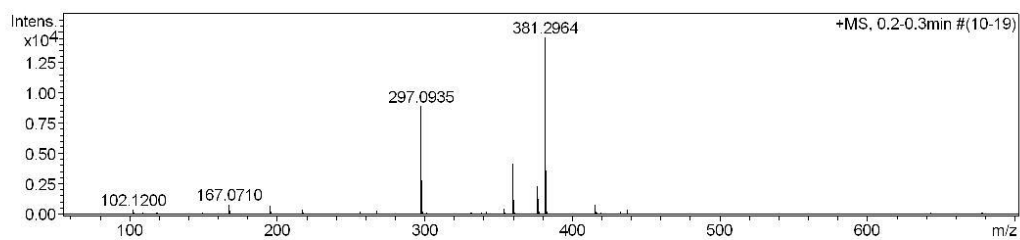


HRMS Spectrum for 42

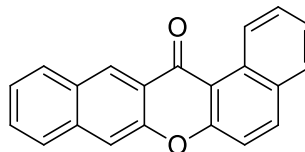
Analysis Info		Acquisition Date	4/12/2013 3:02:53 PM
Analysis Name	D:\Data\041213\3481-4.JZ-N1-P43B.d	Operator	Nonka Sevova
Method	cal80-1550.m	Instrument / Ser#	micrOTOF 10314
Sample Name	JZ-N1-P43B		
Comment	in CH3CN		

Acquisition Parameter

Source Type	ESI	Ion Polarity	Positive	Set Nebulizer	0.3 Bar
Focus	Not active	Set Capillary	4500 V	Set Dry Heater	180 °C
Scan Begin	50 m/z	Set End Plate Offset	-500 V	Set Dry Gas	4.0 l/min
Scan End	3000 m/z	n/a	n/a	Set Divert Valve	Source



Meas. m/z	#	Formula	m/z	err [ppm]	Mean err [ppm]	rdb	N-Rule
297.0935	1	C ₂₁ H ₁₃ O ₂	297.0910	-8.3	-8.0	15.5	ok



HRMS Spectrum for 72

Mass Spectrometry & Proteomics Facility **Mass Spectrum SmartFormula Report**

Analysis Info

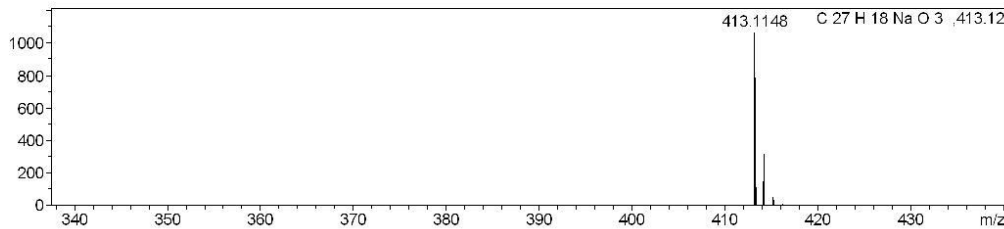
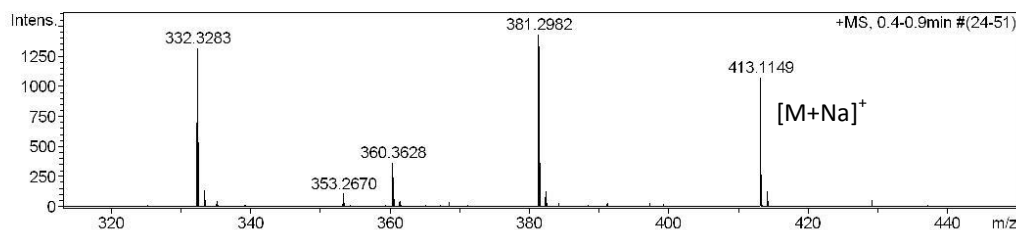
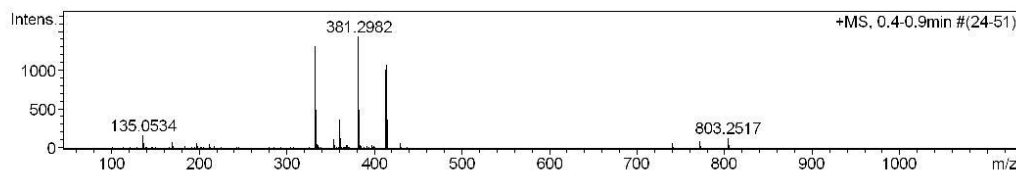
Analysis Name D:\Data\091014\25981-3.JZ-n1-p98.d
 Method cal100-1600.m
 Sample Name 3.JZ-n1-p98
 Comment in CH3CN

Acquisition Date 9/10/2014 4:27:00 PM

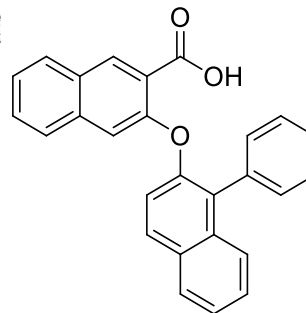
Operator Nonka Sevova
 Instrument / Ser# micrOTOF 10314

Acquisition Parameter

Source Type	ESI	Ion Polarity	Positive	Set Nebulizer	0.3 Bar
Focus	Not active	Set Capillary	4500 V	Set Dry Heater	180 °C
Scan Begin	50 m/z	Set End Plate Offset	-500 V	Set Dry Gas	4.0 l/min
Scan End	3000 m/z	n/a	n/a	Set Divert Valve	Source



Meas. m/z	#	Formula	m/z	err [ppm]	Mean err [ppm]	rdb	N-Rule
413.1149	1	C 27 H 18 Na O 3	413.1148	-0.1	0.3	18.5	ok



HRMS Spectrum for 73

Analysis Info

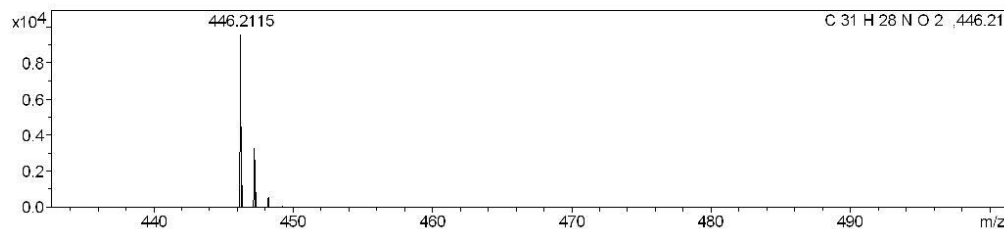
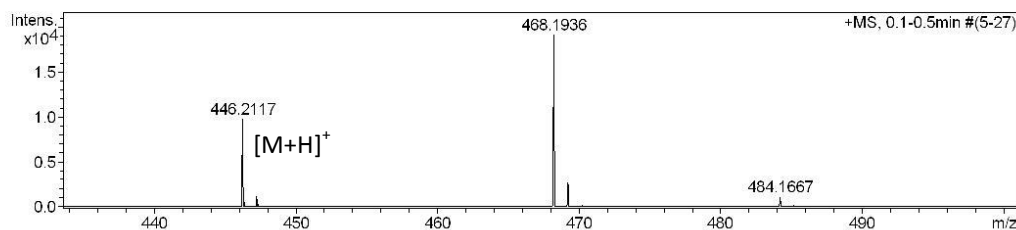
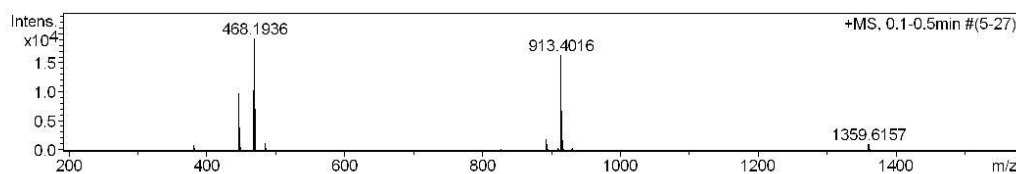
Analysis Name D:\Data\091014\25981-4.JZ-n1-p99.d
 Method cal100-1600.m
 Sample Name 4.JZ-n1-p99
 Comment in CH3CN

Acquisition Date 9/10/2014 4:29:49 PM

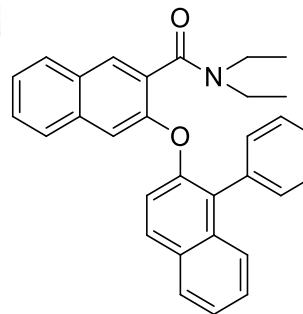
Operator Nonka Sevova
 Instrument / Ser# micrOTOF 10314

Acquisition Parameter

Source Type	ESI	Ion Polarity	Positive	Set Nebulizer	0.3 Bar
Focus	Not active	Set Capillary	4500 V	Set Dry Heater	180 °C
Scan Begin	50 m/z	Set End Plate Offset	-500 V	Set Dry Gas	4.0 l/min
Scan End	3000 m/z	n/a	n/a	Set Divert Valve	Source



Meas. m/z	#	Formula	m/z	err [ppm]	Mean err [ppm]	rdb	N-Rule
446.2117	1	C 31 H 28 N O 2	446.2115	-0.6	-1.0	18.5	ok



HRMS Spectrum for 74

Analysis Info

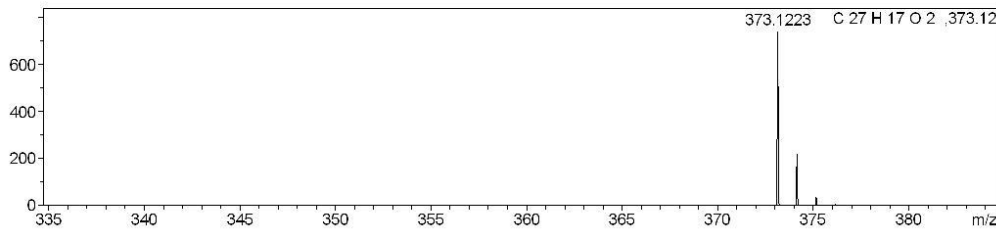
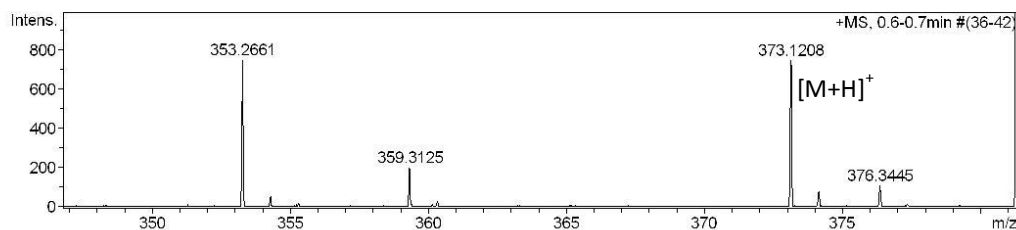
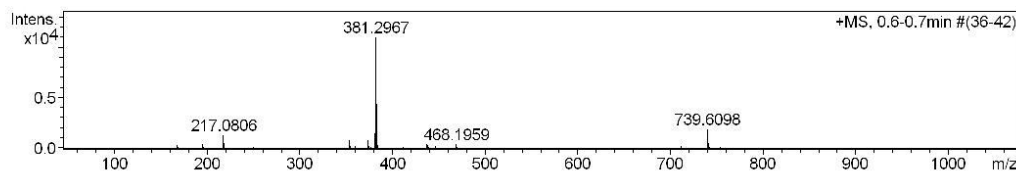
Analysis Name D:\Data\091714\26254-s5.JZ-n1-p100 .d
 Method cal100-1600.m
 Sample Name s5.JZ-n1-p100
 Comment in CH3CN

Acquisition Date 9/17/2014 1:58:28 PM

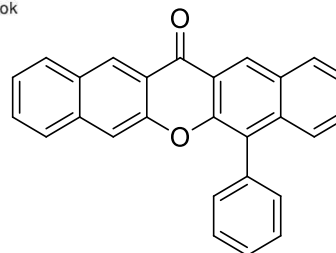
Operator Nonka Sevova
 Instrument / Ser# micrOTOF 10314

Acquisition Parameter


Source Type	ESI	Ion Polarity	Positive	Set Nebulizer	0.3 Bar
Focus	Not active	Set Capillary	4500 V	Set Dry Heater	180 °C
Scan Begin	50 m/z	Set End Plate Offset	-500 V	Set Dry Gas	4.0 l/min
Scan End	3000 m/z	n/a	n/a	Set Divert Valve	Source



Meas. m/z	#	Formula	m/z	err [ppm]	Mean err [ppm]	rdb	N-Rule
373.1208	1	C 27 H 17 O 2	373.1223	4.1	4.0	19.5	ok



HRMS Spectrum for 78

 Mass Spectrometry & Proteomics Facility

Mass Spectrum SmartFormula Report

Analysis Info

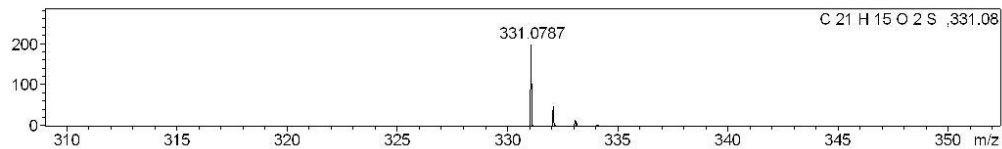
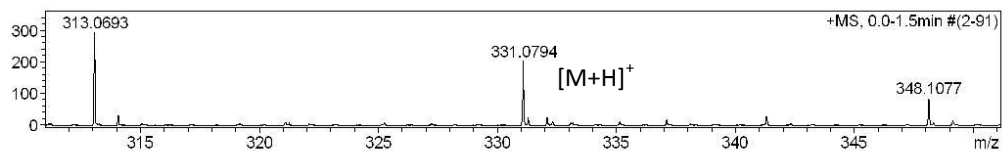
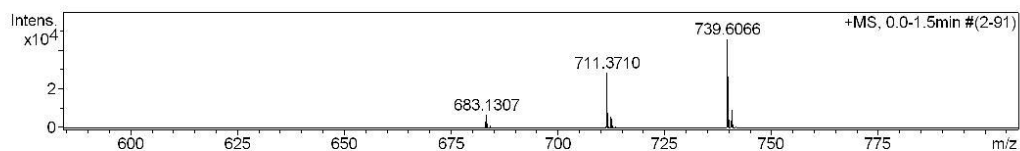
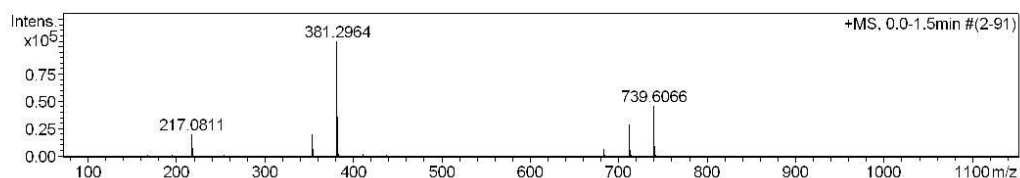
Analysis Name D:\Data\091714\26254-s11.JZ-n2-p26.d
 Method cal100-1600.m
 Sample Name s11.JZ-n2-p26
 Comment in CH3CN

Acquisition Date 9/17/2014 3:16:29 PM

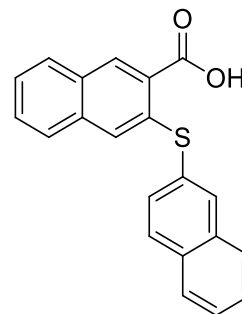
Operator Nonka Sevova
 Instrument / Ser# micrOTOF 10314

Acquisition Parameter

Source Type	ESI	Ion Polarity	Positive	Set Nebulizer	0.3 Bar
Focus	Not active	Set Capillary	4500 V	Set Dry Heater	180 °C
Scan Begin	50 m/z	Set End Plate Offset	-500 V	Set Dry Gas	4.0 l/min
Scan End	3000 m/z	n/a	n/a	Set Divert Valve	Source



Meas. m/z	#	Formula	m/z	err [ppm]	Mean err [ppm]	rdb	N-Rule
331.0794	1	C 21 H 15 O 2 S	331.0787	-1.9	-1.9	14.5	ok

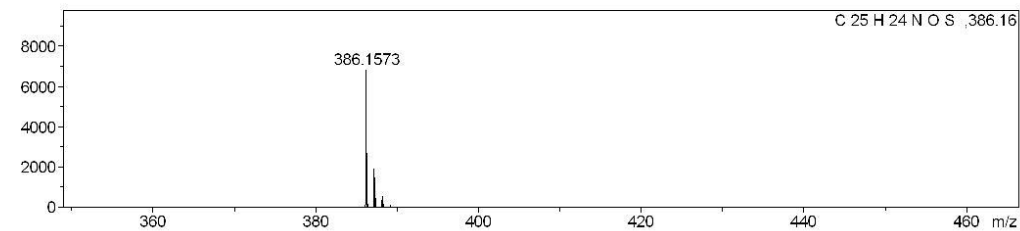
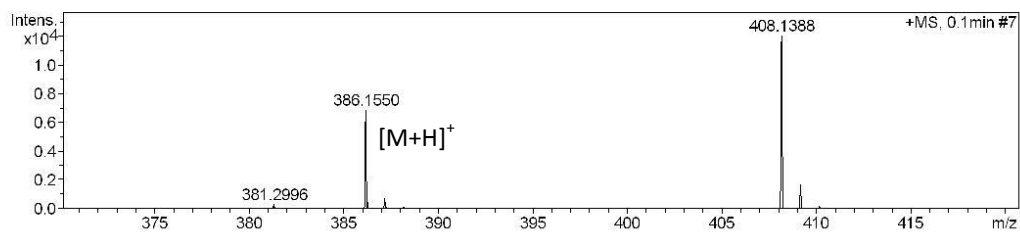
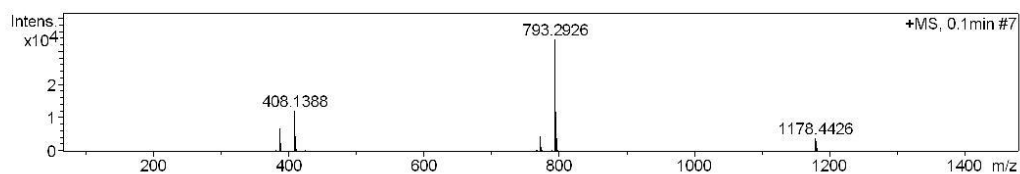


HRMS Spectrum for 79

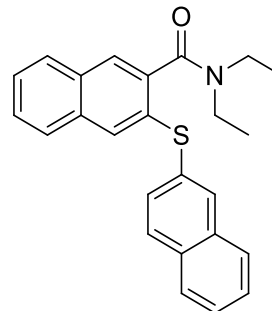
Analysis Info		Acquisition Date	9/17/2014 3:22:30 PM	
Analysis Name	D:\Data\091714\26254-s12.JZ-n2-p27.d	Operator	Nonka Sevova	
Method	cal100-1600.m	Instrument / Ser#	micrOTOF	10314
Sample Name	s12.JZ-n2-p27			
Comment	in CH3CN			

Acquisition Parameter

Source Type	ESI	Ion Polarity	Positive	Set Nebulizer	0.3 Bar
Focus	Not active	Set Capillary	4500 V	Set Dry Heater	180 °C
Scan Begin	50 m/z	Set End Plate Offset	-500 V	Set Dry Gas	4.0 l/min
Scan End	3000 m/z	n/a	n/a	Set Divert Valve	Source



Meas. m/z	#	Formula	m/z	err [ppm]	Mean err [ppm]	rdb	N-Rule
386.1550	1	C ₂₅ H ₂₄ NOS	386.1573	6.0	5.7	14.5	ok



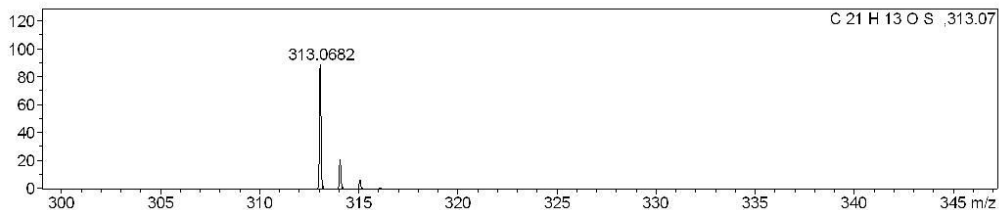
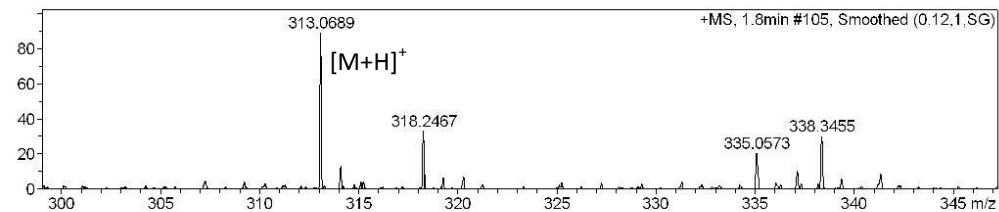
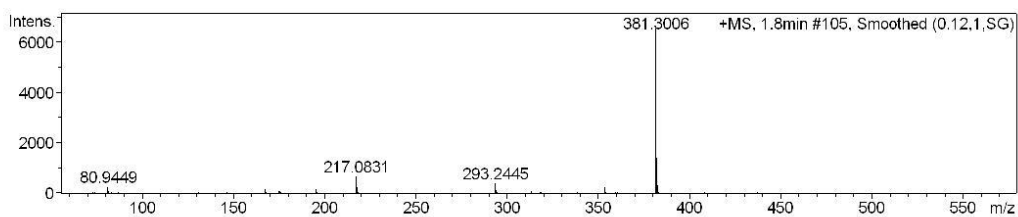
HRMS Spectrum for 80

 Mass Spectrometry & Proteomics Facility Mass Spectrum SmartFormula Report

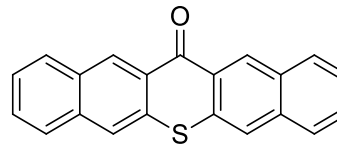
Analysis Info		Acquisition Date	9/25/2014 3:02:56 PM
Analysis Name	D:\Data\092514\26661-s13.JZ-n2-p43.d	Operator	Nonka Sevova
Method	cal100-1600.m	Instrument / Ser#	micrOTOF 10314
Sample Name	s13.JZ-n2-p43		
Comment	in CH3CN		

Acquisition Parameter

Source Type	ESI	Ion Polarity	Positive	Set Nebulizer	0.3 Bar
Focus	Not active	Set Capillary	4500 V	Set Dry Heater	180 °C
Scan Begin	50 m/z	Set End Plate Offset	-500 V	Set Dry Gas	4.0 l/min
Scan End	3000 m/z	n/a	n/a	Set Divert Valve	Source



Meas. m/z	#	Formula	m/z	err [ppm]	Mean err [ppm]	rdb	N-Rule
313.0689	1	C ₂₁ H ₁₃ O ₂ S	313.0682	-2.2	-2.2	15.5	ok



HRMS Spectrum for 83

Analysis Info

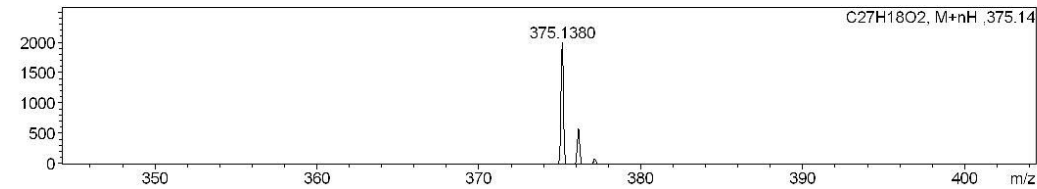
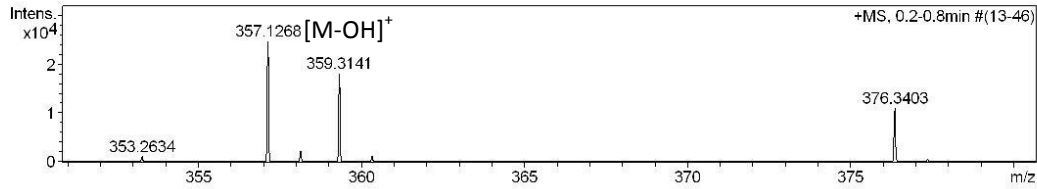
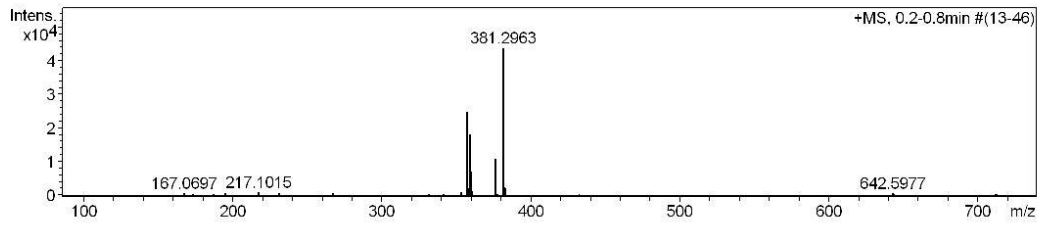
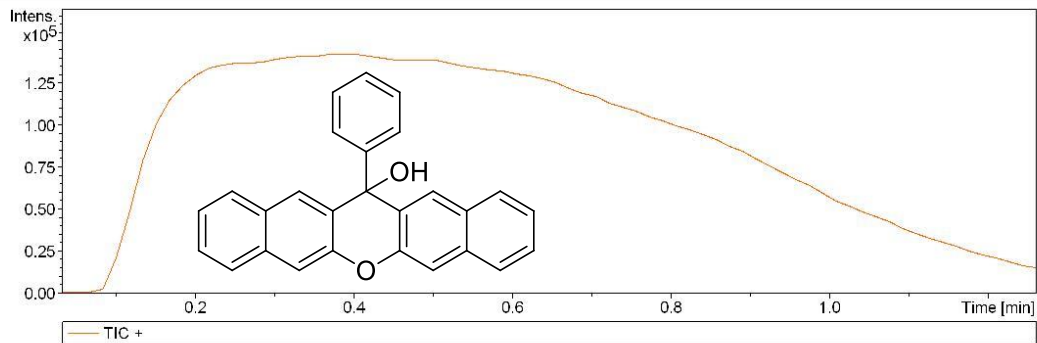
Analysis Name D:\Data\041213\3481-5.JZ-N1-P45.d
Method cal80-1550.m
Sample Name JZ-N1-P45
Comment in CH3CN

Acquisition Date 4/12/2013 3:12:29 PM

Operator Nonka Sevova
Instrument micrOTOF

Acquisition Parameter

n/a	n/a	Ion Polarity	Positive	n/a	n/a
n/a	n/a	n/a	n/a	n/a	n/a
n/a	n/a	n/a	n/a	n/a	n/a
n/a	n/a	n/a	n/a	n/a	n/a

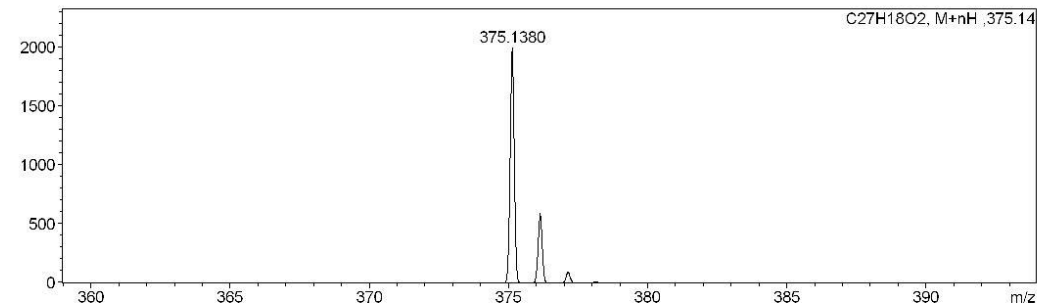
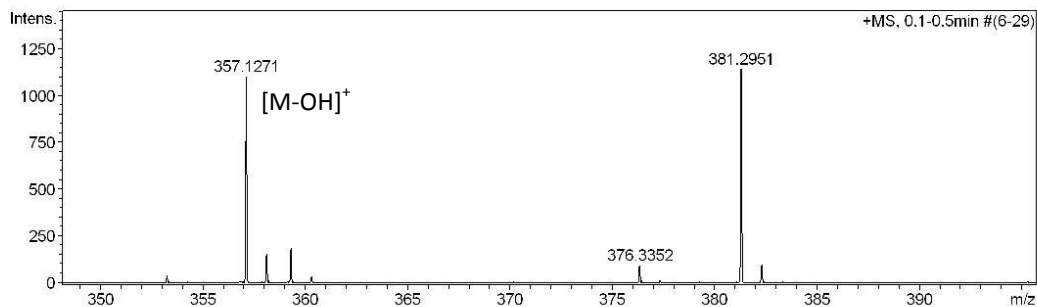
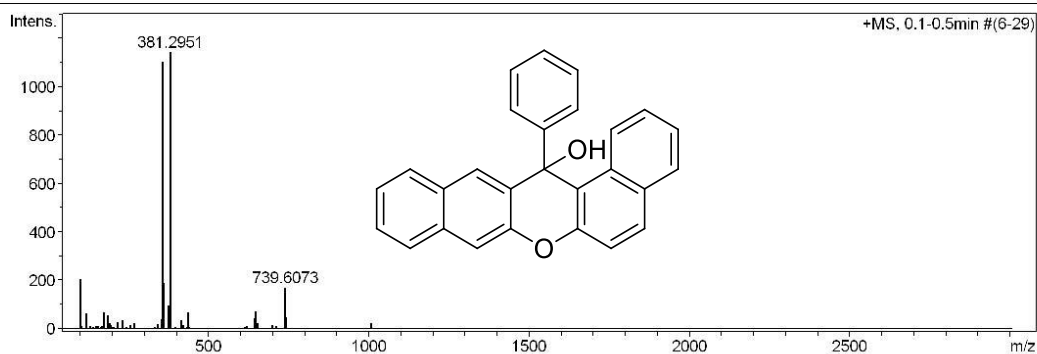


The Center for Environmental Science & Technology contributed to the purchase of the Bruker MicrOTOF-II

HRMS Spectrum for 82

Analysis Info		Acquisition Date	4/12/2013 3:15:18 PM
Analysis Name	D:\Data\041213\3481-6.JZ-N1-P46.d	Operator	Nonka Sevova
Method	cal80-1550.m	Instrument	micrOTOF
Sample Name	JZ-N1-P46		
Comment	in CH3CN		

Acquisition Parameter					
n/a	n/a	Ion Polarity	Positive	n/a	n/a
n/a	n/a	n/a	n/a	n/a	n/a
n/a	n/a	n/a	n/a	n/a	n/a
n/a	n/a	n/a	n/a	n/a	n/a



HRMS Spectrum for 85

 Mass Spectrometry & Proteomics Facility
Mass Spectrum SmartFormula Report

Analysis Info

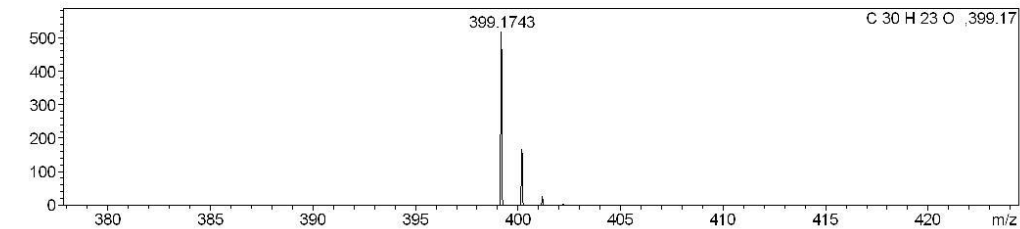
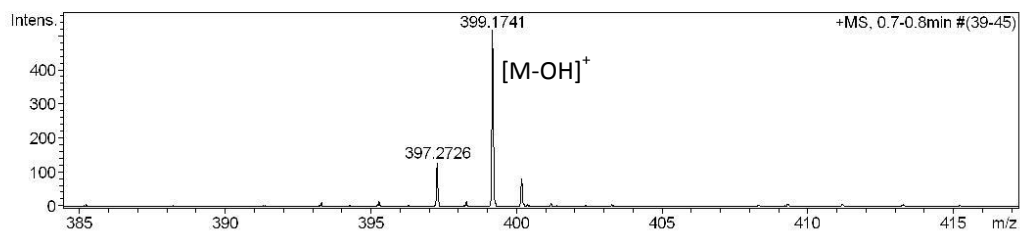
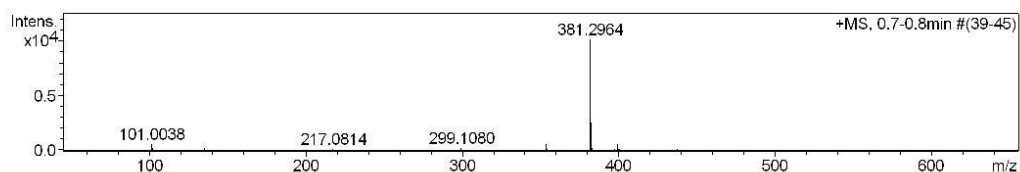
Analysis Name D:\Data\091014\25981-1.JZ-n1-p95-1.d
 Method cal100-1600.m
 Sample Name 1.JZ-n1-p95-1
 Comment in CH3CN

Acquisition Date 9/10/2014 4:17:52 PM

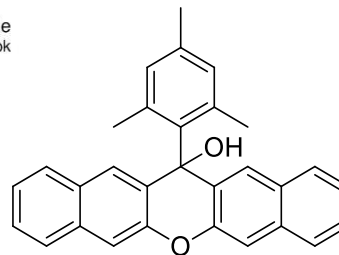
Operator Nonka Sevova
 Instrument / Ser# micrOTOF 10314

Acquisition Parameter

Source Type	ESI	Ion Polarity	Positive	Set Nebulizer	0.3 Bar
Focus	Not active	Set Capillary	4500 V	Set Dry Heater	180 °C
Scan Begin	50 m/z	Set End Plate Offset	-500 V	Set Dry Gas	4.0 l/min
Scan End	3000 m/z	n/a	n/a	Set Divert Valve	Source



Meas. m/z	#	Formula	m/z	err [ppm]	Mean err [ppm]	rdb	N-Rule
399.1741	1	C 30 H 23 O	399.1743	0.6	0.6	19.5	ok



HRMS Spectrum for 87

 Mass Spectrometry & Proteomics Facility Mass Spectrum SmartFormula Report

Analysis Info

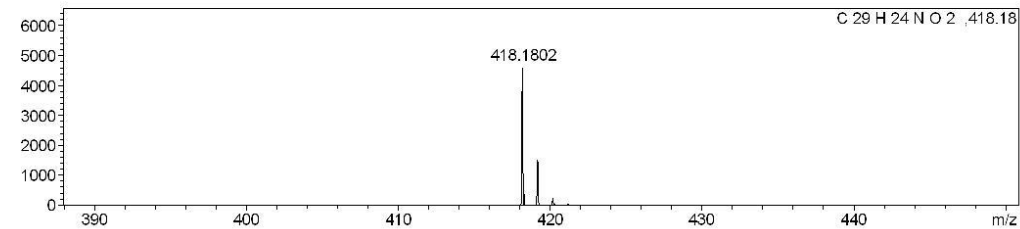
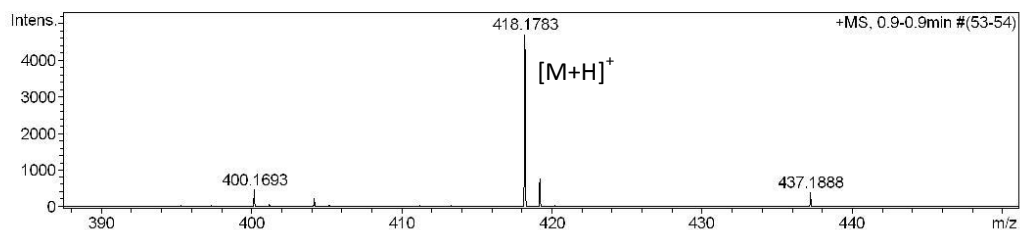
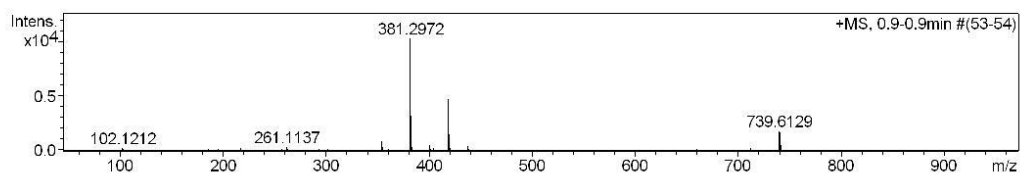
Analysis Name D:\Data\091714\26254-s6.JZ-n2-p1.d
 Method cal100-1600.m
 Sample Name s6.JZ-n2-p1
 Comment in CH3CN

Acquisition Date 9/17/2014 2:05:40 PM

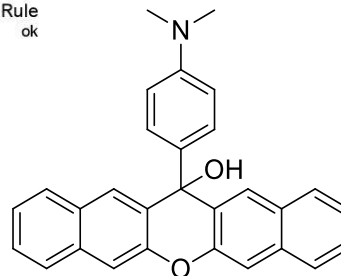
Operator Nonka Sevova
 Instrument / Ser# micrOTOF 10314

Acquisition Parameter

Source Type	ESI	Ion Polarity	Positive	Set Nebulizer	0.3 Bar
Focus	Not active	Set Capillary	4500 V	Set Dry Heater	180 °C
Scan Begin	50 m/z	Set End Plate Offset	-500 V	Set Dry Gas	4.0 l/min
Scan End	3000 m/z	n/a	n/a	Set Divert Valve	Source



Meas. m/z	#	Formula	m/z	err [ppm]	Mean err [ppm]	rdb	N-Rule
418.1783	1	C ₂₉ H ₂₄ N ₁ O ₂	418.1802	4.3	3.2	18.5	ok



HRMS Spectrum for 88

Analysis Info

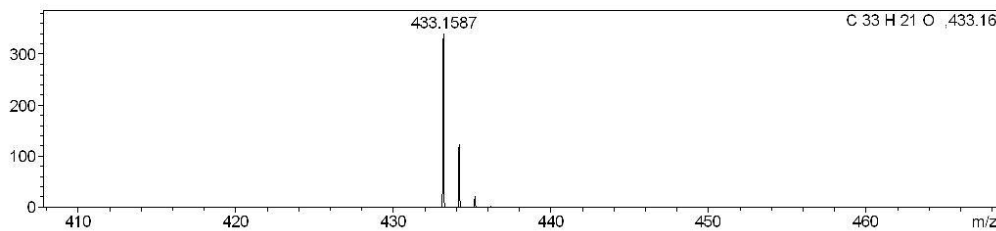
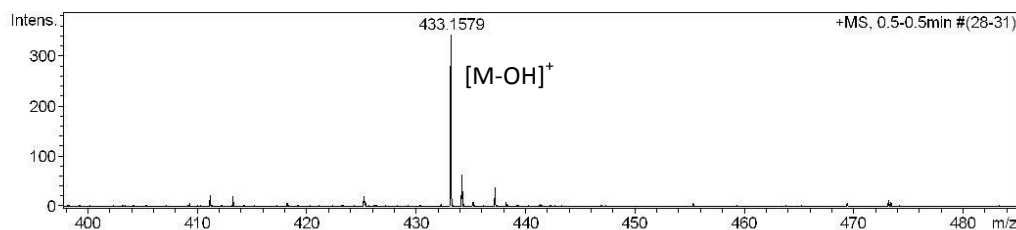
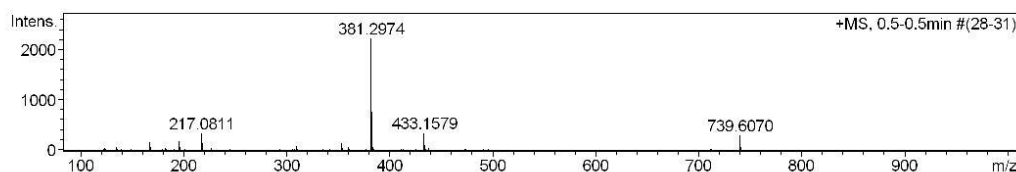
Analysis Name D:\Data\091714\26254-s7.JZ-n2-p2.d
 Method cal100-1600.m
 Sample Name s7.JZ-n2-p2
 Comment in CH3CN

Acquisition Date 9/17/2014 2:09:33 PM

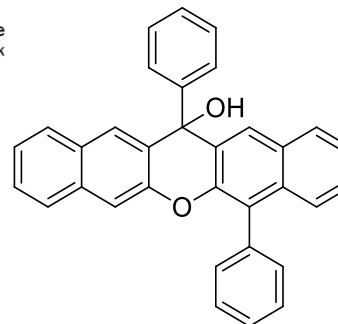
Operator Nonka Sevova
 Instrument / Ser# micrOTOF 10314

Acquisition Parameter

Source Type	ESI	Ion Polarity	Positive	Set Nebulizer	0.3 Bar
Focus	Not active	Set Capillary	4500 V	Set Dry Heater	180 °C
Scan Begin	50 m/z	Set End Plate Offset	-500 V	Set Dry Gas	4.0 l/min
Scan End	3000 m/z	n/a	n/a	Set Divert Valve	Source



Meas. m/z	#	Formula	m/z	err [ppm]	Mean err [ppm]	rdb	N-Rule
433.1579	1	C 33 H 21 O	433.1587	1.7	1.7	23.5	ok



HRMS Spectrum for 89

Analysis Info

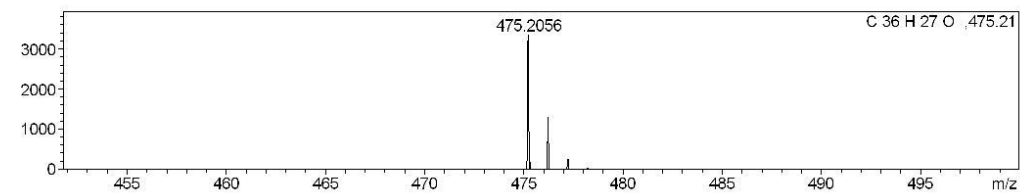
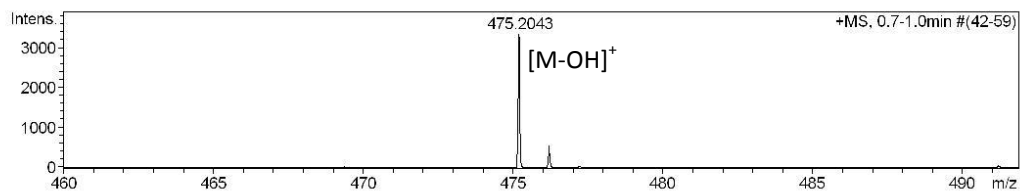
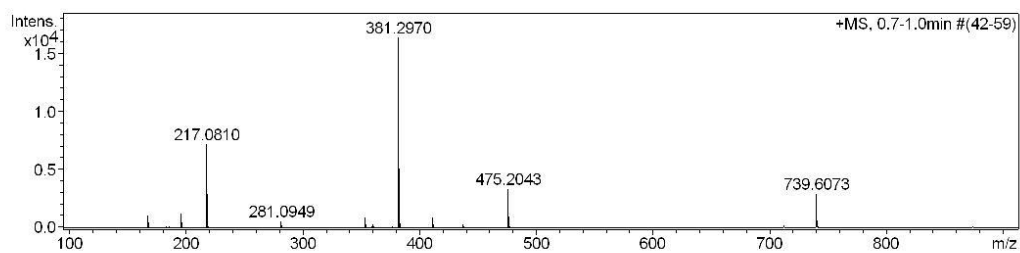
Analysis Name D:\Data\091714\26254-s10.JZ-n2-p10.d
 Method cal100-1600.m
 Sample Name s10.JZ-n2-p10
 Comment in CH3CN

Acquisition Date 9/17/2014 3:13:12 PM

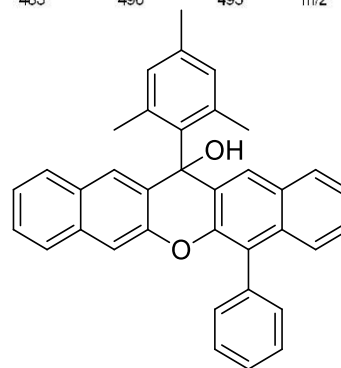
Operator Nonka Sevova
 Instrument / Ser# micrOTOF 10314

Acquisition Parameter

Source Type	ESI	Ion Polarity	Positive	Set Nebulizer	0.3 Bar
Focus	Not active	Set Capillary	4500 V	Set Dry Heater	180 °C
Scan Begin	50 m/z	Set End Plate Offset	-500 V	Set Dry Gas	4.0 l/min
Scan End	3000 m/z	n/a	n/a	Set Divert Valve	Source



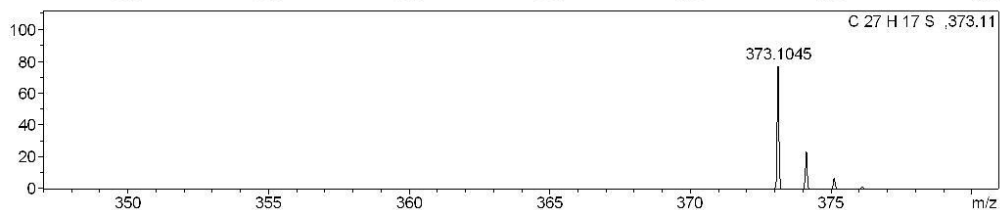
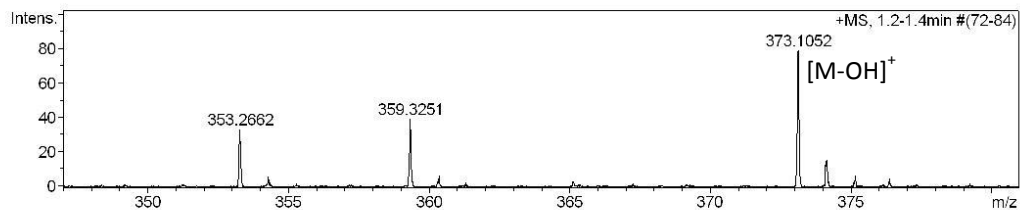
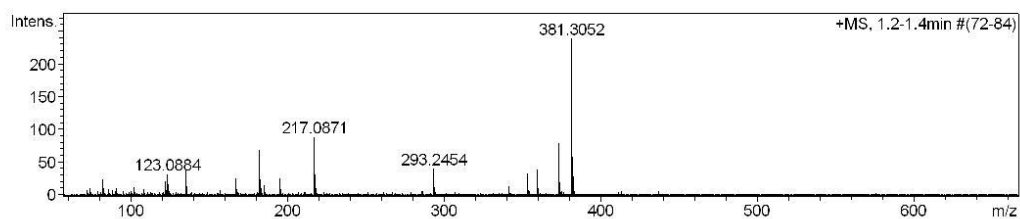
Meas. m/z	#	Formula	m/z	err [ppm]	Mean err [ppm]	rdb	N-Rule
475.2043	1	C 36 H 27 O	475.2056	2.9	3.5	23.5	ok



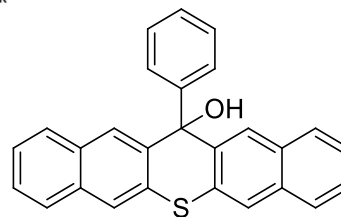
HRMS Spectrum for 90

Analysis Info		Acquisition Date	9/25/2014 3:11:23 PM
Analysis Name	D:\Data\092514\26661-s14.JZ-n2-p44.d	Operator	Nonka Sevova
Method	cal100-1600.m	Instrument / Ser#	micrOTOF 10314
Sample Name	s14.JZ-n2-p44		
Comment	in CH3CN		

Acquisition Parameter					
Source Type	ESI	Ion Polarity	Positive	Set Nebulizer	0.3 Bar
Focus	Not active	Set Capillary	4500 V	Set Dry Heater	180 °C
Scan Begin	50 m/z	Set End Plate Offset	-500 V	Set Dry Gas	4.0 l/min
Scan End	3000 m/z	n/a	n/a	Set Divert Valve	Source



Meas. m/z	#	Formula	m/z	err [ppm]	Mean err [ppm]	rdb	N-Rule
373.1052	1	C 27 H 17 S	373.1045	-1.6	-1.6	19.5	ok



HRMS Spectrum for 91

Mass Spectrometry & Proteomics Facility **Mass Spectrum SmartFormula Report**

Analysis Info

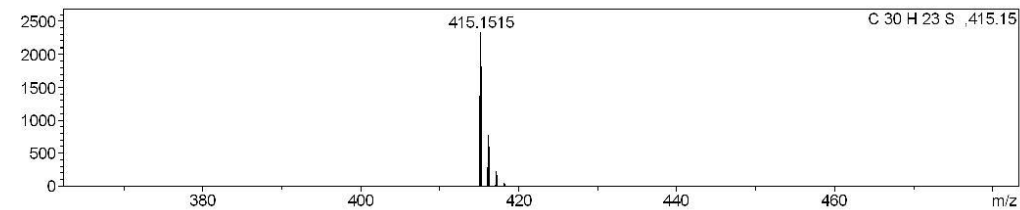
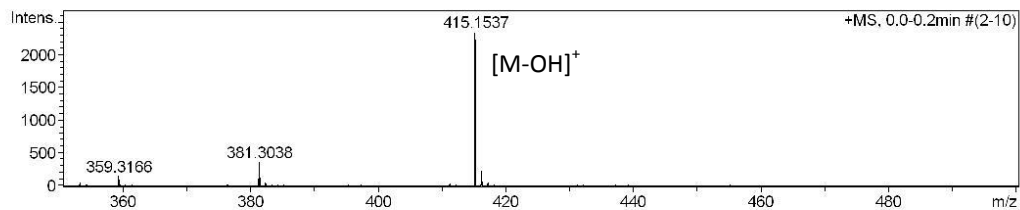
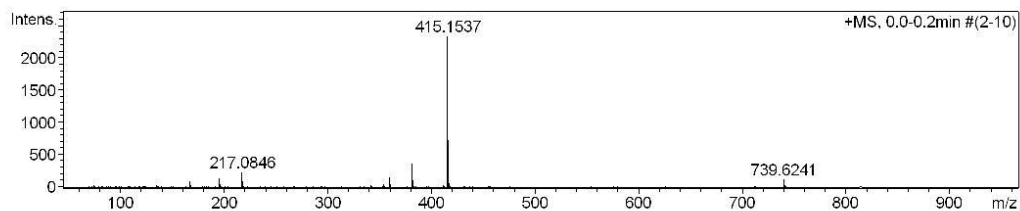
Analysis Name D:\Data\092514\26661-s16.JZ-n2-p51.d
 Method cal100-1600.m
 Sample Name s16.JZ-n2-p51
 Comment in CH3CN

Acquisition Date 9/25/2014 3:21:43 PM

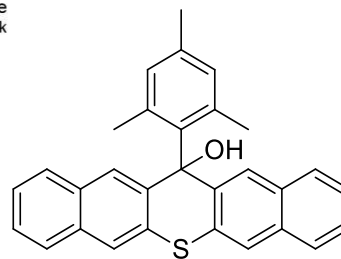
Operator Nonka Sevova
 Instrument / Ser# micrOTOF 10314

Acquisition Parameter


Source Type	ESI	Ion Polarity	Positive	Set Nebulizer	0.3 Bar
Focus	Not active	Set Capillary	4500 V	Set Dry Heater	180 °C
Scan Begin	50 m/z	Set End Plate Offset	-500 V	Set Dry Gas	4.0 l/min
Scan End	3000 m/z	n/a	n/a	Set Divert Valve	Source



Meas. m/z	#	Formula	m/z	err [ppm]	Mean err [ppm]	rdb	N-Rule
415.1537	1	C 30 H 23 S	415.1515	-5.4	-4.2	19.5	ok



HRMS Spectrum for 94

 Mass Spectrometry & Proteomics Facility

Mass Spectrum SmartFormula Report

Analysis Info

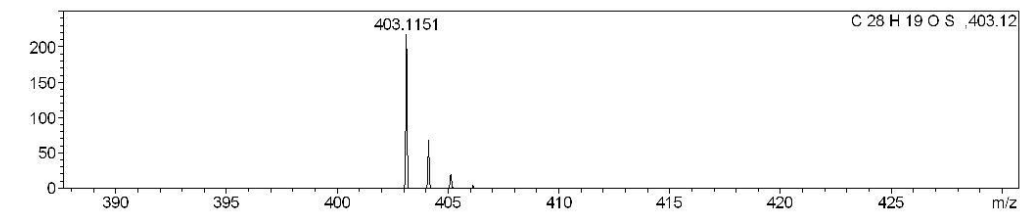
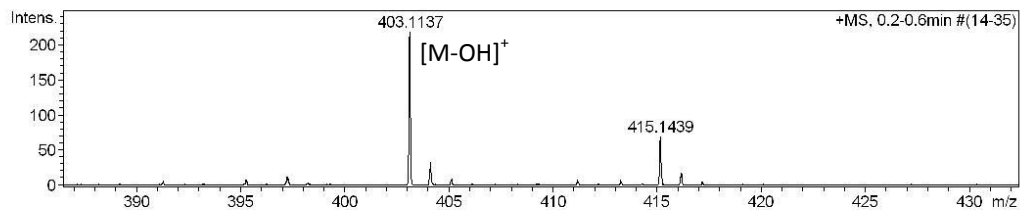
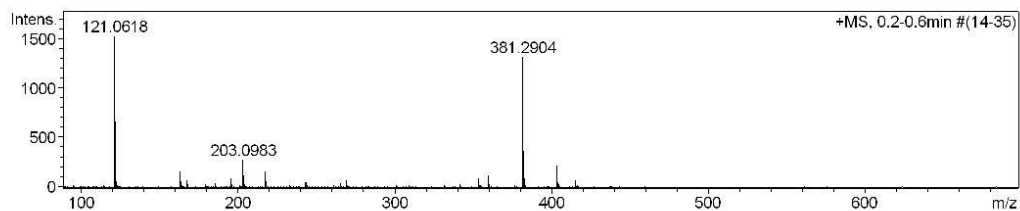
Analysis Name D:\Data\092514\26661-s18.JZ-n2-p57.d
 Method cal100-1600.m
 Sample Name s18.JZ-n2-p57
 Comment in CH3CN

Acquisition Date 9/25/2014 3:30:51 PM

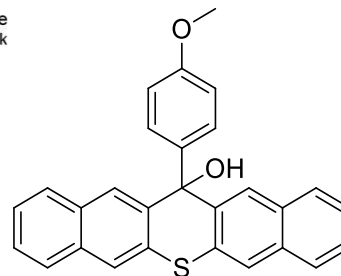
Operator Nonka Sevova
 Instrument / Ser# micrOTOF 10314

Acquisition Parameter

Source Type	ESI	Ion Polarity	Positive	Set Nebulizer	0.3 Bar
Focus	Not active	Set Capillary	4500 V	Set Dry Heater	180 °C
Scan Begin	50 m/z	Set End Plate Offset	-500 V	Set Dry Gas	4.0 l/min
Scan End	3000 m/z	n/a	n/a	Set Divert Valve	Source



Meas. m/z	#	Formula	m/z	err [ppm]	Mean err [ppm]	rdb	N-Rule
403.1137	1	C 28 H 19 O S	403.1151	3.5	3.5	19.5	ok



HRMS Spectrum for 99

Analysis Info

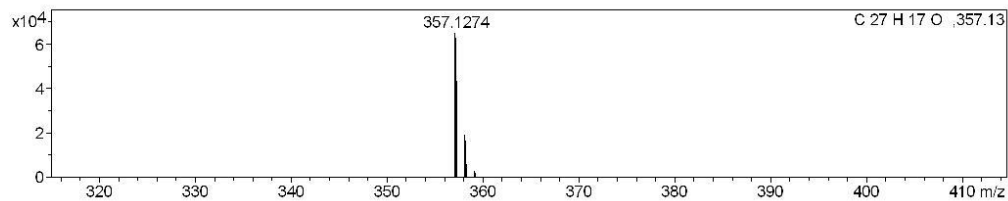
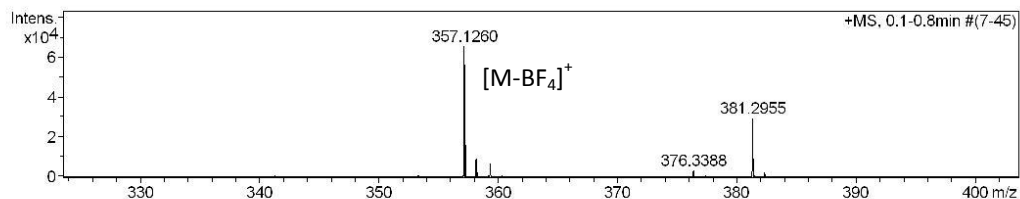
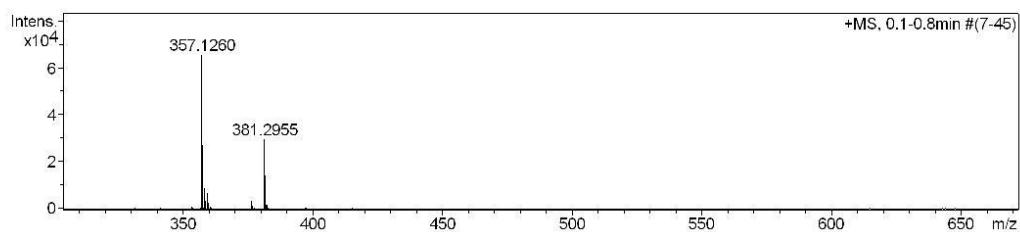
Analysis Name D:\Data\041213\3481-7.JZ-N1-P47.d
 Method cal80-1550.m
 Sample Name JZ-N1-P47
 Comment in CH3CN

Acquisition Date 4/12/2013 3:17:10 PM

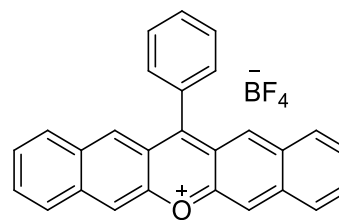
Operator Nonka Sevova
 Instrument / Ser# micrOTOF 10314

Acquisition Parameter

Source Type	ESI	Ion Polarity	Positive	Set Nebulizer	0.3 Bar
Focus	Not active	Set Capillary	4500 V	Set Dry Heater	180 °C
Scan Begin	50 m/z	Set End Plate Offset	-500 V	Set Dry Gas	4.0 l/min
Scan End	3000 m/z	n/a	n/a	Set Divert Valve	Source



Meas. m/z	#	Formula	m/z	err [ppm]	Mean err [ppm]	rdb	N-Rule
357.1260	1	C 27 H 17 O	357.1274	4.0	4.3	19.5	ok



HRMS Spectrum for 100

Mass Spectrometry & Proteomics Facility **Mass Spectrum SmartFormula Report**

Analysis Info

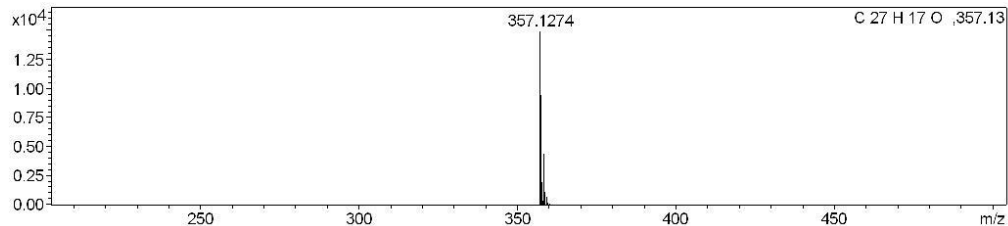
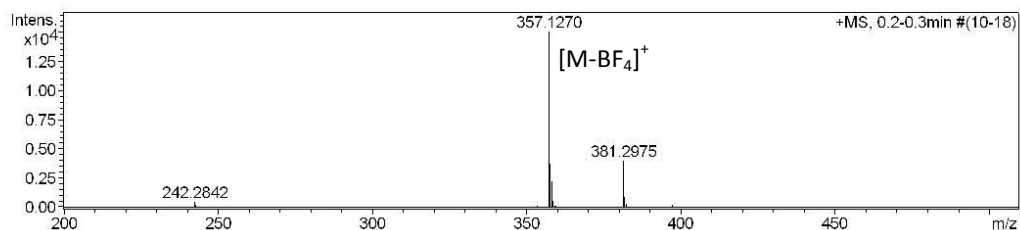
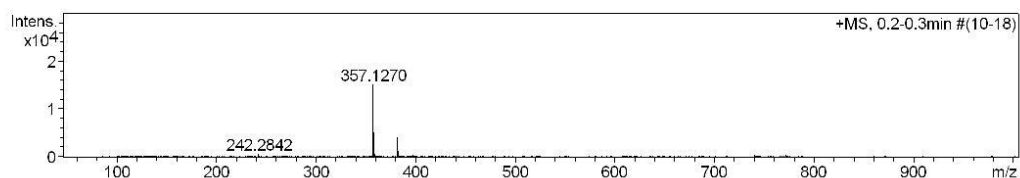
Analysis Name D:\Data\062113\6333-JZ-N1-P58.d
 Method cal80-1550.m
 Sample Name JZ-N1-P58
 Comment in CH₂Cl₂

Acquisition Date 6/21/2013 2:10:51 PM

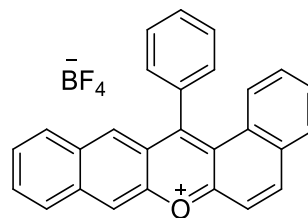
Operator Nonka Sevova
 Instrument / Ser# micrOTOF 10314

Acquisition Parameter

Source Type	ESI	Ion Polarity	Positive	Set Nebulizer	0.3 Bar
Focus	Not active	Set Capillary	4500 V	Set Dry Heater	180 °C
Scan Begin	50 m/z	Set End Plate Offset	-500 V	Set Dry Gas	4.0 l/min
Scan End	3000 m/z	n/a	n/a	Set Divert Valve	Source



Meas. m/z	#	Formula	m/z	err [ppm]	Mean err [ppm]	rdb	N-Rule
357.1270	1	C 27 H 17 O	357.1274	1.2	1.7	19.5	ok



HRMS Spectrum for 101

Analysis Info

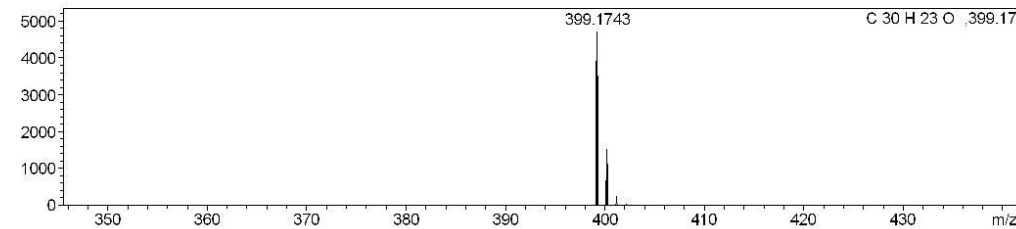
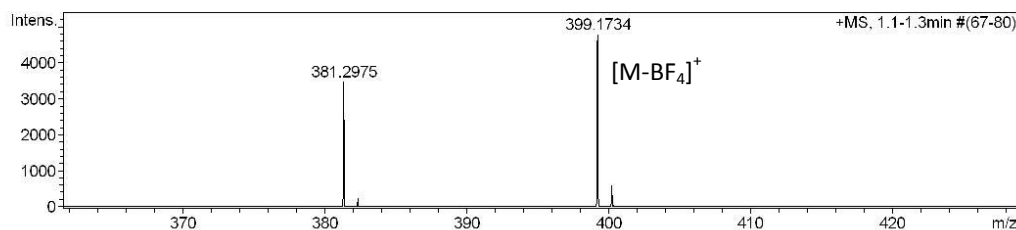
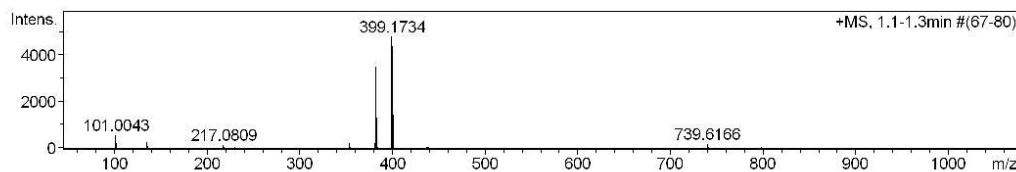
Analysis Name D:\Data\091014\25981-2.JZ-n1-p96.d
 Method cal100-1600.m
 Sample Name 2.JZ-n1-p96
 Comment in CH3CN

Acquisition Date 9/10/2014 4:22:33 PM

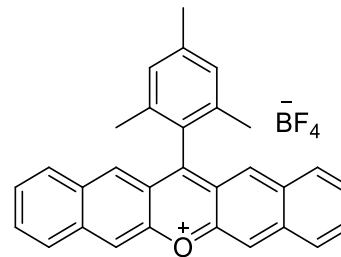
Operator Nonka Sevova
 Instrument / Ser# micrOTOF 10314

Acquisition Parameter

Source Type	ESI	Ion Polarity	Positive	Set Nebulizer	0.3 Bar
Focus	Not active	Set Capillary	4500 V	Set Dry Heater	180 °C
Scan Begin	50 m/z	Set End Plate Offset	-500 V	Set Dry Gas	4.0 l/min
Scan End	3000 m/z	n/a	n/a	Set Divert Valve	Source



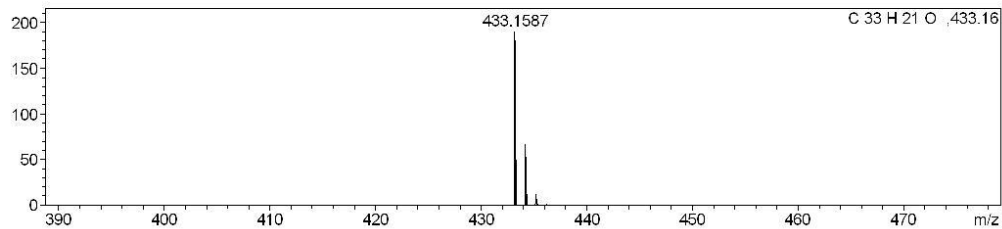
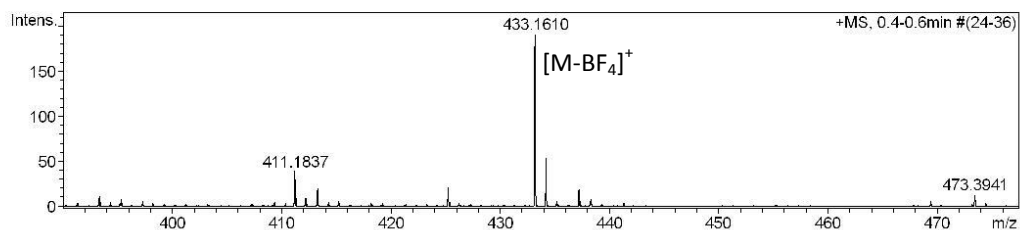
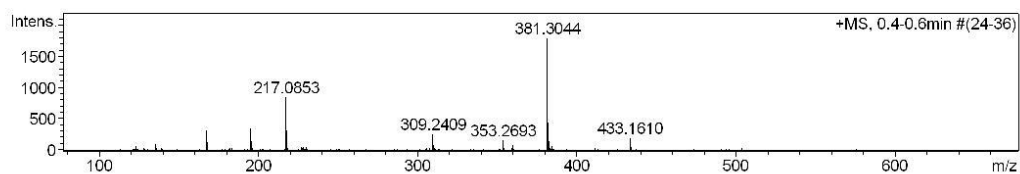
Meas. m/z	#	Formula	m/z	err [ppm]	Mean err [ppm]	rdB	N-Rule
399.1734	1	C 30 H 23 O	399.1743	2.4	3.1	19.5	ok



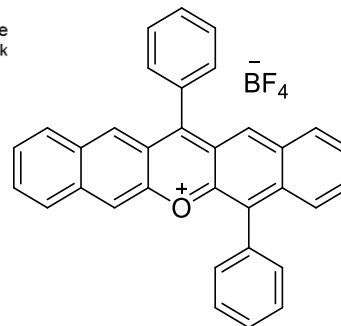
HRMS Spectrum for 103

Analysis Info		Acquisition Date	9/17/2014 2:14:43 PM	
Analysis Name	D:\Data\091714\26254-s8.JZ-n2-p3.d	Operator	Nonka Sevova	
Method	cal100-1600.m	Instrument / Ser#	micrOTOF	10314
Sample Name	s8.JZ-n2-p3			
Comment	in CH3CN			

Acquisition Parameter					
Source Type	ESI	Ion Polarity	Positive	Set Nebulizer	0.3 Bar
Focus	Not active	Set Capillary	4500 V	Set Dry Heater	180 °C
Scan Begin	50 m/z	Set End Plate Offset	-500 V	Set Dry Gas	4.0 l/min
Scan End	3000 m/z	n/a	n/a	Set Divert Valve	Source



Meas. m/z	#	Formula	m/z	err [ppm]	Mean err [ppm]	rdB	N-Rule
433.1610	1	C 33 H 21 O	433.1587	-5.3	-5.2	23.5	ok



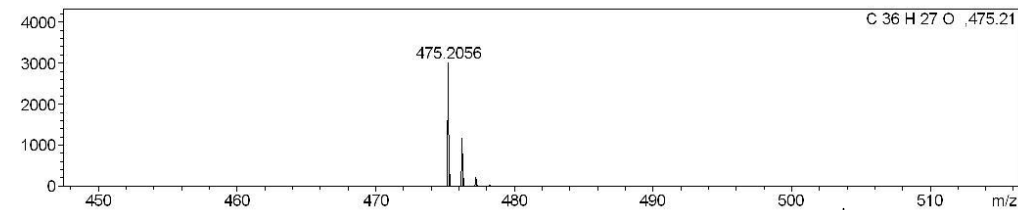
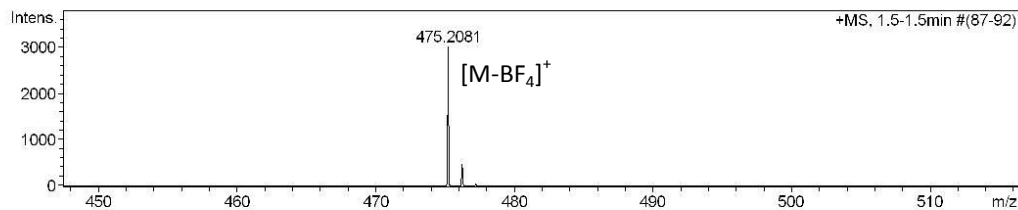
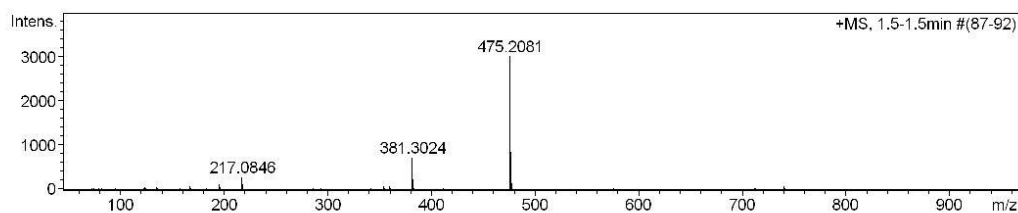
HRMS Spectrum for 104

Mass Spectrometry & Proteomics Facility **Mass Spectrum SmartFormula Report**

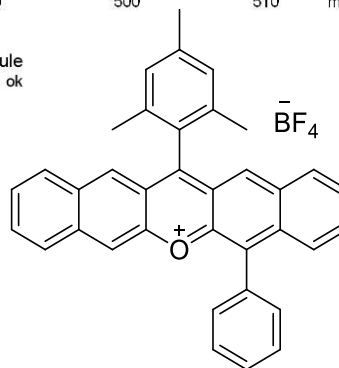
Analysis Info
 Analysis Name: D:\Data\092514\26661-s15.JZ-n2-p46 .d
 Method: cal100-1600.m
 Sample Name: s15.JZ-n2-p46
 Comment: in CH3CN
 Acquisition Date: 9/25/2014 3:17:11 PM
 Operator: Nonka Sevova
 Instrument / Ser#: micrOTOF 10314

Acquisition Parameter

Source Type	ESI	Ion Polarity	Positive	Set Nebulizer	0.3 Bar
Focus	Not active	Set Capillary	4500 V	Set Dry Heater	180 °C
Scan Begin	50 m/z	Set End Plate Offset	-500 V	Set Dry Gas	4.0 l/min
Scan End	3000 m/z	n/a	n/a	Set Divert Valve	Source



Meas. m/z	#	Formula	m/z	err [ppm]	Mean err [ppm]	rdb	N-Rule
475.2081	1	C 36 H 27 O	475.2056	-5.1	-5.3	23.5	ok



HRMS Spectrum for 105

Analysis Info

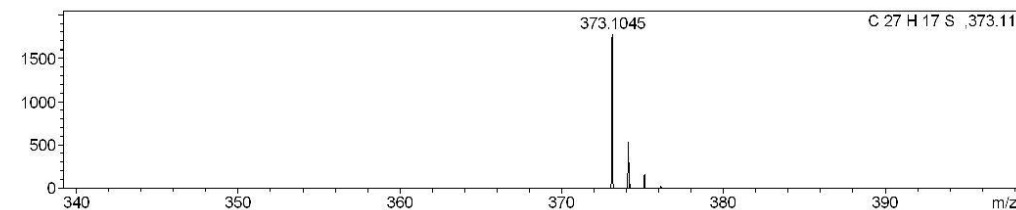
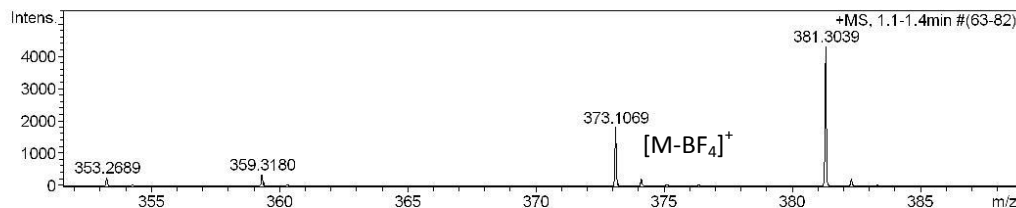
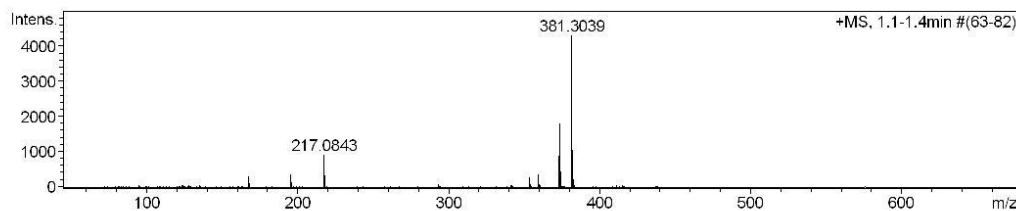
Analysis Name D:\Data\092514\26661-s20.JZ-n2-p60.d
 Method cal100-1600.m
 Sample Name s20.JZ-n2-p60
 Comment in CH3CN

Acquisition Date 9/25/2014 3:43:21 PM

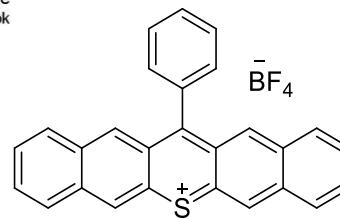
Operator Nonka Sevova
 Instrument / Ser# micrOTOF 10314

Acquisition Parameter

Source Type	ESI	Ion Polarity	Positive	Set Nebulizer	0.3 Bar
Focus	Not active	Set Capillary	4500 V	Set Dry Heater	180 °C
Scan Begin	50 m/z	Set End Plate Offset	-500 V	Set Dry Gas	4.0 l/min
Scan End	3000 m/z	n/a	n/a	Set Divert Valve	Source



Meas. m/z	#	Formula	m/z	err [ppm]	Mean err [ppm]	rdb	N-Rule
373.1069	1	C 27 H 17 S	373.1045	-6.2	-7.8	19.5	ok



HRMS Spectrum for 106

Analysis Info

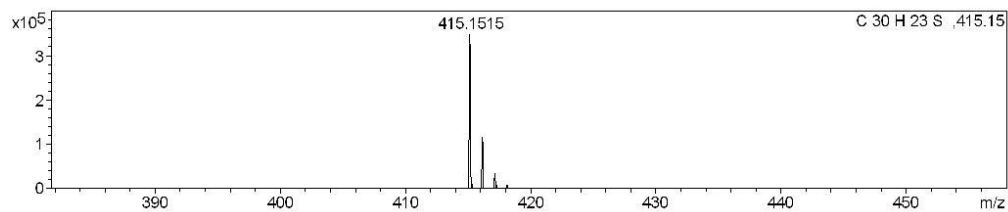
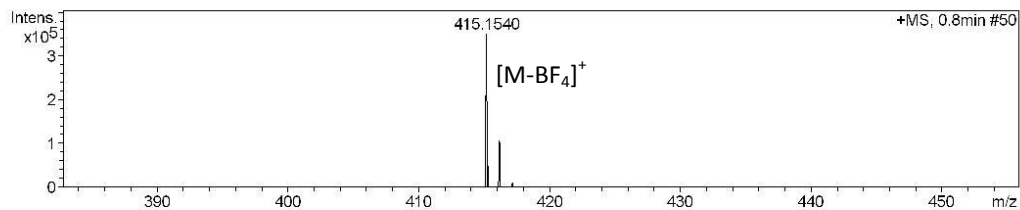
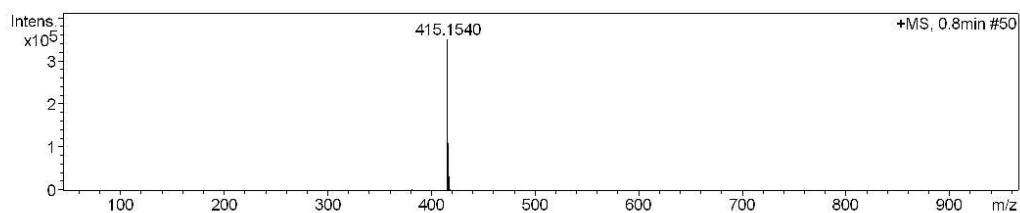
Analysis Name D:\Data\092514\26661-s17.JZ-n2-p52 .d
 Method cal100-1600.m
 Sample Name s17.JZ-n2-p52
 Comment in CH3CN

Acquisition Date 9/25/2014 3:25:38 PM

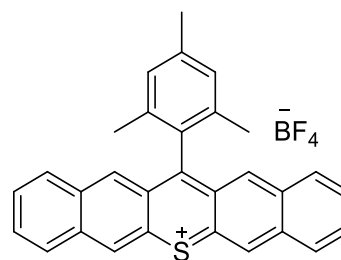
Operator Nonka Sevova
 Instrument / Ser# micrOTOF 10314

Acquisition Parameter

Source Type	ESI	Ion Polarity	Positive	Set Nebulizer	0.3 Bar
Focus	Not active	Set Capillary	4500 V	Set Dry Heater	180 °C
Scan Begin	50 m/z	Set End Plate Offset	-500 V	Set Dry Gas	4.0 l/min
Scan End	3000 m/z	n/a	n/a	Set Divert Valve	Source



Meas. m/z	#	Formula	m/z	err [ppm]	Mean err [ppm]	rdb	N-Rule
415.1540	1	C 30 H 23 S	415.1515	-6.0	-5.6	19.5	ok



HRMS Spectrum for 109

Mass Spectrometry & Proteomics Facility

Mass Spectrum SmartFormula Report

Analysis Info

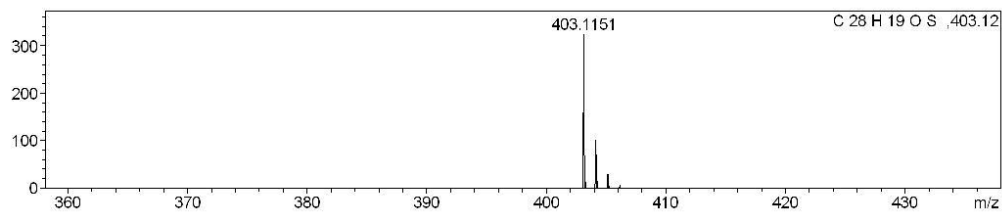
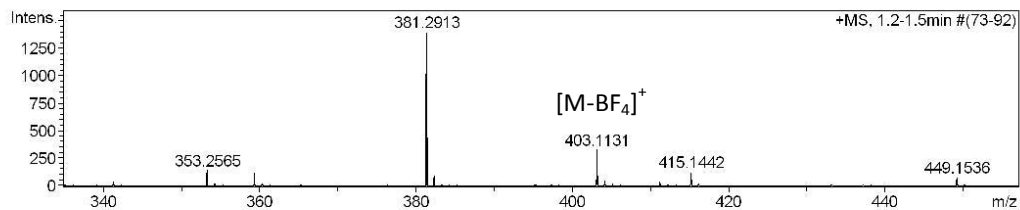
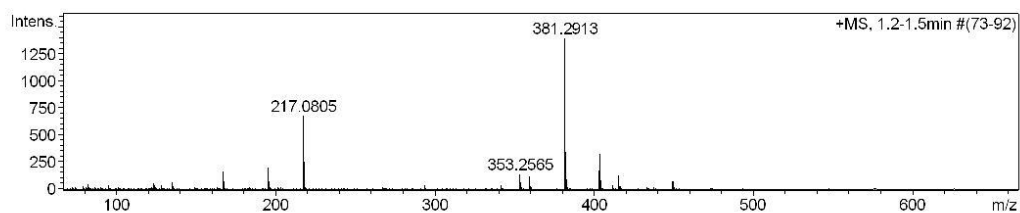
Analysis Name D:\Data\092514\26661-s19.JZ-n2-p58.d
 Method cal100-1600.m
 Sample Name s19.JZ-n2-p58
 Comment in CH3CN

Acquisition Date 9/25/2014 3:38:39 PM

Operator Nonka Sevova
 Instrument / Ser# micrOTOF 10314

Acquisition Parameter

Source Type	ESI	Ion Polarity	Positive	Set Nebulizer	0.3 Bar
Focus	Not active	Set Capillary	4500 V	Set Dry Heater	180 °C
Scan Begin	50 m/z	Set End Plate Offset	-500 V	Set Dry Gas	4.0 l/min
Scan End	3000 m/z	n/a	n/a	Set Divert Valve	Source



Meas. m/z	#	Formula	m/z	err [ppm]	Mean err [ppm]	rdb	N-Rule
403.1131	1	C ₂₈ H ₁₉ O ₂ S	403.1151	4.9	4.9	19.5	ok

